Investigating the roles of Notch and Vascular Endothelial Growth Factor in Hepatic Cell Fate Decisions and Architectural Establishment in Development and Disease

By

Teagan Jo Walter

Dissertation

Submitted to the Faculty of the

Graduate School of Vanderbilt University

in partial fulfillment of the requirements

for the degree of

DOCTOR OF PHILOSOPHY

in

Cell and Developmental Biology

December, 2013

Nashville, Tennessee

Approved:

Stacey S. Huppert, Ph.D.

H. Scott Baldwin, M.D.

Chin Chiang, Ph.D.

Andrea Page-McCaw, Ph.D.

Alvin C. Powers, M.D.

ACKNOWLEDGEMENTS

Funding

This work was supported by grants from the National Institutes of Health to C.V. (T32CA106183), from the NIH to S.S.H (R01DK078640), from the Howard Hughes Medical Institute (HHMI) through the HHMI/Vanderbilt University Certificate Program in Molecular Medicine to T.J.W. (GRDOT56006779), from the NIH to the Vanderbilt Cancer Center (P30CA068485), the Vanderbilt Diabetes Research and Training Center (P30DK020593), the Vanderbilt Digestive Disease Research Center (P30DK058404), and the Cincinnati Children's Hospital Medical Center Digestive Health Center (P30DK078392) for providing financial support for microscopy and pathology Core Services.

Experimental

I am indebted to the many people who have contributed to the research shown in this dissertation. For mouse lines, I thank Mark Magnuson, Maureen Gannon, Tasuku Honjo, Guoqiang Gu, Al Powers, Napoleone Ferrara, and Peter Campochiaro. For mouse and rat tissues, I thank Jorge Bezerra, Pranav Shivakumar, S. Paul Monga, and David Rudnick. For human tissue samples, I thank M. Kay Washington. For immunohistochemistry of human tissues, and general immunohistochemistry assistance, I thank Anna Means. For technical assistance, I thank the several current and former Huppert lab members: Holly Poling, Charles Vanderpool, Erin Sparks, Kari Huppert, Donghyun Lee, Kevin Song, and Ruth Yan.

Academic and Personal

There are many people who have contributed invaluably to my personal and scientific progress over my time in graduate school. I would like to first thank my advisor, Stacey Huppert, who has played a crucial role in the path I have taken. Stacey has helped me to develop scientifically and encouraged me to pursue opportunities to enhance my graduate experience, such as participating in the Certificate Program in Molecular Medicine. For her mentorship and guidance, I am very grateful. Secondly, I would like to thank the faculty members who have contributed to my scientific development and progress, including my committee members, Scott Baldwin, Chin Chiang, Andrea Page-McCaw, and Al Powers, and the Certificate Program in Molecular Medicine leadership, Lou Muglia and Mark deCaestecker. I would also like to thank my clinical mentors, Lynette Gillis, Chan Chung, and Alexandra Menchise. I additionally need to thank the several colleagues who have provided both scientific and personal support. Elise Pfaltzgraff has been an irreplaceable friend and has shared in both my struggles and my triumphs. I am unbelievably lucky to have been able to rely on her for so many various things over the past several years. Holly Poling has generously shared her time and her insight, and I couldn't have wished for a better lab-mate. I am also grateful for the new friends who have provided a lot of support in Cincinnati: Dan Giles, Kyle Bednar, Akash Verma, and Giovanni Morabito. Finally, I have to thank my family, who has done immeasurably more than anyone else in shaping my life over the past 26 years. My parents, Bill and Susan, and my sisters, Kyla and Elissa, have been dependably there for whatever I need. I cannot express how much I love and value them. Most importantly, I would like to specifically thank my mom. She is the most inspiring person I know. She has believed in me unconditionally and has taught me to believe in myself. I would have none of the amazing things that are a now a part of my life without her support, guidance, and love.

TABLE OF CONTENTS

Page

Appendix

LIST OF TABLES

LIST OF FIGURES

LIST OF ABBREVIATIONS

AAF	Acetylaminofluorene
ALGS	Alagille syndrome
ALT	Alanine aminotransferase
BA	Biliary atresia
BA	Total bile acids
BDL	Bile duct ligation
BEC	Biliary epithelial cell
CCl_4	Carbon tetracholoride
CDE	choline-deficient diet supplemented with ethionine
CK19	Cytokeratin19
CPS1	Carbamoyl phosphate synthetase 1
CV	Central vein
DBA	Dolichos biflorus agglutinin
DDC	3,5-diethoxycarbonyl-1,4-dihydrocollidine
DKO	Double knockout
Dll	Delta-like
E	Embryonic
EC	Endothelial cell
EHBD	Extrahepatic bile duct
ELISA	Enzyme-linked immunosorbent assay
EYFP	Enhanced yellow fluorescent protein
Fgf	Fibroblast growth factor
Fox	Forkhead homeobox
Fz	Frizzled
GK	Glucokinase
GS	Glutamine synthetase
H&E	Hematoxylin and eosin
HA	Hepatic artery
HCC	Hepatocellular carcinoma
HIF	Hypoxia inducible factor
Hnf1β	Hepatocyte nuclear factor 1β
Hnf4α	Hepatocyte nuclear factor 4α
Hnf6	Hepatocyte nuclear factor 6
HPC	Hepatic progenitor cell
IHBD	Intrahepatic bile duct
LSEC	Liver sinusoid endothelial cell
NICD	Notch intracellular domain
P	Postnatal
PBC	Primary biliry cirrhosis
PBS	Phosphate-buffered saline
PECAM	Platelet-cell derived endothelial cell adhesion molecule
PEPCK	Phosphoenolpyruvate carboxykinase

PHx	Partial hepatectomy
PSC	Primary sclerosing cholangitis
PV	Portal vein
Rbpj	Recombination signal binding protein J κ
RFP	Red fluorescent protein
RRV	Rhesus rotavirus
SCL	Stem cell leukemia
SMA	Smooth muscle actin
Sox9	Sry-related HMG box transcription factor 9
STM	Septum transversum mesenchyme
TB	Total bilirubin
Ttr	Transthyretin
VEGF	Vascular endothelial growth factor
VEGFR	VEGF receptor
VFOE	VEGF overexpression
VKO	VEGF knockout
wsCK	Wide spectrum cytokeratin

CHAPTER 1

INTRODUCTION

Cell Fate Decisions

Role of cellular fate determination in development and function

All cells of the body, comprising several organs and tissues, arise from a single fertilized zygote. The process by which a single, pluripotent cell yields the numerous highly specialized and incredibly varied cell types of the body is a complex and tightly regulated process. The process is, quite obviously, a very important one, for without the coordinated differentiation of our cells, complex multi-cellular organisms could not exist.

The various differentiated cell types of the body, despite all having the same DNA, differ in their cell shape, gene expression, and function. Differentiated cell fates are acquired progressively over the course of development through a sequence of cell fate decisions that simultaneously restrict a cell's lineage potential and refine a unique and specialized gene expression profile. A cell fate decision is the process through which a cell that has the potential to follow two or more distinct differentiation paths makes the decision to follow one specific path at the expense of other options.

One of the first lineage decisions made by cells comprising an embryo proper is which germ layer they will become. This decision is made during gastrulation and defines three germ layers: the ectoderm, mesoderm, and endoderm (Loebel et al., 2003). After that decision, cells will proceed on through further lineage-refinement decisions. Within the endoderm, cells decide

whether to become, for example, liver, lung, thyroid, pancreas, or intestine. Cells that have been specified first as endoderm and then as liver are called hepatoblasts, and they can give rise to two cell types: hepatocytes and biliary epithelial cells (BECs; also known as cholangiocytes) (Figure 1.1). Similar lineage decisions take place in all organs and tissues, and through this progressive series of cell fate decisions, an organism obtains a large variety of highly distinct cell types comprising unique functional organs and organ systems.

Influence of extrinsic and intrinsic signals in cell fate decisions

Several intrinsic and extrinsic factors, including intercellular signals, intracellular signals, mechanical forces, and cell-extracellular matrix (ECM) interactions, contribute to the fate decision process of a cell by directly or indirectly influencing gene expression (Discher et al., 2009; Guilak et al., 2009; Streuli, 2009).

Extrinsic signals, including molecular signals that mediate cell-cell communication, are especially important and prominent in the process of cell differentiation. Extrinsic intercellular signals can originate from a neighboring cell within the same tissue, a different tissue within an organ, or even from a different organ. Cell-cell communication can promote cellular differentiation in processes that generate cellular boundaries in organs, ensure proper cell ratios, and ensure proper cell spatial relationships. The receipt of extracellular signals can change gene expression and can activate or suppress intracellular signaling pathways in a cell to change cell behaviors and drive cell fate decisions.

The temporal and spatial coordination of signals is crucial during development in order to have proper cell differentiation in all organs of the body. Similarly, some signals are also important for homeostasis and function of tissues, and often times certain signaling pathways can be

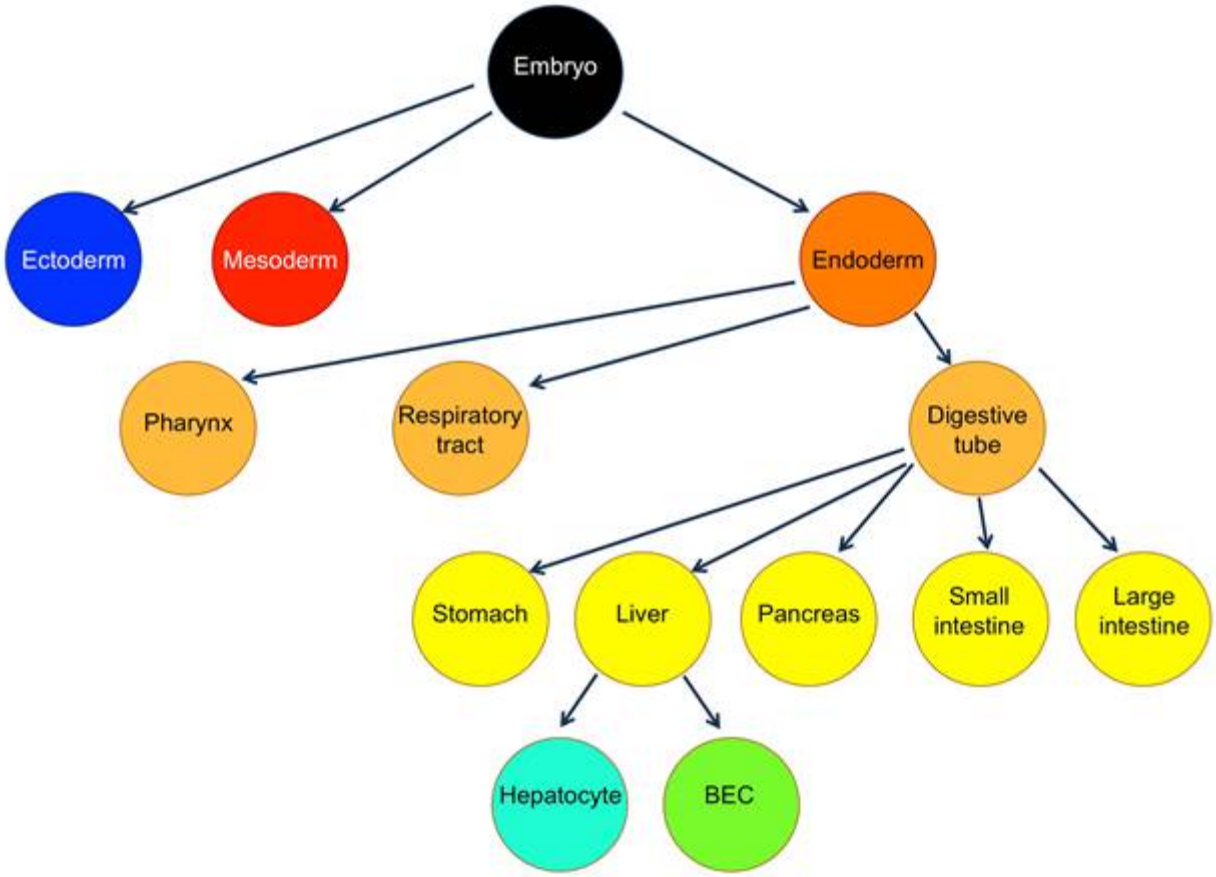

Figure 1.1. Cell fate decisions during development. The diagram demonstrates the general sequence of cell fate decisions made to generate hepatocytes and BECs, the two hepatic epithelial cells types. First, the cells of the embryo are specified as either ectoderm, mesoderm, or endoderm. Within the endoderm germ layer, there is a further differentiation into pharynx, respiratory tract, and digestive tube. The cells of the digestive tube give rise to several organs, including the stomach, liver, pancreas, small intestine, or large intestine. The cells that become specified as liver give rise to two hepatic epithelial cell lineages: hepatocytes and biliary epithelial cells (BECs).

reactivated in the adult state; these signals can either contribute to a beneficial regenerative response to injury or can alternatively generate or promote an injury, such as cancer.

Intercellular Communication in Organ Development

Coordination of multiple cell types in organ development and function

Organs consist of multiple cell types that often have different morphologies, functions, and locations, but that are all required to work together in order for an organ to function properly. In order to generate a properly functioning organ, proper regulation of the number and location of all of the involved cells during development is crucial.

The functions of each organ vary, and as such, so do the ways in which cell types must interact during development. For all organs, the number and location of blood vessels must be regulated so that all cells have access to oxygen and nutrients from the blood stream. The nervous system integration into an organ must also be regulated so that all cells that require sensory input for function are in contact with a nerve. Several organs have endocrine functions requiring that the cells that produce hormones have immediate access to a blood stream into which to secrete hormones. Similarly, for organs that generate and excrete products, like the liver, pancreas, and kidneys, ductal systems must be established to connect the cells that produce and/or modulate an excretion product with the intended destination of that product. Even cells that do not directly interact with one another often must still have a precise spatial organization in relation to each other; in the eye, the spatial organization of rod and cones cells must be precisely regulated to ensure that the eye can detect both light and color from all areas of the visual field. As all organs of the body must function in coordination to support a functional

organism, so must the cells and tissues within each organ interact and work together to form a functional organ.

Role of intercellular signaling in defining cellular and morphological organ features

Intercellular signaling during development is important for coordinating organ characteristics such as cell type ratios and cellular boundaries within an organ and organ size. There are multiple types of signals, distinguished by the range of the signal. Endocrine signals are transported in the bloodstream and can access virtually any tissue in the body. Paracrine signals can diffuse within a tissue and penetrate several cell layers from the source. Juxtacrine signaling occurs between neighboring cells, often as the result of the signaling molecules being tethered to the cell membranes. Finally, autocrine signals act on the same cell in which they are generated.

During development, paracrine signals are frequently used to set up gradients of morphogens. Morphogen gradients are used to differentiate multiple cell fates based on the concentration on the morphogen received by each cell (Dessaud et al., 2008). Morphogens can also be used to control directional growth of tissues; vascular and nervous tissues, for example, use pathfinding led by morphogen gradients to grow directionally into a tissue or towards the source of the signal (Eichmann et al., 2005). Juxtacrine signaling is used to set up strict boundaries within a tissue (Bolós et al., 2007). Juxtacrine signaling is also used for lateral inhibition during cell fate decisions to ensure proper cell type ratios; a cell that adopts a specific fate can signal to its neighbors to adopt a different fate, thereby regulating both the ratios and the spacing of different cell types during development (Owen et al., 2000).

Correct signaling between the different cells and tissues of an organ during development is important in order to generate a mature, functional organ. Improper signaling can lead to malformed or non-functional organs, and can be a causal factor in the development of cancers.

Liver Architectural Establishment

Early liver development

The liver is specified from the anterior definitive endoderm (Tremblay and Zaret, 2005) at the 5-6 somite stage, around embryonic day (E)8.0-8.5 in mice (Gualdi et al., 1996). By E9.0-9.5, the specified hepatic progenitor cells, called hepatoblasts, activate the expression of liver specific genes, such as albumin and α-fetoprotein. The cells begin to proliferate and evaginate into a liver bud (Figure 1.2). After the breakdown of extracellular matrix ECM around this bud, the hepatoblasts migrate into the septum transversum mesenchyme (STM) that is adjacent to the hepatic bud. The continued proliferation and further differentiation of these cells gives rise to the adult liver.

Liver architecture and function within the organism

The liver plays crucial functions in nutrient regulation, and its anatomy in relationship to the vascular and digestive systems reflect these functions. In one of its roles, the liver produces and secretes bile salts into the intestine. The bile produced serves in the predigestive emulsification of ingested fats. For this function, the liver maintains a direct connection with both the intestine and the gall bladder, which stores bile. The liver also has several metabolic roles and regulates the storage and circulation of both lipids and carbohydrates. The location of the liver within the vascular system aids in these tasks; the majority of the blood flow into the liver enters via the

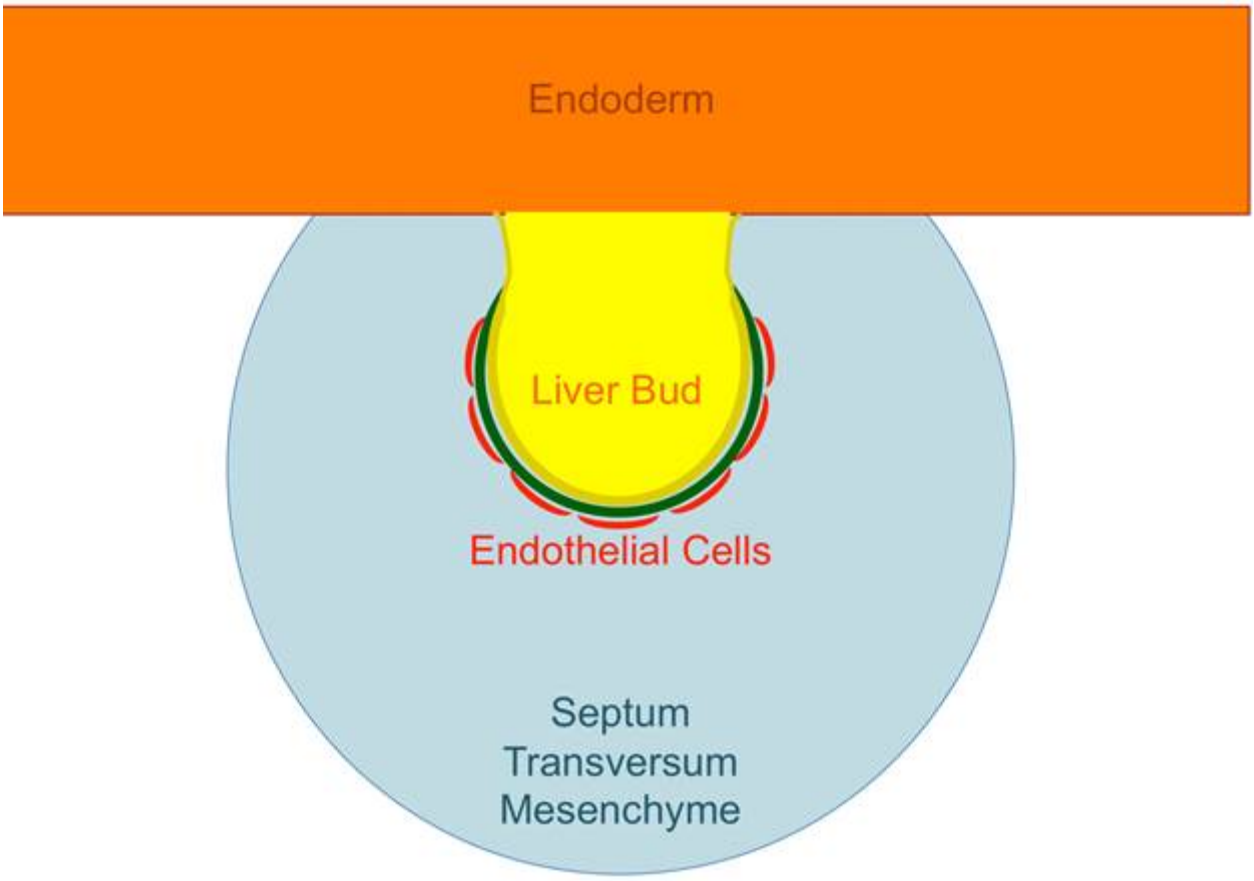

Figure 1.2. Endothelial cells surround the liver bud at the time of evagination and delamination. When the liver bud (yellow) evaginates from the endodermal gut tube (orange), it is lined by endothelial cells (red). The liver bud (yellow) is comprised of several bipotential hepatoblasts that form a columnar epithelial sheet surrounding a hollow extension off of the hollow endodermal gut tube (orange). After hepatoblasts activate the expression of hepatic-lineage genes, such as Albumin, they transition from a columnar epithelial sheet to a pseudostratified epithelium, the ECM surrounding the liver bud (green) is broken down, and the hepatoblasts delaminate from the gut tube, invading the septum transversum mesenchyme (light blue) comprised of multiple mesenchymal cells.

portal vein (PV), a venous system that collects blood from the other gastrointestinal organs and carries it to the liver. As nutrients are absorbed from the digestive organs into the blood stream, they are taken directly to the liver for efficient processing and regulation. This vascular anatomy is also important for the detoxification functions of the liver. Drugs and pathogens that are orally ingested enter the body through the gastrointestinal tract. As they pass through the PV system, these agents are metabolized within the liver prior to reaching other tissues. For these highlighted functions of the liver, a specific architectural relationship of the liver to the gastrointestinal and vascular systems is crucial.

Importance of liver three-dimensional architecture for function

The architecture of the cells and tissues within the liver is also crucial for the liver to perform its various functions. The liver includes several tissues that have a specific 3-dimensional architecture, including the PV, central vein (CV), and hepatic artery (HA) vascular tissues, the intrahepatic bile duct (IHBD), the hepatic nerves, and the hepatocytes.

Proper liver function requires a precise spatial arrangement of the aforementioned tissues. The importance of the spatial associations of liver tissues is apparent in the structure and function of the hepatic lobule (Figure 1.3). Lobules are proposed to be the smallest functional unit of the liver. The architecture of the lobule is defined by the spatial arrangement of several liver tissues, including the PV, HA, IHBD, and the CV. Lobules, in two dimensions, have a hexagonal shape with a portal vein at each vertex and a CV branch in the middle. The HA and IHBD branches also appear at the vertices in close association with PV branches in structures known as portal triads. Hepatocytes arranged in cords fill in the space between the PV and the CV (blue shaded regions in Figure 1.3). Along the basal sides of the hepatocytes run the sinusoids, specialized capillary structures that connect the PV and HA to the CV and supply blood to all hepatocytes.

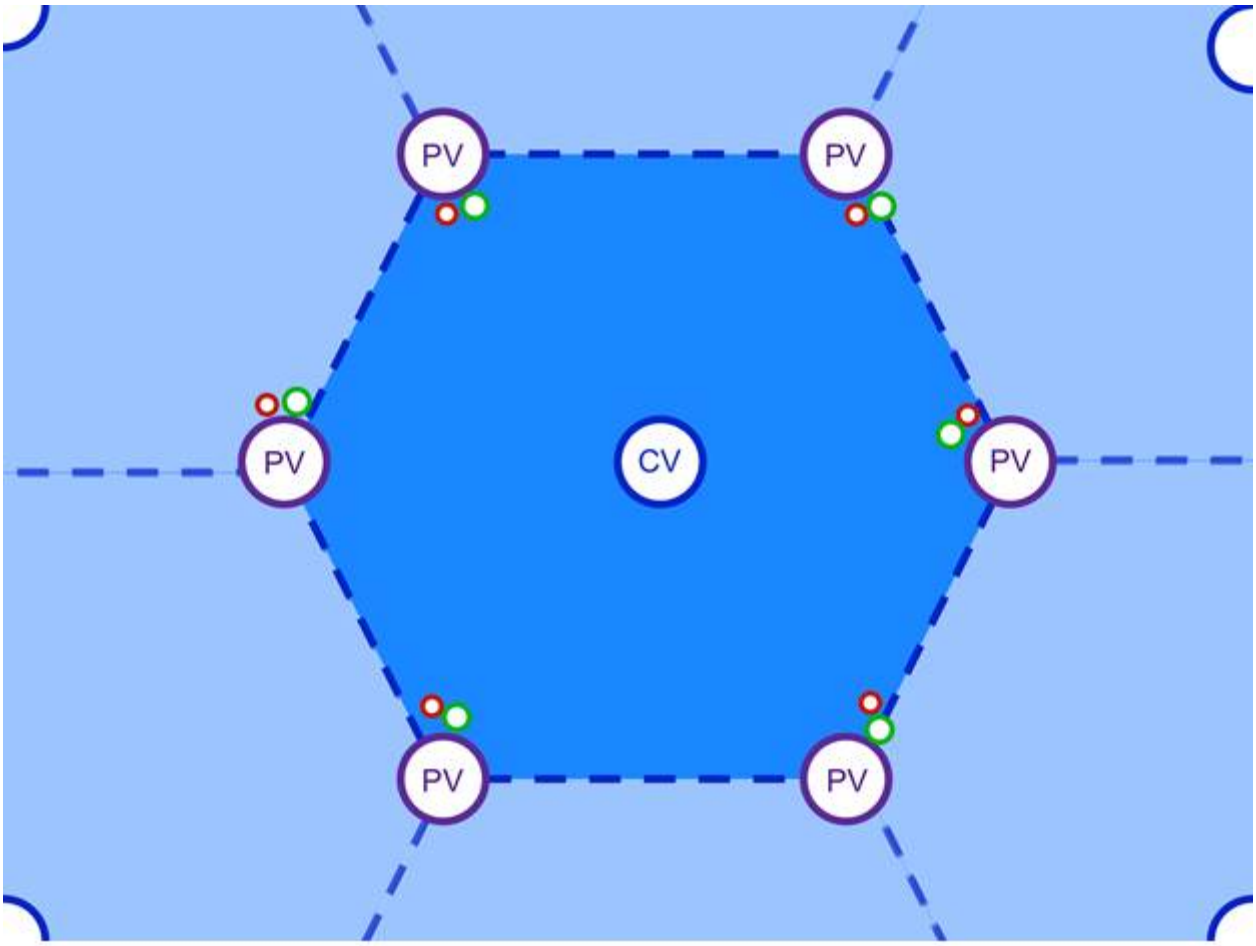

Figure 1.3. Structure of the hepatic lobule. The hepatic lobule (dark blue) has a hexagonal shape with portal vein branches (PV) at the vertices and a central vein branch (CV) at the center. Intrahepatic bile ducts (green) and hepatic arteries (red) are spatially associated with PVs. Within the lobule (dark blue), many hepatocytes are arranged into cords that extend across the PV-CV axis.

Along the apical sides of the hepatocytes are canaliculi, small structures that transport bile produced by hepatocytes into the IHBDs (Figure 1.4).

The spatial organization of the vascular and epithelial tissues within the lobule is required for proper liver function. While the precise organization of the PV, HA, and CV are required to generate proper blood flow within the liver, the organization of hepatocytes and IHBDs are also crucial for the drainage of bile, and the precise layout of all of these structures are required to generate the hepatic lobule units. Apart from their relationship in the lobule, each of these epithelial and vascular tissues also has its own architecture and spatial organization.

Hepatic vascular development and architecture

The PV and HA both supply blood to the liver and their architecture is important for proper liver function. The PV collects nutrient-rich effluent blood from the other peritoneal organs and brings it to the liver, where hepatocytes filter the blood and regulate the nutrients in circulation as previously described. In humans, the portal vein supplies approximately 75% of the afferent hepatic blood flow. The other 25% of hepatic blood flow is supplied by the HA (Lautt, 2009; Tygstrup et al., 1962). The PV and HA both empty into the hepatic sinusoids, which line hepatocyte cords, forming a specialized capillary network (Figure 1.4). The CV collects the blood that has passed through the sinusoids and returns it to the inferior vena cava.

The PV and CV have a unique mechanism of development as extrapolated from the analysis of human fetuses (Collardeau-Frachon and Scoazec, 2008; Gouysse et al., 2002; Lassau and Bastian, 1983) and mouse embryos (T.J.W. and S.S.H, unpublished)(Crawford et al., 2010). Both vessels derive from the fetal vitelline and umbilical veins. At the time of liver bud delamination and expansion, the hepatoblasts surround and disrupt the vitelline and umbilical

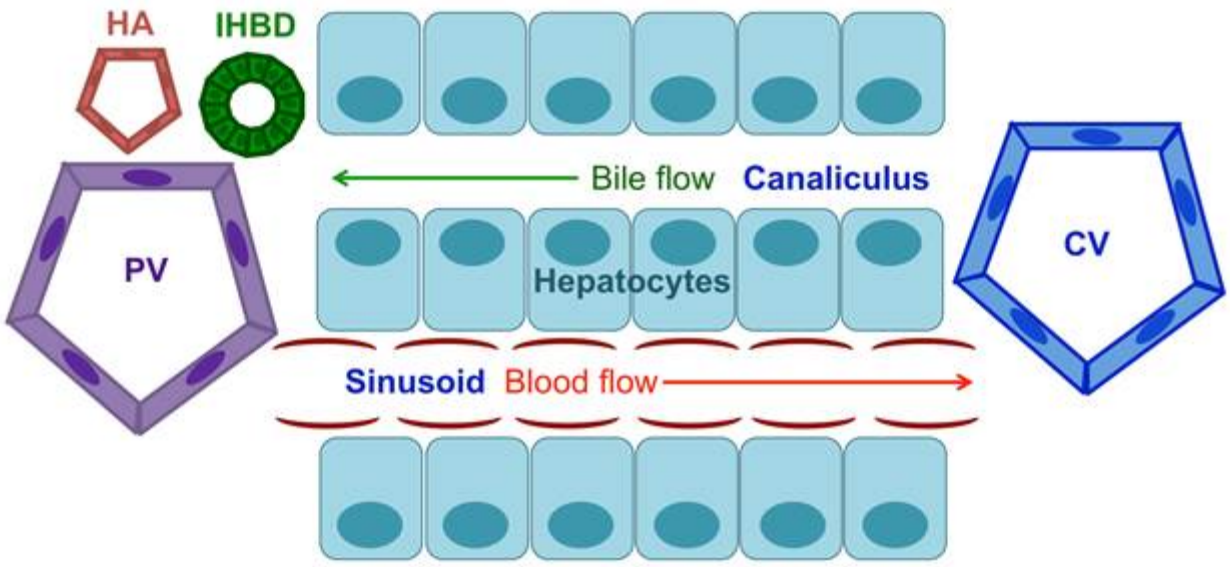

Figure 1.4. Organization of structures within the hepatic lobule. Hepatocyte cords (blue) run along the radius of the lobule between PVs and CVs. Along the apical hepatocyte membrane, bile is secreted into small canalicular channels and transported to the IHBD. Along the basal hepatocyte membrane, the sinusoidal capillaries carry blood from the PV and HA past the hepatocytes and ultimately into the CV.

veins. The veins remodel into a modified fetal circulatory network. The pre-hepatic and post-hepatic portions of the veins remain intact and give rise to the bases of the PV and CV (Figure 1.5) (Collardeau-Frachon and Scoazec, 2008; Gouysse et al., 2002). The origin of the HA is not completely understood, but it appears after birth, after the formation of the PV and CV, and is understood to develop as an angiogenic sprout originating from the dorsal aorta (Collardeau-Frachon and Scoazec, 2008; Gouysse et al., 2002).

The PV, CV, and HA all display hierarchical branching architectures, with progressively smaller branches that extend throughout the hepatic parenchyma. The architecture of the HA follows that of the PV, indicative of functional relationship between the two structures, as both supply blood to the hepatic sinusoids. (Please see Figure 1.6 for a representative image of the 3-dimensional structure of the left lobe PV and Appendix D for further information on the 3-dimensional relationship between the PV and IHBD).

There is also a presumed developmental relationship between the HA and the IHBD. HAs form after birth and after the remodeling and maturation of the IHBDs (Collardeau-Frachon and Scoazec, 2008; Gouysse et al., 2002). Anatomically, HAs follow the architectural pattern of the IHBDs, being spatially associated with IHBDs through their structure. It is proposed that signals derived from the IHBD direct the development of the HA. This is supported by a failure to generate mature HAs in a genetic mouse model where IHBD morphogenesis is genetically impaired (Fabris et al., 2008).

The sinusoids, lined by liver sinusoidal endothelial cells (LSECs), traverse the lobule, bridging the PV and the CV. The origin of LSECs in the liver is not known, but they are presumed to arise from endothelial cells (ECs) resident in the septum transversum mesenchyme (STM), including the ECs that surround that hepatic bud at the time of evagination and delamination.

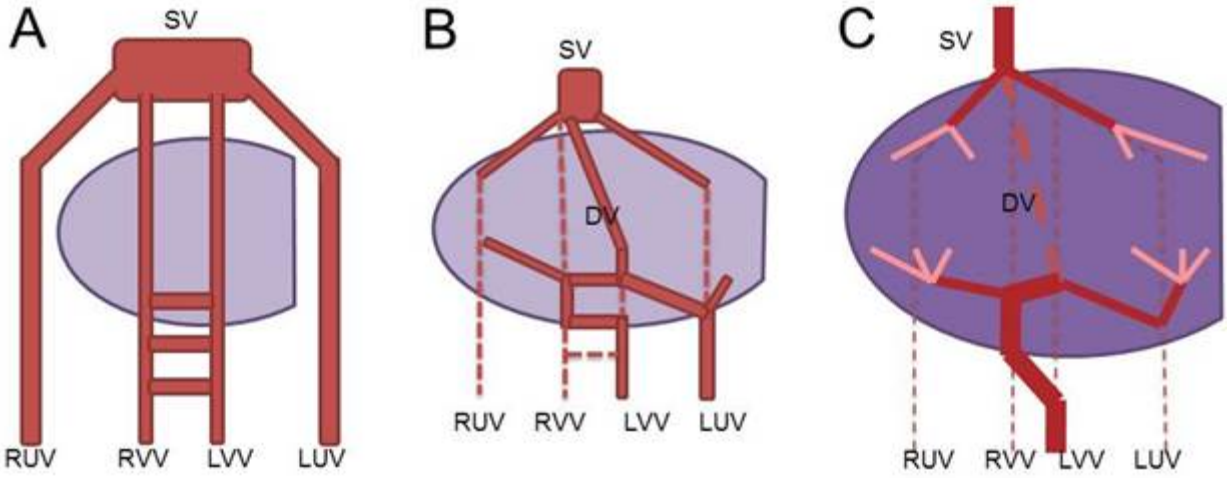

Figure 1.5. The vestigial hypothesis of PV and CV development. According to histological studies of human fetuses, the PV and CV are hypothesized to emerge from the remodeled fetal vitelline and umbilical veins. A. Prior to liver bud formation, the right umbilical vein (RUV), left umbilical vein (LUV), right vitelline vein (RVV), and left vitelline vein (LVV) empty into the sinus venosus (SV). B. As the fetal liver bud expands, it envelops these fetal vessels and causes a remodeling event, generating a new structure, the ductus venosus (DV). C. At the time of birth, the DV collapses. Hepatic circulation after birth goes only through the PV and CV, which are believed to retain components of the fetal veins.

Figure 1.6. 3-dimensional hierarchical branching structure of the PV. The left lobe PV is shown here in a representative image. The PV structure demonstrates progressive branching into smaller veins. These small veins reach through the liver periphery. The CV and IHBD show similar hierarchical branching structures (data not shown).

LSECs provide a lenient selective barrier between the sinusoidal blood and the hepatocytes, allowing for particles to pass through them to the hepatocytes. The scavenging functions of LSECs, allowing them to take up particles from the blood and transmit them to hepatocytes, are aided by several key features, including: 1. the presence of multiple fenestrae, arranged into sieve plates, on the LSECs; 2. The absence of a basal lamina; 3. The discontinuous organization of LSECs and corresponding absence of cell-junction proteins (Aird, 2007; Wisse et al., 1985). The maintenance of these LSEC characteristics has been shown to require VEGF signaling (DeLeve et al., 2004). In experiments with cultured primary LSECs, the loss of fenestrae and upregulation of the platelet-derived endothelial cell adhesion molecule (PECAM) expression occur within days after isolation unless the cells are either treated with exogenous VEGF or co-cultured with a VEGF-producing cell type, including either hepatocytes or stellate cells (DeLeve et al., 2004). Due to the close spatial relationship between LSECs and hepatocytes, it is likely that the hepatocytes are a source of VEGF that maintains LSEC identity *in vivo*.

One interesting feature of the hepatic lobule, generated by the arrangement of the blood vessels, is the gradient of oxygen across the lobule. The blood oxygen tension in the sinusoid ranges from approximately 65 mm Hg in the periportal zone to approximately 30-35 mm Hg in the pericentral zone in rats and humans (Figure 1.7) (Jungermann and Keitzmann, 1996; Lautt, 2009). The oxygen gradient within the sinusoid also generates a gradient in intracellular oxygen tension in hepatocytes. The hepatocyte oxygen tensions are considered to range from 45-50 mm Hg in the periportal hepatocytes to 15-20 mm Hg in the pericentral hepatocytes (Jungermann and Kietzmann, 2000).

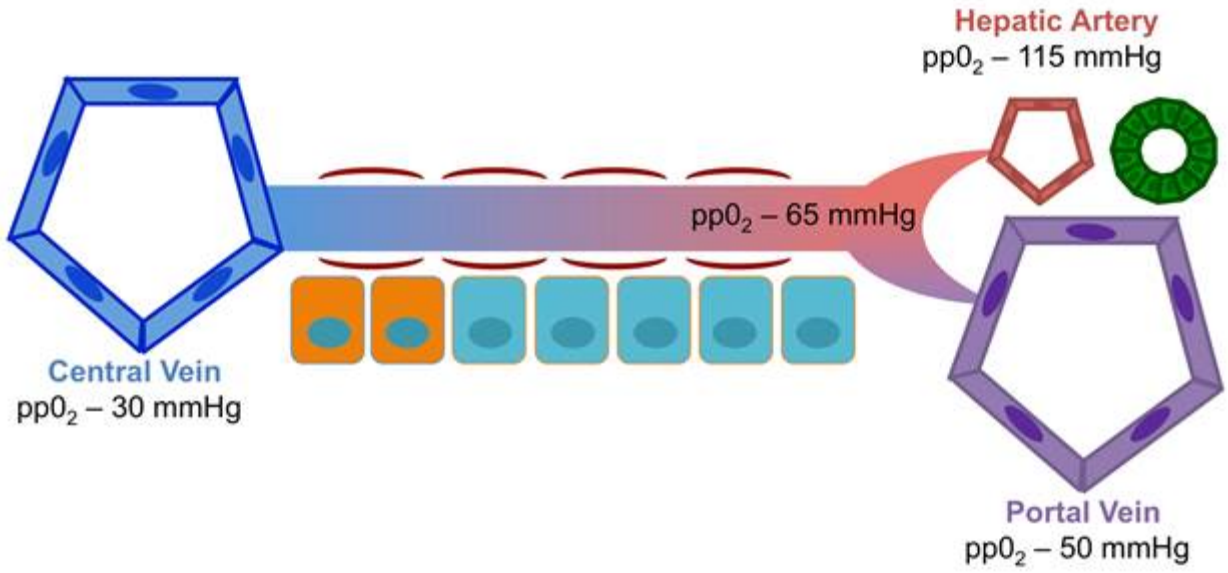

Figure 1.7. Oxygen tensions vary within the different vascular compartments of the liver. The highest oxygen tension is found within the HA, in which oxygen tension is about 115 mg Hg. In the PV, oxygen tensions are lower, around 50 mm Hg, and they are lower still, about 30 mm Hg in the CV. Within the sinusoids, there is a gradient in oxygen tension. In the periportal sinusoids, oxygen tension is around 65 mm Hg, while in the pericentral sinusoids, oxygen tension is about 30-35 mm Hg. Orange squares represent zone 3 pericentral hepatocytes, which are located near the CV, and turquoise squares represent zones 1 and 2 hepatocytes, located near the PV and in the intermediate spaces of the lobule.

IHBD development and architecture

The IHBD also has a hierarchical branching architecture that follows the branching pattern of the PV. This architectural relationship results from a developmental connection. The IHBD develops through a process called ductal plate morphogenesis. During mid-gestational liver development, the liver is comprised of bipotential hepatic progenitor cells, called hepatoblasts, which give rise to both hepatocytes and BECs. In the first step of IHBD morphogenesis, a single cell layer of hepatoblasts adjacent to the portal vein mesenchyme activate expression of BEC marker genes such as Sry-related HMG box 9 (Sox9) and wide spectrum cytokeratins (wsCK). After this, a second cell layer of hepatoblasts activates Sox9 and wsCK expression in the areas where IHBDs will form. The specified BECs then undergo a remodeling event during which the double cell layers become polarized and generate a lumen; the ductal plate cells that do not become incorporated into IHBDs regress, turning off the BEC markers, and become periportal hepatocytes (Figure 1.8) (Antoniou et al., 2009; Carpentier et al., 2011; Si-Tayeb et al., 2010). Due to this developmental connection, the architecture of the IHBD follows the pattern of the PV.

The smallest branches of the IHBD, called canaliculi, collect bile as is it secreted from hepatocytes and transport it into the peripheral branches of the IHBDs. The small peripheral IHBD branches merge into fewer, larger branches, until finally one single branch carries the bile out of the liver and transports it into the gallbladder for storage and ultimately into the intestine to aid in digestion. The IHBD relies on its highly regulated 3-dimensional structure to access all of the hepatocytes and effectively clear bile out of the liver. The process of IHBD architectural formation is a highly complex and regulated one, process of IHBD maturation and ductal plate

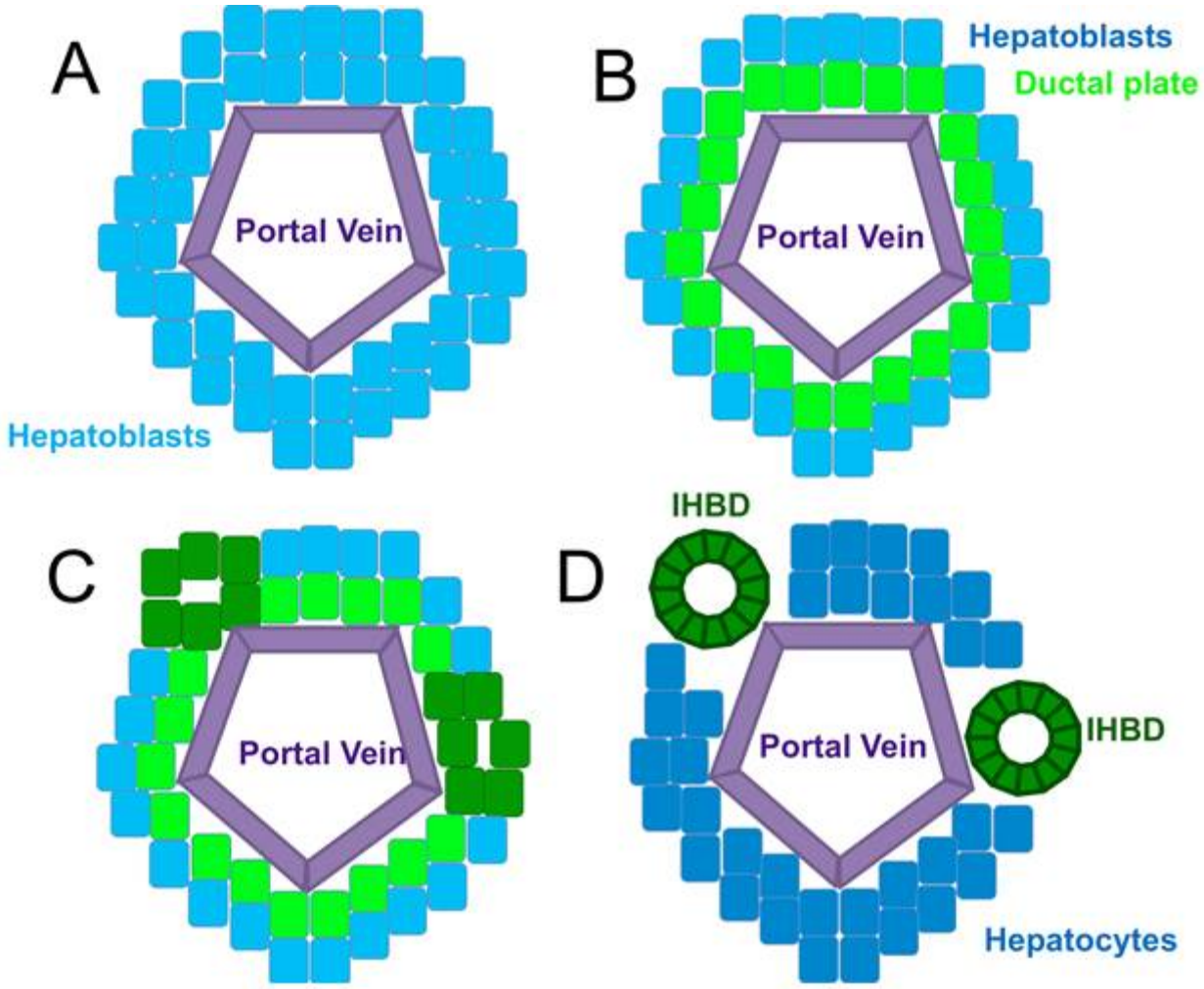

Figure 1.8. Ductal plate morphogenesis. The diagram represents the steps of ductal plate morphogenesis. This process occurs progressively along the proximal-distal axis of the liver. A. At the onset of ductal plate morphogenesis, the portal vein is surrounding by bipotential hepatoblasts. B. Starting around E13.5, the cells immediately adjacent to the portal vein become specified as BECs and activate BEC markers such as Sox9 and cytokeratin19. C. In certain locations around the PV, a second cell layer begins to activate BEC markers. In these locations, the ductal plate cells become polarized and form a lumen. D. The ductal plate double cell layers mature into functional IHBD branches, while the ductal plate cells not incorporated into IHBDs regress and differentiate into hepatocytes.

regression has to occur in a coordinated fashion along the 3-dimensional PV network to form a IHBD network that connects with the canaliculi supporting every hepatocyte within the liver.

Hepatocyte zonal organization

Approximately 15-25 hepatocytes span the distance between the portal and central veins in the rat liver, forming a series of hepatocyte plates that radiate between the central vein and the portal vein vertices (Colnot and Perret, 2011). Within the lobule, there is spatial organization of hepatocytes that is important for function. The hepatocytes collectively perform a wide variety of tasks, including gluconeogenesis, urea genesis, β-oxidation, and liponeogenesis (Bhatia et al., 1996). These functions are segregated between different subpopulations of hepatocytes that are organized into three spatial zones within the lobule: zone 1 is the periportal zone, zone 2 is the intermediate zone, and zone 3 is the pericentral zone (Figure 1.9).

Hepatocytes exhibit zonal heterogeneity in several ways, including gene expression and metabolic function, cell size, and oxygen pressure. Zone 1 hepatocytes specialize in gluconeogenesis and urea formation, while zone 3 hepatocytes specialize in liponeogenesis, glutamine synthesis, and glycolysis (Colnot and Perret, 2011). Accordingly, the expression of metabolic genes varies between the zones. For example, in rats and mice, one enzyme involved in urea synthesis, glutamine synthetase, is only expressed in the 1-2 cell layers of hepatocytes that immediately juxtapose the central veins. Cell morphologies also change zonally in the rat liver; periportal hepatocytes are smaller, approximately 7-15 μm in diameter, than pericentral hepatocytes, measuring approximately 30-40 μm (Bhatia et al., 1996).

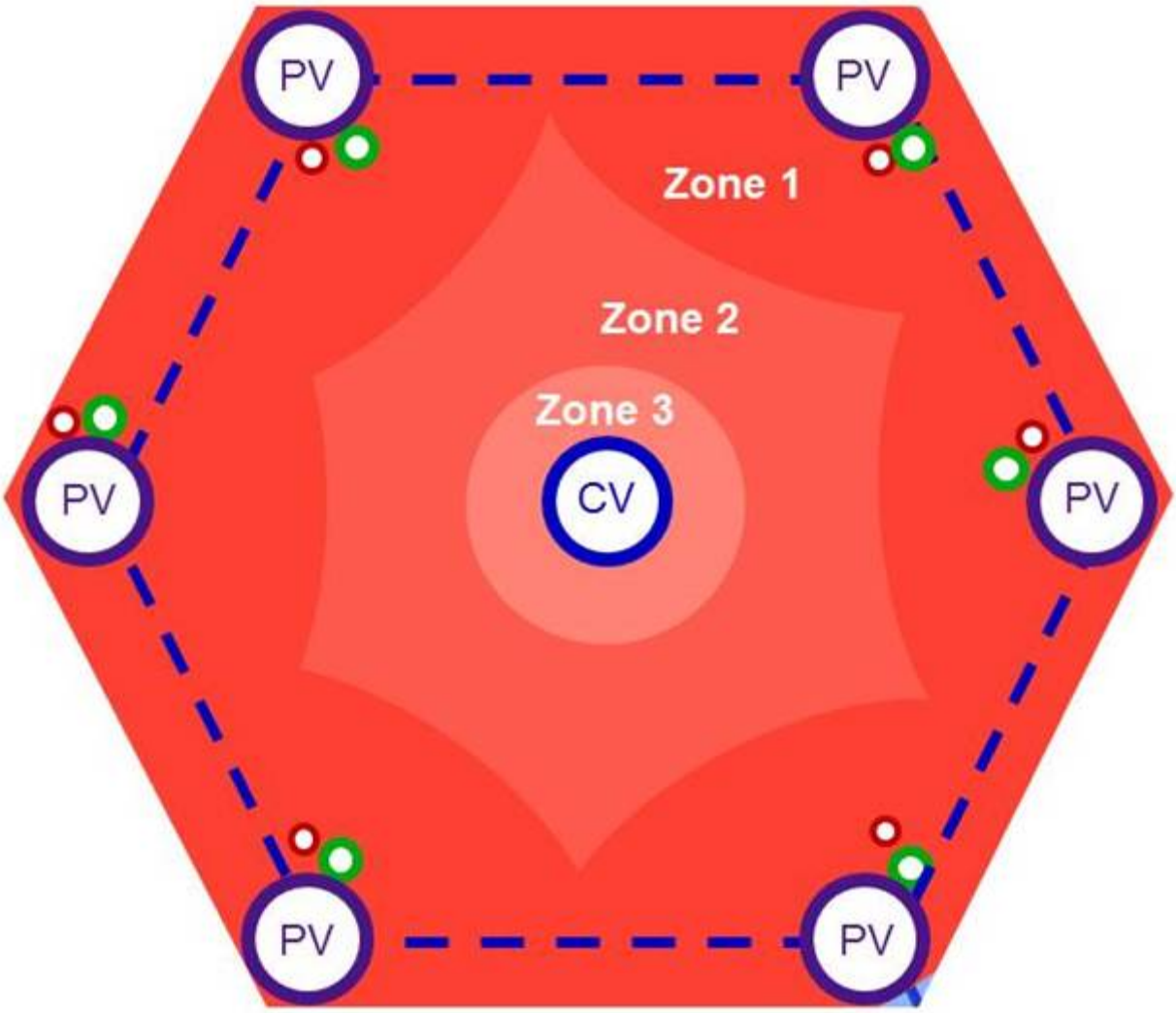

Figure 1.9. Hepatocyte zonation. Hepatocytes form three zones in the mouse and rat liver based on their differential metabolic functions and gene expression. Zone 1 consists of periportal hepatocytes closest to the PV(purple circles), zone 2 is intermediate hepatocytes, and zone 3 contains pericentral hepatocytes closest to the CV (blue cirle). Zones 1 and 2 are roughly equivalent sizes, while zone 3 is smaller, incorporating only 1-2 cell layers around the CV. The relative locations of IHBDs (green circles) and HAs (red circles) to the hepatocyte zones are shown.

Signaling in Hepatic Development and Cell Fate Decisions

Signaling pathways that drive hepatic specification and early development

At the first stage of hepatic specification, a combination of Fgf1 and Fgf2 signaling from the cardiac mesoderm and Bmp4 signaling from the STM, starting at E8.0-8.5, are crucial for the activation of liver specific gene expression in the pre-hepatic endoderm. (Gualdi et al., 1996; Jung et al., 1999; Rossi et al., 2001). After specification, the hepatic endoderm begins to express several important transcription factors, including Hepatocyte nuclear factor (Hnf)1α and β, Hnf4α, Hnf6, Forkhead homeobox (Fox)a1, Foxa2, Foxa3, Hex, Prox1, Gata4, and Gata6 (Kaestner, 2005). The Foxa gene group is redundantly required for liver specification; knocking out Foxa1 and Foxa2 together in the endoderm results in the inability to specify the liver primordium (Lee et al., 2005). Mutations in the transcription factors Hex, Hnf4α, Hnf1β, Hnf6, Prox1, Gata4, and Gata6 result in liver developmental abnormalities that occur after liver specification (Bort et al., 2006; Clotman et al., 2002; Coffinier et al., 2002; Kaestner, 2005; Parviz et al., 2003; Sosa-Pineda et al., 2000; Watt et al., 2007; Zhao et al., 2005). The abnormalities occur at different stages in hepatic development. Alterations in Gata6 or Hex result in abnormalities early in liver bud specification; Gata6 mutants fail to express the liver gene Albumin and Hex mutant liver buds fail to transition from a columnar epithelium to a pseudostratified epithelium. Gata4 and Prox1 mutants have abnormalities slightly later in development, as they activate expression of liver bud genes and transition to a pseudostratified epithelium, but do not invade the STM. Mutations in Hnf4α, Hnf1β, and Hnf6 occur later in liver development and affect liver cell maturation and architecture. Hnf4α mutants display problems in hepatocyte maturation and epithelium formation, while Hnf6 and Hnf1β mutants fail to organize IHBD structures. Together, these genetic manipulations reveal several crucial steps in hepatogenesis where precise signaling and gene expression is required for development.

Signaling pathways driving IHBD morphogenesis

The primary pathway that has been implicated in IHBD morphogenesis is Notch signaling. Notch is a conserved signaling pathway that plays a role in cell fate decisions in several organs and timepoints during development. Notch signaling has known roles in stem cell maintenance, cell fate decisions, proliferation, and tissue patterning (Andersson et al., 2011). In mammals, there are five canonical Notch ligands across two families (Delta1, 3, and 4, and Jagged1 and 2) and four Notch receptors (Notch1, 2, 3, and 4). Notch ligands and receptors are both membrane bound and participate in juxtacrine signaling between adjacent cells. Upon binding between a Notch ligand and receptor, a conformational change in Notch allows a proteolytic cleavage by γ-secretase, releasing the Notch intracellular domain (NICD) from the cell membrane. NICD translocates to the nucleus, where it interacts with the DNA-binding co-factor Rbpj (also known as CSL) and initiates the transcription of Notch-responsive genes (Andersson et al., 2011). Rbpj is required for canonical Notch signaling via all four Notch receptors.

Ductal plate morphogenesis begins at E13.5, at which time the mesenchymal cells surrounding the PV express the Notch ligand Jagged1. Jagged1 interacts with the fundamental Notch2 receptor expressed on bipotential hepatoblasts surrounding the portal vein to activate Notch signaling (Hofmann et al., 2010). Notch signaling is required for remodeling of the specified BECs into mature, lumenal IHBDs and the expression of a constitutively activated form of Notch2 or Notch1 is sufficient to promote BEC differentiation (Geisler et al., 2008; Hofmann et al., 2010; Jeliazkova et al., 2013; Lozier et al., 2008a; McCright et al., 2002; Sparks et al., 2010; Tanimizu and Miyajima, 2004). Ductal plates are first observed in the proximal hilar regions of the liver and appear in the more distal regions progressively following the PV during embryonic and early postnatal development.

In addition to Notch signaling, the transcription factors Sox9, Hnf1β, and Hnf6 are important for biliary morphogenesis; without each of these genes, delays or disruptions in biliary development are observed in mice (Antoniou et al., 2009; Clotman et al., 2002; Coffinier et al., 2002). It is likely that Notch acts upstream of Sox9 during biliary morphogenesis, as Sox9 is a known target of Notch signaling in several organs (Chen et al., 2012; Haller et al., 2012; Muto et al., 2009). Sox9 has also been found to be regulated by HIF signaling; however, this association not been examined in the liver (Zhang et al., 2011). Additionally, Hnf6 and Hnf1β are known to function in the same pathway, as Hnf6 can regulate the expression of Hnf1β (Clotman et al., 2002).

Signaling pathways controlling vascular morphogenesis

The main pathway implicated in regulating vascular morphogenesis is vascular endothelial growth factor (VEGF) signaling. VEGF is a crucial signaling pathway governing vascular development and behavior throughout the body. In mammals, there is one principal VEGF ligand and two principal receptors, VEGF receptor 1 (VEGFR1, also known as Flt1) and VEGFR2 (also known as KDR and Flk1) (Ferrara and Davis-Smyth, 1997). Related molecules include the ligands VEGF-B, VEGF-C, and placental growth factor and the receptor VEGFR3 (also known as Flt4) (Ferrara and Davis-Smyth, 1997). The VEGF signaling pathway is essential during development, as mice with a homozygous gene deletion for either VEGFR1 or VEGFR2, as well as mice with either a homozygous or heterozygous deletion for VEGF, are embryonic lethal due to impaired or altered vascular development and failed blood-island formation (Carmeliet et al., 1996; Ferrara et al., 1996; Fong et al., 1995; Shalaby et al., 1995).

VEGF has several known functions in vascular development and homeostasis, including in angiogenic directional growth and branching behavior, vascular permeability, endothelial

fenestration, endothelial proliferation, and endothelial cell survival (Carpenter et al., 2005; Connolly et al., 1989; Gerber et al., 2002; Gerhardt et al., 2003; Krueger et al., 2011; Lee et al., 2007; Leung et al., 2013).

Angiogenesis is the process of vascular development by which new vessels are generated and grow by sprouting off of an existing vessel and extending directionally. The directionality of the angiogenic growth is directed by the graded concentration of VEGF protein. During angiogenesis ECs in the growing vessel can take on one of two identities: tip or stalk (Phng and Gerhardt, 2009). Tip cells are located at the tips of growing blood vessels and display filopodial extensions. Tip cells are responsible for pathfinding and directionality. Stalk cells are all cells of the new vessel that trail behind the tip cell. These cells form a luminal structure and perform the proliferation required for vessel extension and growth.

Tip and stalk cells engage in lateral inhibition through VEGF and Notch signaling. Both tip and stalk cells express VEGFR2. Upon exposure to VEGF protein, VEGFR2 is activated, leading to the upreguation of the Notch ligand Delta-like4 (Dll4) and, in a positive feedback loop, VEGFR2 (Phng and Gerhardt, 2009). Dll4 interacts with and activates Notch receptors expressed on surrounding cells. The activation of Notch inhibits the expression of VEGFR2 and upregulates VEGFR1, making the Notch-activated cell less sensitive to VEGF protein (Figure 1.10) (Phng and Gerhardt, 2009). Through these feedback loops, one cell adopts the tip cell identity while the surrounding cells are designated as stalk cells. The functions of Notch and VEGF in the tip/stalk designation have recently been defined in detail in several papers, mainly using the cultured mouse retina as a model system (Benedito et al., 2009; Gerhardt et al., 2003; Hellström et al., 2007; Lobov et al., 2007; Suchting et al., 2007; Trindade et al., 2008).

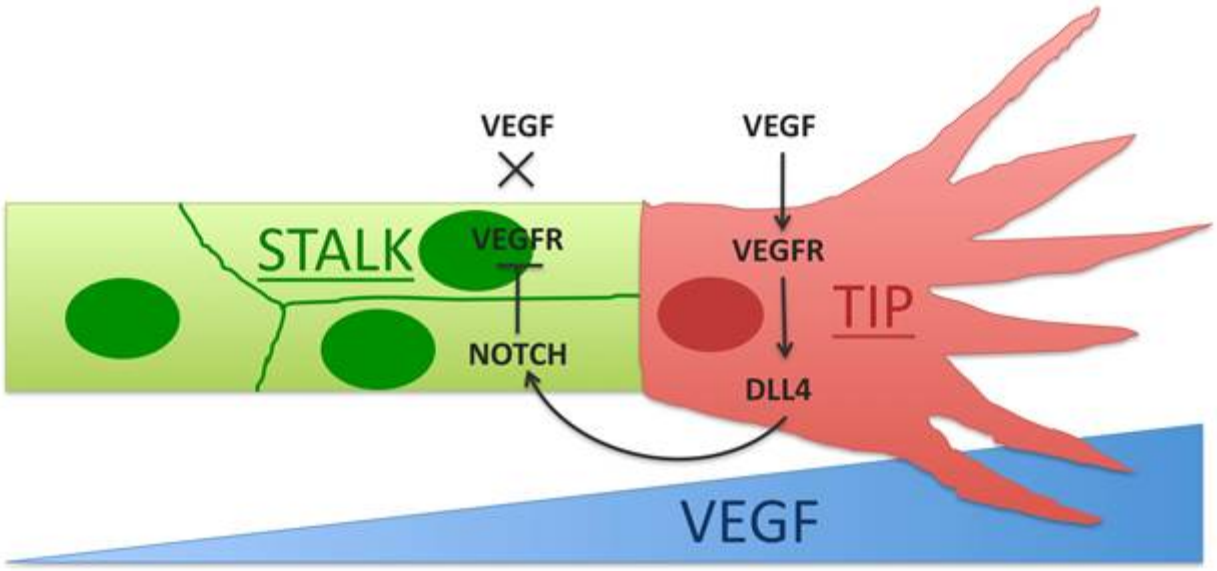

Figure 1.10. Notch and VEGF signaling collaborate to specify tip and stalk cells during angiogenesis. Angiogenic growth is directed by a gradient of VEGF protein (blue). The tip cell (red) expresses VEGF receptor (VEGFR), allowing it to respond to VEGF protein. Activation of VEGFR causes the upregulation of Dll4 and VEGFR in the tip cell. Dll4 signals to activate Notch in stalk cells (green). The activation of Notch causes the downregulation of VEGFR, making the stalk cells less responsive to environmental VEGF protein. Together, Notch and VEGF generate positive feedback loops that reinforce the separate tip and stalk cell identities.

VEGF expression and consequent angiogenesis is often promoted by hypoxia. Under hypoxic conditions, cells stabilize the hypoxia inducible factor1α (HIF1α) protein, and the HIF1α/β heterodimer binds enhancer sequences of the *Vegf* gene, stimulating the production of VEGF protein (Hoeben et al., 2004). Secretion of VEGF protein from a region of hypoxic tissue directs angiogenesis towards that area, ultimately increasing blood flow to alleviate the hypoxic condition.

There is relatively little known about the signaling pathways that regulate the development of vasculature in the liver. A limited number of studies have confirmed that VEGF and Notch signaling do influence liver vasculature (Carlson et al., 2005; Carpenter et al., 2005; Gerber et al., 2002). However, these studies to date have been unable, due to their experimental systems, to address the question of whether the different vascular tissues in the liver form through angiogenesis and whether Notch and VEGF are involved in liver vascular development in the same way as they are in other organs.

Several studies have analyzed the role of VEGF signaling in the maintenance of LSECs. These studies have consistently found that LSECs require VEGF signaling in order to maintain several unique LSEC features, including fenestration, scavenger function, lack of platelet cell-derived endothelial cell adhesion molecule (PECAM) expression, and lack of an organized basement membrane (DeLeve et al., 2004). The majority of these studies were performed on cultured primary LSECs. Primary LSECs lose their identity and unique features within a few days in culture unless they are either treated with exogenous VEGF or co-cultured with another liver cell type, including either hepatocytes or stellate cells, that produces VEGF (DeLeve et al., 2004). Another known role of VEGF in the liver is to regulate the expression of erythropoietin in hepatocytes (Tam et al., 2006).

Signals controlling lobular hepatocyte zonation

Within the liver, the main factor implicated in the establishment and maintenance of hepatocyte zonation is Wnt/β-catenin signaling. β-catenin stabilization is both necessary and sufficient for expression of the pericentral enzyme glutamine synthetase (GS) *in vivo* in the mouse liver (Colnot and Perret, 2011). In a normal liver, stabilized β-catenin is observed only in the pericentral hepatocytes. In a liver-specific β-catenin knockout mouse model, the expression of GS is completely absent from the liver. Contrastingly, the liver-specific knockout of Apc, a negative regulator of β-catenin stabilization, activates the expression of GS in all hepatocytes in the liver (Benhamouche et al., 2006; Colnot and Perret, 2011). β-catenin expression in pericentral hepatocytes is dependent on Wnt signaling (Benhamouche et al., 2006). The expression of Wnt liagands has been found in several liver cell types, including: hepatocytes, BECs, LSECs, stellate cells (pericytes in the liver sinusoids), and Kupffer cells (resident macrophages in the liver) (Zeng et al., 2007). At this time, it remains unknown which Wnt proteins, secreted from which cells in the liver, are responsible for establishing and maintaining hepatocyte zonation. It has been hypothesized, although without any concrete evidence, that Wnt signaling in the pericentral zone is directed by LSECs (Colnot and Perret, 2011).

Another key molecule mediating hepatic zonation is Hnf4α. Hnf4α opposes Wnt signaling to promote the expression of periportal hepatocyte genes and inhibit the expression of pericentral hepatocyte genes (Colletti et al., 2009). In the liver deficient for Hnf4α, the expression of pericentral hepatocyte genes, including GS, is expanded into the periportal zone (Stanulović et al., 2007). There is evidence that Hnf4α and β-catenin, along with its DNA-binding co-factors Tcf/Lef, directly compete for binding on the same consensus motifs on the enhancer regions of zonal hepatocyte genes (Colletti et al., 2009; Colnot and Perret, 2011).

Finally, the last recognized factor in regulating hepatic zonation is oxygen pressure. As previously described, the oxygen pressure both in the sinusoids and in the hepatocytes is graded along the axis of the hepatic lobule between the PV and the CV. There is evidence that hepatocytes are able to sense oxygen tension through a non-respiratory chain ferro-heme protein, which reveals a potential pathway for oxygen to regulate hepatocyte zonal gene expression (Kietzmann et al., 1992; Kietzmann et al., 1993). In cultured primary rat hepatocytes, oxygen tensions influence the gene expression of some zonal genes, including the periportal gene phosphoenolpyruvate carboxykinase (PEPCK, involved in gluconeogenesis) and the pericentral gene glucokinase (GK, involved in glycolysis) (Jungermann and Keitzmann, 1996; WÖLfle and Jungermann, 1985). However, it appears that only certain classes of zonal hepatocyte genes are sensitive to oxygen tension. Genes involved in glucose and drug metabolism are more readily influenced by blood flow and oxygen tension, while genes involved in ammonia detoxification and glutamine synthesis have a more stable and defined expression pattern in the face of oxygenation manipulations (Allen and Bhatia, 2003; Bhatia et al., 1996; Colnot and Perret, 2011; Jungermann and Kietzmann, 1997; Wagenaar et al., 1993; Wagenaar et al., 1994). While it appears clear that oxygen pressure can influence hepatocyte zonation, in *in vivo* mechanism through which the regulation occurs and the importance of oxygen pressure during developmental zone establishment and homeostasis remain unknown.

Cell Plasticity in Injury

Reactivation of developmental pathways in regeneration

Often times, the signaling pathways and mechanisms that control embryonic cell fates and tissue architecture retain function during adult homeostasis and are re-activated during organ

regeneration. In the liver, several signaling pathways with known roles during hepatogenesis, including VEGF, Notch, Wnt, and Sox9, have roles during injury and regeneration as well.

Very recently, Sox9 has been under investigation for its role in marking liver progenitor cells. This examination began in large part with a publication claiming that Sox9-expressing cells constitute a bipotential liver progenitor, giving rise to both hepatocytes and cholangiocytes under injury and regeneration conditions as well as over time during the normal homeostatic process (Furuyama et al., 2010). This paper was widely recognized in the liver field, where the identity of the "hepatic stem cell" has been an elusive object of investigation and controversy. A following study refuted some of the findings presented by Furuyama et al. (2010), but added evidence that a Sox9-expressing progenitor present during embryonic development did give rise to a bipotential liver progenitor cell that had potential to differentiate into both hepatoctyes and BECs during regeneration (Carpentier et al., 2011).

Sox9 has also gained the interest of many researchers due to recent findings that Sox9 is highly expressed in a population of liver cells that have bipotential differentiation capability *in vitro* (Dorrell et al., 2011). The implications of Sox9 playing a role in, or at least marking cells that are capable of, multi-lineage differentiation is of interest because Sox9-expressing "hepatobiliary intermediate cells," expressing lineage markers of both hepatocytes and BECs, have been found in human liver disease (Yanger et al., 2013). Also of interest, Sox9 has been implicated as a marker of hepatocyte-to-BEC conversion during liver injury in mice, suggesting that some components of the ductal plate differentiation program may be utilized for the generation of new BECs in injured livers of adult mice (Yanger et al., 2013). If Sox9 does denote a hepatic progenitor population or play a role in hepatic cell plasticity, the protein would be of high interest for future studies on *in vivo* cell-based therapies for liver disease.

In many organs, Sox9 is regulated downstream of Notch signaling (Chen et al., 2012; Haller et al., 2012; Hardingham et al., 2006; Muto et al., 2009). In the liver, Sox9 it is a direct target of Notch signaling in the ductal plate (Zong et al., 2009). During liver injury in adult mice, disrupting Notch signaling is demonstrated to reduce the expression of Sox9 in hepatocytes and to consequently restrict the process of hepatocyte-to-BEC conversion, confirming the link between Notch signaling and Sox9 in cell lineage decisions and plasticity in both the embryonic and adult liver (Yanger et al., 2013).

Endothelial-epithelial interactions in disease and regeneration

Several epithelial-endothelial interactions have been observed during injury and regeneration in the liver. The connection between epithelial and endothelial tissues in disease is elucidated by the vascular phenotypes observed in human liver diseases of malformed IHBDs. In diseases where the ductal plate does not remodel, resulting in IHBD abnormalities (such as autosomal dominant polycystic kidney disease and Caroli's disease), BECs express abnormally high VEGF and the microvasculature around the IHBD is expanded and very dense (Fabris et al., 2006). In some patients with IHBD malformations, unremodeled ductal plates are frequently associated with abnormal "Pollard willow" branching patterns of the portal vein, in which the portal veins develop too many branches that are too small and too densely spaced (Desmet, 1992). These human studies provide evidence that the epithelial and endothelial tissues can affect each other in a disease circumstance. In addition to being altered in genetic diseases, VEGF also appears to mediate epithelial-endothelial interactions in situations of acute liver injury and regeneration. VEGF expression from both hepatocytes and non-parenchymal cells is upregulated after necrosis in the rat liver. In this case, it is proposed that this VEGF promotes liver regeneration by promoting vascular endothelial cell and LSEC proliferation (Ishikawa et al., 1999). A hepatocyte-endothelial signaling loop is also proposed to enhance regeneration after partial

hepatectomy; VEGF secreted by the hepatocytes promotes the proliferation of ECs and the revascularization of the growing liver tissues, while the ECs in turn produce hepatocyte growth factor (HGF), which stimulates hepatocyte proliferation and demonstrate the VEGF is an important mediator of epithelial-endothelial interactions (Bockhorn et al., 2007; Ding et al., 2010; Oe et al., 2004; Shimizu et al., 2005; Shimizu et al., 2001; Taniguchi et al., 2001; Yamamoto et al., 2010).

Increases in VEGF signaling are also observed in rodent experimental models of acetaminophen hepatotoxicity, bile duct ligation, polycystic kidney disease, and biliary cirrhosis (Gaudio et al., 2006; Kato et al., 2011; Ren et al., 2011; Rosmorduc et al., 1999; Tanaka et al., 2007). In these studies, VEGF expression was found in the hepatocytes and BECs. Together, these studies indicate a characteristic collaboration between epithelial and endothelial lineage during regeneration.

Ductular reactions in liver injury

A frequent manifestation of liver disease is the presence of a ductular reaction (Desmet, 2011; Desmet et al., 1995; Gouw et al., 2011). Ductular reactions are comprised of semi-polarized proliferative BECs that expand outside of the portal triad into the hepatic parenchyma. Ductular reactions are seen both in human liver disease and in rodent models of liver injury. The BECs that comprise the ductual reaction are sometimes referred to as “oval cells” due to their cell shape. It remains unclear if the ductular reaction is merely a byproduct of liver injury or if the structure serves some function, either negative or positive, during the injury and regeneration process.

Studies have demonstrated that Notch signaling plays a role in the generation of the ductular reaction in rats and in mice, as inhibiting Notch signaling can reduce or delay the formation of the ductular reaction (Darwiche et al., 2011; Fiorotto et al., 2013). Notch2 is also sufficient to direct biliary differentiation in adult hepatocytes and generating ductual reactions (Jeliazkova et al., 2013).

In addition to Notch, Wnt signaling has also been examined for its role in directing cell fate decisions in the regenerating adult rodent liver. Current thinking suggests that Notch and Wnt may have opposing roles in directing cell fate decisions during liver regeneration, with Notch promoting BEC specification and Wnt promoting hepatocyte fates (Boulter et al., 2012; Strazzabosco and Fabris, 2013). These data suggest that Notch signaling retains its ability to direct BEC specification in the adult liver, and that Notch is involved in the response to injury and generation of reactive ductules.

In an interesting study, the hepatic progenitor cells (HPCs, referring to the BECs of the reactive ductules) in a variety of acute and chronic human liver diseases were analyzed to see whether they had activated Notch and/or Wnt signaling (Spee et al., 2010). The diseases analyzed were classified as either parenchymal (injuring the hepatocytes) or biliary diseases. This study found a strong activation of Wnt signaling in the HPCs arising in acute necrotizing hepatitis, a parenchymal disease, but a high activation of Notch in the HPCs present in the biliary disease primary biliary cirrhosis (PBC). These data support the idea that Notch and Wnt oppose each other to promote biliary and hepatic cell fates, respectively, and also supports the idea that different regenerative responses occur in the liver depending on the mechanism (including which cells and tissues are affected) and extent of injury. Together, the findings in humans and mice indicate that cell therapies targeting cell populations and signaling pathways may be differentially effective in the context of different liver diseases.

Hepatocyte and BEC inter-lineage conversion

The study of signaling pathways during liver regeneration is aimed at answering the base questions: what progenitor populations exist in the liver, and how can we activate them to promote liver regeneration? As previously described, recent studies have discovered that there is a high degree of cell plasticity in the adult liver and that Notch signaling plays a role in the ability of seemingly differentiated cell types to adopt a different cell fate (Jeliazkova et al., 2013; Yanger et al., 2013). The concept of hepatocyte-to-BEC conversion had previously been suggested by expression studies and demonstrated by transplantation experiments to occur during liver injury in a rat model (Limaye et al., 2010; Limaye et al., 2008b; Michalopoulos et al., 2005; Michalopoulos et al., 2002).

To further explore the potential of differentiated hepatocytes and BECs to undergo lineage conversion, several groups have recently performed lineage tracing studies whereby they indelibly label either hepatocytes or BECs in mice and then injure the liver through several common chemical and surgical liver injury models. These studies are intended to demonstrate whether a cell with bipotential progenitor or interlineage conversion capacities reside within either the hepatocyte or BEC lineage and is activated by the injury model.

Thus far, some of these lineage tracing studies have yielded conflicting results (Español-Suñer et al., 2012; Malato et al., 2011; Yanger et al., 2013). Despite the specific discords between the studies (Table 1.1), it appears as though there is at least the potential that interlineage conversion from hepatocyte-to-BEC and BEC-to-hepatocyte can occur in specific injury situations.

Reference	Lineage tracing model	Injury	Result
Malato et al. (2011)	AAV8-Ttr-Cre *Hepatocyte lineage tracing*	Homeostasis	All hepatocytes labeled
		Acute CCl4	All hepatocytes labeled
		Chronic CCl_4	1.3% hepatocytes not labeled
		2/3 PHx	1.4% hepatocytes not labeled
		BDL	No labeled BECs; some unlabeled hepatocytes
		DDC	No labeled BECs; some unlabeled hepatocytes
Español-Suñer et al. (2012)	Osteopontin-CreER *BEC lineage tracing*	Homeostasis	0.006% hepatocytes labeled
		CCl_4	0.038% hepatocytes labeled
		2/3 PHx	0 hepaocytes labeled
		CDE	2.45% hepatocytes labeled
		DDC	0 hepatocytes labeled
Yanger et al. (2013)	AAV8-TBG-Cre and AAV8-CMV-Cre *Hepatocyte lineage tracing*	PHx	0.0% BECs labeled
		BDL	2.0% BECs labeled
		DDC	14.3% BECs labeled

Table 1.1. Summary of recent studies on hepatocyte or BEC lineage tracing during injury

Oncogenic implications of cell plasticity and intercellular signaling

While cell plasticity has an obvious therapeutic importance for liver regeneration, the flexibility in cell lineages and the retained proliferative ability of hepatocytes and cholangiocytes can also yield negative consequences in disease situations, most notably cancer. The signaling pathways Notch and Wnt, as previously explained, contribute to cell fate decisions, but both pathways also have roles in cancer progression in the liver.

Recent findings have demonstrated that the overexpression of Notch signaling in hepatocytes can promote to both hepatocyte-to-BEC conversion and to cellular proliferation, ultimately contributing to the development of cholangiocarcinoma in a mouse model (Fan et al., 2012; Sekiya and Suzuki, 2012). In mice, overexpression of Notch2 increases proliferation and promotes tumor progression in both hepatocytes and BECs (Dill et al., 2013). Studies analyzing the expression of Notch in human hepatocellular carcinoma (HCC) have found conflicting results on the role of Notch in HCC; while some studies suggest that Notch signaling can actually play a pro-differentiation role in hepatocellular carcinoma and function to suppress hepatocellular carcinoma (Wang et al., 2009; Yao and Mishra, 2009), others find correlations between Notch expression and tumor size, tumor grade, and poor prognosis (Ahn S, 2013; Zhou et al., 2013).

In addition to Notch, Wnt/β-catenin signaling also has oncogenic potential in the liver (Moeini et al., 2012). Nuclear β-catenin is frequently found in hepatocellular carcinoma and correlates with tumor grade (Wang et al., 2009). Interestingly, one study analyzing human hepatocellular carcinomas found a negative correlation between β-catenin expression and Notch1/Jagged1 expression, where tumor grade was positively correlated with β-catenin expression but

negatively correlated with Jagged1/Notch1 expression (Wang et al., 2009). This finding may indicate that the Wnt/Notch duality that governs cell fates during liver regeneration may also dictate hepatocellular carcinoma tumor types and differentiation status, ultimately influencing tumor progression. These findings indicate that a very careful control of Notch and Wnt is required within the liver to balance the potential positive effects in regeneration and avoid oncogenic effects.

Like Notch, the misregulation of VEGF signaling can also be pathogenic in the context of liver injury, especially cancer. VEGF expression is upregulated in hepatocellular carcinoma and is correlated with tumor size (Kwon et al., 2012; Marschall et al., 2001; Moon et al., 2003). The VEGF-mediated neovascularization of hepatocellular carcinoma may reflect a negative manifestation of a developmental epithelial-endothelial signaling interaction. In another example of a signaling pathway that can both promote regeneration and fuel tumor growth, we see that a precise understanding of signaling between tissues, specifically mediated by VEGF, will be important for the understanding of liver homeostasis and regeneration and for the future exploration of *in vivo* therapies for liver disease.

Cell plasticity and the associated signaling pathways that influence cell fate changes have both an exciting potential for therapeutic applications and potential negative consequences in disrupting normal organ behavior and promoting disease. A thorough understanding of the process of cell fate regulation and the involvement of pathways such as Notch and VEGF will be important in order to understand normal development and physiology, disease, and regeneration.

Aims of the Dissertation

It is clear that the regulation of cell fates and architecture in the liver are crucial for proper liver development, function, and regeneration.

This dissertation intends to focus on the role of inter- and intracellular signaling in directing cell fate decisions and architectural establishment during hepatic development and regeneration in response to injury.

First, I will investigate the requirement for Notch signaling in the regeneration of the three-dimensional IHBD network in a genetic model of IHBD paucity and the rule of Sox9 in the regenerative process (Please refer to Chapter 3). Next, I will explore the mechanism of regeneration in regard to Sox9 expression in a variety of liver injuries and diseases, both human and rodent models (Please refer to Chapter 4). Finally, I will examine the role of epithelial VEGF signaling in directing vascular cell identities and architecture during liver development and the effects of vascular manipulation on hepatocyte zonal identity.

In summary, this dissertation will address the role of Notch signaling, VEGF signaling, and Sox9 in directing the architecture of the IHBD, vasculature, and hepatic lobule, and in directing the cell fates and identities of vascular and epithelial cells during development and regeneration.

CHAPTER 2

MATERIALS AND METHODS

Mouse Lines

Double Knockout (DKO) Mice

DKO mice were generated by crossing *Tg(Alb-cre)*^{21Mgn} (*Albumin-Cre*)(Postic and Magnuson, 2000), *Rbpj*^{tm1Hon} (*Rbp*^{flox}) (Han et al., 2002), and *Onecut1*$^{tm1.1Mga}$ (*Hnf6*^{flox}) (Zhang et al., 2009) mouse lines.

VEGF Knockout (VKO) Mice

VEGF-knockout (VKO) mice were generated by crossing *Albumin-Cre* (Postic et al., 2000) and *Vegfa*^{tm2Gne} (Gerber et al., 1999) mouse lines to generate *Albumin-Cre;VEGF*$^{flox/flox}$ mice.

Genotyping

Mouse genotypes were confirmed by polymerase chain reaction using previously established primer pairs.

Animal Care and Use

All breeding and experimental procedures were performed with approval from the Institutional Animal Care and Use Committees at Vanderbilt University Medical Center, Cincinnati Children's

Hospital, University of Pittsburgh Medical Center, and Washington University School of Medicine.

Livery Injury Models

DDC Feeding

Adult mice were fed a diet of chow supplemented with 0.1% 3,5-diethoxycarbonyl-1,4-dihydrocollidine (DDC) (Bio-Serve, Frenchtown, NJ) for a maximum of 4 weeks. Control littermate mice were kept on normal chow without DDC.

Partial Hepatectomy (PHx)

Adult 8-12 week old male mice on a mixed genetic background (C57Bl/6-6x129) were subjected to 2/3 partial hepatectomy (PHx) and allowed to recover for 12 hours, 24 hours, 36 hours, 3 days, 7 days, or 14 days. Control mice were subjected to a sham surgery. Surgeries were performed as previously described(Shteyer et al., 2004).

2-AAF/PHx

Male Fisher rats were received an intraperitoneal implantation of a 70mg (28-day slow release) 2-acetylaminofluorene (2-AAF) tablet. 7 days after tablet implantation, rats were subjected to 2/3 PHx. Control rats received a sham surgery. Implantations and surgeries were performed as previously described(Apte et al., 2008; Petersen et al., 1998).

Bile Duct Ligation (BDL)

Adult 4-6 week old female mice on a mixed genetic background (C57Bl/6-6-SJL-Swiss Black) were subjected to bile duct ligation (BDL) and allowed to recover for 1, 7, 14, or 21 days. Control mice were subjected to a sham surgery. Surgeries were performed as previously described(Campbell et al., 2004).

Rhesus Rotavirus (RRV) Injection

Postnatal day 1 (P1) Balb/c mice were injected with Rhesus rotavirus (RRV). Mice were analyzed 14 days after injection. Control littermate mice were injected with saline. Injections were performed as previously described(Mohanty et al., 2006).

Human Tissue Samples

De-identified formalin-fixed, paraffin-embedded human tissue samples from patients with Alagille syndrome (ALGS), primary biliary cirrhosis (PBC), primary sclerosing cholangitis (PSC), or biliary atresia (BA) were obtained from the pathology archives of Vanderbilt University Medical Center by Dr. Kay Washington (IRB protocol 010294, Tennessee Valley Cooperative Human Tissue Network). Research on human tissue samples was performed at Vanderbilt in accordance with Vanderbilt University Institutional Review Board (120649-SSH; 120047-ALM) and conforms to the ethical guidelines of the 1975 Declaration of Helsinki.

Serum Chemistry

Blood was collected from postmortem mice and tested for serum total bilirubin (TecoDiagnostics, Anaheim, CA), total bile acids (Diazyme, Poway, CA), and alanine aminotransferase (TecoDiagnostics, Anaheim, CA).

Immunohistochemistry and Immunofluorescence

Paraffin-Embedded Tissue

Murine liver tissue was fixed overnight at 4°C in 4% paraformaldehyde, processed and embedded in paraffin. Sodium citrate pH6 antigen retrieval was performed in heat and high pressure for 15 minutes. Sections were incubated in 1° antibody overnight at 4°C and 2° antibody for 2 hours at room temperature in 1% bovine serum albumin in phosphate-buffered saline. Sections were cut at 6 μm. Antibodies and reagents are listed in Table 2.1. Mayer's hematoxylin or bisbenzimide were used as counterstains.

Frozen-Embedded Tissue

Murine liver tissue was either fixed overnight at 4°C in 4% paraformaldehyde, washed in PBS, and equilibrated in sucrose, or was put directly into sucrose without fixation. Equilibrated tissues were embedded in OCT (Tissue-Tek, Torrence, CA). Sections were cut at 10 μm. Unfixed frozen tissue was fixed for 5 minutes in acetone after sectioning. Sections were incubated in 1° antibody overnight at 4°C and 2° antibody for 2 hours at room temperature in 1% bovine serum albumin in phosphate-buffered saline. Sections were cute at 6 μm. Antibodies and reagents are

Table 2.1: Antibodies and reagents used for immunohistochemistry

A.

Primary antibodies used for IHC					
Antigen	Retrieval	Dilution	Host	Company	Amplification
CK19 (TromaIII)	Na citrate	1:200	rat	DSHB	ABC; DAB (chromogenic)
CK19	Na citrate	1:200	mouse	Dako	ABC; TSA-FITC
CPS1	Na citrate	1:500	rabbit	Abcam	
Cytokeratin, wide spectrum	Na citrate	1:300	rabbit	Dako	
DBA-biotin	Na citrate	1:500		Vector	
EYFP (GFP)	Na citrate	1:500	rabbit	Novus	
Endomucin	Na citrate	1:200	goat	R&D	
Glutamine synthetase	Na citrate	1:1000	mouse	BD Transduction	
HepPar1	Na citrate	1:500	mouse	Dako	ABC; TSA-FITC
Hnf1	Na citrate	1:500	rabbit	From Joo-Seop Park	
HNF1β	Na citrate	1:2000	goat	Santa Cruz	ABC; TSA-FITC
HNF4α	Na citrate	1:1000	goat	Santa Cruz	ABC; TSA-FITC
HNF6	Na citrate	1:200	rabbit	Santa Cruz	ABC; TSA-FITC
Hypoxyprobe	Na citrate	1:100	mouse	NPI	Vector Blue
IsolectinB4-biotin	Na citrate	1:100		Sigma	ABC; DAB
Ki67	Na citrate	1:200	mouse	BD Pharmingen	
Ki67	Na citrate	1:200	rabbit	Thermo Neomarkers	
PECAM (CD31)	Na citrate	1:100	rat	BD Pharmingen	
RBPJ-κ (T6709)	AUS H3300	1:100	rat	CosmoBio	ABC; TSA-Biotin; TSA-FITC
Sox9	Na citrate	1:500	rabbit	Millipore	
VEGF	Na citrate	1:100	rabbit	Abcam	

B.

Secondary Antibodies used for IHC					
Antibody		Dilution	Host	Company	
α rabbit-biotin		1:500	donkey	Jackson ImmunoResearch	
α rabbit-cy3		1:300	donkey	Jackson ImmunoResearch	
α rat-Alexa488		1:300	donkey	Jackson ImmunoResearch	
α rat-biotin		1:1000	goat	Jackson	

				ImmunoResearch	
α goat-biotin		1:500	donkey	Jackson ImmunoResearch	
α mouse-biotin		1:500	goat	Jackson ImmunoResearch	
α mouse-alkaline phosphatase (AP)		1:1000		Jackson ImmunoResearch	
streptavidin-cy2		1:300		Jackson ImmunoResearch	
streptavidin-HRP		1:500		Vector	

C.

Reagents					
Reagent	Company				
ABC	Vector				
Apoptag kit	Millipore				
AUS H3300	Vector				
TSA-Biotin	PerkinElmer				
TSA Plus-FITC	PerkinElmer				
Vector Blue	Vector				

listed in Table 2.1. Bisbenzimide was used as a counterstain.

Imaging

Images were acquired using either an Axioplan2 microscope and QImaging RETIGA EXi camera or an Olympus BX51 scope and Olympus DP71 camera. Post-capture image processing was performed with Adobe Photoshop.

Histology

For H&E stains, paraffin-embedded tissues sections were stained with Harris Hematoxylin (PolyScientific, Bay Shore, NY) and eosin Y alcoholic (Sigma Aldrich, St. Louis, MO).

Cell and Structure Counts

Hilar and peripheral bile duct counts

Paraffin sections of the left liver lobe were stained for CK19 and DBA. The number of peripheral (DBA-) and hilar (DBA+) IHBDs per section were counted. Counts from multiple tissue sections, including sections from proximal, intermediate, and distal liver segments, were added and divided by the total area of liver tissue in section analyzed to provide numbers of IHBDs/mm^2 liver tissue.

Portal vein counts

Paraffin sections of the left liver lobe were stained for DBA and GS to count portal veins. Portal veins were determined as any vein not surrounded by GS+ hepatocytes and were characterized as hilar or non-hilar by the presence of absence, respectively, of an associated DBA^+ IHBD. The numbers of portal veins were counted on multiple tissue sections, including sections from proximal, intermediate, and distal liver segments, were added and divided by the total area of liver tissue in section analyzed to provide numbers of vessels/mm^2 liver tissue.

Hepatic artery counts

Paraffin sections of the left liver lobe were stained for smooth muscle actin (SMA) to count hepatic arteries. Hepatic arteries were determined as any vessel with a thick SMA^+ muscle layer and associated with a portal vein. The numbers of hepatic arteries were counted on multiple tissue sections, including sections from proximal, intermediate, and distal liver segments, were added and divided by the total area of liver tissue in section analyzed to provide numbers of vessels/mm^2 liver tissue.

$Sox9^+$ cell counts

Paraffin section of the left liver lobe were stained for Sox9 and Hnf4α. Random fields of the liver were imaged and counted for Sox9+ single-positive and Sox9+Hnf4α+ double-positive cells. The numbers of cells were added and divided by the total area of the liver tissue analyzed to provide numbers of cells/mm^2 liver tissue.

Resin Casting and Tissue Clearance

Retrograde resin injection of the common bile duct and tissue clearance were performed as previously described (Walter et al., 2012). See Appendix D for further details. The left liver lobes were photographed using a Leica MZ 16 FA stereoscope and QImaging RETIGA 4000R camera for IHBD casts and were photographed using an Olympus SZX12 stereoscope and a Diagnostic Instruments Spot Insight Color 3.2.0 camera for PV casts.

Visualization of Hypoxia

Hypoxyprobe (NPI, Inc., Bulington, MA) was used as directed. Approximately 0.6mg/g Hypoxyprobe was injected into mice. Mice were sacrificed 90 minutes after injection. Immunohistochemistry for Hypoxyprobe was performed on paraffin-embedded tissue.

Quantification of VEGF Protein in Liver Tissue and Serum

Liver tissue (caudate lobes at P30; caudate, right, and medial lobes at P15 and P3; whole liver at E16.5) was digested with Complete protease inhibitor cocktail (Roche, Mannheim, Germany). Serum was isolated from mouse blood at the time of harvest. VEGF protein was measured with using ELISA as directed (R&D, Minneapolis, MN). Total protein for normalization was measured with a Pierce BCA Protein Assay Kit as directing (Thermo Scientific, Rockford, IL).

Circulating Blood Cell Analysis

Blood samples were collected from the inferior vena cava in Microvette EDTA tubes at the time of sacrifice. Blood was analyzed with a Hemavet machine.

Statistical Analysis

One-tailed unpaired Student's t-tests were used to analyze statistical differences.

CHAPTER 3

INTRAHEPATIC BILE DUCT REGENERATION IN MICE DOES NOT REQUIRE HNF6 OR NOTCH SIGNALING VIA RBPJ.

Introduction

Studies have demonstrated that bipotential progenitors may be present in the liver that are capable of giving rise to both hepatocytes and biliary epithelial cells (BECs) (Carpentier et al., 2011; Dorrell et al., 2011; Sackett et al., 2009; Shin et al., 2011). It remains unknown, however, what degree of *in vivo* capacity specific stem, progenitor, or liver epithelial cells have to regenerate a functional IHBD system, and whether endogenous hepatic cells hold potential therapeutic benefit to treat bile duct insufficiency or ductopenic liver diseases.

In addition to human studies of Alagille syndrome (ALGS) etiology, mouse models have elucidated the importance of Notch signaling in IHBD morphogenesis (Geisler et al., 2008; Hofmann et al., 2010; Lozier et al., 2008a; Sparks et al., 2010; Zong et al., 2009). The Jagged1 ligand, expressed in portal vein (PV) mesenchyme, activates Notch receptors on bipotential hepatoblasts to promote intrahepatic bile duct (IHBD) formation (Hofmann et al., 2010). The DNA-binding co-factor recombination signaling binding protein immunoglobulin kappa J (Rbpj) is required for canonical Notch signaling within hepatoblasts. Along with Notch signaling, Hepatocyte nuclear factor 6 (Hnf6) is also important for BEC specification of bipotential hepatoblasts during embryonic development (Clotman et al., 2002).

Rbpj/Notch signaling and Hnf6 are central mediators of the known differentiation pathway for BECs (Si-Tayeb et al., 2010). In the current model of BEC specification, inhibiting both

Notch/Rbpj and Hnf6 blocks all known arms of the BEC specification signaling cascade, and would be hypothesized to cause a blockade in IHBD morphogenesis (Si-Tayeb et al., 2010). Previous work in our laboratory has demonstrated that the *Albumin-Cre*-mediated (Postic and Magnuson, 2000) hepatoblast-specific deletion of both *Rbpj* (Han et al., 2002) and *Hnf6* (Zhang et al., 2009) produces a synergistic defect whereby Rbpj and Hnf6 double-knockout (DKO) mice are developmentally unable to form peripheral IHBDs (Vanderpool et al., 2012). Early in life IHBD paucity causes severe cholestasis, hepatic necrosis, and fibrosis in these mice. However, DKO mice eventually generate BECs in reactive ductules (Vanderpool et al., 2012). The DKO mouse provides a unique and unprecedented model in which to study regeneration from a true IHBD paucity model.

In this study, we demonstrate that DKO mice are indeed capable of forming communicating peripheral IHBDs subsequent to the emergence of a ductular reaction. This indicates that Notch and Hnf6 are together dispensable for IHBD regeneration in adult mice. This is a surprising result that demonstrates that alternate mechanisms for IHBD morphogenesis exist that are different than the mechanism of embryonic ductal plate morphogenesis. This finding may explain the recovery of cholestasis that occurs in some ALGS patients while providing a new concept for investigation of potential Notch-independent IHBD regenerative therapies.

Results

Adult peripheral IHBDs form in the absence of Rbpj and Hnf6.

To examine IHBD regeneration, we utilized the bile duct insufficiency *Albumin-Cre Rbpj*$^{flox/flox}$ *Hnf6*$^{flox/flox}$ (DKO) mouse model (Vanderpool et al., 2012). At postnatal day (P)15, DKO mice lack peripheral IHBDs, but have normal appearing hilar and extrahepatic bile ducts. DKO mice also demonstrate extensive hepatocyte necrosis at P15 (Figure 3.1B). However, by P60, DKO mice display a cytokeratin 19 $(CK19)^{+}$ ductular reaction (Figure 3.1D). At P120, DKO mice exhibit a reduction in reactive ductules and display patent regenerated peripheral IHBDs (Figure 3.1F).

To quantify the extent of IHBD paucity and regeneration, hilar and peripheral IHBD branches in DKO and control mice were counted in tissue section at P15 and P120. Among the $CK19^{+}$ cells, localization of the lectin Dolichos Biflorus Agglutinin (DBA) was used to define and distinguish hilar from peripheral IHBDs. At P15, DKO mice display no difference in the number of hilar IHBD branches (Figure 3.2A). However, there is a dramatic and significant decrease in peripheral IHBD branches in DKO mice as compared to controls. At P120, there remained no difference in hilar IHBD branches between control and DKO mice (Figure 3.2B). At P120, some DKO mice displayed a complete recovery in peripheral IHBD branches to control levels; however, some DKO mice still exhibited a reduction in the number of peripheral IHBD branches as compared to control (Figure 3.2B).

We performed IHBD resin casting (Walter et al., 2012) to determine if the peripheral IHBDs observed in section contributed to the 3-dimensional communicating IHBD

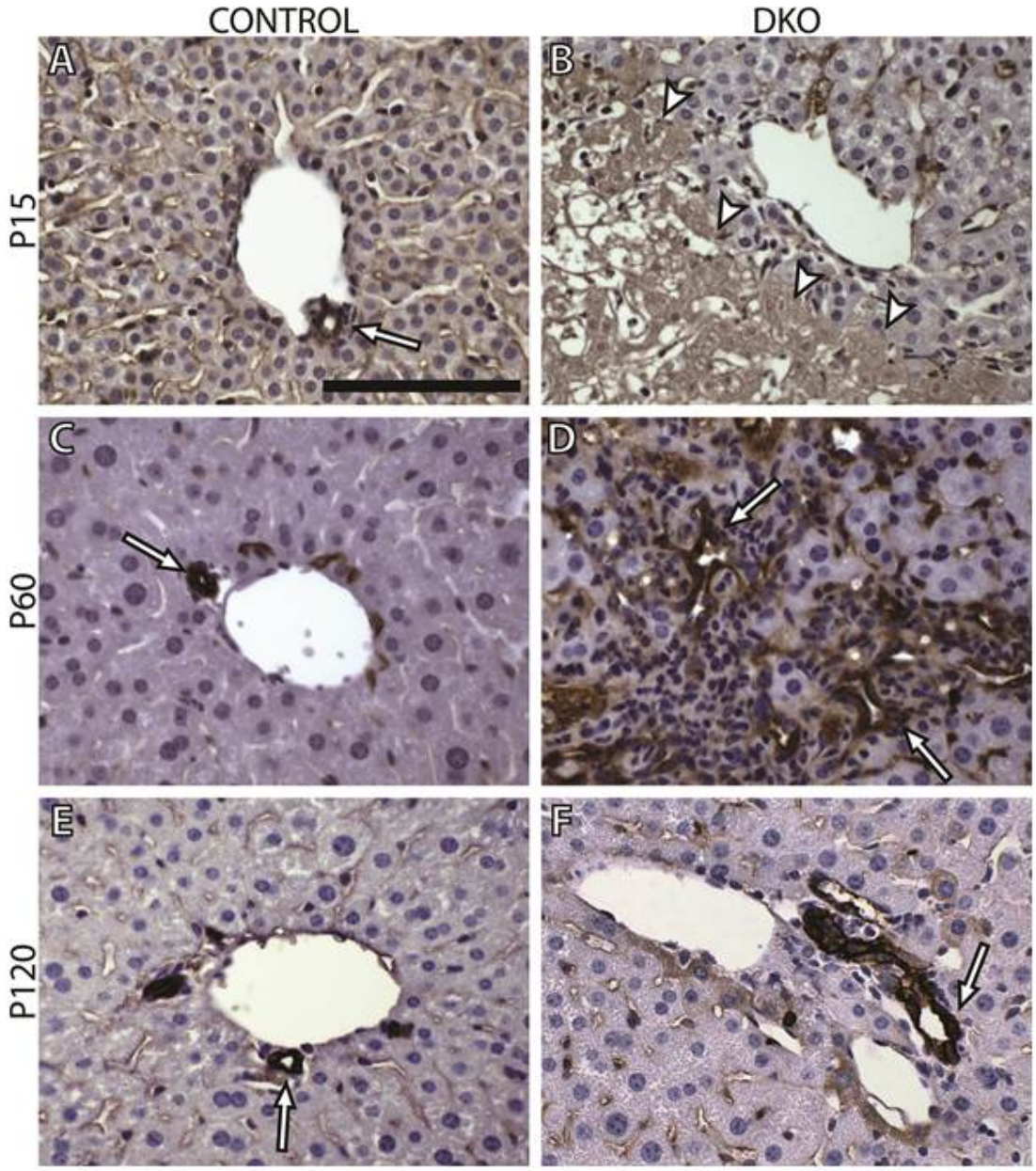

Figure 3.1. DKO mice exhibit histological recovery of peripheral IHBD paucity by P120. Paraffin sections of DKO and control (lacking *Albumin-Cre* transgene) mouse livers at P15 (A,B), P60 (C,D) and P120 (E,F) are immunostained for CK19 to mark BECs and counterstained with Mayer's hematoxylin. At P15, control mice have well-formed IHBDs (A; arrow) while DKO mice lack peripheral IHBDs and exhibit areas of focal necrosis (B; necrotic area highlighted by arrowheads). At P60, DKO mice display a large increase in peripheral CK19^{+} BECs (D; arrows), which form reactive ductules. By P120, many of the reactive ductules have resolved to patent peripheral IHBDs in the DKO (F; arrow). Scale bar is 100 μm. Details regarding serum total bilirubin levels and histological severities provided in Supplemental Table 2A.

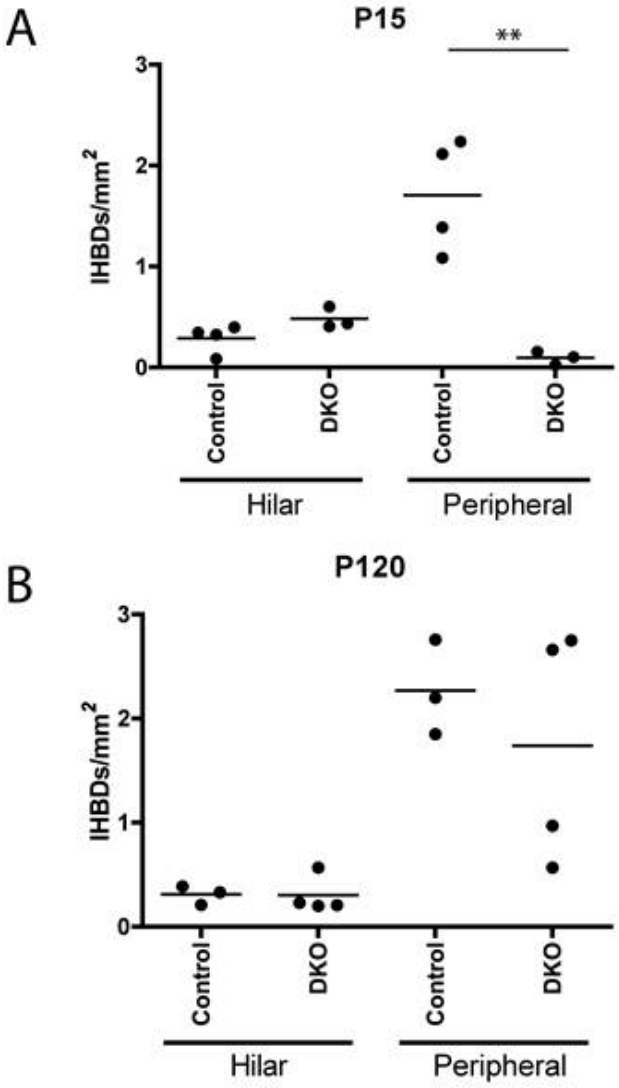

Figure 3.2. DKO mice display a lack of peripheral IHBDs at P15 and partial recovery of peripheral IHBDs at P120. P15 and P120 control and DKO mouse liver sections were stained for CK19 and stained with the lectin DBA. DBA only marks cholangiocytes comprising the hilar IHBDs. At P15, DKO mice have a statistically significant decrease in the number of DBA$^-$ peripheral IHBDs per area, but no change in DBA$^+$ hilar IHBDs (A). At P120, some DKO mice display a full recovery in the number of DBA$^-$ peripheral IHBDs per area, while some DKO mice do not recover to control levels (B). Compared to control, there was no statistically significant difference in peripheral or hilar IHBDs at P120. The two P120 DKO mice that exhibited recovery in peripheral IHBDs had normal levels of total bilirubin in serum of 0 and 1.12 mg/dL; the two P120 DKO mice that did not exhibit full recovery had total bilirubin levels in serum of 27.1 and 1.27 mg/dL. (See Supplemental Table 2 for further details of DKO phenotypes.) 3-4 animals were analyzed for each genotype at each time. At least 6 (P15) or 3 (P120) sections of liver, and a minimum area of 63 (P15) or 56 (P120) mm^2 of liver tissue was analyzed for each animal. **$p<0.01$.

architecture. At P60 in DKO mice, only the hilar branches of the IHBD are communicating with the extrahepatic bile duct system (Figure 3.3C). However, DKO mice at P120 display regenerated peripheral IHBD branches (Figure 3.3D). P120 DKO mice also demonstrate recovery from cholestasis, as measured by total bilirubin levels in serum (Table 3.1). There was some variation within the DKO mice in terms of extent of IHBD paucity in casts and in total bilirubin levels (Table 3.1). Representative cast images with the corresponding total bilirubin are shown at each timepoint: for P60 DKOs, the most common phenotype is “only hilum” cast and for P120 DKOs, the most common phenotype is “moderate”.

BECs in ductular reactions and regenerated peripheral IHBDs do not express Rbpj or Hnf6

To determine whether the ductular reaction and regeneration of peripheral IHBDs can truly occur without Rbpj and Hnf6, we examined the expression of each protein in BECs. If the recovery is due to either (1) an expansion of BECs that retain Rbpj and/or Hnf6 expression, or (2) a conversion of cells from a non-Albumin-Cre expressing cell lineage into BECs, we would expect to find that all or most BECs at P60 and P120 will retain expression of one or both of these proteins.

We performed immunohistochemistry for Hnf6 in P60 and P120 DKO and control mice. Hnf6 is present throughout the tissue in hepatocytes and BECs at both P60 and P120 (Figure 3.4A,C). In DKO mice, however, hepatocytes and BECs express no detectable Hnf6 at P60 or P120, demonstrating that the BECs constituting both reactive ductules and regenerated peripheral IHBDs are formed in the absence of Hnf6 protein (Figure 3.4B,D).

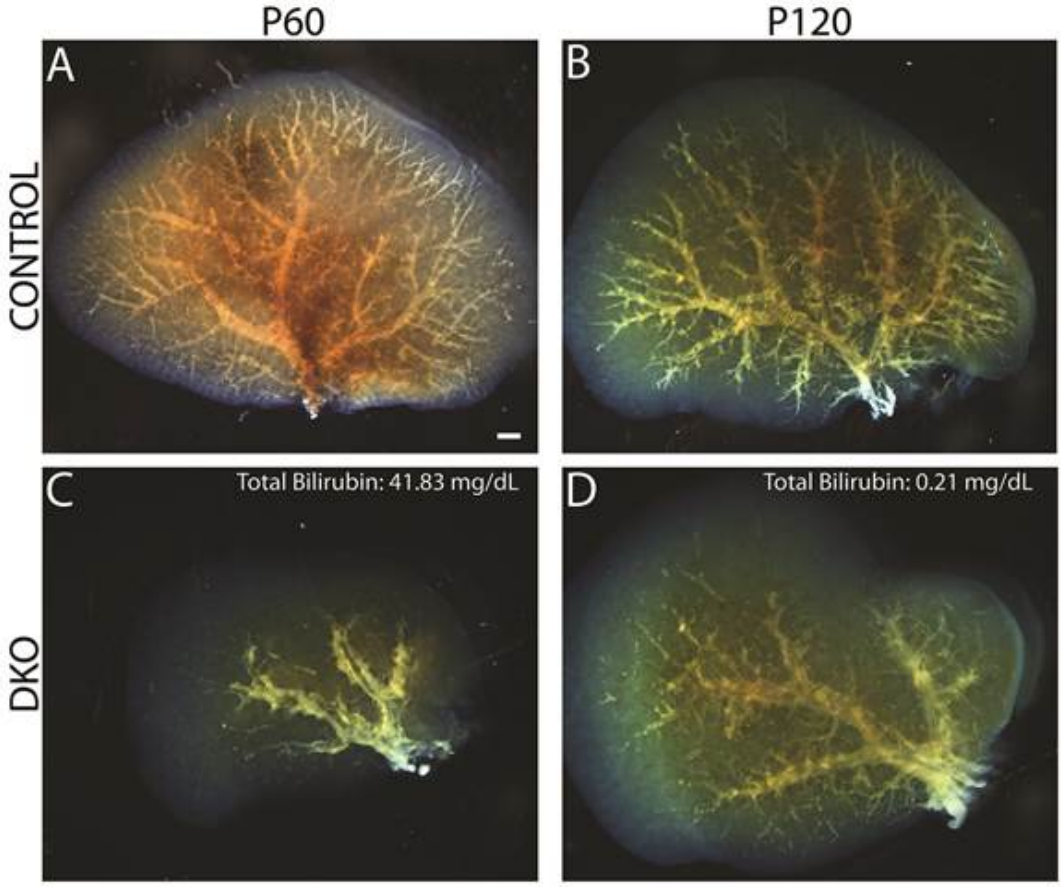

Figure 3.3. 3-dimensional hepatic architecture improves in DKO mice. Liquid resin/catalyst mixture was injected retrograde into the common bile duct to generate a cast of the communicating IHBD structure in P60 and P120 control (A,B) and DKO mice (C,D). At P60, the DKO cast exhibits a severe lack of communicating peripheral IHBDs (C). However, by P120, the DKO IHBD structure exhibits partial recovery with a visual increase in peripheral IHBD branches (D). Total bilirubin levels for the representative DKO IHBD resin cast is displayed (C,D). Scale bar is 1 mm. Details on serum total bilirubin levels and cast severities are provided in Table 3.1B.

A.

Mice examined for chromogenic CK19 immunohistochemistry								
		Serum Total Bilirubin (mg/dL)					Histology	
	N=	<1.2	1.2-10.0	>20	Average	Range	Normal-Mild	Moderate-Severe
p60	5	1	0	4	26.15	0.57-46.1	2	3
p120	6	5	1	0	0.56	0-1.27	6	0

B.

Mice examined for 3-dimensional IHBD cast architecture									
		Serum Total Bilirubin (mg/dL)					Cast architecture		
	N=	<1.2	1.2-10.0	>20	Average	Range	Normal	Moderate	Only hilum
p60	8	3	2	3	8.12	0.10-41.38	1	3	4
p120	8	6	2	0	1.3	0.21-5.64	1	7	0

Histology:

- Normal-mild: Low to no focal necrosis. Few to no reactive ducts.
- Moderate-severe: Large amount of necrosis. Large number of reactive ducts, bridging portal tracts.

Cast architecture:

- Normal: Many peripheral IHBD branches apparent, extending to liver periphery.
- Moderate: Peripheral IHBD branches visible, but reduced in number and density and not extending to liver periphery.
- Only hilum: No peripheral IHBD branches visible. IHBD cast is only visible in the proximal part of the liver in the large, hilar branches.

Table 3.1. DKO mouse phenotypes.

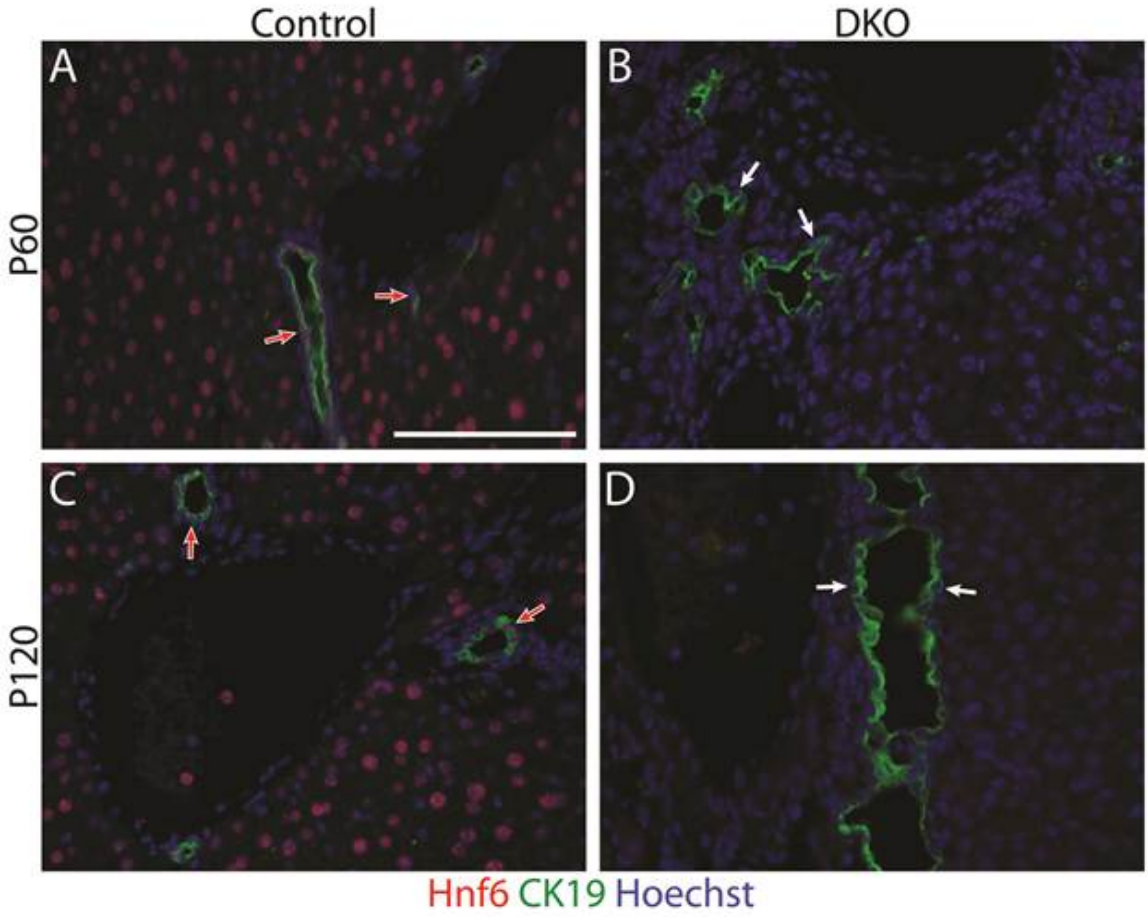

Figure 3.4. DKO mice do not express Hnf6 in BECs or hepatocytes. P60 and P120 control and DKO mouse liver sections were stained for Hnf6 (red), CK19 (green), and Hoechst (blue). In P60 (A) and P120 (C) control mice, Hnf6 is present in hepatocytes and BECs (red arrows). In P60 (B) and P120 (D) DKO mice, Hnf6 is not detected in hepatocytes or BECs in either reactive ductules or remodeled IHBDs (white arrows). Scale bar is 100 μm.

To determine whether Rbpj is present in reactive and regenerated peripheral BECs, we performed immunostaining for Rbpj protein. Rbpj is expressed not only in cells with activated Notch signaling, but is ubiquitously expressed in all cell types (Hamaguchi et al., 1992). The levels of Rbpj protein are normally very low in liver epithelial cells, and the protein can only be detected with multiple steps of amplification for immunostaining performed on paraffin embedded tissue. In control mice at P15, P60, and P120, Rbpj is consistently observed in both wide spectrum cytokeratin (wsCK)+ BECs and in the surrounding stromal cells (Figure 3.5A,C,E, white arrowheads). In P15 DKO mice, the majority of BECs in hilar IHBDs express no detectable Rbpj protein; however, a small number of rare BECs do still express Rbpj (Figure 3.5B, white arrowhead). The presence of some Rbpj-expressing cells in the hilar IHBDs may indicate that these cells underwent BEC-specification prior to *Albumin-Cre* transgene expression, thus avoiding Albumin-Cre mediated recombination and deletion of Rbpj. At P60 and P120, the vast majority of BECs present in either reactive ductules or regenerated IHBDs express no detectable Rbpj protein. Only very rare BECs that express Rbpj are present in the liver at P60 and P120 (Figure 3.5D,F, white arrowheads). We detect no indication that undeleted populations of BECs are preferentially expanding and contributing to regenerated IHBDs in the DKO mice.

Ductular reactions occur surrounding all peripheral portal veins and not in isolated locations.

To assess the extent of the ductular reaction and IHBD regeneration over time within the hepatic architecture context, we immunostained for CK19 to mark BECs and glutamine synthetase (GS) to marks pericentral hepatocytes. This allows us to discriminate between portal veins, where IHBDs are normally associated, and central veins (Figure

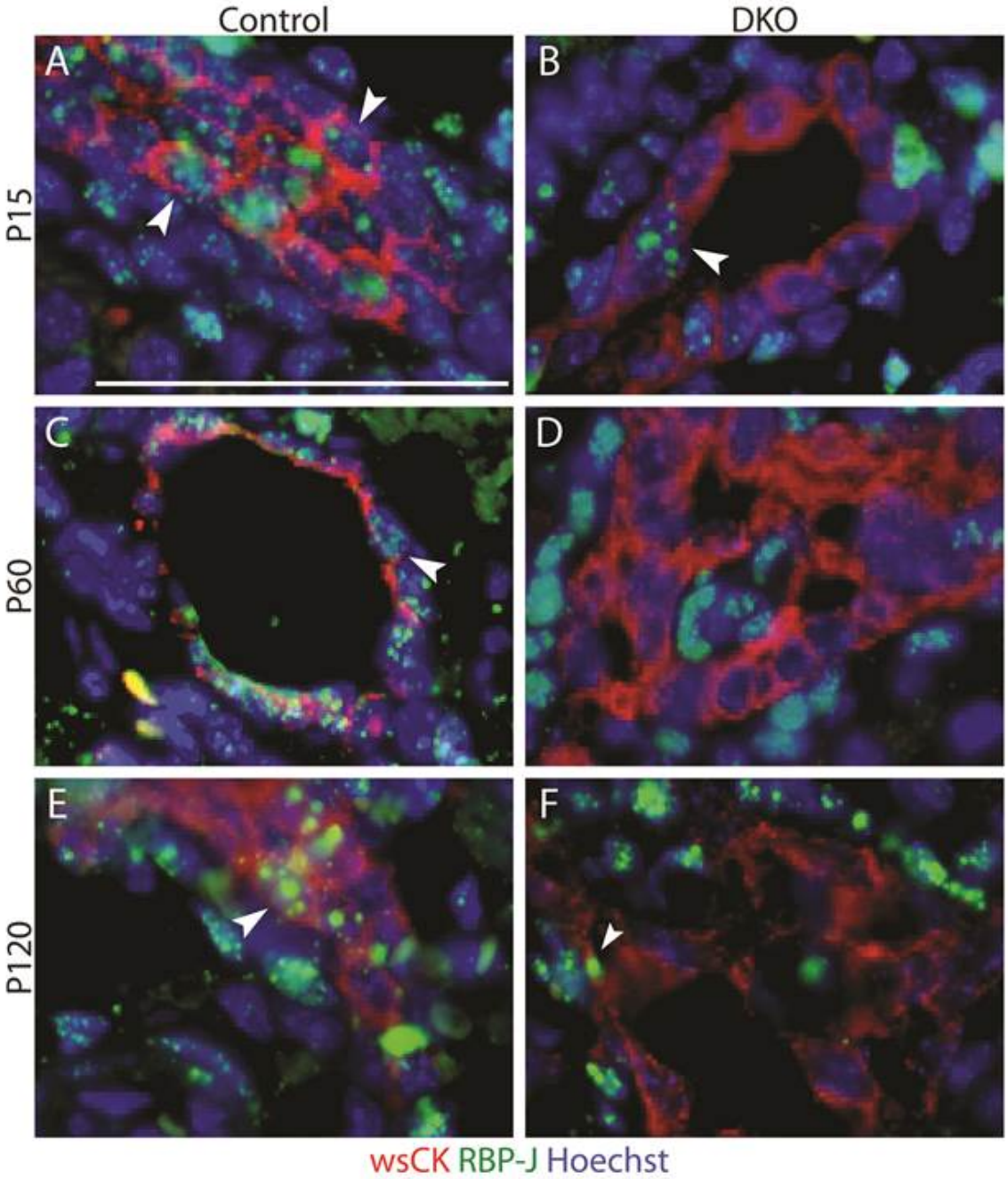

Figure 3.5. DKO mice do not express Rbpj in nearly all BECs of reactive ductules and IHBDs. P15, P60, and P120 control and DKO liver sections were stained for wide spectrum cytokeratin (wsCK; red), Rbpj (green), and Hoechst (blue). Rbpj is expressed in all cells and BECs in control mice at P15 (A), P60 (C), and P120 (E). P15 DKO mice only have formed hilar IHBDs, and within these, most BECs do not have detectable Rbpj protein, but a small number of BECs do retain Rbpj expression (B, white arrowhead). Similarly, in P60 (D) and P120 (F) DKO mice, nearly all wsCK$^+$ BECs in reactive ductules and IHBDs express no Rbpj protein. Rare Rbpj$^+$ wsCK$^+$ BECs are marked with white arrowheads. Scale bar is 50 μm.

3.6A,C,E,G). If new BECs arise from rare cells in the liver, for example, a small number of cells that retain Rbpj and/or Hnf6 expression, we would expect to see localized expansions of $CK19^+$ cells. Instead, we see that at P60, the $CK19^+$ ductular reaction extends throughout the liver, with reactive ductules surrounding all peripheral portal vein branches (Figure 3.6B,D). At P120, the $CK19^+$ reactive ductules have resolved and patent IHBDs are present in regions of GS^- hepatocyte-associated portal veins (Figure 3.6F,H).

Reactive BECs are not derived from hilar DBA^+ IHBDs.

To explore the hypothesis that cells contributing to pre-existing IHBDs give rise to ductular reactions and peripheral IHBDs, we analyzed the relationship between CK19 expressing cells and DBA^+ hilar ducts. We looked at a timepoint between P15, when no peripheral BECs are present and P60 when a full ductular reaction has developed; at P30, reactive $CK19^+$ BECs are just beginning to appear (Figure 3.7B-F, white arrowheads compared to Figure 3.6). To determine whether these emerging $CK19^+$ reactive BECs are coming from differentiated hilar BECs, we assessed the expression of CK19 and DBA in three dimensions on serial liver sections. We examined serial sections of the P30 DKO mouse liver in areas where $CK19^+$ reactive BECs were found. These cells exist in small clusters that extend in three-dimensions but do not juxtapose DBA^+ hilar IHBDs on any spatial axis, as visible in the Figure 3.7A image captured from a hilar region. These results suggest that the initial $CK19^+$ reactive BECs are not emerging directly from formed hilar IHBDs.

Next, we examined the expression of the BEC marker Sex determining region Y-related HMG box transcription factor 9 (Sox9). Normally, Sox9 expression is activated during

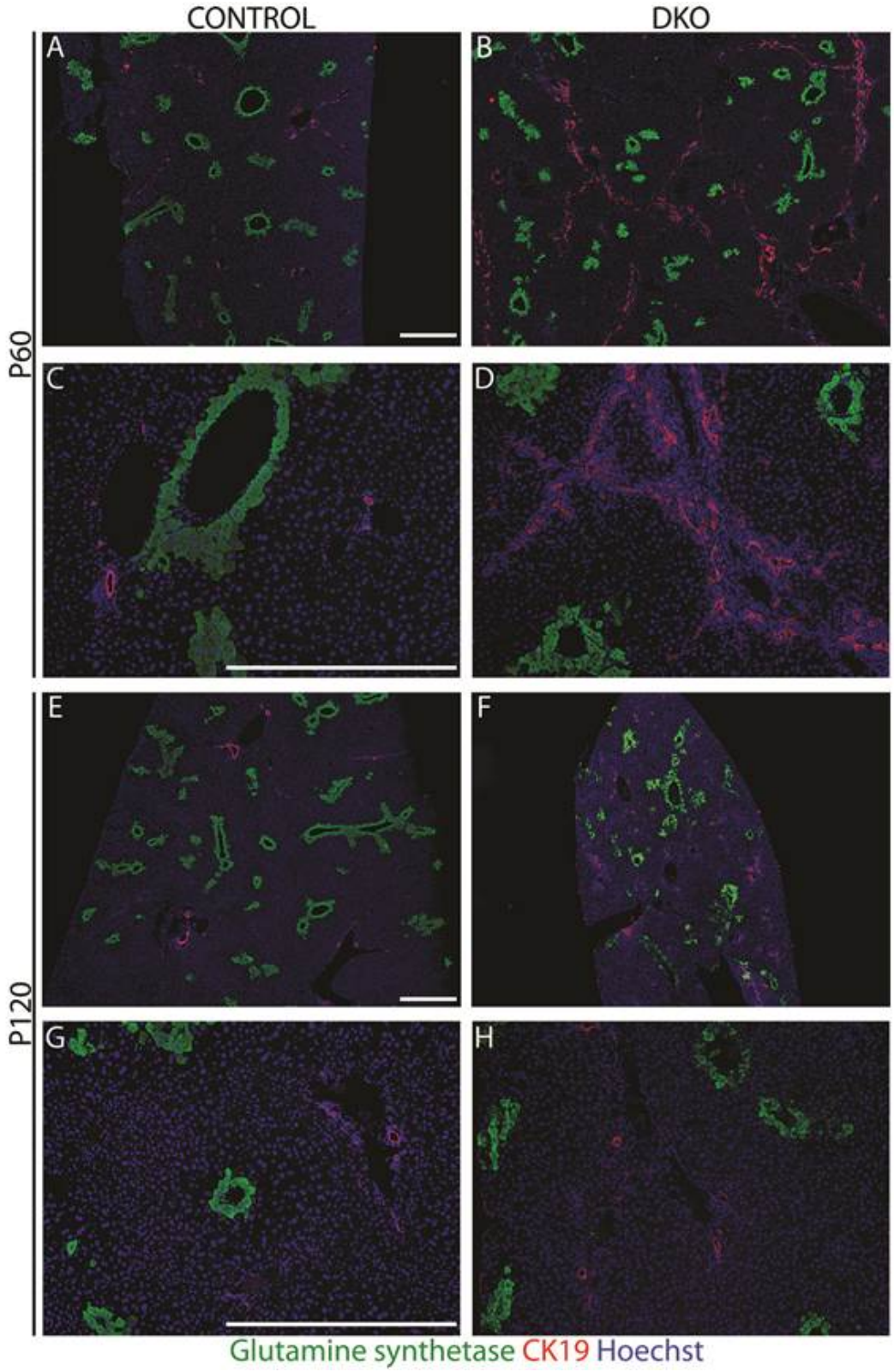
CONTROL
DKO
A
B
C
D
E
F
G
H
P60
P120
Glutamine synthetase CK19 Hoechst

Figure 3.6. Atypical ducts arise surrounding all peripheral portal vein branches by P60 and are partially resolved by P120. P60 and P120 control and DKO mouse liver sections were stained for glutamine synthetase (green), CK19 (red), and Hoechst (blue). Glutamine synthetase expression demarcates hepatocytes adjacent to central versus portal veins at low (A,B,E,F) and high (C,D,G,H) magnifications. $CK19^+$ reactive ductules appear in P60 DKO mice throughout the liver in all regions surrounding peripheral portal vein branches (B,D). In P120 DKO mice, reactive ductules have largely resolved and patent bile ducts have formed adjacent to peripheral portal veins throughout the tissue (F,H). Scale bar is 500 µm.

DBA CK19 Hoechst
Sox9 CK19 Hoechst
A
A'
x µm
B
B'
x+12 µm
C
C'
x+24 µm
D
D'
x+36 µm
E
E'
x+48 µm
F
F'
x+72 µm

Figure 3.7. Reactive CK19+ BECs emerge juxtaposed to Sox9+ intermediate cells but not juxtaposed to DBA+ formed hilar IHBDs. Serial sections of a P30 DKO mouse liver were stained for CK19 (green), or Sox9 (A'-F') (red), and Hoechst (blue). At P30, formed hilar IHBDs bind the lectin DBA (A'A"). $CK19^+$ reactive BECs (white arrowheads) were found in small clusters that extended in three dimensions. These BECs, representing the beginning of the ductular reaction and formation of peripheral IHBDs, were found in areas in which there was close proximity of $Sox9^+$ intermediate cells but not juxtaposed to DBA^+ hilar IHBDs (green arrowheads). $Sox9^+CK19^-$ cell (red arrowheads) were frequently observed in the vicinity of reactive BECs. Scale bar is 100 μm.

ductal plate differentiation of BECs (Antoniou et al., 2009), expressed in mature BECs, enriched in adult mouse hepatic progenitor cell (HPC) populations (Dorrell et al., 2011), and has been demonstrated to be a marker of hepatocyte-to-BEC conversion (Yanger et al., 2013). To examine the spatial relationship between the $Sox9^+$ cells, emerging $CK19^+$ reactive BECs, and DBA^+ IHBDs, we performed immunostaining for Sox9 and CK19 on serial liver sections in P30 DKO mice (Figure 3.7A'-F'). Sox9 is expressed widely throughout the hepatic tissue of DKO mice. $Sox9^+$ cells (Figure 3.7A'-F', red arrowheads) are present outside of $CK19^+DBA^+$ hilar IHBDs (Figure 3.7A', green arrowhead) and $CK19^+DBA^-$ peripheral BECs (Figure 3.7B'-F', white arrowheads). $CK19^+DBA^-$ peripheral BECs are consistently found in close spatial association with $Sox9^+CK19^-$ cells. While small clusters of $Sox9^+$ cells do exist in close proximity to DBA^+ IHBDs, they are already widespread in the peripheral tissue by P30.

To further assess whether these $Sox9^+$ cells may be arising from hilar IHBDs, we also analyzed the spatial relationship between $Sox9^+$ cells and DBA^+ hilar IHBDs through immunofluorescence on serial liver sections at P15 (Figure 3.8). $Sox9^+$ cells are found surrounding necrotic patches (Figure 3.8B-F, dashed outline). At P15, $Sox9^+$ cells extend in three-dimensions surrounding areas of focal necrosis. The areas of focal necrosis are apparent by cell morphology and the sticking of the lectin DBA. Importantly, we find that these areas of $Sox9^+$ cells do not juxtapose hilar IHBDs in any area examined. Although this analysis does not definitively determine that the $Sox9^+$ cells do not arise from DBA^+ IHBDs, our data strongly support this conclusion.

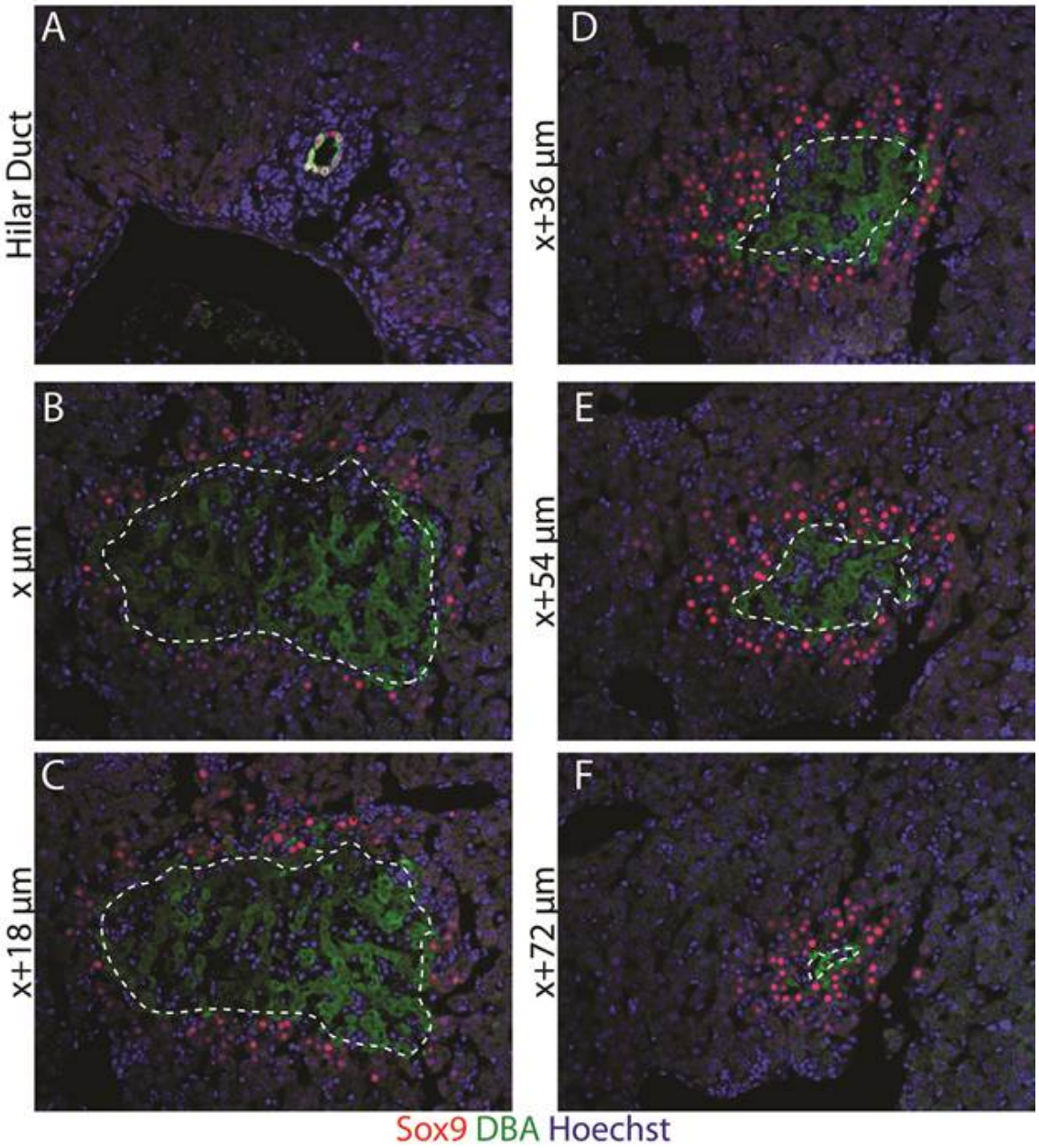

Figure 3.8. Sox9⁺ intermediate cells in P15 DKO mice do not arise from hilar BECs. Serial sections of a P15 DKO mouse liver were stained for Sox9 (red), DBA (green), and Hoechst (blue). At P15, formed hilar IHBDs bind the lectin DBA (A). Areas of Sox9⁺ intermediate cells surrounding focal necrotic areas (circled with dotted line) were followed through at least 72 µm of tissue (B-F). Sox9⁺ intermediate cells were not found to juxtapose or be spatially associated with DBA⁺ hilar ducts at any tissue depth. Scale bar is 100 µm.

DKO mice exhibit Sox9$^+$ "intermediate" cells.

To assess the cellular identity of the observed Sox9$^+$ cells in DKO mice, we performed immunohistochemistry for Sox9. Sox9 expression is observed in cells that histologically appear as BECs in P15 and P60 control livers (Figure 3.9A,C). In P15 DKO mice, Sox9 is seen not only in IHBDs (Figure 3.9B"), but also in non-IHBD cells surrounding necrotic patches throughout the liver (Figure 3.9B'). These cells morphologically resemble hepatocytes. Although they are found near necrotic patches, these Sox9$^+$ cells are not undergoing apoptosis (Figure 3.10). In P60 DKO mice, Sox9 expression is found both in IHBDs (Figure 3.9D") and within the liver parenchyma in cells that morphologically resemble hepatocytes (Figure 3.9D').

We further characterized the identity of Sox9+ cells by performing co-immunostaining with markers of BECs or hepatocytes. In DKO mice at P15, Sox9$^+$ cells surrounding necrotic areas co-express the hepatocyte marker Hnf4α (Figure 3.11A) and do not express the BEC markers Hnf1β (Figure 3.11B) or CK19 (Figure 3.11C). The Sox9$^+$ cells display cell fate markers of both the hepatocyte marker Hnf4α and the BEC marker Sox9 and therefore represent a population of "intermediate" cells. In DKO mice at P60, Sox9 was again found in intermediate cells co-expressing Hnf4α (Figure 3.11D) as well as in Hnf1ß$^+$ and CK19$^+$ reactive BECs (Figure 3.11F, red arrowheads). The Sox9$^+$ intermediate cells that juxtapose central veins co-express glutamine synthetase (GS), an enzyme expressed in pericentral hepatocytes, supporting the hypothesis that these cells originate from hepatocytes and active the expression of BEC markers (Figure 3.12). The number of Sox9$^+$ intermediate cells is significantly higher in DKO mice than in controls at P15, P60 and P120, but decreases over time (Figure 3.13A).

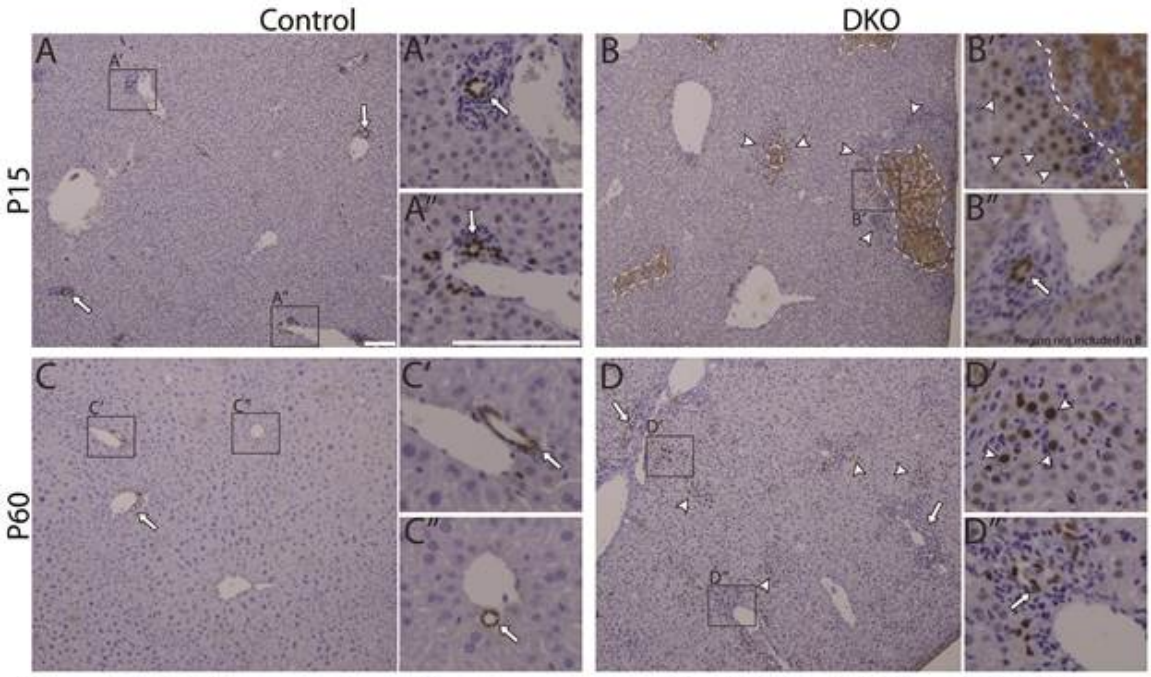

Figure 3.9. Sox9-expressing cells are present outside of IHBDs in P15 and P60 DKO mice. Liver sections were immunostained for the BEC marker Sox9 and counterstained with Mayer's hematoxylin. Sox9 is observed in P15 (A) and P60 (C) control mice IHBDs (arrows). In P15 DKO mice, Sox9 appears in cells surrounding necrotic areas that morphologically resemble hepatocytes (B, B' arrowhead). At P60, DKO mice exhibit a large visible increase in Sox9 expressing cells (D) and Sox9 is observed in cells that resemble both BECs (D, D", arrow) and hepatocytes (D, D' arrowhead). Boxed regions are magnified in A-D' and A-D", except for B". As IHBDs are very rare in P15 DKO mice, the image in B" was taken from a hilar region of the tissue. Scale bar is 50 µm.

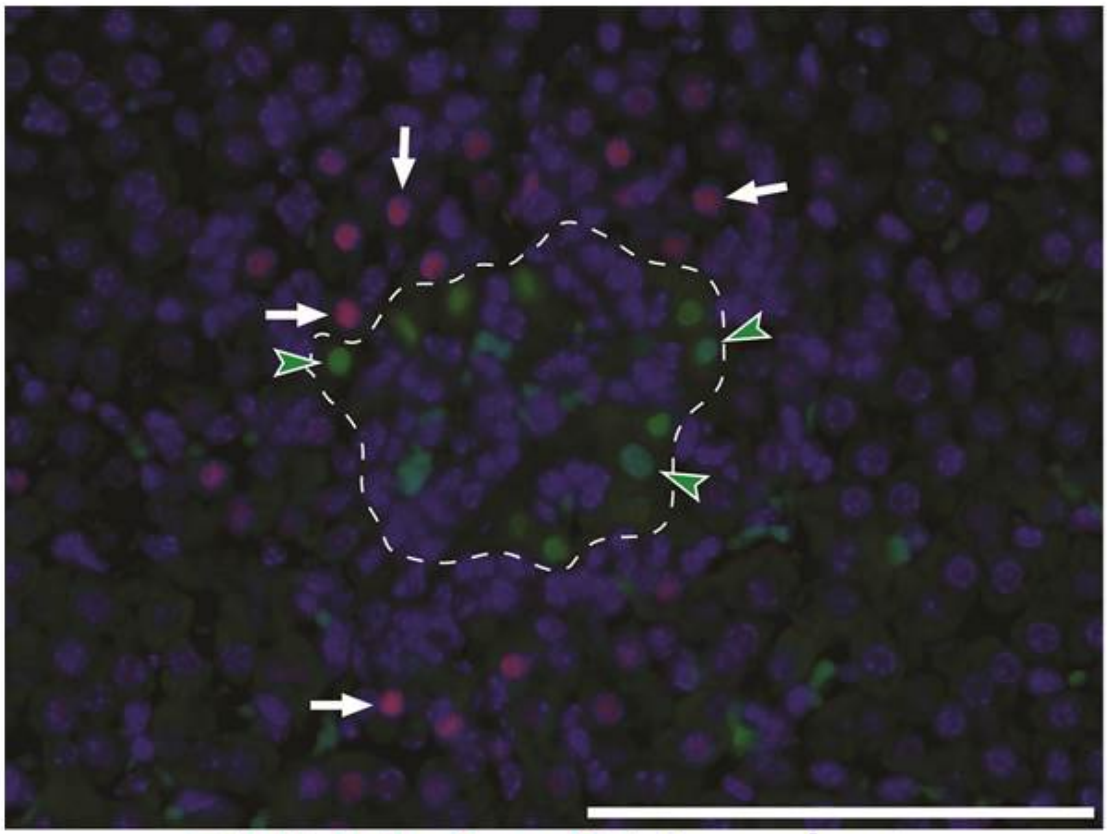

Figure 3.10. Sox9⁺ intermediate cells are not apoptotic. P15 DKO mouse liver sections were stained for Sox9 (red), TUNEL (green), and Hoechst (blue). TUNEL⁺ cells (green arrowhead) were present within necrotic areas (circled with dotted line). Sox9⁺ cells (arrows) surrounding the necrotic areas did not stain positive for TUNEL. Scale bar is 100 um.

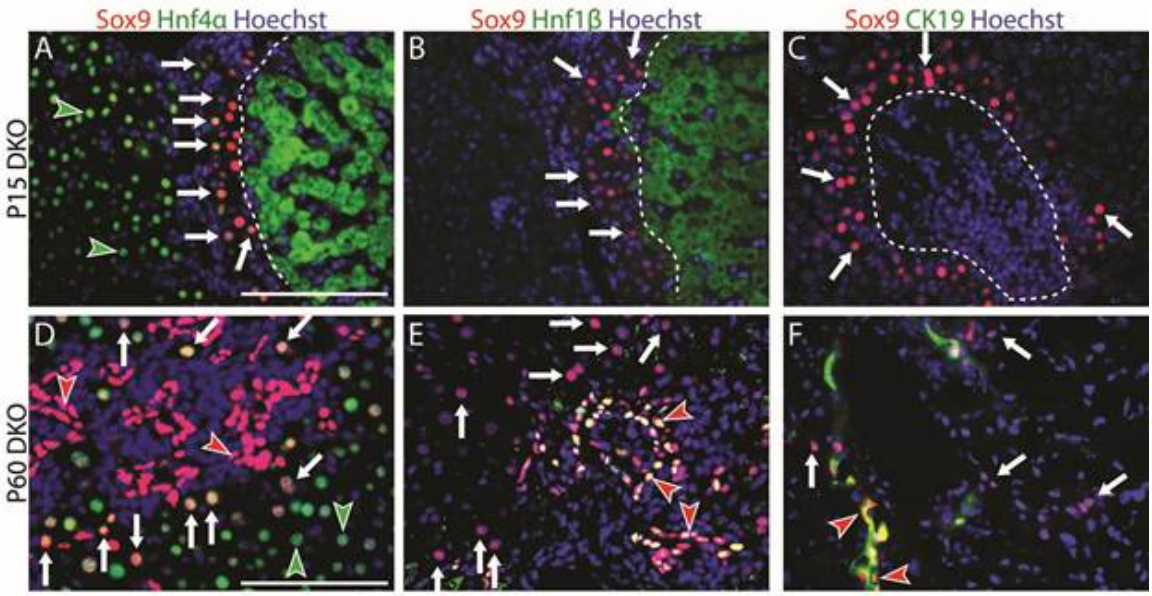

Figure 3.11. Sox9-expressing cells express hepatocyte markers in P15 and P60 DKO mice. Liver sections were immunostained for Sox9 (red), Hoechst (blue), and the differentiation markers Hnf4α, Hnf1β, or CK19 (green). In P15 DKO mice, $Sox9^+$ cells surrounding focal necrotic areas co-express the hepatocyte marker Hnf4α (A) and do not co-express the BEC markers Hnf1β (B) or CK19 (C). In P60 DKO mice, $Sox9^+Hnf4\alpha^+$ intermediate cells are present (D). The $Sox9^+$ intermediate cells do not express the BEC markers Hnf1β (E) and CK19 (F). At P60, Sox9 is also expressed in BECs, determined morphologically or by co-expression of Hnf1ß or CK19 (D-F, red arrowheads). $Sox9^+Hnf4\alpha^+$ intermediate cells (arrows) appear yellow while $Sox9^-Hnf4\alpha^+$ hepatocytes appear green (green arrowheads) (A,D). $Sox9^+Hnf1\beta^+$ or $Sox9^+CK19^+$ BECs appear yellow (red arrowheads) while $Sox9^+CK19^-$ intermediate cells (arrows) appear red (B,C,E,F). Scale bar is 100 um.

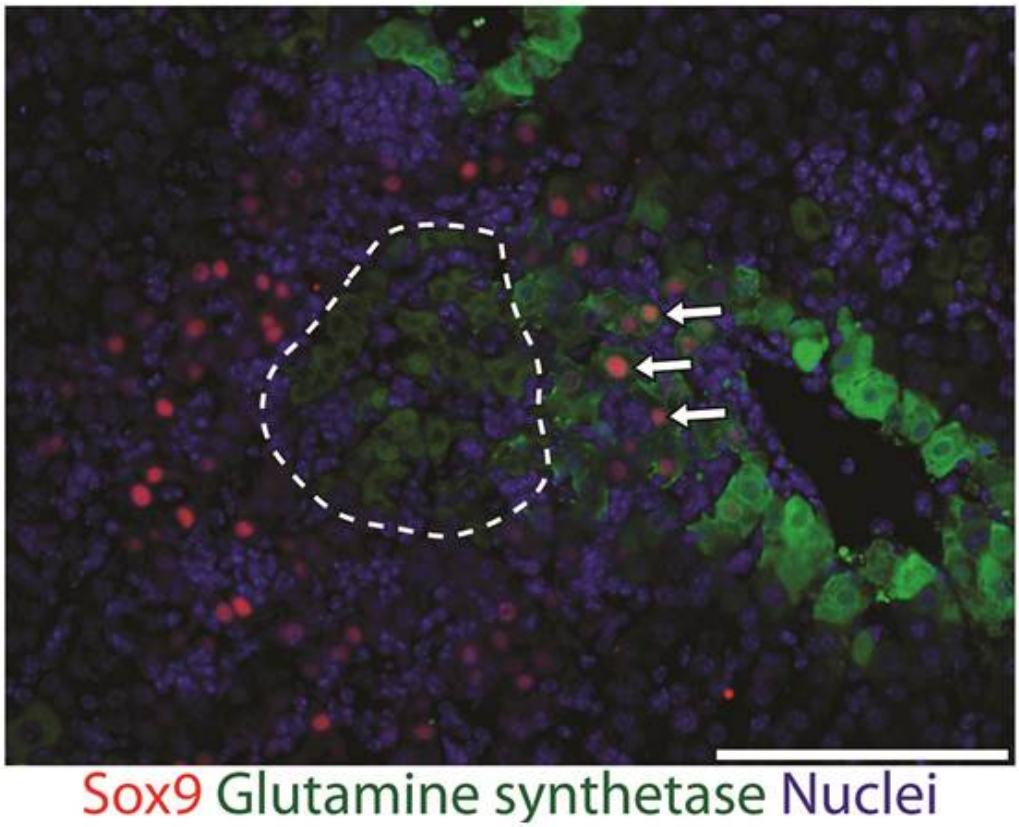

Figure 3.12. Sox9 is expressed in glutamine synthetase-expressing pericentral hepatocytes. P15 DKO mouse liver section was stained for Sox9 (red) and the pericentral hepatocyte marker glutamine synthetase (green). Due to the tight restriction of glutamine synthetase expression within hepatocytes, most Sox9+ hepatocyte cells did not co-express glutamine synthetase; however, some necrotic areas (dotted line) were located close to central veins, and Sox9 expression was visualized in glutamine synthetase+ hepatocytes (arrows). Scale bar is 100 um.

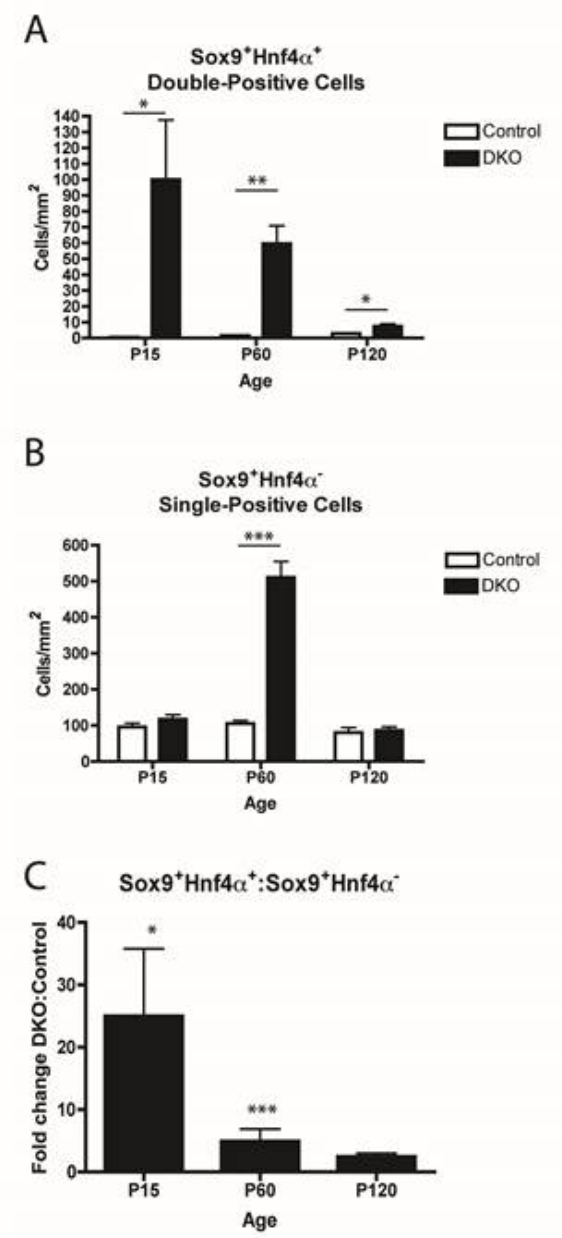

Figure 3.13. DKO mice have increased Sox9⁺Hnf4α⁺ double-positive hepatocytes. P15, P60, and P120 DKO and control mouse liver sections were stained for Sox9 and Hnf4α. Random sections were imaged and counted for Sox9⁺ single-positive (A) and Sox9⁺Hnf4α⁺ double-positive cells (B). Three animals for each genotype at each time point were analyzed. A minimum of 688 (P15), 854 (P60), or 866 (P120) cells was counted for each animal. Sox9⁺Hnf4α⁺ double-positive cells were increased in DKO mice over controls at P15, P60, and P120 (A). Sox9⁺ single-positive cells were increased over controls at P60 only (B). The ratio of Sox9⁺Hnf4α⁺ double-positive cells to Sox9⁺ single-positive cells is displayed in (C). The ratio of double-positive-to-single-positive cells is increased in DKO animals over controls at P15 and P60. *p<0.05; **p<0.01; ***p<0.001.

We examined proliferation to determine whether Sox9^{+} intermediate cells represent an expanding progenitor population. In DKO mice at P15, Sox9^{+} intermediate cells did not express the proliferation marker Ki67, despite high amounts of proliferation in surrounding hepatocytes (Figure 3.14B). Sox9^{+} intermediate cells were also non-proliferative at P60 in DKO mouse livers (Figure 3.14D). This suggests that these cells do not represent a proliferative progenitor population.

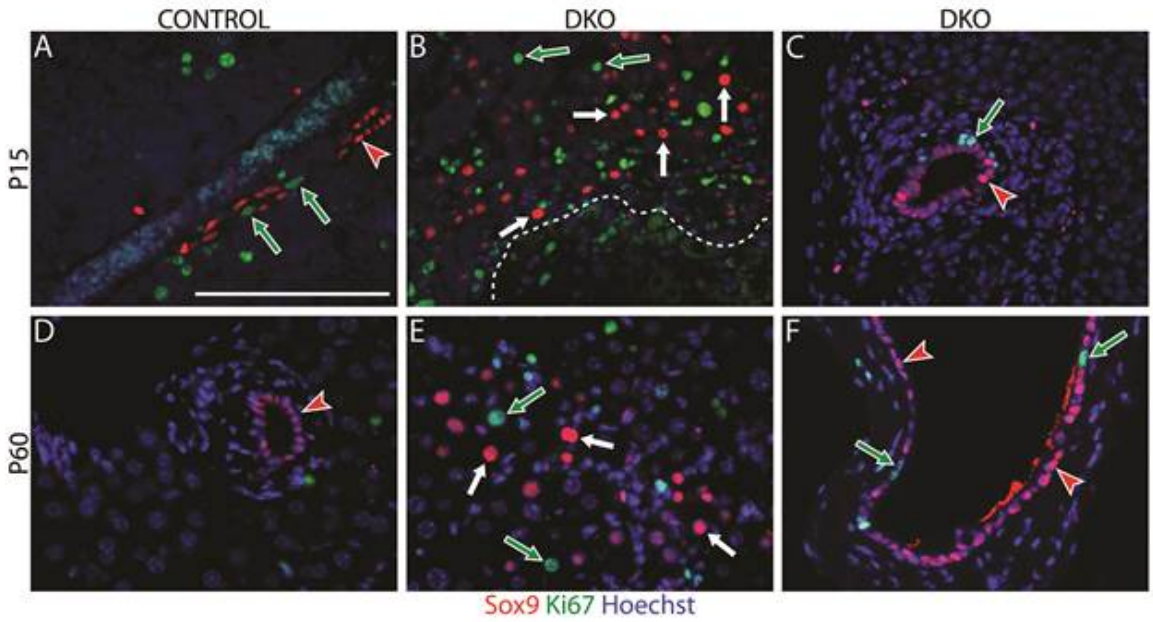

Figure 3.14. Sox9-expressing hepatocyte cells are non-proliferative. P15 and P60 control and DKO mouse liver sections were stained for Sox9 (red), Ki67 (green) for proliferating cells, and Hoechst (blue) for nuclei. In the control mice, frequent BEC proliferation was seen at P15 (A, green arrows) but little was observed at P60 (D). In the DKO mice, overall there was increased BEC proliferation compared to control, likely due to liver injury conditions (B,C,E,F). However, the Sox9-expressing hepatocyte cells (white arrows) infrequently co-expressed the proliferative marker Ki67 at both P15 (B) and P60 (E). Proliferative BECs (green arrows) display low levels of Sox9 relative to non-proliferative BECs (red arrowheads) within the IHBD in P15 control mice (A) and P60 DKO mice (F). Focal necrosis is indicated by dotted white line. Scale bar is 100 um.

Conclusion

Sox9^{+} BECs and a communicating IHBD are able to form without Notch/Rbpj signaling and Hnf6.

The involvement of Notch and Hnf6 in ductal plate IHBD development has been well-characterized (Antoniou et al., 2009; Clotman et al., 2002; Hofmann et al., 2010; Lozier et al., 2008a). During ductal plate morphogenesis, hepatoblasts surrounding the portal vein are specified as BECs, become polarized, and remodel into a luminal IHBD structure (Antoniou et al., 2009). The initial peripheral IHBD paucity observed in DKO mice indicates that ductal plate IHBD morphogenesis cannot occur without Notch signaling and Hnf6 (Figure 3.1). However, the regeneration of peripheral IHBDs in DKO mice (Figures 3.2, 3.3) despite the absence of Rbpj and Hnf6 protein from nearly all BECs and hepatocytes (Figures 3.4, 3.5) (Vanderpool et al., 2012) excludes an absolute cell-autonomous requirement of these genes for BEC differentiation during injury.

Recent studies have demonstrated that the cell autonomous over-activation of Notch signaling is capable of driving hepatocyte-to-BEC conversion and that deleting Rbpj impairs efficient hepatocyte-to-BEC conversion in liver injury models (Jeliazkova et al., 2013; Yanger et al., 2013). For example, Yanger et al. (2013) demonstrate that deleting Rbpj decreases the number of Sox9^{+} lineage-labeled hepatocytes arising during liver injury, but does not completely block the response. Similarly, inhibiting Notch signaling reduced the extent of the ductular reaction mounted in response to injury (Fiorotto et al., 2013). Our data add to this story through the indication that Rbpj, and canonical Notch signaling, is not absolutely required. In a Notch loss model, it may take longer to reach intracellular thresholds to activate Sox9 expression. We hypothesize that one or more signaling pathways may converge to activate Sox9 expression

and, in coordination with Sox9, overcome the loss of Notch signaling in the DKO model. Contributing signaling molecules may originate from infiltrating immune cells to initiate expression of Sox9 localized around necrotic lesions. There is precedent for immune and endothelial cells communicating with the liver epithelium during injury (Boulter et al., 2012; Wang et al., 2012) to promote liver regeneration. Previous studies investigating hepatocyte-to-BEC conversion in mice and rats have identified Akt, HGF, EGF, and PI3K as potential mediators of the transdifferentiation process (Fan et al., 2012; Limaye et al., 2008b) in a Notch signaling-capable background. Further studies are required to determine which extra- and intracellular signaling pathways are driving the Notch-independent alternate BEC differentiation mechanism observed in DKO mice.

Interestingly, although $Sox9^+$ intermediate cells are observed in both Notch loss and Notch over-activation models, the molecular regulation may be different. In Notch over-activation, the biliary cell marker Hnf1β becomes activated in hepatocytes co-expressing Hnf4α (Yanger et al., 2013); however, the co-expression of these markers is not observed in the DKO mouse model, where Hnf1β is expressed in $Sox9^+$ cells that have already downregulated Hnf4α (Figure 3.11). This suggests that the regulation of Sox9 expression may be quite different in the presence or absence of Notch signaling. The two different models may have complementary clinical implications, with Notch over-activation modeling carcinogenesis and the Notch loss more closely resembling a chronic cholestatic disease injury.

Reactive BECs that arise in peripheral regions originate from liver epithelium but not from hilar IHBDs.

There are several possible origins of the peripheral reactive BECs and regenerated IHBDs in the DKO mouse models, including: differentiated DBA^+ hilar IHBDs, extrahepatic bile ducts

(EHBDs), EHBD associated peribiliary glands (Carpino et al., 2012), hepatocytes (Fan et al., 2012; Michalopoulos et al., 2005; Yanger et al., 2013), mesenchymal/stellate cells (Tao et al., 2009; Yang et al., 2008), endothelial cells (Goldman et al., 2013), or hematopoietic cells (Petersen et al., 1999). As we are not able to perform *Cre-mediated* lineage tracing in this *Cre-generated* genetic deficiency model, we cannot definitively rule out any of these possibilities. However, based on the finding that almost every BEC observed in P60 and P120 DKO mice are deleted for both Rbpj and Hnf6 strongly indicates that new BECs come from an *Albumin-Cre*-derived intrahepatic cell and not from a non-hepatic source (Figures 3.4, 3.5). This makes it highly unlikely that the new BECs would originate from the EHBDs, peribiliary glands, mesenchymal cells, endothelial cells, or hematopoietic cells. While the existing hilar IHBDs at P15 are restricted to the proximal base of the liver, the reactive BECs are present throughout the liver periphery. It is difficult to imagine how cells from either the hilar IHBD would distribute throughout the liver periphery, either by cell migration or proliferation, in the time it takes before reactive BECs are seen throughout the tissue (Figure 3.6). This dissuades the idea that the new BECs are arising from the existing Albumin-Cre derived IHBDs. Similarly, the observation that the first peripheral appearing $Sox9^+$ $CK19^+$ BECs that form reactive ductules emerge within the parenchyma, not juxtaposing differentiated DBA^+ hilar IHBDs, strongly indicates that the BECs of the ductular reaction are arising through a *de novo* differentiation process and not originating from pre-existing formed hilar IHBDs (Figures 3.7, 3.8).

A remaining possibility is that the new BECs arise from Albumin-Cre derived hepatocytes. This idea is supported by two observations. First, the BECs contributing to the ductular reaction and the regenerated peripheral IHBDs do not express Rbpj and Hnf6 protein. Second, we observe expression of Sox9, a biliary and progenitor cell marker, in intermediate $Hnf4\alpha^+$ cells of the DKO liver (Figure 3.11). Sox9 has previously been shown to be an early marker of interlineage conversion (Yanger et al., 2013) and may mark cells beginning a conversion process in the

DKO model as well. Indeed, new peripherally localized BECs are found in areas dense with $Sox9^+$ cells that do not express CK19 (Figure 3.7, white arrowheads). Therefore, it remains formally possible that the $Sox9^+$ intermediate cells give rise to the new $CK19^+$ BECs.

The combined loss of Rbpj and Hnf6 has a synergistic effect on the injury condition that may be crucial for the observed regenerative response.

The liver-specific single deletion of *Rbpj* (Rbpj KO) decreases the number of IHBD branches, and no recovery in IHBD branch number was found to occur with age in that model (Sparks et al., 2011). We propose three explanations for the difference in regenerative capacity between Rbpj KO and DKO mice: 1. The more severe degree of hepatic injury observed in DKO mice is required to induce the proper stimulus or signal to drive adult IHBD regeneration; 2. The Rbpj KO mice undergo a low level of IHBD regeneration and replenishment that is below the resolution of our previous resin cast microCT analysis (20μm limitation) (Sparks et al., 2011); or 3. The absence of Hnf6 in a Notch deficient background is required for adult IHBD regeneration. The presence of $Sox9^+$ intermediate cells in Rbpj KO mice (Jeliazkova et al., 2013) (T.J.W. and S.S.H., unpublished) indicates that the absence of Hnf6 is not required for the emergence of intermediate cells, but it remains possible that Hnf6 functions to inhibit later stages of IHBD regeneration. Interestingly, hepatic Hnf6 levels have been found to decrease after bile duct ligation in mouse, and forced overexpression of Hnf6 inhibits IHBD regeneration through decreasing BEC proliferation (Holterman et al., 2002). Thus, Hnf6 may potentially play an active role in mediating IHBD regeneration. This is an active area of investigation in our laboratory. At this time, we cannot rule out any of these explanations with certainty.

De novo BEC differentiation may be a common and targetable phenomenon in human liver disease and regeneration.

The occurrence of $Sox9^+$ intermediate cells in human liver disease samples has previously been observed in cases of hepatocellular injury and fibrosis (Yanger et al., 2013). These findings indicate that the intermediate cells seen in the DKO mouse model may be a common feature of cholestatic liver diseases (Figure 3.1), situations of IHBD regeneration, and are especially relevant to the Notch-associated disease ALGS (Oda et al., 1997). Histopathological studies have shown that ALGS patients display large accumulations of intermediate "hepatobiliary" cells which co-express hepatocyte and BEC markers (Desmet, 2011; Fabris et al., 2007; Roskams et al., 2003). Additional studies will be required to determine whether $Sox9^+$ intermediate cells correlate with ALGS disease severity or outcome.

To date, Hnf6 mutations have not been found to contribute to ALGS. However, the loss of Hnf6 greatly increases the severity of injury caused by Rbpj deletion in mouse liver (Vanderpool et al., 2012). This finding may reflect how epigenetic changes of Hnf6, and/or genetic or epigenetic changes of other liver genes, could modulate Notch loss in ALGS patients and influence disease severity between patients. Further detailed analysis will be required to characterize the role of other genes in modulating the varied disease severity and recovery in ALGS patients.

Our findings in DKO mice demonstrate that new BECs may be able to alleviate cholestasis in patients with ALGS despite the persistent Notch impairment. Hopefully, further investigation on the potential of intermediate cells in mice and more in depth studies analyzing human tissues will identify alternate signaling mechanisms that may be utilized therapeutically to drive Notch-independent IHBD regeneration in patients, especially given the potential cholangiocellular carcinogenic outcome of Notch over-activation (Fan et al., 2012; Sekiya and Suzuki, 2012).

CHAPTER 4

HEPATOCYTE IDENTITY RESPONSE IS BASED ON THE NATURE OF THE LIVER INJURY

Introduction

The liver has an incredible capacity for regeneration; in rats, 2/3 of the liver can be removed and within 5 to 7 days, it will return to its original mass (Michalopoulos and DeFrances, 1997). In this model of acute liver injury, “regeneration” occurs through the compensatory growth of the remaining liver tissue and involves the proliferation of all existing mature cell types in the liver (Michalopoulos and DeFrances, 1997). However, the innate ability of the liver to regenerate is frequently compromised in situations of chronic liver disease. The use of cell-based therapies to aid liver regeneration and avoid transplantation would be an important therapeutic advance in the treatment of liver disease.

Different liver injuries and diseases can be highly variable in the pathological manifestation and course of progression and/or regeneration. Before we can explore and utilize cell-based therapies for treatment of hepatobiliary diseases, we must classify the different and temporal cellular responses inherent to specific liver disease types. This will provide a foundation for using cell markers for diagnostic and prognostic purposes and also allow for the identification of the most appropriate *in vivo* models for studying human liver disease progression.

Several groups have previously demonstrated the differential cellular response in different rodent liver injury models (Español-Suñer et al., 2012; Malato et al., 2011; Yanger et al., 2013). Lineage-tracing studies have demonstrated that biliary epithelial cell (BEC)-to-hepatocyte conversion occurs in response to a choline-deficient diet supplemented with ethionine (CDE),

but not in response to 2/3 partial hepatectomy (PHx), carbon tetrachloride (CCl_4) administration, or 3,5-diethoxycarbonyl-1,4-dihydrocollidine (DDC) feeding (Español-Suñer et al., 2012). On the other hand, studies have provided contradictory data as to whether hepatocyte-to-BEC conversion occurs in response to several liver injury models, including 2/3 PHx, bile duct ligation (BDL), and DDC feeding (Malato et al., 2011; Yanger et al., 2013). These studies indicating different regenerative responses in different liver injury models, as well as the ensuing conflict in the field regarding the degree of hepatic interlineage conversion between hepatocytes and cholangiocytes during liver injury, demonstrate the need for further study of specific cell markers in different injury models.

The investigation of human pathological samples has demonstrated that the variation in cellular response to different injuries extends to human liver disease (Fabris et al., 2007; Falkowski et al., 2003; Gouw et al., 2011). For example, although the pediatric diseases Alagille syndrome (ALGS) and biliary atresia (BA) are both characterized by ductopenia and cholestasis, the cellular responses to these injuries are highly varied: BA is characterized by a pronounced ductular reaction not observed in AGS while AGS patient samples show a much higher number of “intermediate hepatobiliary cells,” displaying markers of both hepatocytes and BECs, than BA patient samples (Fabris et al., 2007). The differences observed in these otherwise phenotypically similar human diseases suggest that the same cellular observations could mean different phenomena in terms of diagnosis and prognosis, and that the mechanism of hepatic cell renewal or regeneration occurs differently in these different human liver diseases.

At this point in time, the functional significance of intermediate hepatobiliary cells in liver disease is unknown. Alagille syndrome patients have varying disease severities and outcomes, and cellular indicators like intermediate hepatobiliary cells have the potential to be helpful in disease prognosis; however, no thorough studies have characterized the normal disease progression in

terms of intermediate cell presence or attempted to correlate intermediate cell presence with disease severity or outcome. As such, we cannot be sure if the presence of intermediate hepatobiliary cells is a positive indicator, indicating cellular reprogramming to generate new BECs, or a negative indicator, indicating a complete block in the BEC-differentiation process. If markers of cellular fates and responses are to be useful for clinical diagnostic and prognostic purposes, we must fully understand the temporal response of the cellular markers over the course of the injury and their prognostic meaning, if any. Similarly, if we intend to target *in vivo* progenitor therapies to treat human liver diseases, we must fully understand the origin and differentiation potential of possible progenitor cells such as intermediate hepatobiliary cells. Mouse and rat models will be essential to probe these important questions; however, the field with new lineage-tracing tools is just beginning to thoroughly investigate the cellular responses and contributions in different rodent liver injuries.

Hepatocyte-to-BEC transdifferentiation has also been demonstrated to occur in several liver injury models and suggested to occur by marker analysis in human disease through a process by which hepatocytes begin to co-express biliary markers (Español-Suñer et al., 2012; Limaye et al., 2008a; Limaye et al., 2010; Yanger et al., 2013). One marker that has been found to denote cells undergoing the hepatocyte-to-BEC reprogramming is Sox9(Yanger et al., 2013), a protein that has received recent attention as a possible stem/progenitor cell marker in the developing and adult liver (Carpentier et al., 2011; Dorrell et al., 2011). As an early marker of hepatocytes undergoing conversion to BECs, and identifying cells with bipotential and clonogenic potentials in culture (Dorrell et al., 2011; Yanger et al., 2013), Sox9 has a high potential for being an important marker of liver regeneration and also of hepatic interlineage conversion and regenerative progress.

This study attempts to address a portion of the required in depth characterization of liver injury models by investigating the temporal response of Sox9 expression in a variety of commonly utilized acute and chronic rodent liver injury models. Examining the presence of $Sox9^+$ hepatocytes or progenitor cells over time in hepatocyte proliferation-competent and non-competent rodent liver injury models will help to better understand the cellular response. We find that $Sox9^+CK19^-$ and $Sox9^+Hnf4\alpha^+$ cells appear after DDC and BDL injuries in mouse but not after PHx in mouse or 2-acetylaminofluorene (2-AAF)/PHx in rat. This indicates that there are different cellular responses to different injury models in rodents. Of note, the activation of a ductular reaction does not appear to be directly related to the appearance of $Sox9^+CK19^-$ and $Sox9^+Hnf4\alpha^+$ cells. In the 2-AAF/PHx model, in which hepatocyte proliferation was fully impaired, $Sox9^+CK19^-$ and $Sox9^+Hnf4\alpha^+$ cells were not observed coincident with the ductular reaction. Specifically, activation of Sox9 expression in hepatocytes was observed in the models of cholestasis, DDC and BDL. $Sox9^+CK19^-$ and $Sox9^+Hnf4\alpha^+$ cells were found to display low rates of proliferation. Similar to rodent injury models, we observed $Sox9^+CK19^-$ and $Sox9^+Hnf4\alpha^+$ cells in a variety of liver samples from patients with cholestatic liver disease: AGS, BA, primary biliary cirrhosis (PBC), and primary sclerosing cholangitis (PSC). The extent of $Sox9^+CK19^-$ and $Sox9^+Hnf4\alpha^+$ cells varied widely between the samples assayed. Therefore, a thorough examination of each human disease will have to be performed to assess if the presence $Sox9^+CK19^-$ and $Sox9^+Hnf4\alpha^+$ cells correlate to disease stage, severity, and/or prognosis.

Results

SOX9 expression is activated in Hnf4α^{+} and CK19^{-} cells in cholestatic human liver disease.

To first assess the expression of SOX9 in several human cholestatic liver diseases, we performed immunofluorescence for Sox9 protein in human patient liver samples of AGS, BA, PBC, and PSC. Previous studies have found that within the normal human liver, SOX9 is expressed exclusively within BECs (Furuyama et al., 2011). We found the expression of SOX9 in all four liver diseases we examined. To characterize the lineages of the cells that express SOX9, we performed co-immunostaining with the BEC marker CK19 (Figure 4.1A-D) or the human hepatocyte marker HepPar1 (Figure 4.1E-H). In all samples, Sox9 expression was found within CK19^{+} BECs and also within cells that express HepPar1 and do not express CK19, resembling hepatocytes. Nevertheless, there is variation in the extent of SOX9 expression between individuals diagnosed and tissue examined with the same disease. Additionally, there is a difference in the presence of ductular reactions between the different types of human cholestatic liver disease. A ductular reaction was observed in the PSC sample but not in the other three types of cholestatic liver disease. Previous work has found the expression of SOX9 in other non-cholestatic liver diseases, including Joubert's syndrome, chronic Hepatitis C Virus infection, and INH-induced massive hepatic necrosis (Yanger et al., 2013). Taken together, these results indicate that the expression of SOX9 in hepatocytes may be a common feature of human liver diseases.

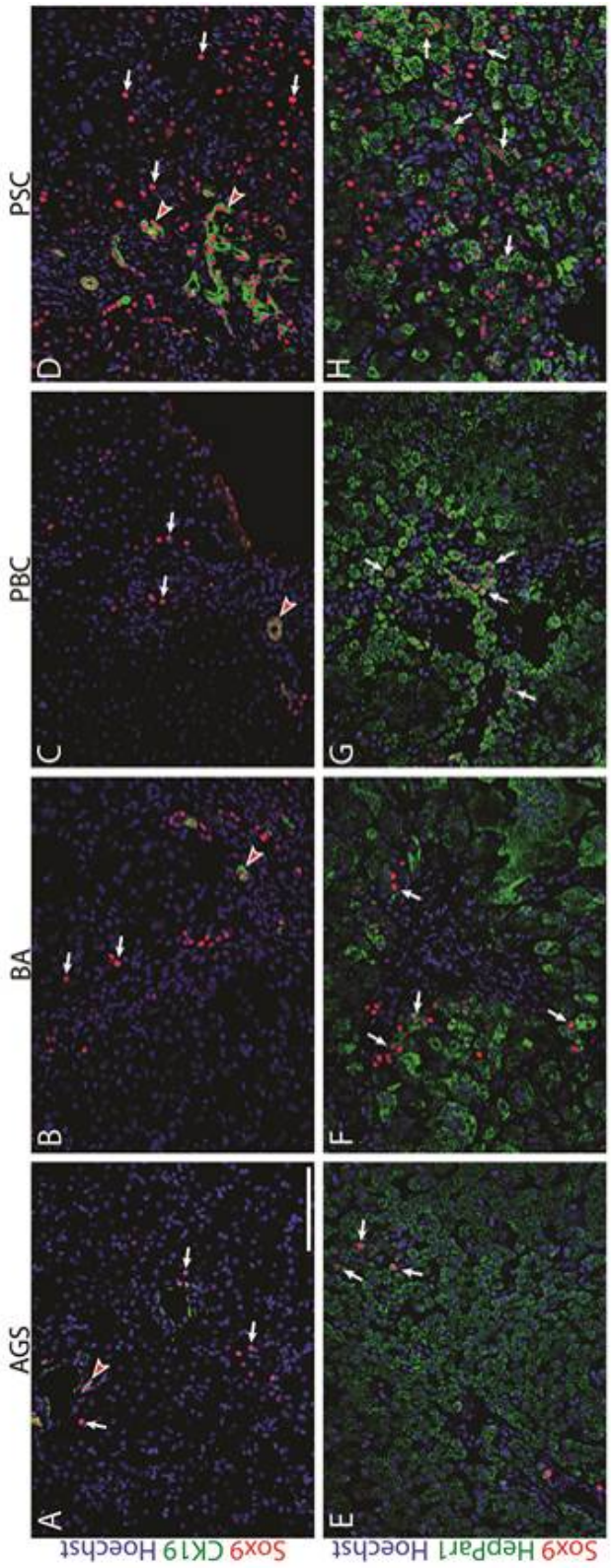
AGS
BA
PBC
PSC
A
B
C
D
E
F
G
H
Sox9 CK19 Hoechst
Sox9 HepPar1 Hoechst

Figure 4.1. Figure 7: Sox9+ "intermediate" cells are observed in human cholestatic liver diseases. Human liver tissue samples from patients with AGS (A,A'), BA (B,B'), PBC (C,C'), and PSC (D,D') were immunostained for Sox9 (red), CK19 or the hepatocyte marker HepPar1 (green), and Hoechst (blue). In AGS, BA, PBC, and PSC liver samples, Sox9+ cells were present that morphologically resembled hepatocytes, did not express CK19, and co-expressed HepPar1 (arrows). Sox9+CK19+ BECs in IHBDs were also present (red arrowheads). Scale bar is 100 um.

Sox9 expression is activated in Hnf4α^{+} co-expressing hepatocytes in response to cholestasis-inducing liver injuries.

To determine whether hepatocyte expression of Sox9 is a general liver injury response, we characterized the response of Sox9 expression in several injury models, including PHx in mice, 2-AAF/PHx in rats, BDL in mice, DDC feeding in mice, and RRV injection in mice. BDL and DDC both induce chronic cholestatic injury, while PHx provides an acute injury model. The treatment of 2-AAF prior to PHx suppresses hepatocyte proliferation, providing a model of hepatocyte impairment. Finally, RRV injection provides a model of neonatal immune-induced obstructive cholestasis similar to biliary atresia.

To examine the expression of Sox9 in the rodent liver injury models, we performed co-immunostaining for Sox9 and either CK19 (Figure 4.2) or Hnf4α (Figure 4.3). Intermediate timepoints at which there was a response to injury were chosen for DDC, PHx, BDL, and 2-AAF/PHx based on previous literature (Apte et al., 2008; Campbell et al., 2004; Ohno-Matsui et al., 2002; Preissegger et al., 1999; Shteyer et al., 2004) and our own analysis of injury progression. In DDC and BDL injuries, Sox9^{+}CK19^{-} and Sox9^{+}Hnf4α^{+} cells were found that morphologically and histologically resemble hepatocytes. These cells are loosely localized to periportal zones. However, Sox9^{+}CK19^{-} and Sox9^{+}Hnf4α^{+} cells were not found in either PHx or 2-AAF/PHx injuries. In the RRV injury, Sox9^{+}CK19^{-} and Sox9^{+}Hnf4α^{+} cells were observed around portal veins. However, as these early postnatal mice are still undergoing the final stages of ductal plate morphogenesis, it is not possible to definitively discriminate between injury-induced cells and those that appear normally during the process of ductal plate morphogenesis.

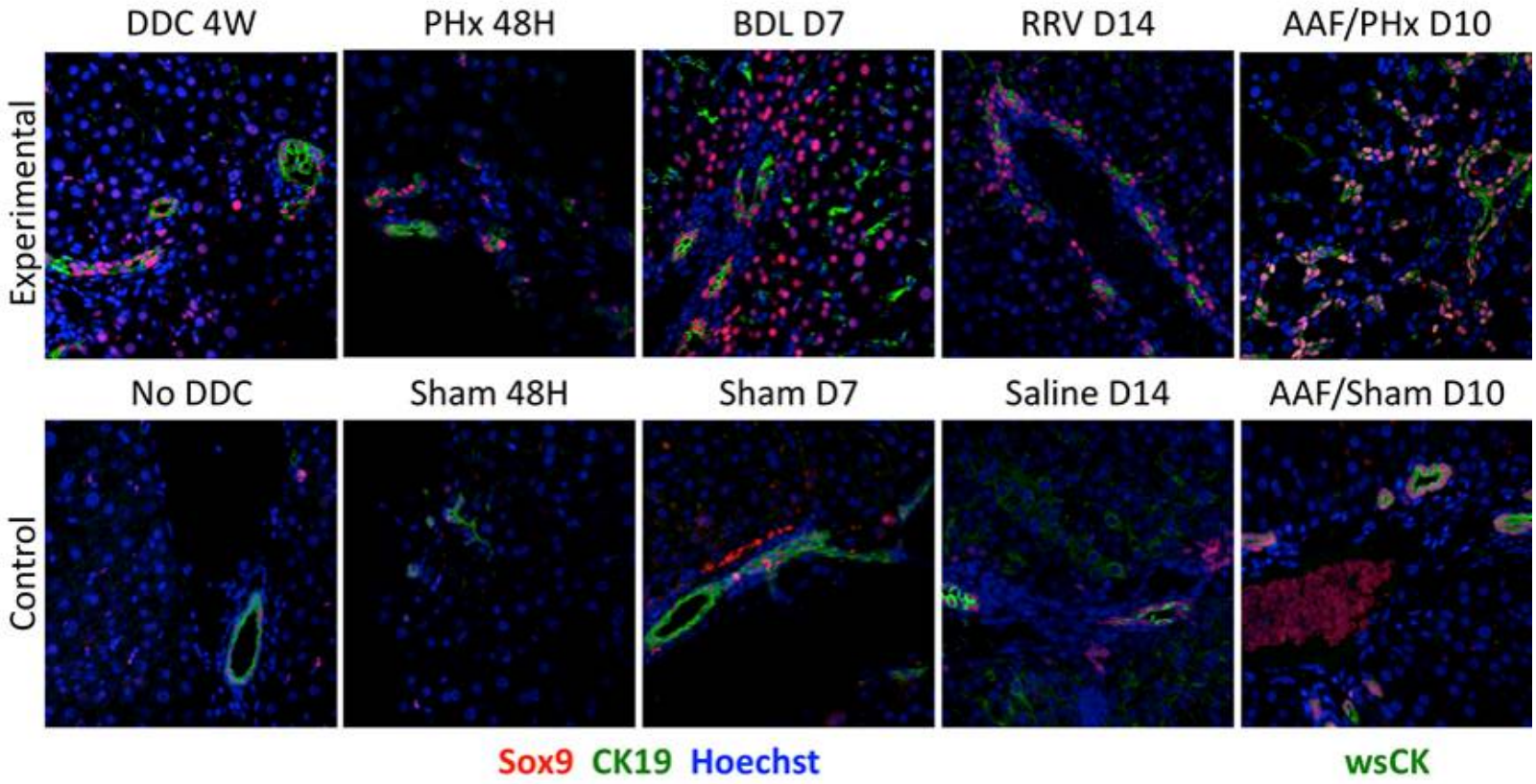
DDC 4W
PHx 48H
BDL D7
RRV D14
AAF/PHx D10
Experimental
No DDC
Sham 48H
Sham D7
Saline D14
AAF/Sham D10
Control
Sox9 CK19 Hoechst
wsCK

Figure 4.2. Expression of Sox9 in CK19$^-$ cells occurs in some but not all liver injury models. Mouse (A-D, F-I) and rat (E, J) livers were subjected to various injuries: DDC feeding (A), 2/3 PHx (B), BDL (C), RRV injection (D), and AAF feeding followed by 2/3 PHx (E). Uninjured control livers were also examined (F-J). Liver sections were stained for Sox9 (red), CK19 (green), and Hoechst (blue). Sox9$^+$CK19$^-$ cells are observed in DDC feeding (A) and BDL (C) and but in PHx (B) and AAF/PHx (E). Some Sox9$^+$CK19$^-$ cells were observed in RRV-injected livers around the portal vein (D), but due to the age of these mice, the cells could not be definitively distinguished from normally-occurring ductal plate cells, which appear in saline-injected mice as well (I). Scale bar is 100 μm

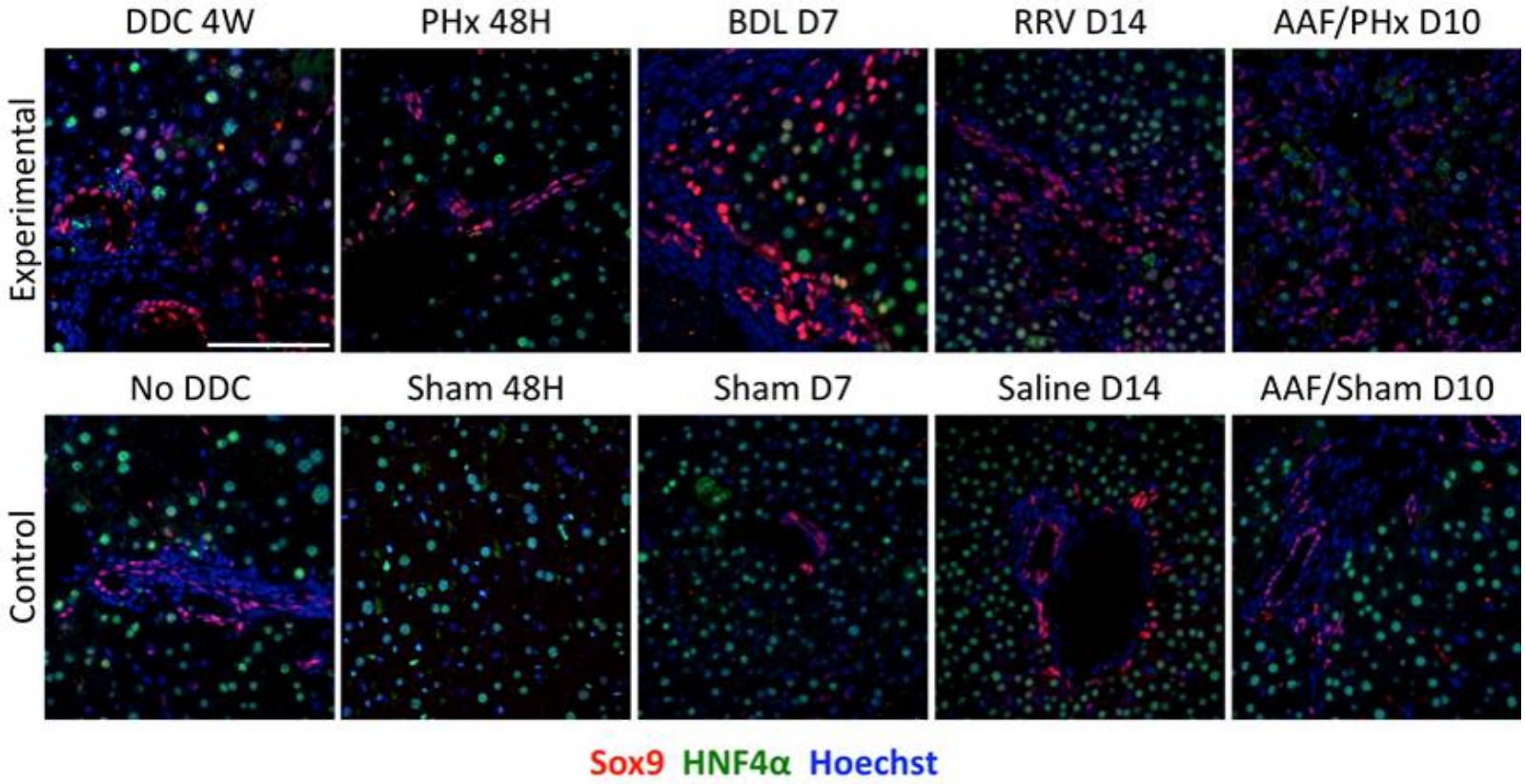
DDC 4W
PHx 48H
BDL D7
RRV D14
AAF/PHx D10
Experimental
No DDC
Sham 48H
Sham D7
Saline D14
AAF/Sham D10
Control
Sox9 HNF4α Hoechst

Figure 4.3. Co-expression of Sox9 and Hnf4α is observed in chronic cholestatic liver injuries but not in acute injuries or hepatocyte injuries. Mouse (A-D, F-I) and rat (E, J) livers were subjected to various injuries: DDC feeding (A), 2/3 PHx (B), BDL (C), RRV injection (D), and AAF feeding followed by 2/3 PHx (E). Uninjured control livers were also examined (F-J). Liver sections were stained for Sox9 (red), Hnf4α (green), and Hoechst (blue). Sox9 expression is observed in Hnf4α co-expressing cells in livers subjected to DDC feeding (A), BDL (C), or RRV injection (D). In control uninjured livers (F-J), $Sox9^{+}Hnf4\alpha^{+}$ co-expressing cells are very rarely observed. No increase in $Sox9^{+}Hnf4\alpha^{+}$ co-expressing cells was observed in PHx (B) or AAF/PHx (E) injury models. Scale bar is 100 μm.

At no time after PHx are Sox9$^+$CK19$^-$ and Sox9$^+$Hnf4α$^+$ cells present.

Following PHx, a model of acute injury in the liver, the hepatic cells rapidly expand in number to replace the lost mass. During this process, hepatocyte mass is recovered through the proliferation of previously-differentiated hepatocytes. Lineage-labeling studies suggest that PHx does not result in the interlineage conversion of hepatocytes to BECs or vice versa (Malato et al., 2011). To test whether Sox9$^+$CK19$^-$ and Sox9$^+$Hnf4α$^+$ cells occur at any point during the injury and recovery from PHx, we analyzed a timecourse post-PHx injury. We assessed mice at 12 hours, 24 hours, 36 hours, 3 days, 7 days, and 14 days after PHx (Figure 4.4). These timepoints cover an initial change in gene expression and normalization (Shteyer et al., 2004), timepoints of peak proliferation, and recovery of liver mass (Factor et al., 1997; Jungermann and Keitzmann, 1996; Shteyer et al., 2004). At no point during this timecourse did we see an increase in Sox9$^+$CK19$^-$ and Sox9$^+$Hnf4α$^+$ cells over sham levels. A very small number of rare Sox9$^+$Hnf4α$^+$ cells are observed in control liver tissue, but PHx did not cause any increase in this cellular compartment.

Sox9$^+$CK19$^-$ and Sox9$^+$Hnf4α$^+$ cells appear rapidly and persist after BDL injury.

BDL, a model of human chronic obstructive cholestatic liver disease, causes a toxic accumulation of bile acids subsequently causing hepatocyte apoptosis, fibrosis, and proliferation of BECs and hepatocytes (Bai et al., 2012; Miyoshi et al., 1999; Prado et al., 2003). There is some evidence that BDL injury causes a small number of hepatocytes to undergo interlineage conversion and become BECs (Yanger et al., 2013) and contribute to reactive ductules. To characterize the Sox9 expression in response to BDL, we analyzed intrahepatic tissue at 7 days, 14 days, and 21 days after BDL (Figure 4.5).

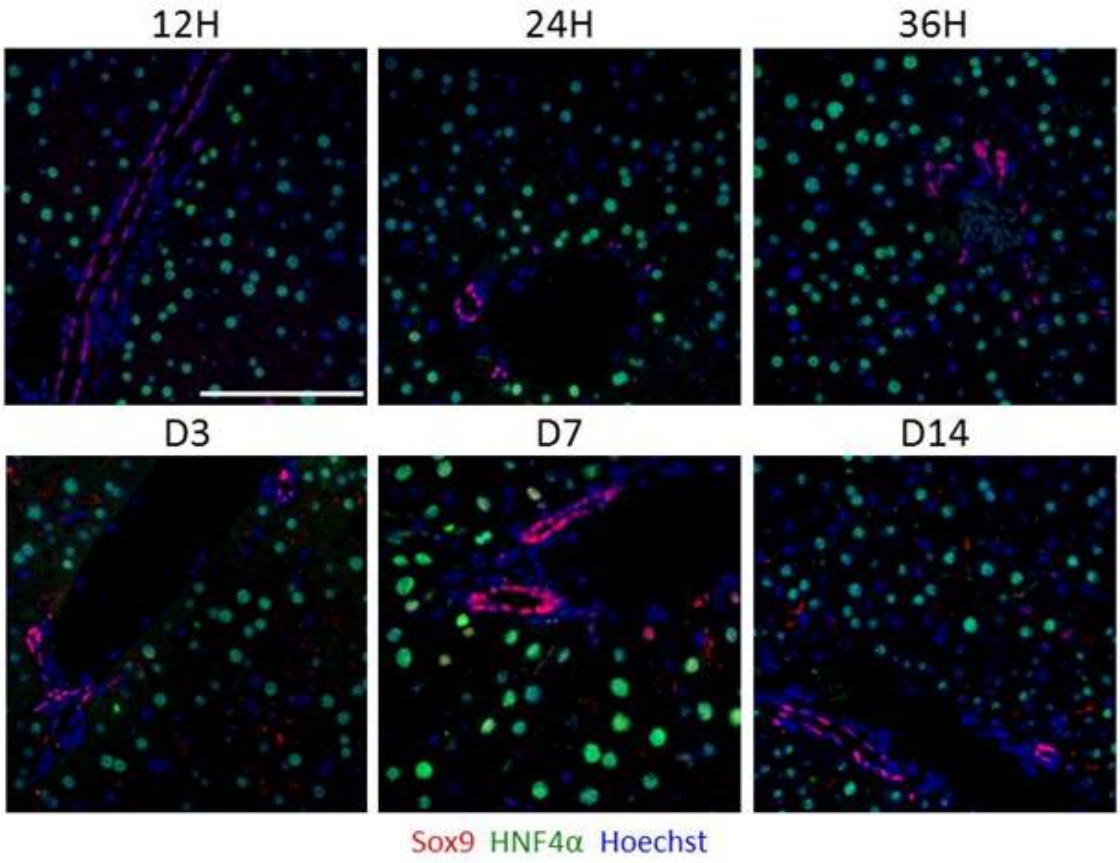

Figure 4.4. Sox9⁺Hnf4α⁺ co-expressing cells are not observed at any time after PHx injury. Mouse livers were subjected to 2/3 PHx and analyzed after 12 hours (A), 24 hours (B) 36 hours (C), 3 days (D), 7 days (E), and 14 days (F). Liver sections were stained for Sox9 (red), Hnf4α (green), and Hoechst (blue). Sox9⁺Hnf4α⁺ co-expressing cells were observed only very rarely and were not increased over the very low number observed in control sham liver tissue (Figure 2). Scale bar is 100 μm.

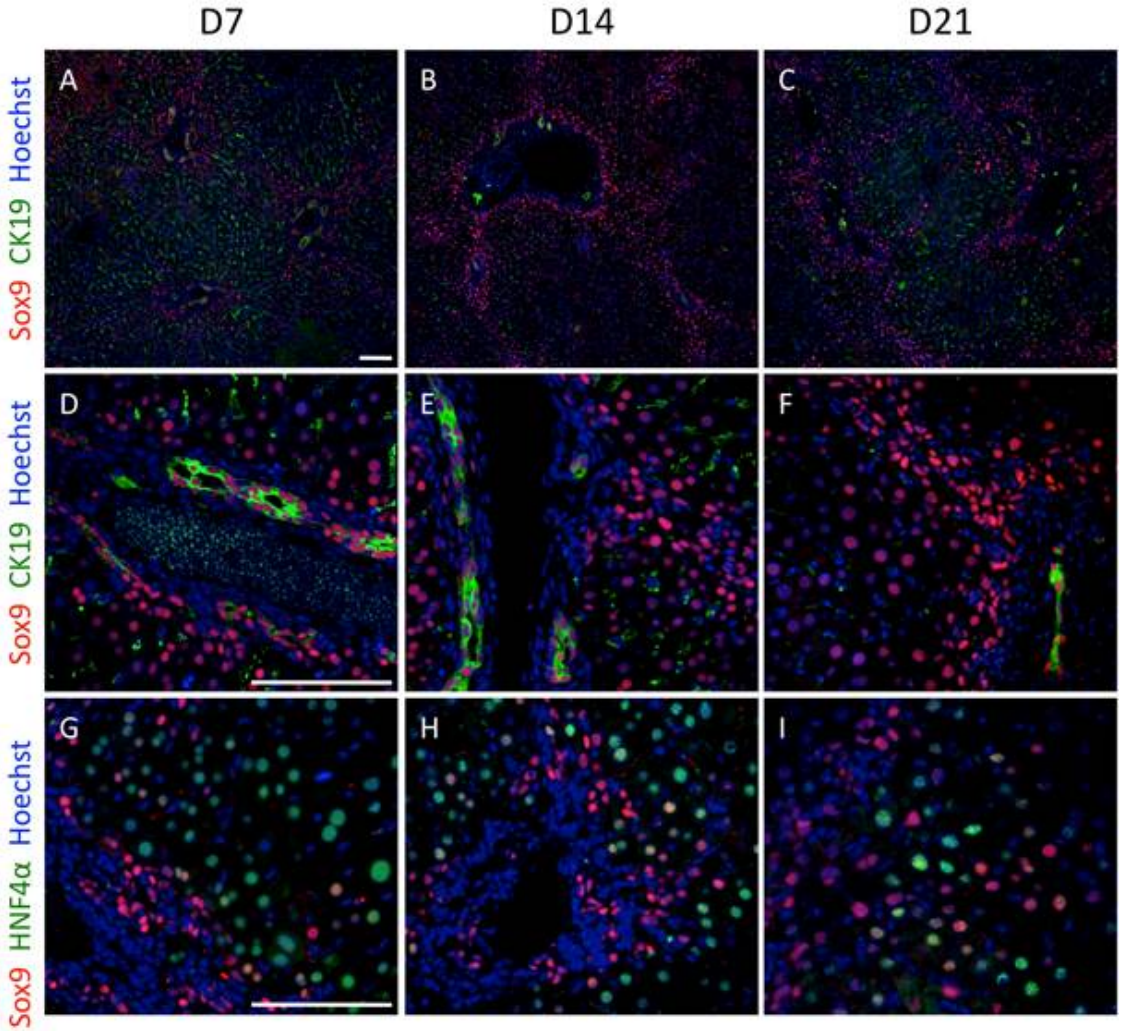

Figure 4.5. Increased Sox9 expression occurs quickly and persists after BDL. Mouse livers were subjected to BDL and analyzed after 7 (A,D,G), 14 (B,E,H), and 21 (C,F,I) days. Liver sections were stained for Sox9 (red), CK19 (A-F) or Hnf4α (G-I) (green), and Hoechst (blue). Some $Sox9^{+}CK19^{-}$ and $Sox9^{+}Hnf4\alpha^{+}$ cells were observed at 7 days after BDL (A,D,G) in periportal areas. The number of $Sox9^{+}CK19^{-}$ and $Sox9^{+}Hnf4\alpha^{+}$ cells further increased at 14 (B,E,H) and 21 (C,F,I) days after BDL. Scale bar is 100 μm.

$Sox9^+CK19^-$ and $Sox9^+Hnf4\alpha^+$ cells are visible in periportal areas by 7 days post-BDL (Figure 4.5A,D,G). At 14 (Figure 4.5B,E,H) and 21 (Figure 4.5C,F,I) day post-BDL, the number of $Sox9^+Hnf4\alpha^+$ cells increases and the cells are localized throughout the parenchyma. The cells still surround portal tracts and additionally extend throughout the parenchyma in tracks that bridge portal triads. In these bridging tracts, the cells begin to condense and morphologically resemble BECs in terms of their cell size and shape; however, they do not express CK19 and thus would not necessarily be considered mature BECs.

$Sox9^+CK19^-$ and $Sox9^+Hnf4\alpha^+$ cells progressively increase with time of DDC feeding injury.

DDC is a chemical-induced liver injury that models chronic cholestatic liver disease (Preisegger et al., 1999). DDC feeding induces the appearance of a ductular reaction, however, hepatocytes and cholangiocytes are still able to proliferate (Preisegger et al., 1999). During DDC treatment, reactive BECs are highly proliferative. To assess the progression of Sox9 expression over time during DDC injury, we performed co-immunostaining of Sox9 with either CK19 (Figure 4.6A-C) or Hnf4α (Figure 4.6D-F) at 3 days, 4 weeks, or 8 weeks of injury. During this time course, the extent of the ductular reaction progressively increases, such that no ductular reaction is observed at 3 days of DDC, but a profound ductular reaction is present after 8 weeks. After 3 days of DDC, there are a small number of $Sox9^+CK19^-$ and $Sox9^+Hnf4\alpha^+$ cells present around portal areas. The number of $Sox9^+CK19^-$ and $Sox9^+Hnf4\alpha^+$ cells increase over time and are higher after 4 weeks of injury and 8 weeks of injury.

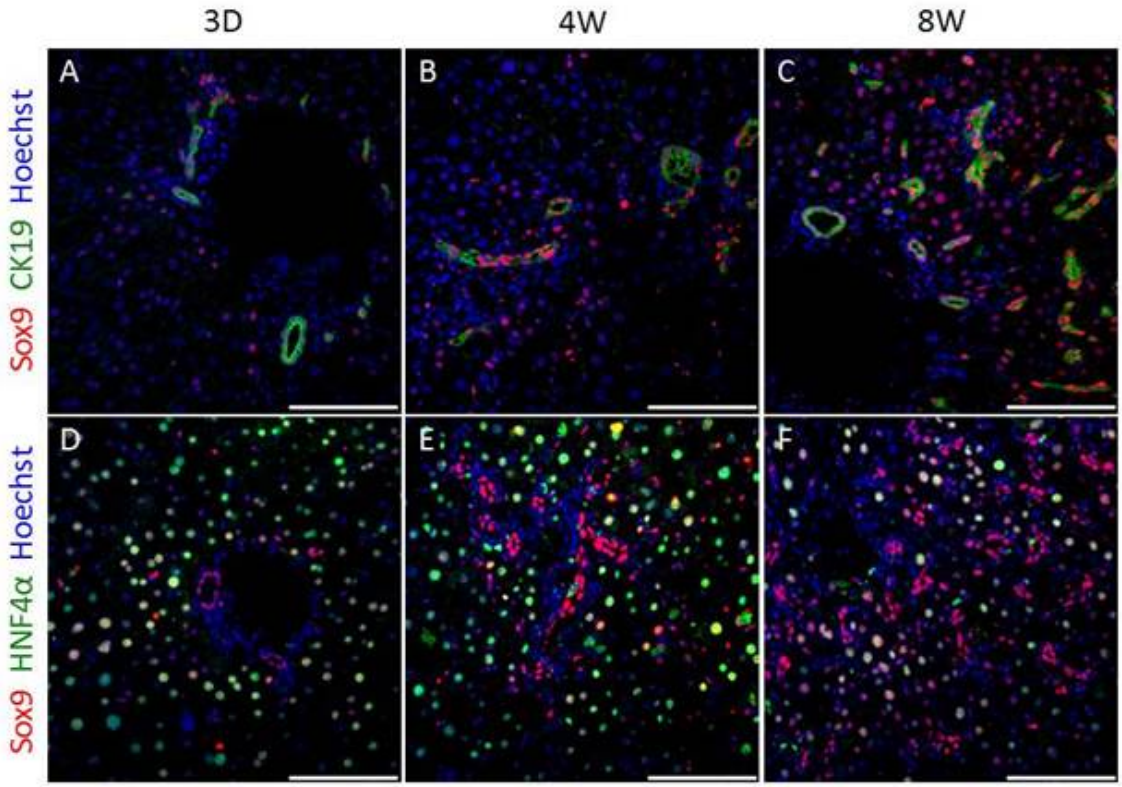

Figure 4.6. Sox9⁺Hnf4α⁺ hepatocytes increase with time during DDC treatment. Mouse livers were subjected to DDC feeding and analyzed after 3 days (A,D), 4 weeks (B,E), and 8 weeks (C,F). Liver sections were stained for Sox9 (red) CK19 (A-C) or Hnf4α (D-F) (green), and Hoechst (blue). Some Sox9⁺CK19⁻ and Sox9⁺Hnf4α⁺ cells were observed in periportal areas as early as after 3 days of treatment (A,D). The number of Sox9⁺CK19⁻ and Sox9⁺Hnf4α⁺ cells increased with longer treatment times at 4 weeks (B,E) and 8 weeks (C,F). After 4 and 8 weeks of treatment, expansion of Sox9⁺CK19⁺ cells in ductular reactions was also observed (B-C,E-F). Scale bar is 100 μm.

Sox9^{+}Hnf4α^{+} cells present in BDL and DDC injury are not highly proliferative.

To determine whether the large number of Sox9^{+}Hnf4α^{+} cells present after BDL injury may represent the expansion of a proliferative progenitor population, we assessed the expression of Sox9 and the proliferative marker Ki67 by dual-immunofluorescence (Figure 4.7). Intrahepatic proliferation was observed at the timepoints where a high number of Sox9^{+}Hnf4α^{+} cells are present in the liver post-BDL (Figure 4.5). However, proliferation was very rare in the prevalent Sox9^{+} cells at 7, 14 and 21 days post-BDL. This suggests that the Sox9^{+}Hnf4α^{+} cells are not highly proliferative, amplifying progenitors.

To determine whether the Sox9^{+}Hnf4α^{+} cells that appear during DDC injury represent an amplifying progenitor population, we performed co-immunostaining with Sox9 and Ki67 to assess the proliferative status of Sox9^{+}Hnf4α^{+} cells (Figure 4.8). At 7 days of DDC feeding (Figure 4.8A), there is very low proliferation both within Sox9^{+}Hnf4α^{+} cells and throughout the tissue. By 28 days of injury (Figure 4.8B), there is proliferation occurring in both hepatocytes and BECs; however, the very few Sox9^{+}Hnf4α^{+} cells are actively proliferating. These data indicate that Sox9^{+}Hnf4α^{+} cells that arise in a DDC injury model most likely do not constitute a rapidly amplifying progenitor population.

Sox9 expression in BECs is inversely correlated with proliferative status in uninjured mice during postnatal IHBD morphogenesis and homeostasis.

The finding that Sox9^{+} hepatocytes display very low rates of proliferation, despite proliferation in surrounding hepatocytes prompted us to wonder whether the expression of Sox9 had a fundamental correlation with proliferation, either through directly or

D1
D7
D14
D21
A
B
C
D
Sox9 Ki67 Hoechst

Figure 4.7. Sox9^{+}Hnf4α^{+} hepatocytes display very low proliferation during BDL injury. Mouse livers were subjected to BDL and analyzed after 1 (A), 7 (B), 14 (C), and 21 (D) days. Liver sections were stained for Sox9 (red), Ki67 (green), and Hoechst (blue). Proliferation is observed in the liver in response to injury at 7, 14, and 21 days. However, Sox9^{+}Hnf4α^{+} hepatocytes display a very low rate of proliferation at these timepoints, with almost all Sox9^{+}Hnf4α^{+} hepatocytes not co-expressing the proliferative marker Ki67. Scale bar is 100 μm.

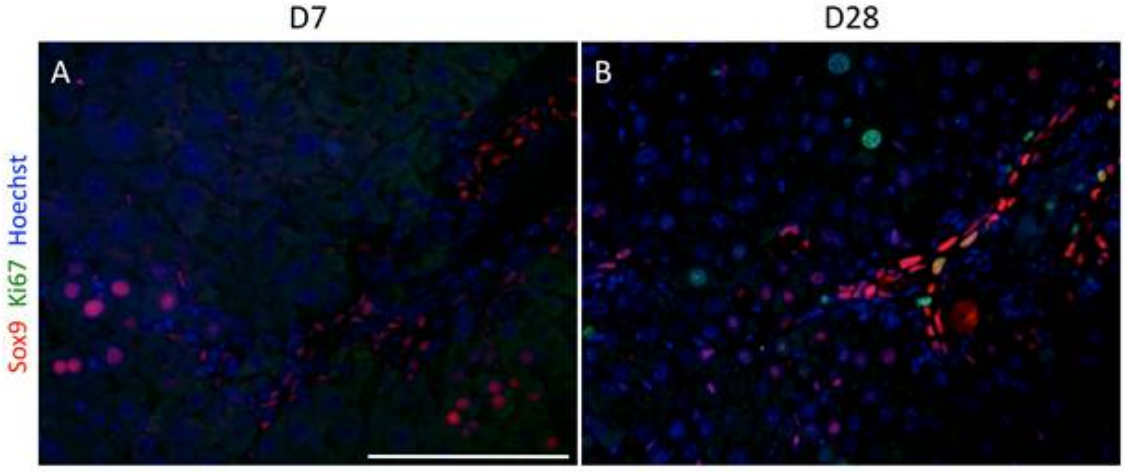

Figure 4.8. Sox9^{+}Hnf4α^{+} hepatocytes display very low proliferation during DDC injury. Mouse livers were subjected to DDC and analyzed after 7 (A) and 28 (B) days. Liver sections were stained for Sox9 (red), Ki67 (green), and Hoechst (blue). At 7 days, there is very low overall proliferation within the liver (A). By 28 days of treatment, there is proliferation observed in both BECs and hepatocytes (B). However, Sox9^{+}Hnf4α^{+} hepatocytes display a very low rate of proliferation at these timepoints, with almost all Sox9^{+}Hnf4α^{+} hepatocytes not co-expressing the proliferative marker Ki67. Scale bar is 100 μm.

indirectly decreasing proliferation or as a marker of a cellular subpopulation that has a different progenitor status or capacity for proliferation. To test the correlation between Sox9 and proliferation in non-injury conditions, we examined Sox9 and Ki67 expression in control postnatal mice in mature IHBDs (Figure 4.9). Previous work has demonstrated that during ductal plate morphogenesis, ductal plate cells that activate Sox9 expression do not proliferate despite the extremely high rates of proliferation in surrounding $Sox9^-$ hepatoblasts during embryonic development (Carpentier et al., 2011). At P3 and P15, proliferation, as marked by Ki67 expression, is observed within IHBDs. Interestingly, the cells that express Ki67 express relatively low or undetectable Sox9 protein as compared to the surrounding, non-proliferative BECs. This indicates that Sox9 correlates inversely within proliferating cells even in control, uninjured livers and in embryonic hepatoblasts (Carpentier et al., 2011), hepatocytes, and BECs. From this data, we cannot discriminate whether low levels of Sox9 may demarcate a permanent subpopulation of BECs that maintain proliferative capacities and are therefore able to act as progenitors, or Sox9 expression may be downregulated transiently during the cell cycle.

Sox9 is expressed surrounding nectrotic patches in multiple injury models.

Although $Sox9^+CK19^-$ and $Sox9^+Hnf4\alpha^+$ cells were not normally found in PHx injury, rare $Sox9^+$ cells that morphologically resemble hepatocytes surrounding the small number of necrotic patches in the liver (Figure 4.10A). This was also observed in RRV-injected livers (Figure 4.10B). The necrotic patches in both PHx and RRV injuries were in the middle of the parenchyma and not juxtaposing veins or bile ducts.

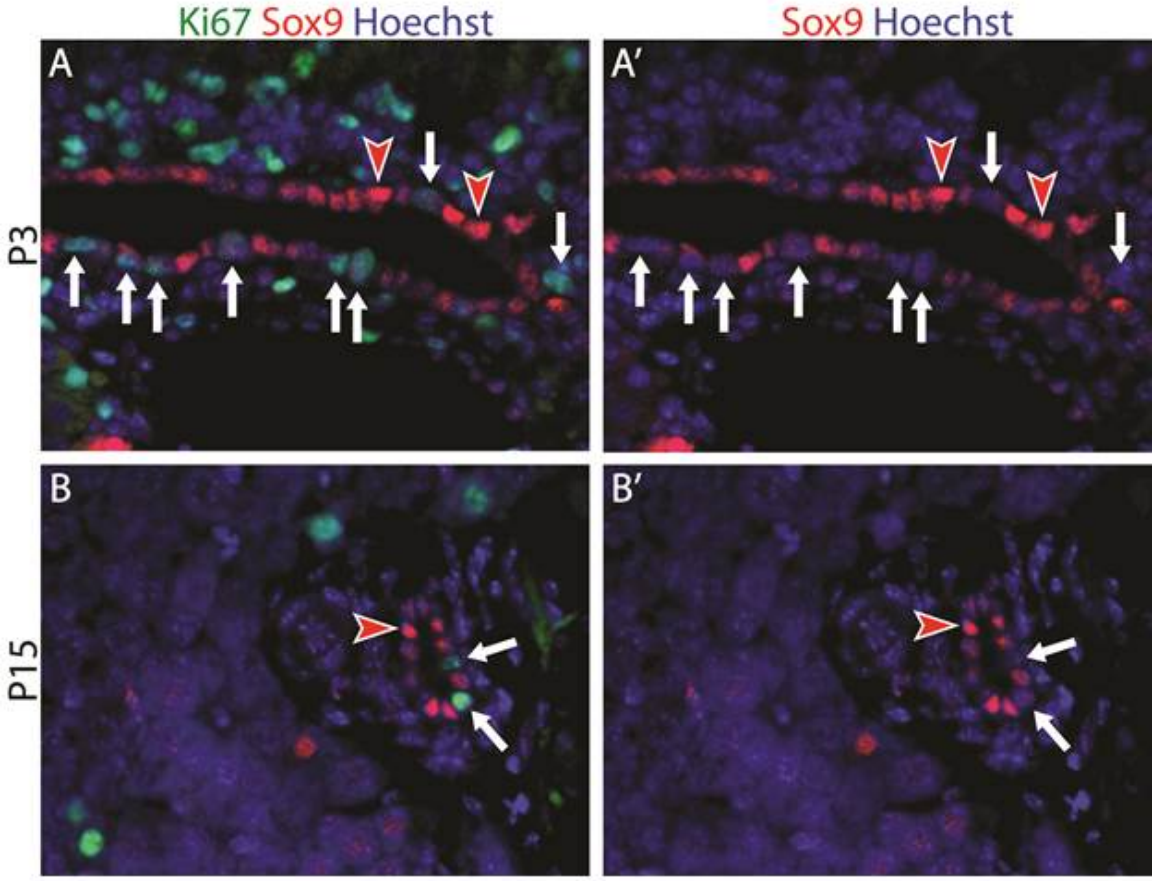

Figure 4.9: Sox9-expressing cells do not proliferate during IHBD morphogenesis and homeostasis. Liver sections of control mice were stained for Sox9 (red), Ki67 for proliferation (green), and Hoechst for nuclei (blue) at P3 (A), and P15. Sox9+ cells (red arrowheads) are observed within IHBDs at these postnatal timepoints. Within IHBDs, proliferating BECs (arrow) express low or undetectable levels of Sox9 relative to the non-proliferating Sox9+ BECs. A'-D' show Sox9 and Hoechst channels only. Scale bar is 50 um.

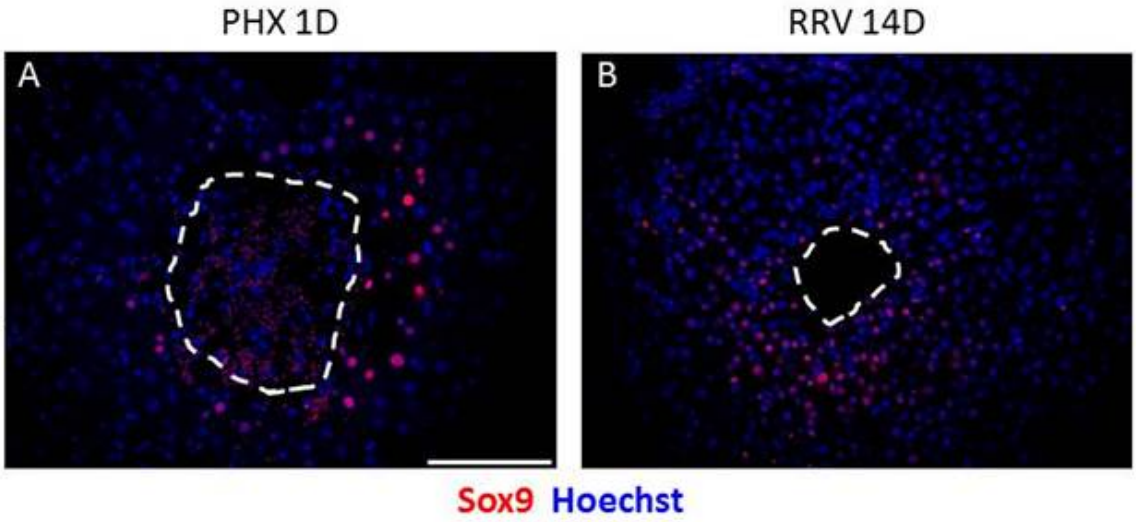

Figure 4.10. Sox9 is expressed surrounding necrotic patches in PHx and RRV injury models. Mice were subjected to 2/3 PHx (A) or RRV injection (B). Liver sections were stained for Sox9 (red) and Hoechst (blue). Sox9 expression is observed in cells surrounding areas of focal necrosis (dotted lines). Scale bar is 100 μm.

Conclusion

Expression of Sox9 in hepatocytes may be regulated by spatially-restricted signals or zones of competence.

Previous work has demonstrated that only specific zones of hepatoblasts and hepatocytes in mouse liver are competent to respond autonomously to Notch overactivation and to adopt a BEC fate (Jeliazkova et al., 2013; Sparks et al., 2010; Yanger et al., 2013). The cells that were competent to respond to Notch activation were found within hepatocyte zones 1 and 2, including the periportal and intermediate range hepatocytes, but not within zone 3, which is comprised of pericentral hepatocytes. This data aligns with the spatial restrictions of Sox9 expression observed in this study. In BDL, the injury model with the most widespread activation of Sox9, a very high number of cells turn on Sox9 but the spatial pattern of Sox9 is restricted; Sox9 is only expressed around portal tracts and in bridging tracts between portal tracts, leaving many areas devoid of any $Sox9^{+}$ cells (Figure 4.5).

This pattern may be the result of two possible causes: 1. Specific zones of hepatocytes may be competent and non-competent to respond to injury-derived signals and express Sox9, or 2. Specific signals that activate Sox9 expression may be spatially restricted and only reach hepatocytes within a certain distance of portal tracts. The second possibility may indicate that a specific protein signal is involved in the injury response and may derive from cells within the periportal regions, such as periportal mesenchyme or infiltrating immune cells.

Sox9^{+}Hnf4α^{+} cells do not represent highly proliferative amplifying progenitors.

The finding that very few Sox9^{+} cells that morphologically resemble hepatocytes are active in the cell cycle suggests that these cells do not constitute a population of transit rapidly amplifying progenitor cells. In both BDL (Figure 4.7) and DDC (Figure 4.8) injury models, Sox9^{+} hepatocytes cells display very low proliferation, consistent with direct lineage conversion instead of amplification of a progenitor.

The additional finding that Sox9 negatively correlates with the proliferative status of BECs in control animals indicates that the expression of Sox9 in non-proliferative hepatocytes may not be arbitrary; Sox9 may mark subpopulations of both hepatocytes and BECs, or hepatic progenitors, which have a lower proliferative capacity or some type of progenitor characteristic. Alternately, Sox9 may somehow directly or indirectly impede proliferation and may be transiently downregulated in cells undergoing proliferation.

Studies of Sox9's role in differentiation and proliferation in the liver and in other organs have yielded conflicting results (Delous et al., 2012; Ramalingam et al., 2012; Seymour et al., 2007). Both positive and negative correlations between Sox9 expression and patient tumor grade and survival have been found in gastroenterological tumors (Abdel-Samad et al., 2011; Guo et al., 2012; Mazur et al., 2012). In a recent study, an HPC population capable of clonal expansion and bipotential differentiation was found to be enriched for Sox9 expression (Dorrell et al., 2011). However, only 1 in 34 cells within this population had clonal expansion capacity; our findings would suggest that the uncommon proliferative progenitors may, in fact, be cells with low or absent Sox9 expression within the population.

The prevalence and expression pattern of Sox9 in response to liver injury varies between different human liver diseases and rodent liver injury models.

This study finds that Sox9 expression in Hnf4α^{+} and CK19^{-} cells occurs, but to different extents, in four different human cholestatic liver diseases, and in the mouse BDL and DDC injury models. This phenomenon is not a general liver injury response, as Sox9^{+}CK19^{-} and Sox9^{+}Hnf4α^{+} cells are absent from PHx and 2-AAF/PHx rodent injury models.

The variation in both human and rodent liver injuries could represent different mechanisms of injury and/or regeneration. Hepatocyte-to-BEC conversion has been previously suggested in human liver disease based on immunohistochemistry and demonstrated with lineage tracing in rodent liver injury models. We hypothesize, based on this and published studies, that the expression of Sox9 in hepatocytes marks cells undergoing the process of interlineage conversion. If this is so, these cells may only appear in situations where hepatocyte-to-BEC conversion is required for recovery, namely injuries that damage BECs and where BEC proliferation is not sufficient to recover from the injury. This would be consistent with presence of Sox9^{+}CK19^{-} and Sox9^{+}Hnf4α^{+} cells in BDL and DDC, where there is chronic cholestasis, but not in PHx, where proliferation alone is sufficient for recovery, or 2-AAF/PHx, where the primary injury is to the hepatocytes, not the BECs.

Lineage tracing experiments have previously demonstrated that different rodent liver injury models have different responses in terms of hepatocyte-to-BEC or BEC-to-hepatocyte transdifferentiation (Español-Suñer et al., 2012; Yanger et al., 2013). However, the current few works on lineage-tracing hepatocytes or BECs under different injury conditions has provided some conflicting results on whether, and in what injury models, transdifferentiation occurs (Español-Suñer et al., 2012; Malato et al., 2011; Yanger et al., 2013). Despite contradictions

between studies in specific injury models, there are strong findings within studies that different injuries produce different cellular responses in terms of interlineage conversion, either hepatocyte-to-BEC or BEC-to hepatocyte (Español-Suñer et al., 2012; Yanger et al., 2013).

Interestingly, in our BDL experimental paradigm, we find a large increase in the number of hepatocytes expressing Sox9, consistent with the idea that hepatocytes are undergoing a conversion into BECs. However, even at 21 days we see no evidence of a ductular reaction and the $Sox9^+$ hepatocytes do not express CK19 (Figure 5). While these cells may be undergoing a change in cell identity, we do not find any evidence suggesting that these cells do eventually complete the process of transdifferentiation and activate CK19 expression, specifically in the BDL model.

This study supports the previously published findings that different injury models elicit different cellular responses and that hepatocytes can adopt BEC-like identities in response to certain injuries (Yanger et al., 2013). We add information regarding the expression of Sox9 in hepatocytes ($CK19^-$ and $Hnf4\alpha^+$) over the progressive response of multiple injury models.

What remains unknown is how the expression of Sox9 correlates with disease progression, severity, and outcome in human patients. In both BDL and DDC injuries, the number of $Sox9^+CK19^-$ and $Sox9^+Hnf4\alpha^+$ cells were found to increase over time. Similarly, the expression of Sox9 in human liver disease could be used to assess disease progression or, similarly, extent of injury. Given that this study was performed on de-identified human tissue samples, the patient data is unknown. A thorough study of these human diseases tracking Sox9 expression over time in patients and correlating Sox9 expression with eventual disease outcome will be necessary in order to be able to use Sox9 as an informative disease marker.

As Sox9 has a potential role in defining intralineage cellular subpopulations it may have the potential to be used to promote progenitor cell or hepatocyte conversion toward a BEC fate in cholestatic diseases. Identifying the subpopulations marked by Sox9 and their specific properties and potentials for regeneration could inform future research on the specific cells with the highest therapeutic potential and serve as a regenerative marker in therapeutic testing in both rodents and humans.

CHAPTER 5

VASCULAR AND EPITHELIAL MORPHOGENESIS IN THE LIVER IS DEPENDENT ON EPITHELIAL-DERIVED VEGF SIGNALING

Introduction

VEGF signaling is an essential mediator of vascular growth and behavior in both development and disease. In the liver, the secretion of VEGF from hepatocytes and cholangiocytes is believed to play an important role in liver protection and regeneration (Ishikawa et al., 1999; Mancinelli et al., 2009; Shimizu et al., 2001; Taniguchi et al., 2001) but to also promote the progression of liver tumors (Marschall et al., 2001; Moon et al., 2003; Park et al., 2000). This communication between hepatocytes, cholangiocytes, and endothelial cells via VEGF must be understood and regulated in a context-specific manner in order to harness the beneficial impacts of VEGF.

The architecture of the hepatic vascular systems, including the portal vein (PV), hepatic artery (HA), and central vein (CV), are highly precise and stereotypic. It is unknown what signals regulate the architecture of these structures and whether signaling interactions between epithelial and endothelial tissues is crucial to generate the proper vascular patterning. Previous studies have suggested that an epithelial-endothelial VEGF signal from the intrahepatic bile duct (IHBD) is crucial for the development of the HA (Fabris et al., 2008; Morell et al., 2013). Interestingly, several human diseases also display correlated IHBD and vascular paucities, posing the question of how the epithelial and endothelial tissues may interact during development.

VEGF has previously been shown to be important for normal liver development during embryonic and early postnatal periods (Carpenter et al., 2005; Gerber et al., 1999). However, the studies conducted so far have utilized VEGF inhibition methods that ubiquitously block all VEGF signaling either globally in postnatal mice or specifically in the liver of embryonic mice. These methods inhibited the baseline level of signaling required for endothelial cell (EC) survival and homeostasis (Franco et al., 2011; Lee et al., 2007). It is unsurprising that these mice showed decreases in ECs. These studies also found reductions in vascular branching early in embryonic liver development, disorganized sinusoids, dismorphogenic liver sinusoidal endothelial cells (LSECs) and hepatocytes, and reduced lipid uptake into hepatocytes (Carpenter et al., 2005; Gerber et al., 1999). Due to the extreme impact on ECs in these mouse models, the studies conducted thus far have been unable to assess the role of VEGF in the growth and architectural establishment of the PV and HA.

In this study, we utilize a unique mouse model in which liver VEGF signaling is decreased but not completely deleted. We utilized a combination of the transgene *Tg(Alb-cre)*^{21Mgn} and the *Vegfa*^{tm2Gne} allele, *Albumin-Cre; Vegf*$^{flox/flox}$ (hereafter referred to as VKO), to delete VEGF from hepatoblast, bipotential liver progenitor, beginning at mid-gestation. This results in both hepatocyte and cholangiocyte deletion of VEGF. The production of VEGF from non-epithelial cells types is not impaired by this genetic deletion. This mouse model allows us to specifically address the question of whether the hepatic epithelium drives the architectural establishment and growth of the PV and HA through VEGF signaling.

We find that mice are able to survive for several weeks postnatally after mid-gestational deletion of VEGF from the hepatic epithelium, but do display abnormalities in both the epithelial and endothelial tissues. VKO mice show an initial reduction in endothelium in the liver, but recover

postnatally without concomitant elevation of hepatic or serum VEGF. However, these mice display a progressive impairment in the postnatal elaboration of the PV and HA and disruptions in the sinusoidal network and in LSEC identity. These changes correlate with hypoxia in the liver and to alterations in hepatic zonation and gene expression.

We conclude that secretion of VEGF specifically from the hepatic epithelium is required for the postnatal architectural development of the liver vascular systems and for proper hepatic oxygenation and hepatocyte zonal fates. Additionally, epithelial VEGF is required to maintain LSEC identity and function and for the postnatal phase of PV and HA elaboration.

Results

Hepatoblast-specific deletion of VEGF reduces total VEGF levels in the liver at embryonic and adult timepoints.

To determine the extent of VEGF protein reduction in VKO mice, VEGF protein levels in whole liver were analyzed through an ELISA assay. In control mice, the total liver VEGF was highest at embryonic day (E)16.5 and was significantly decreased at each subsequent timepoint (Figure 5.1). The levels of VEGF in the liver of VKO mice were significantly reduced as compared to control at all timepoints analyzed (Figure 5.1). VEGF protein in the VKO liver was reduced, as compared to control, 66.7% at E16.5, 36.3% at P3, 30.7% at P15, and 52.5% at P30.

To determine whether the loss of VEGF in the liver could influence systemic VEGF levels, perhaps to compensate for the hepatic loss of VEGF or as a result of decreased VEGF secretion from the liver into the bloodstream, we also measured VEGF protein in the blood serum. Similar to the pattern in the liver, serum VEGF protein in control mice was highest at the first timepoint measured, P3, and was significantly decreased at P15 and P30 (Figure 5.2). At P3 and P15, no change in serum VEGF protein levels between control and VKO mice. At P30, VKO mice exhibited a significant decrease in serum VEGF protein levels as compared to controls (Figure 5.2).

A

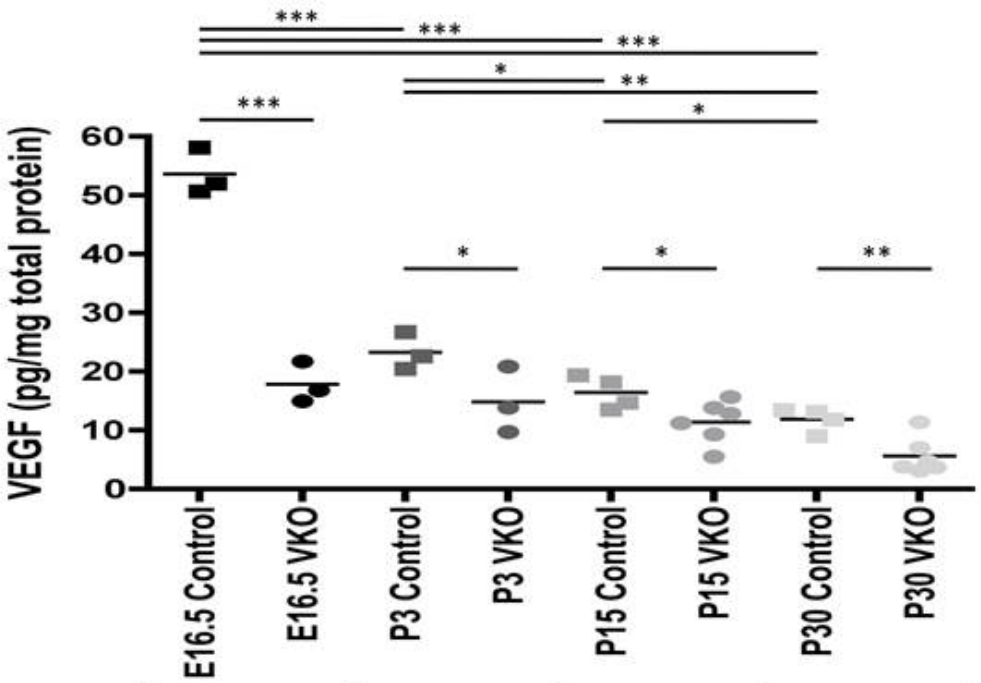

B

	E16.5		P3		P15		P30	
	Control	VKO	Control	VKO	Control	VKO	Control	VKO
VEGF protein (pg/mg total protein)	53.6	17.8	23.3	14.8	16.4	11.4	11.9	5.6
% decrease VEGF protein (Control vs VKO)	66.7%		36.3%		30.7%		52.5%	

Figure 5.1. VKO mice have decreased liver VEGF protein during embryonic and adult timepoints. VEGF protein levels in liver were analyzed by ELISA assay in embryonic and postnatal control and VKO genotypes. Measurements were performed in duplicate and standardized relative to total liver protein. A. Each square or circle represents one biological sample. In controls, liver VEGF levels were highest at E16.5 and decreased progressively over time. At E16.5, P3, P15, and P30, VKO mice have significantly less VEGF protein in the liver than littermate controls. B. The average VEGF protein concentrations in liver tissue are provided for control and VKO mice at all timepoints. The percentage reduction in relative VEGF protein levels between controls and VKO are shown for all timepoints. *$p<0.05$; **$p<0.01$; ***$p\leq0.001$.

A

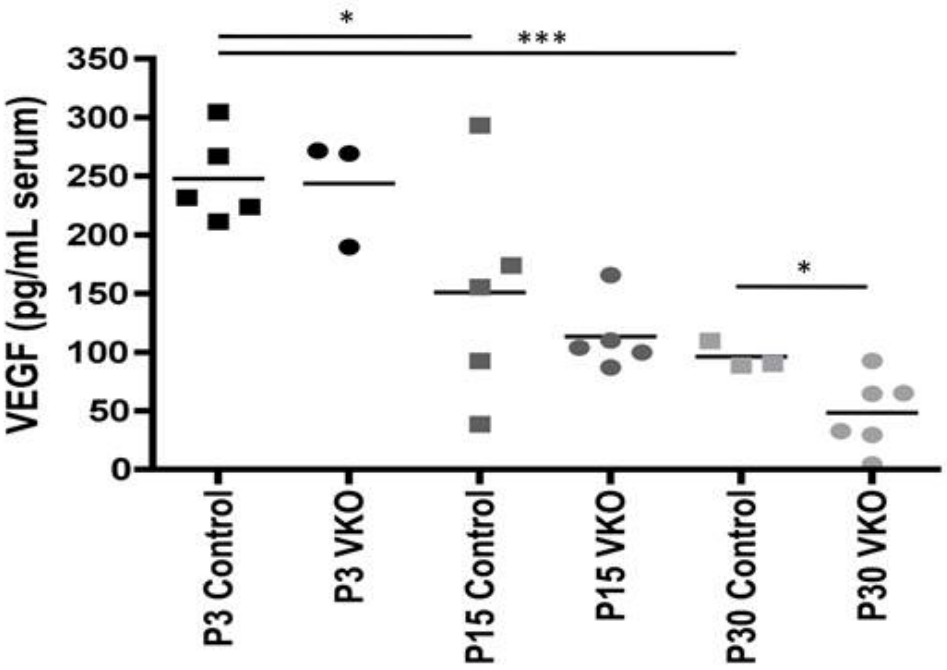

B

	P3		P15		P30	
	Control	VKO	Control	VKO	Control	VKO
VEGF protein (pg/mL serum)	247.7	243.6	150.8	96.2	96.2	48.3
% decrease VEGF protein (Control vs VKO)	No significant change		No significant change		49.8%	

Figure 5.2. There is no compensation in VEGF protein levels in serum of VKO mice. VEGF protein levels in serum were analyzed by ELISA assay for P3, P15, and P30 control and VKO mice. A. Each square or circle represents one mouse. In control mice, a progressive decrease in serum VEGF was observed over time. There was no significant difference in serum VEGF levels between control and VKO mice at P3 or P15. However, at P30, VKO mice display a significant reduction in serum VEGF as compared to controls. B. The average VEGF protein concentrations in serum are displayed for control and VKO mice at all timepoints. The percentage reduction in VEGF between controls and VKO mice is shown for all timepoints at which a statistically significant decrease was found. *$p<0.05$; ***$p\leq0.001$.

VKO mice display global phenotypes, including reduced body mass and indicators of hypertension.

To determine the global effect of the hepatoblast-specific loss of VEGF on mice, we allowed mice to age until P60 and measured body, liver, and spleen mass at several postnatal timepoints. Several VKO mice display poor health and lethality between P30 and P60. While some VKO mice have comparable body masses to their littermate controls, there was a significant decrease in body mass between sex-matched control and VKO mice at P30, P45, and P60 (Figure 5.3). Due to the high rate of lethality before P60, we only analyzed one female VKO mouse that exhibited a lower body mass than all P60 control females.

VKO mice at P30 and older timepoints displayed an obvious and consistent phenotype of peritoneal verices (data not shown). Blood vessels around the abdominal organs, including the stomach, intestine, and pancreas were enlarged. Occasionally, this phenotype was accompanied by death of the gut and/or a pink-toned pancreas, indicative of blood retention in the organ. Combined, these phenotypes can be indicative of hypertension.

To assess hypertension in VKO mice, we utilized the surrogate measurement of splenomegaly. At P30, P45, and P60, VKO mice displayed splenomegaly, having a significantly increased spleen:body mass ratio (Figure 5.3). This suggests that there is hypertension in VKO mice P30 and older. No differences in body mass or spleen:body mass ratio were observed in VKO mice P15 or younger (data not shown).

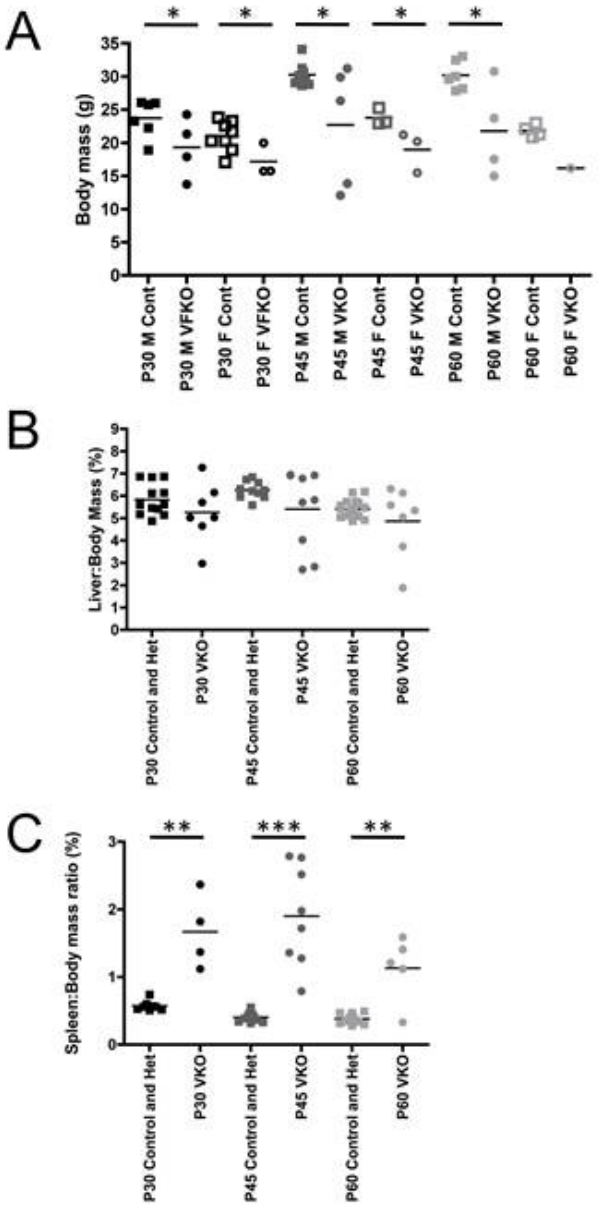

Figure 5.3. Adult VKO mice display decreased body mass and splenomegaly. The body mass and organ mass of P30, P45, and P60 control and VKO mice were measured, and the organ:body mass ratio was calculated for liver and spleen. A. At P30, P45, and P60, several VKO mice display total body masses that are much less than their sex-matched littermate controls. VKO mice, sorted by gender, have significantly lower body masses at all timepoints for both males (M) and females (F). Statistics were not performed for P60 females due to the high lethality before this timepoint and the consequent low number of P60 VKO females obtained. B. Liver:body mass ratio (%) was not significantly different between control and VKO mice at P30, P45, and P60 despite several VKO mice displaying abnormally low liver:body mass ratios. C. VKO mice display splenomegaly, having significantly elevated spleen:body mass ratios at P30, P45, and P60. *$p<0.05$; **$p<0.01$; ***$p\leq0.001$.

Due to the enlarged abdominal blood vessels and a difficulty in extracting serum from blood from VKO mice, we examined whether there were any changes in the circulating blood cell populations (Figure 5.4). We first looked at P60, when mice are visibly sick, but due to the high lethality prior to P60, we did not collect enough mice to perform statistical analysis. The one P60 VKO mouse analyzed displayed a large increase in hematocrit, explaining the phenotype of thickened blood with reduced serum. We also analyzed mice at P30 and found a smaller but significant increase in hematocrit in VKO over controls at that time. The increase in hematocrit is similar to that found in Tam et al. (2006). In the aforementioned study, inhibiting VEGF systemically or specifically in the liver caused an upregulation of hepatocyte-produced erythropoietin, leading to increased hematocrit in a matter of weeks in adult mice. Our phenotype of elevated hematocrit in adult VKO mice is consistent with this previously published report.

P30 VKO mice displayed an increase in the number of circulating red blood cells and neutrophils (Figure 5.5). No other hematopoietic cell populations were significantly changed at P30.

VKO mice have altered liver morphology, health, and function by P30.

To assess the health and function of the liver, we performed blood serum measurements for alanine aminotransferase (ALT), total bile acids (BA), and total bilirubin (TB) in P30 control and VKO mice (Figure 5.6). In P30 VKO mice, ALT and BA were consistently and significantly increased over control littermates. Levels of TB were inconsistent in P30 VKO mice, with some mice having normal or near-normal levels of TB and some mice displaying a mild but abnormal increase in TB. The increase in TB in P30 VKO mice over controls was statistically significant.

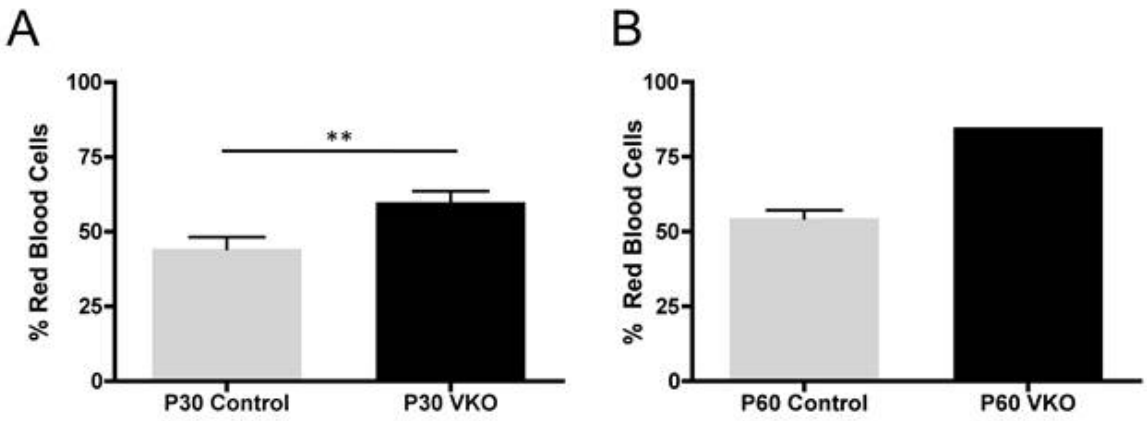

Figure 5.4. VKO mice display an increase in hematocrit. To assess the composition of the circulating blood, a hemavet was used to analyze hematocrit in P30 (A) and P60 (B) control and VKO mice. 8 control mice had an average of 44.33% red blood cells and 6 VKO mice had an average of 59.93% red blood cells in circulating blood at P30. P30 VKO had a significantly higher hematocrit than P30 controls. Due to the high rate of lethality in VKO mice prior to P60, only one P60 mouse was obtained for this experiment. 3 P60 control mice were included. No statistical analysis was performed for the P60 timepoint. **p<0.01.

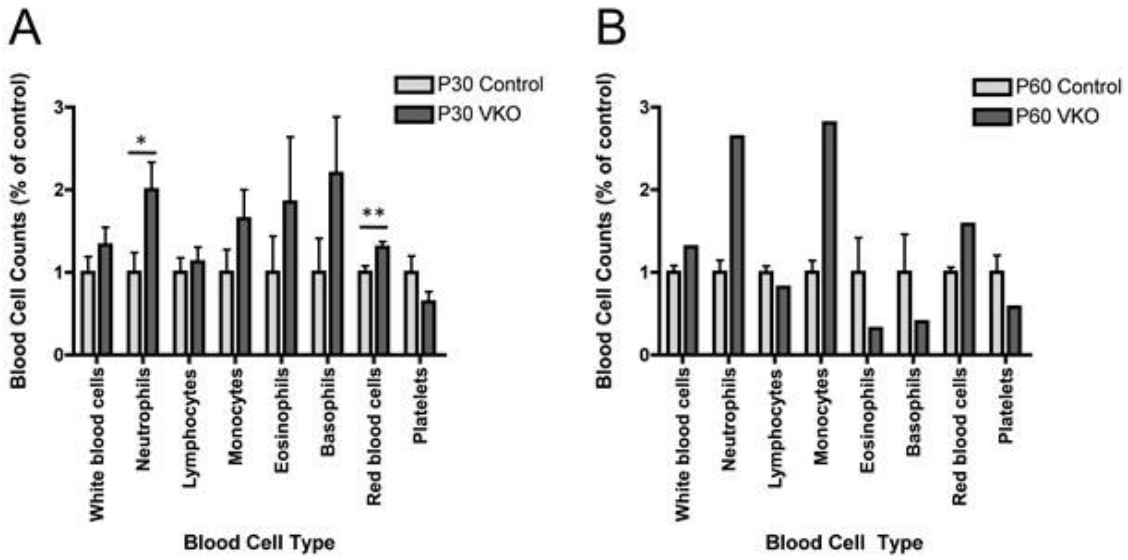

Figure 5.5. VKO mice have altered circulating blood cell numbers. To assess the composition of circulating blood, a hemavet was used to count circulating blood cells in P30 (A) and P60 (B) control and VKO mice. 8 control mice and 6 VKO mice were included at the P30 timepoint. The blood cell counts for each animal are presented as a ratio against the average of the controls for each cell type. P30 VKO mice had significant increases in the number of circulating neutrophils and red blood cells. Due to the high rate of lethality in VKO mice prior to P60, only one P60 mouse was obtained for this experiment. 3 P60 control mice were included. No statistical analysis was performed for the P60 timepoint. *$p<0.05$; **$p<0.01$.

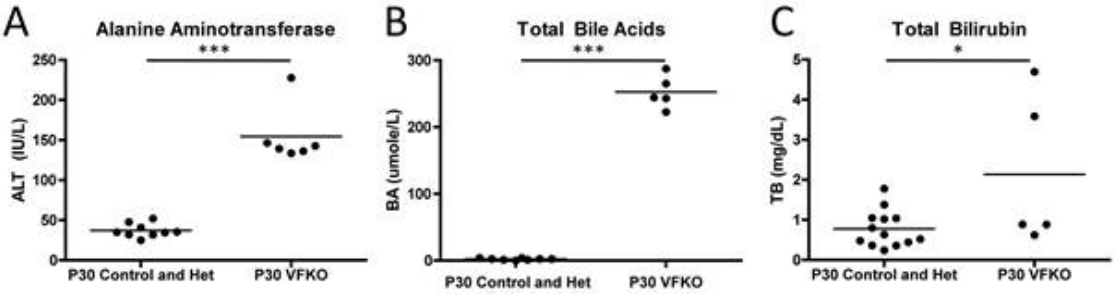

Figure 5.6. VKO mice show indicators of liver damage. Serum from P30 control and VKO mice was tested for alanine aminotransferase (ALT), total bile acids (BA), and total bilirubin (TB). No difference was observed between control and heterozygous mice in any of these analyses. A. VKO mice have elevated levels of ALT in serum at P30. B. VKO mice have elevated levels of BA in serum at P30. C. Some VKO mice have elevated levels of TB in serum at P30. Although some VKO mice display normal levels of TB, the difference between control and VKO mice was statistically significant. *$p<0.05$; ***$p\leq0.001$.

With the serum tests providing evidence that liver health and function was impaired (Figure 5.6), we assessed whether VKO mice displayed any changes in liver morphology. We assessed liver histopathology by hematoxylin and eosin (H&E) staining (Figure 5.7). The H&E stain did not reveal any differences in liver morphology between control and VKO mice at P3 (Figure 5.7A-B). However some differences in hepatocyte cord morphology were observed at P15 (Figure 5.7C-D) and by P30, VKO mice displayed small areas of focal necrosis (white arrows) and dilated sinusoids (white arrowheads) (Figure 5.7E-F).

To examine the zonation of hepatocytes, we assessed the expression of the zone-specific hepatocyte enzymes glutamine synthetase (Figures 5.8, 5.9) and carbamoyl phosphate synthetase 1 (CPS1) (Figure 5.9). GS and CPS1 are enzymes involved in glutamine formation and urea formation, respectively, in hepatocytes (Jungermann and Keitzmann, 1996). GS expression in both VKO and control mice was observed in its normal location, in the hepatocytes surrounding central veins (Figure 5.8). However, the expression region of GS was abnormally expanded in VKO mice; at P15, there was a slight increase in the area of expression in the pericentral zone, and at P30, GS expression was observed in large clusters of hepatocytes not surrounding a CV (Figure 5.8).

In control adult mouse livers, GS and CPS1 expression is mutually exclusive, with GS expressed only in pericentral hepatocytes and CPS1 expressed in periportal and intermediate hepatocytes (Figure 5.9). In P15 VKO mice, in line with the expansion of GS expression, there are a small number of hepatocytes present that co-express GS and CPS1 (Figure 5.9, arrowheads). At P30, the number of GS and CPS1 co-expressing cells has visually increased, and these cells are found both juxtaposing central veins and

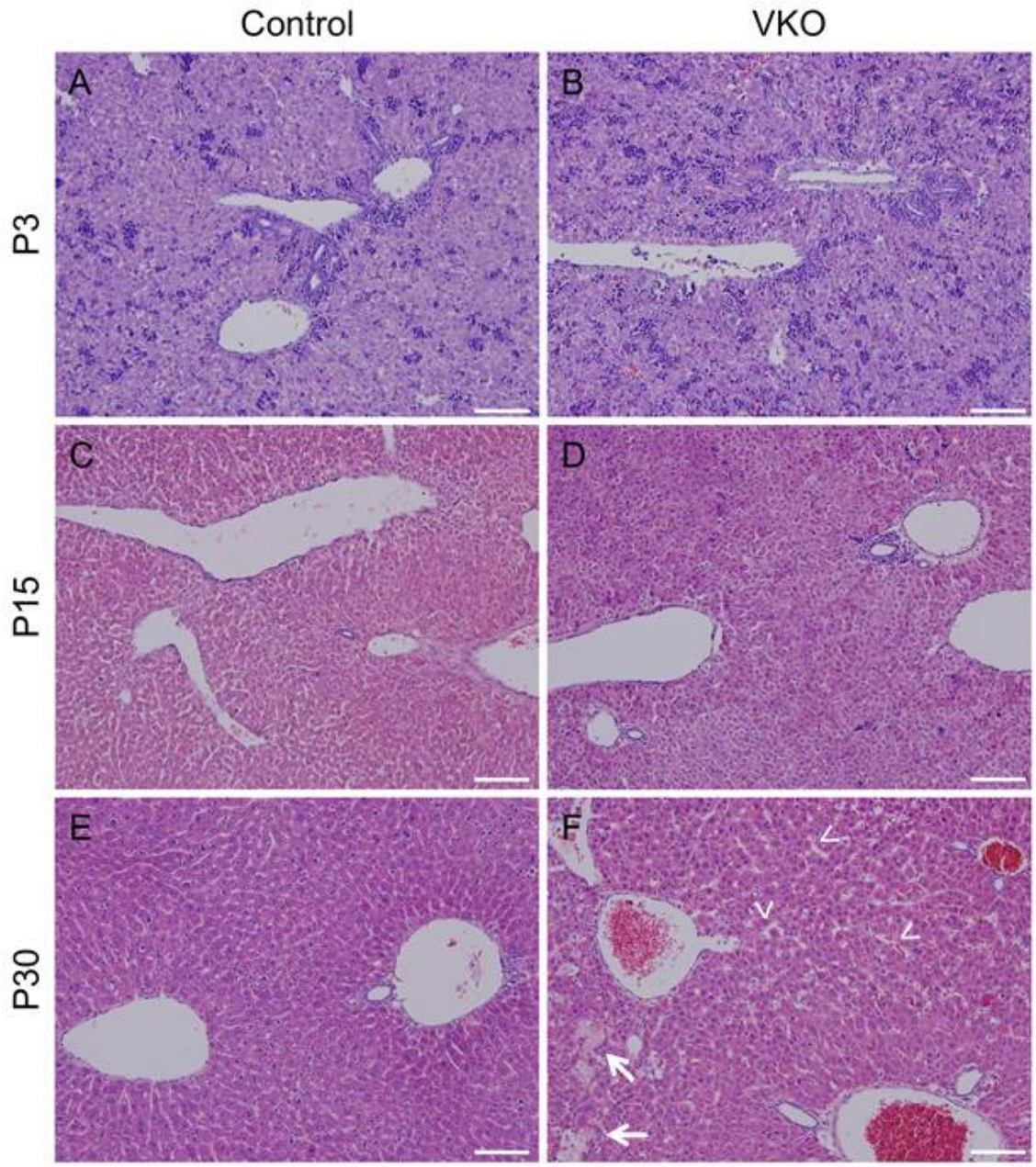

Figure 5.7. VKO mice display disrupted hepatocyte cords and dilated sinusoids. H&E stains were done on P3, P15, and P30 control and VKO livers. At P3, no obvious visual differences were observed between control and VKO mice. At P15, VKO mice exhibited abnormal hepatocyte cord morphology (D) as compared to controls (C). By P30, VKO mice demonstrate dilated sinusoids (F, arrowheads) as compared to control (E). There is also a loss of hepatocyte zonal morphology and focal necrosis (arrows). In the P30 control, an H&E shows subtle differences in the periportal and pericentral hepatocytes; the periportal hepatocytes are more densely associated than the pericentral hepatocytes (E). However, no zonation is apparent in the P30 VKO liver (F). Scale bar is 100 μm.

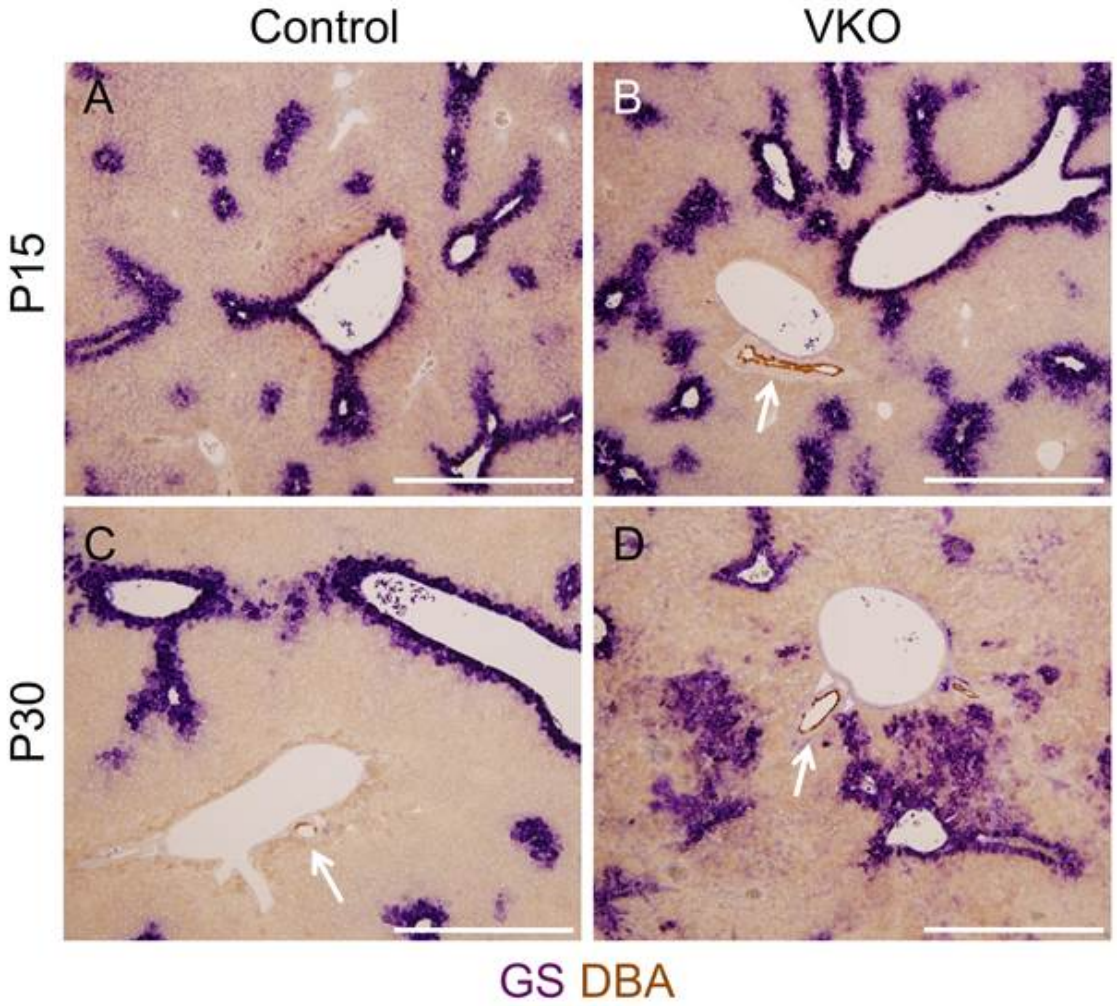

Figure 5.8. VKO mice display expanded pericentral hepatocyte gene expression. To assess hepatocyte zonation in VKO mice, expression of the pericentral hepatocyte marker Glutamine Synthetase (GS) (purple) was assessed with immunohistochemistry. The lectin DBA (brown, white arrows) was used to mark hilar IHBDs next to hilar portal vein branches. In control mice at P15 (A) and P30 (C), the expression of GS is restricted to hepatocytes within a few cell diameters from a central vein. No GS expression is observed around portal veins. In VKO mice, however, a slight visual increase in the area of GS expression is observed at P15 (B). In P30 VKO mice, there is a large increase in the area of GS expression, with several large patches of hepatocytes displaying abnormal GS expression (D). Scale bar is 500 μm.

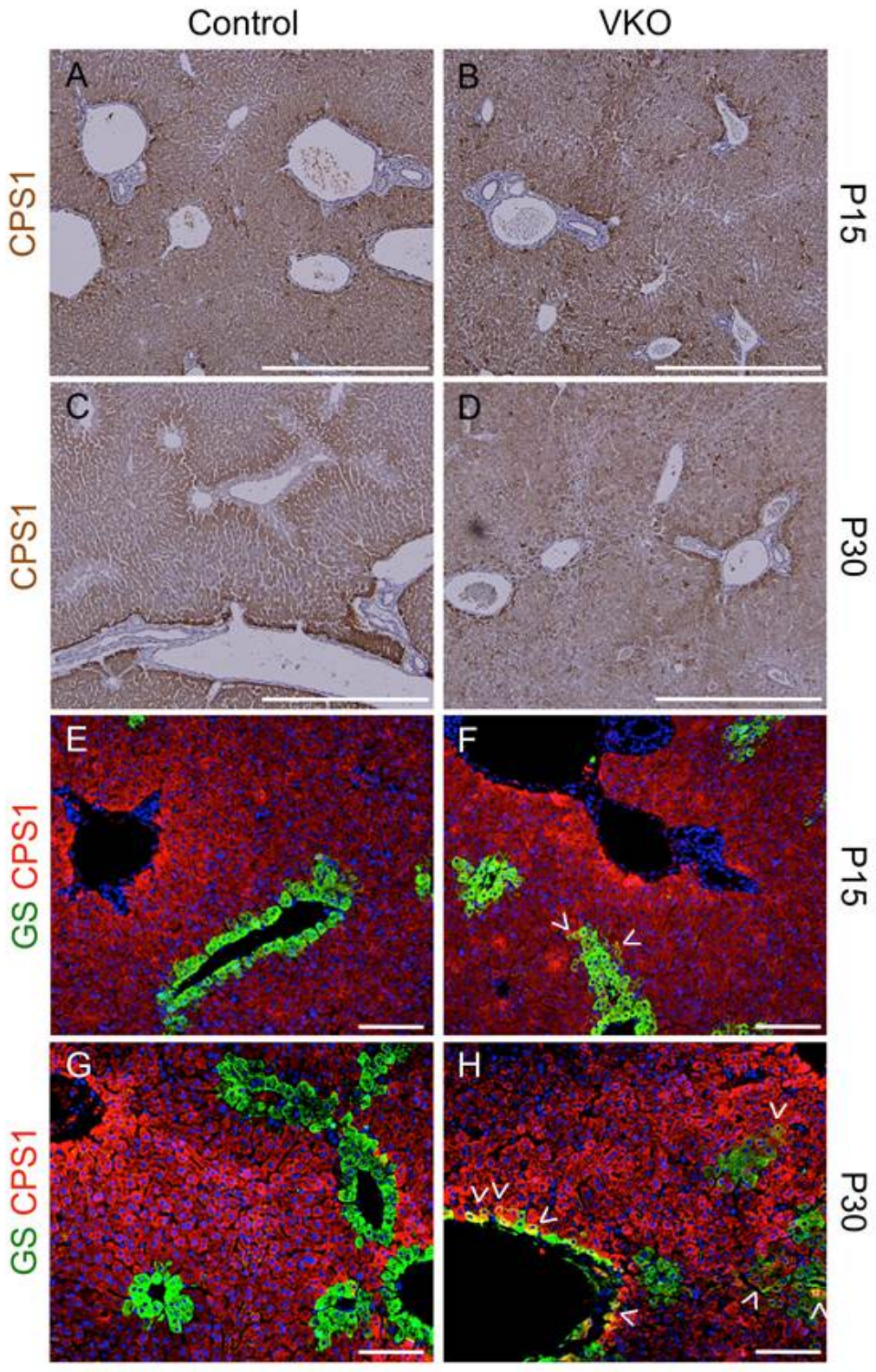
Control
VKO
A
B
C
D
E
F
G
H
CPS1
CPS1
GS CPS1
GS CPS1
P15
P30
P15
P30

Figure 5.9. VKO mice display a loss of hepatocyte zonation and abnormal overlap of hepatocyte zonal markers. To assess hepatocyte zonation in VKO mice, we assessed the expression of CPS1, a marker of periportal and intermediate zone hepatocytes, and the co-expression of CPS1 and GS. In control mice, CPS1 begins to exhibit zonal restriction at P15 (A) and by P30, expression of CPS1 is excluded from pericentral hepatocytes (C). At both P15 and P30, control mice do not display overlap in the expression patterns of CPS1 and GS (E,G). In VKO mice, similar to controls, rough zonal restriction of CPS1 expression is observed at P15 (B). However, by P30, there is a loss of zonal pattern of CPS1 expression in VKO mice (D). VKO mice also display the abnormal co-expression of GS and CPS1 in both pericentral hepatocytes and in intermediate zone hepatocytes that abnormally express GS (arrowheads). This co-expression occurs in rare hepatocytes at P15 (F) but is increased at P30 (H). Scale bar is 500 μm (A-D), 100 μm (E-H).

in the abnormal GS-expression hepatocyte clusters that do not juxtapose central veins (Figure 5.9). This altered gene expression indicates a loss of zonation and a disruption in zone-specific hepatocyte identity.

VKO mice display hypoxia in the liver by P15.

In the consideration that a liver morphogenesis phenotype is already apparent by P30, and increasing hematocrit after P30 may cause secondary effects confounding the immediate role of VEGF in liver development, we hereafter focus on P30 and earlier timepoints. Hepatocyte zonation has been hypothesized to result, at least in part, from the steep gradient in blood oxygen pressure across the hepatic lobule (Colnot and Perret, 2011). This hypothesis is consistent with our experimental model, in which we reduce expression of a known angiogenic factor. To determine if hypoxia may be playing a causative role in the altered zonal identity of hepatocytes, we used Hypoxyprobe to visualize regions of hypoxia in the livers of P15 and P30 VKO and control mice (Figure 5.10). Hypoxyprobe (pimonidazole) binds peptide thiols in hypoxic cells where it competes with oxygen for electrons for activation. The activated form of pimonidazole can be detected in tissue by a specific antibody, thereby identifying regions of low oxygen tension.

In control mice, hypoxia is faintly apparent in a zonal pattern, specifically around central veins marked by GS expression, at P15 and P30 (Figure 5.10B,F). In VKO mice, however, there is a visual increase in the area of hypoxia over controls at both P15 and P30 (Figure 5.10D,H). This indicates that the VKO mice do have abnormally hypoxic livers, which may be contributing to the observed altered hepatocyte zonal identities.

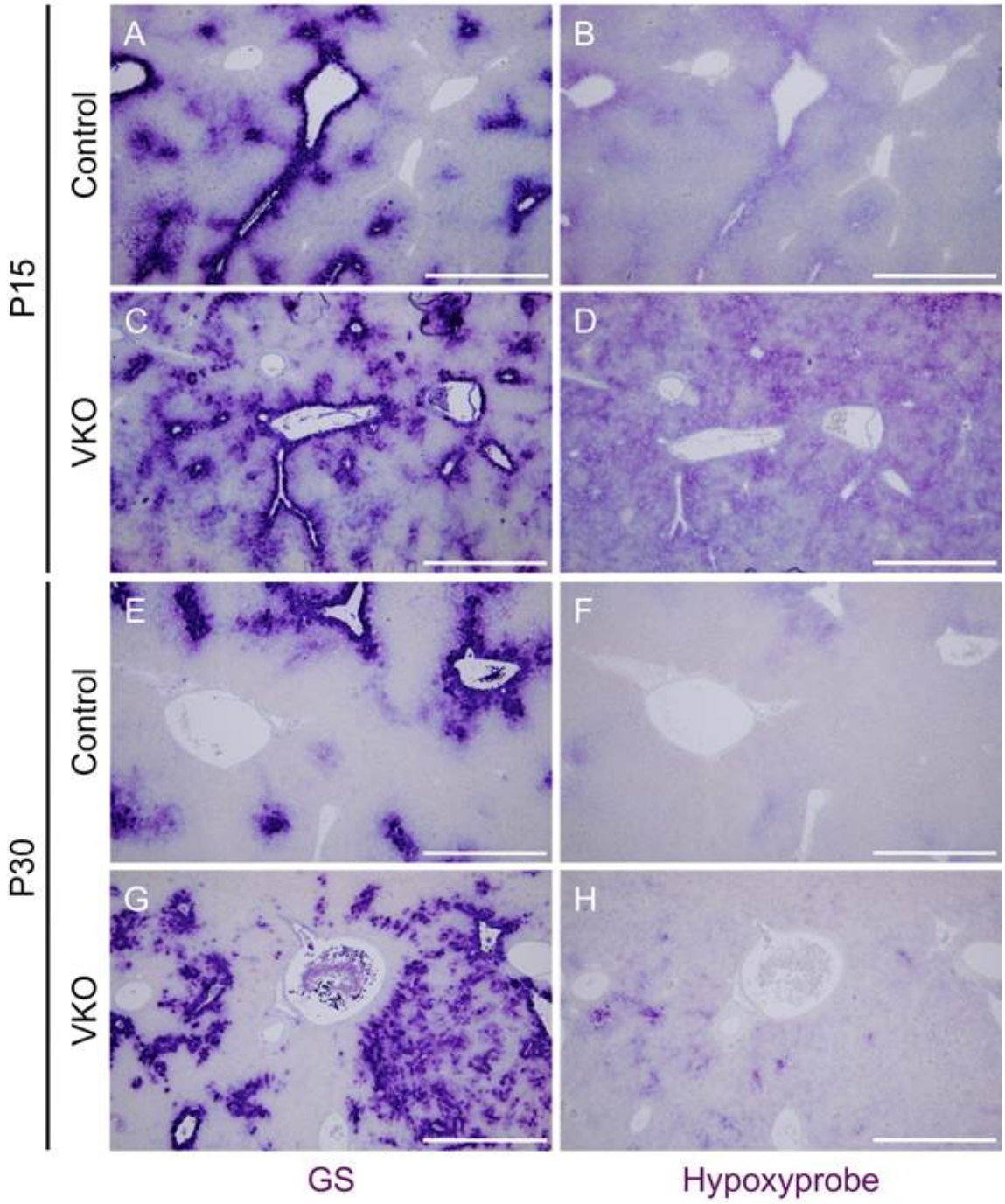
P15
P30
Control
VKO
Control
VKO
A
B
C
D
E
F
G
H
GS
Hypoxyprobe

Figure 5.10. VKO mice demonstrate increased hypoxia in the liver that occurs in close proximity to, but does not necessarily overlap, regions of GS expression. Serial sections were used to assess the association of oxygen levels and GS expression in the livers of VKO mice. Hypoxyprobe was injected into mice 90 minutes prior to sacrifice and assessed by immunohistochemistry (purple, B,D,F,H). At P15 and P30, control mice display low levels of regional hypoxia, specifically around central veins (B,F). In P15 VKO mice, however, the amount of hypoxia is markedly higher than that observed in control and is widespread in the liver (D). This hypoxia is still present in P30 VKO mice, but is not as widespread (H). The regions of hypoxia correspond with regions of GS expression in P15 and P30 controls (A,E). In P15 VKO livers, GS expression correlates with the strongest Hypoxyprobe staining, but not all hypoxic areas express GS (E-F). In P30 VKO livers, Hypoxyprobe occurs in close spatial association with GS expression, but GS and Hypoxyprobe expression frequently occur in different cells (G-H). Scale bar is 500 μm.

To assess whether regions of hypoxia correlate with the areas of expanded GS expression, serial liver sections were stained for GS and Hypoxyprobe (Figure 5.10). In P15 and P30 controls, the areas of GS expression very closely lined up with the areas of faint Hypoxyprobe staining (Figure 5.10A-B, E-F). In P15 VKO livers, hypoxia is very disperse through the tissue, but the regions of GS staining do still correlate with the darkest Hypoxyprobe staining (Figure 5.10C-D). In P30 livers, hypoxia is observed in areas of expanded GS staining; however, there is not a complete overlap between GS and Hypoxyprobe staining (Figure 5.10G-H). Large areas of GS staining exist that are not positive or only weakly positive for Hypoxyprobe. Interestingly, the strongest Hypoxyprobe staining is frequently seen in cells on the border of a GS^+ patch, or in the middle of a GS^+ patch in cells that juxtapose GS staining but do not express GS themselves (Figure 5.10G-H).

VKO mice display an embryonic decrease in endothelial-lineage cells.

After determining that VKO mice did have a liver phenotype in which hypoxia is increased and hepatocyte zonal identities are altered, we examined the different vascular compartments to see if any were abnormal in VKO mice and could be responsible for the aforementioned liver phenotypes. We focused our examination on the portal vein, the hepatic artery, and the hepatic sinusoids.

Previous reports have demonstrated that inhibiting VEGF signaling ubiquitously in the liver results in a reduction in the number of endothelial cells (Carpenter et al., 2005; Gerber et al., 1999). To determine if there is a similar reduction in endothelial cell number when only epithelial-VEGF expression is reduced from a mid-gestational timepoint, we stained with IsolectinB4 (IsoB4) in embryonic and postnatal livers (Figure 5.11). At E16.5 in VKO mice, there

is a reduction in the number of cells that stain positive for IsoB4 as compared to control. However, this reduction is no longer observed at P3 or at P15. This indicates that although there was an initial defect in the number of IsoB4-expressing endothelial-lineage cells, the loss is able to be compensated for postnatally.

VKO mice have reduced portal vein branching and branch diameters at P30.

To determine whether epithelial-VEGF plays a role in portal vein branching, we analyzed the number of portal vein branches in P15 and P30 VKO and control mice. We analyzed both the number of PV branches per liver area as a measure of vessel density and the number of PV branches per transverse section as an assessment of the vessel architectural pattern independent of any consequent reductions in liver size.

Between P15-P30, control mice exhibit an increase in the number of PVs/liver section but a decrease in the number of PVs/liver area. This indicates that new PV branches are being formed during this time, but the rate of PV branch addition is relatively less than the rate of liver growth. At P15, there is no observable decrease in PVs/liver section or PVs/liver area in VKO mice as compared to control. However, there is a reduction in both PVs/liver section and in PVs/liver area in P30 VKO mice as compared to controls (Figure 5.12).

To assess whether the size of the portal vein branches were affected in the VKO mouse liver, we generated 3-dimensional resin casts of the left lobe portal vein in P30 control and VKO mice (Figure 5.13). We examined three stereotypic branch points, which we labeled A, B, and C (Figure 5.13A) and measured the PV diameter on each of the two

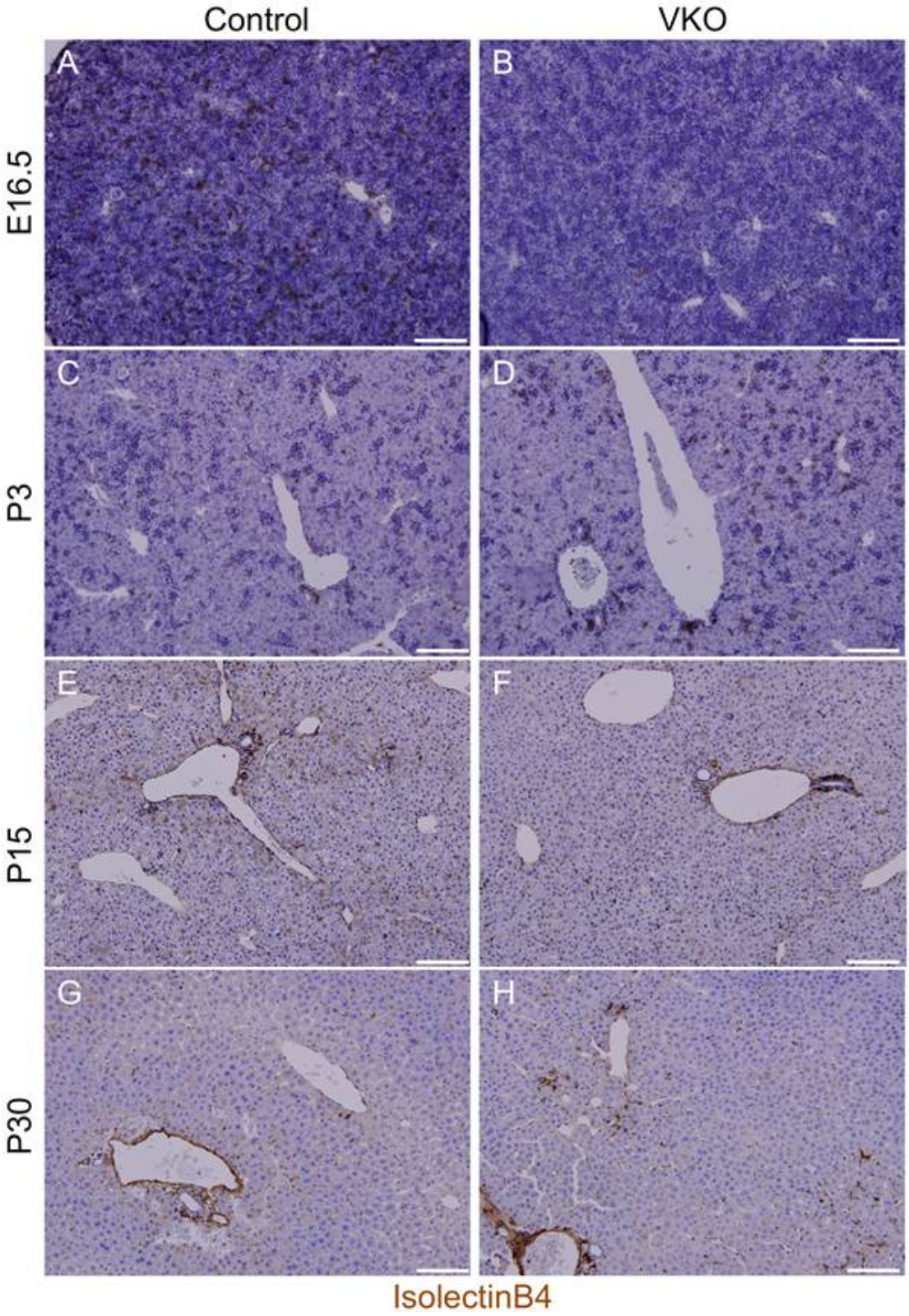
Control
VKO
A
B
E16.5
C
D
P3
E
F
P15
G
H
P30
IsolectinB4

Figure 5.11. An initial endothelial-lineage cell decrease is compensated for in VKO mice. To assess the presence of endothelial-lineage cells in the livers of VKO mice, the endothelial cell marker IsolectinB4 (brown) was visualized with immunohistochemistry and a hematoxylin counterstain. In E16.5 control mice, IsolectinB4 expression is apparent throughout the liver (A). In E16.5 VKO mice, however, there is a marked reduction in the number of cells that stain for IsolectinB4 (B). By P3, VKO mice (D) show a visual increase in IsolectinB4 expression over E16.5 VKO mice, and do not have any reduction in IsolectinB4$^+$ cells as compared to P3 controls (C). In fact, P3 VKO mice demonstrate a slight visual increase in the number of IsolectinB4$^+$ cells as compared to controls. Similarly, no reduction in IsolectinB4 staining is observed in P15 (F) or P30 (H) VKO mice as compared to controls (E,G). Scale bar is 100 μm.

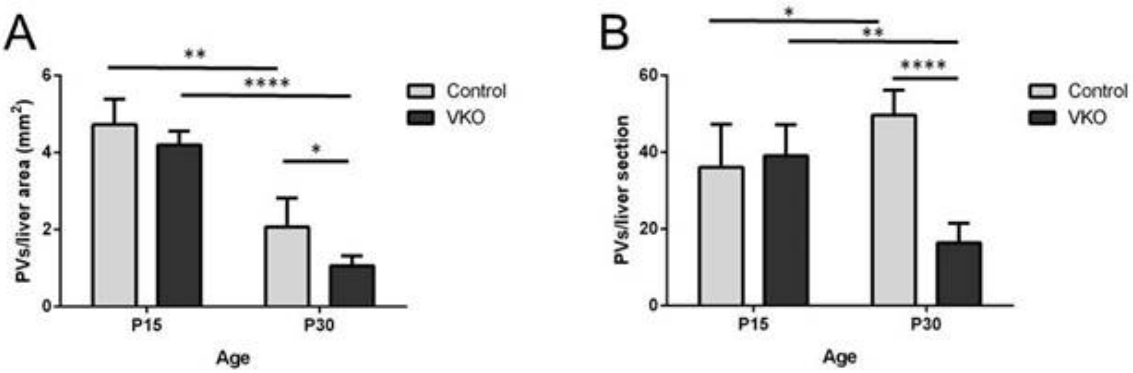

Figure 5.12. VKO mice display a reduction in PV branches. Liver sections were stained with GS to demarcate CVs. PVs, defined as any vein not lined by GS^+ hepatocytes, were counted. The number of branches per liver area (A) and the number of branches per liver cross section (B) were analyzed. At P15, no difference in PVs/liver area or PV/liver section between control and VKO mice was observed. At P30, VKO mice had significantly fewer PVs per liver area and per section. The number of PVs per area decreased between P15 and P30 in both control and VKO mice (A). The number of PVs per liver section increased in control mice but decreased in VKO mice (B). At least six liver sections over two slides per animal were counted. N = 3 (P15) or 4 (P30) for both genotypes. *$p<0.05$; **$p<0.01$; ****$p\leq0.0001$.

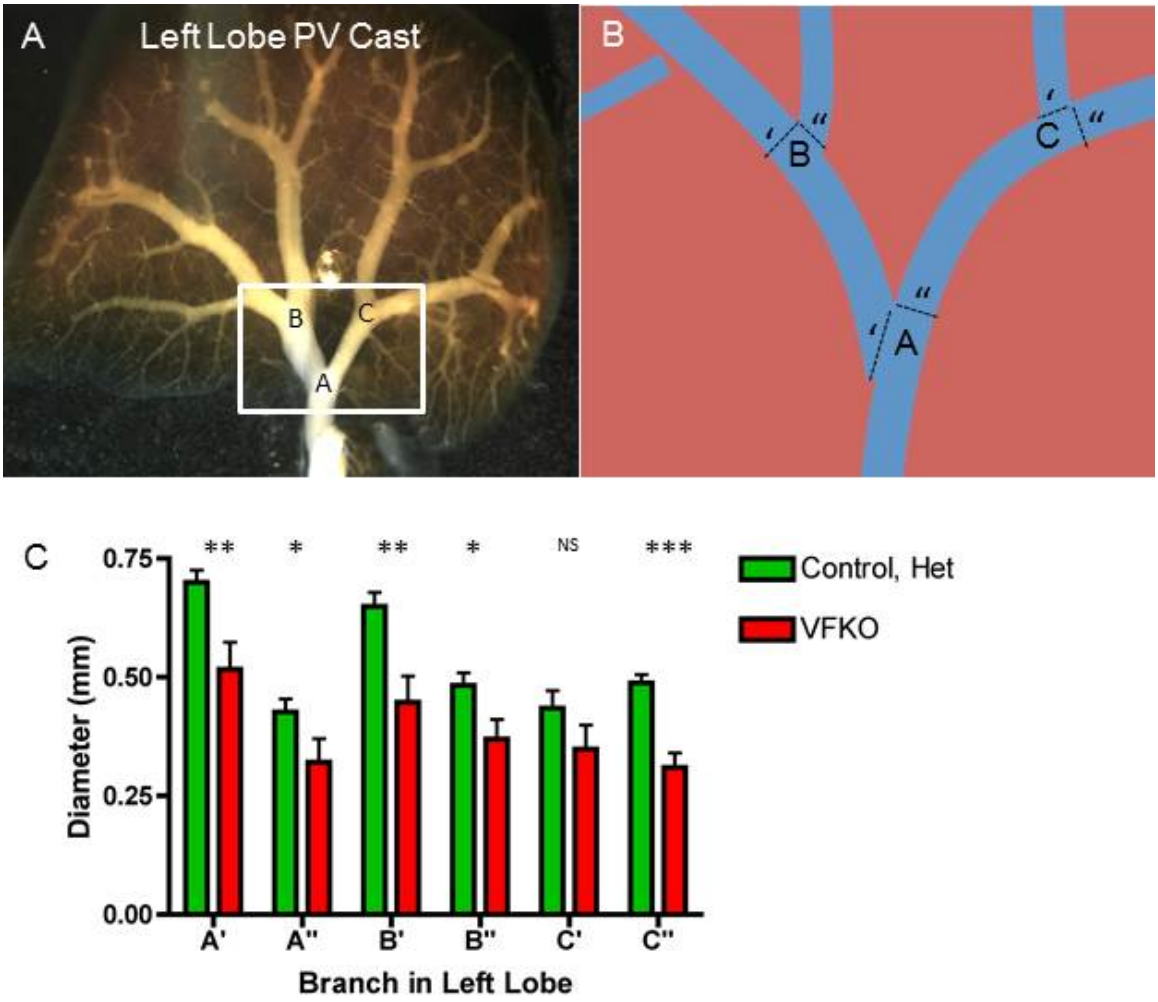

Figure 5.13. VKO mice display a reduction in PV branch diameter. The 3-dimensional structure of the PV in the left liver lobe of P30 control and VKO mice was analyzed by resin cast. In the left liver lobe, several branch points exist which are highly stereotypic. We labeled these branch points A, B, and C, and measured the cast diameters of each branch at these branch points (A,B). For 5 of the 6 locations in which diameter was measured, P30 VKO mice displayed a reduced cast diameter as compared to P30 control mice. The cast diameter at location C' was not significantly changed between VKO and control mice. Control and heterozygous (het) mice were combined as no differences were observed between them. N=7-9 measurements per branch from 10 mice (control and het); 4-6 measurements per branch from 8 mice (VKO). *p<0.05; **p<0.01; ***p≤0.001.

branches generated from each branch point: A', A", B', B", C', and C" (Figure 5.13B). At 5 of the 6 locations assessed (A', A", B', B", and C"), the VKO mice displayed significantly smaller PV diameters than the control mice (Figure 5.13C). At one location (C'), no significant difference was observed between VKO and control mice (Figure 5.13C). This suggests that, in addition to having fewer PV branches, the P30 VKO mice also have narrower PV branches than control mice.

VKO mice have reduced hepatic artery branching at P15 and P30.

To determine whether epithelial-VEGF is required for hepatic artery branching, we assessed HA branches as normalized to liver tissue area and per liver section, the same way the PV branches were analyzed.

Similar to the PV, we found that in control mice between P15 and P30, the number of HA branches/liver area decreases. This indicates that, similarly to the PV, the rate of HA branch addition is less than that of liver parenchymal expansion (Figure 5.14). In VKO mice as compared to controls, there were fewer HAs/liver area and HAs/liver section at P15 and P30.

VKO mice demonstrate a loss of LSEC identity.

To determine whether epithelial-VEGF plays a role in the development of the sinusoid network, we assessed the expression of endothelial markers in the liver. First, we analyzed the expression of endomucin in P15 and P30 VKO and control mouse livers. In control livers at P15 and P30, the expression of endomucin is not uniform over all hepatic endothelial cells: endomucin is expressed in the endothelium of the HA, the CV,

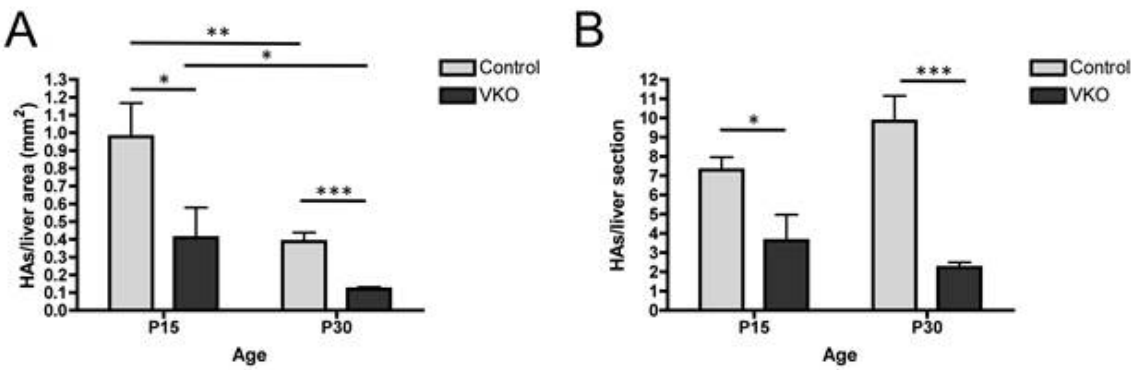

Figure 5.14. VKO mice display a reduction in HA branches. HA branches were visualized by immunohistochemistry for SMA. Expression of SMA in the arterial mesenchyme marks the major HA branches. The number of branches per liver area (A) and the number of branches per liver cross section (B) were analyzed. At both P15 and P30, VKO mice have fewer HA branches per liver area and per liver section as compared to controls (A,B). At least six liver sections per animal were counted. N = 4 (P15) or 6 (P30) for both genotypes. *$p<0.05$; **$p<0.01$; ***$p\leq0.001$.

and the pericentral sinusoids (Figure 5.15). No endomucin expression is observed in the endothelium of the PV or periportal sinusoids. In P15 VKO mice, a slight expansion of endomucin expression is observed as compared to controls. By P30, however, the pattern of endomucin in P30 VKO is highly abnormal (Figure 5.15). The restriction of expression within the hepatic zones is lost and endomucin is now observed in the periportal sinusoidal endothelium. Additionally, the concentration of endomucin^{+} cells is decreased in the regions of pericentral hepatocytes, with additional hepatocyte cords between the endomucin^{+} sinusoidal endothelium.

To assess the differentiated identity of the LSECs, we assessed expression of PECAM. Normally, PECAM is not expressed in LSECs in adult mice. At P3, both PECAM (Figure 5.16) and endomucin (Figure 5.16 and 5.15) were expressed only within venous endothelium in control and VKO mice. In P15 controls, PECAM is expressed primarily in venous endothelium and in some sinusoidal endothelium that co-expresses endomucin (Figure 5.16C). In P15 VKO mice, PECAM is not only expressed in venous endothelium, but the expression of PECAM is also expanded to a greater number of sinusoid endothelial cells (Figure 5.16D). As previously noted, the expression of endomucin is slightly expanded in sinusoids in the P15 VKO liver as compared to control (Figure 5.15), and the pattern of PECAM shows a similar effect (Figure 5.16D). By P30, the expression of PECAM is highly restricted in control mice: PECAM is expressed within the portal vein and central vein endothelium, but not within the sinusoidal endothelium (Figure 5.16E). In contrast, PECAM is expressed not only in venous endothelium, but is also very highly associated with the sinusoidal endothelium in P30 VKO mice (Figure 5.16F). There does not seem to be any zonal or regional restrictions to PECAM expression within the sinusoidal endothelium. The expression of PECAM within LSECs indicates that these cells have lost features of their sinusoidal identity. Oftentimes this is correlated with a

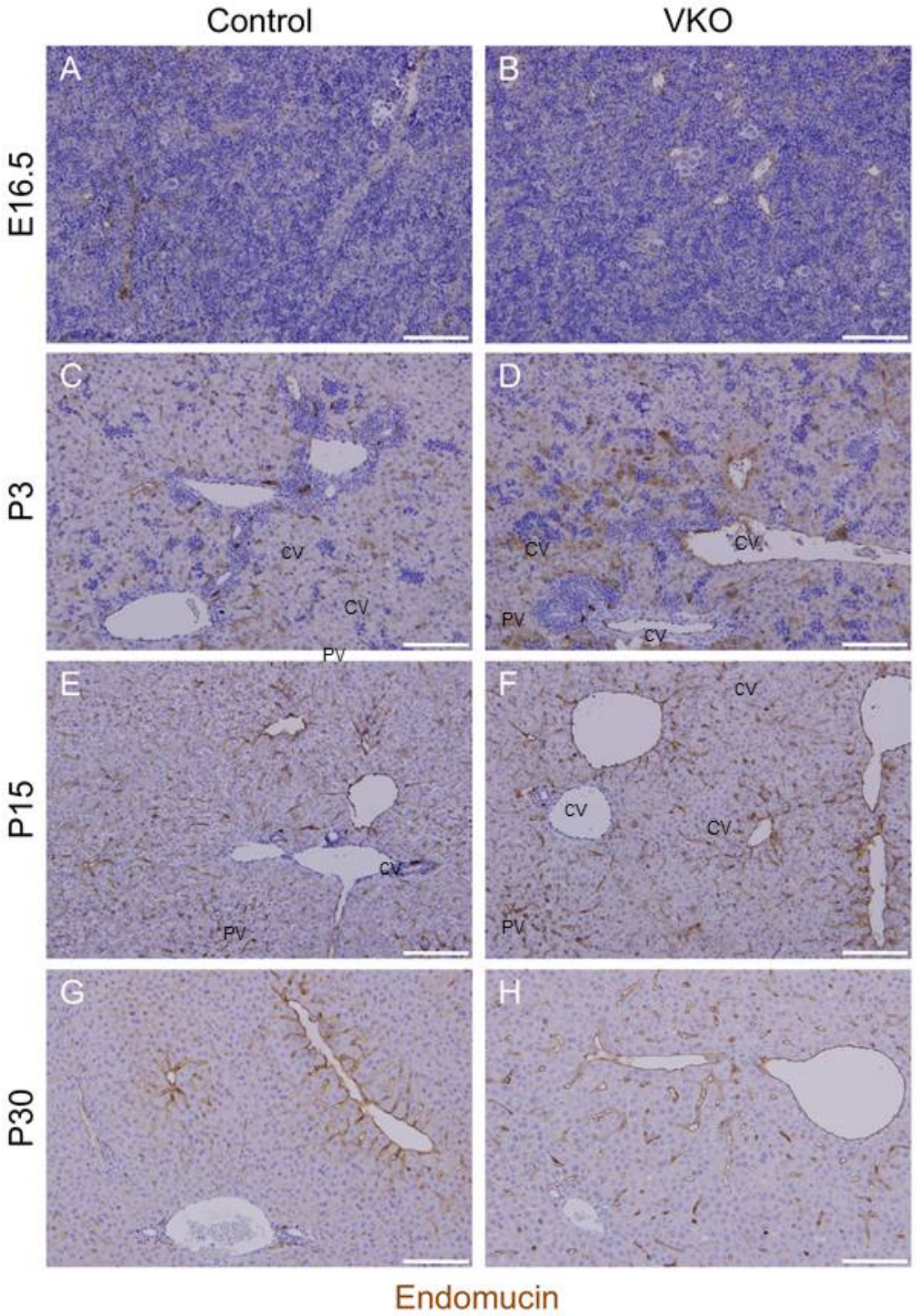
Control
VKO
A
B
E16.5
C
D
P3
CV
CV
PV
CV
CV
PV
CV
E
F
P15
CV
CV
PV
CV
CV
PV
G
H
P30
Endomucin

Figure 5.15. P30 VKO mice have altered sinusoid endothelial cell identity. To assess endothelial cell identity, we assessed the expression of the endothelial cell marker endomucin (brown) with a hematoxylin counterstain. In control mice, endomucin expression is observed in venous endothelium at E16.5 (A), in venous, sinusoidal and peribiliary plexus endothelium at P3 (C) and P15 (E), and by P30, endomucin is expressed in central vein endothelium, pericentral sinusoid endothelium, and peribiliary plexus endothelium (G). Endomucin is not expressed in portal vein endothelium or periportal sinusoid endothelium in P30 control mice (G). In P30 VKO mice, however, the expression of endomucin is altered and endomucin can bee seen in periportal endothelium (H). No difference in endomucin localization is observed in E16.5 (B), P3 (D), and P15 (F) VKO mice as compared to controls. Scale bar is 100 μm.

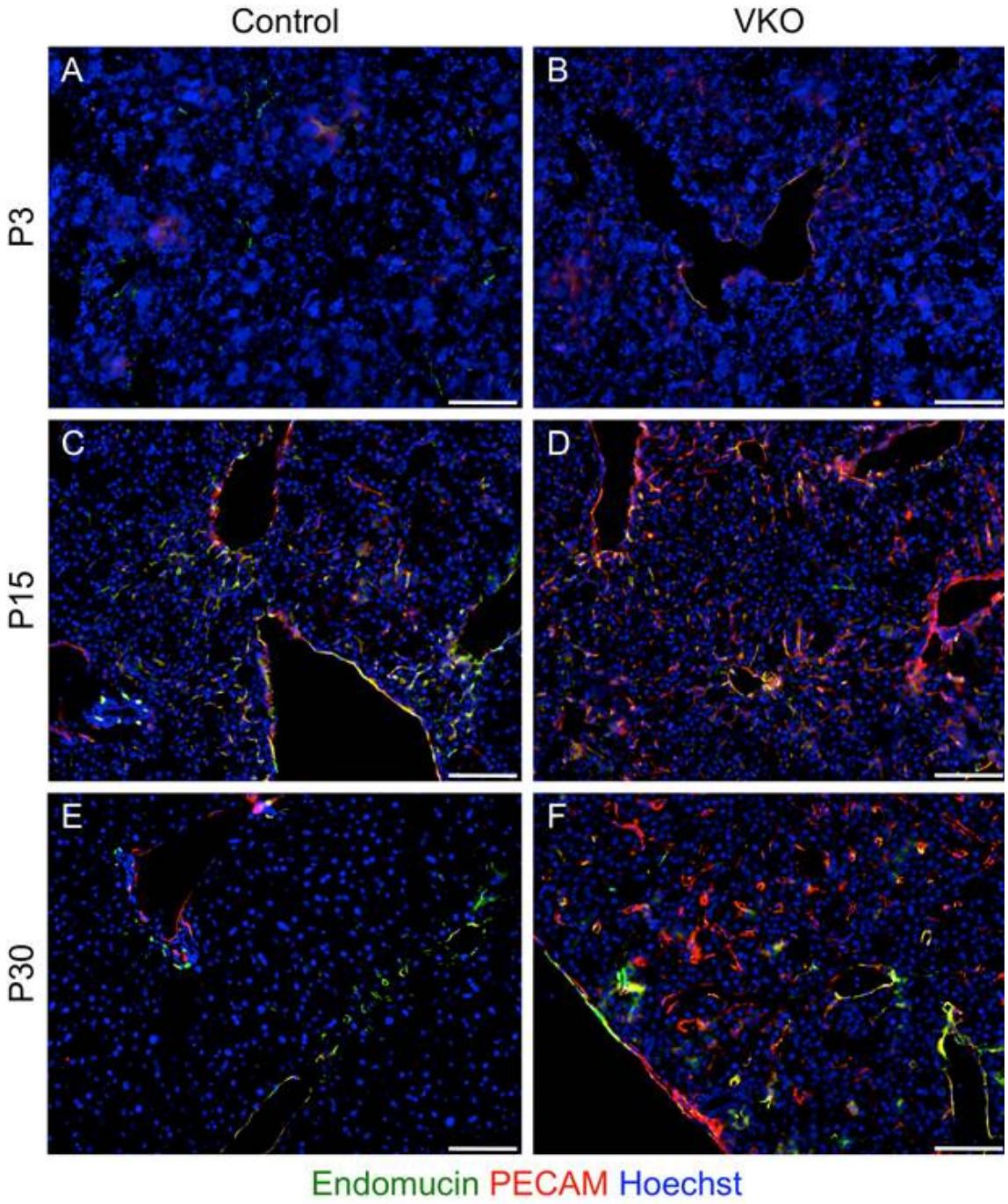
Control
VKO
A
B
C
D
E
F
P3
P15
P30
Endomucin PECAM Hoechst

Figure 5.16. VKO sinusoid endothelial cells display an abnormal expression of PECAM. To assess the differentiation status of sinusoid endothelial cell, the expression of PECAM (red) and endomucin (green) were assessed by immunofluorescence. In P3 control mice, low amounts of PECAM and endomucin are expressed in venous endothelium (A). No difference is observed between control and VKO (B) mice at this time. In P15 control mice, central vein endothelium expresses PECAM and endomucin while portal vein endothelium only expresses PECAM (C). A subset of sinusoid endothelial cells express both PECAM and endomucin. In P15 VKO mice, PECAM is similarly expressed in both portal vein and central vein endothelium while endomucin is expressed in the central vein but not portal vein endothelium (D). Differently from controls, however, P15 VKO mice display an expansion in the expression of PECAM in sinusoid endothelial cells. By P30, control mice express PECAM only in portal and central vein endothelium and express endomucin only in central vein, pericentral sinusoid, and peribiliary plexus endothelium (E). PECAM is not expressed in sinusoid endothelial cells. P30 VKO mice, however, have a large expansion of PECAM expression with PECAM abnormally expressed in a large number of sinusoid endothelial cells (F). The expression of endomucin is similarly expanded, as compared to control, to sinusoid endothelial cells that are not pericentral. Scale bar is 100 μm.

decrease in fenestration and a reduction in *in vivo* function of particle transport (Carpenter et al., 2005; Mitchell et al., 2011). The loss of sinusoidal identity in the VKO mice may be indicative of "capillarization."

Conclusion

VEGF levels differentially affect the PV, HA, and sinusoids.

The VKO displays alterations in PV, HA, and sinusoids as compared to control, but the abnormal phenotypes appear in the different vascular tissues at different times. VKO mice display alterations in IsolectinB4^{+} endothelial-lineage cells as early as E16.5 but that recover by P3. HAs and LSECs show abnormal phenotypes by P15 that persist at P30, and PVs show abnormal phenotypes at P30. Similarly, hepatocytes show abnormalities that are subtle at P15 and become more pronounced by P30.

There are multiple possible explanations for these abnormalities. First, it may be that there are different required levels of VEGF for each vascular tissue. As the levels of VEGF decrease over development in VKO mice, it may be that the absolute hepatic VEGF levels drop below the required level for HA development and LSEC identity sooner than they drop below the level required for PV morphogenesis. This explanation fits with the known role for VEGF in arterial-venous differentiation (Swift and Weinstein, 2009); high levels of VEGF promote arterial fates while ECs not receiving high VEGF signaling adopt a venous fate.

A second explanation is that the different vessels rely primarily on VEGF derived from different tissues. Perhaps the PV receives the majority of its VEGF signal from the mesenchyme, while the sinusoids depend on VEGF from hepatocytes and the HA is directed by VEGF secreted from the IHBD. These alternate potential sources of VEGF could also contribute to the levels of VEGF that are normally received by each vascular tissue and that are required for normal development and function.

Third, it may be that VEGF serves a different function for the different vascular tissues based on the identity and specific mode of development of each tissue. VEGF has been described as having roles in endothelial proliferation, differentiation, branching morphogenesis, cell survival, and vascular permeability (Carpenter et al., 2005; Connolly et al., 1989; Gerber et al., 2002; Gerhardt et al., 2003; Krueger et al., 2011; Lee et al., 2007; Leung et al., 2013). The main role of VEGF may be different in the different endothelium, or may change at different stages of development. Based on our results, it is not possible to distinguish between these possibilities.

Loss of epithelial-VEGF results in an inability to generate PV branches during postnatal growth.

Between P15 and P30, control mice decrease the number of PVs per liver area, but increase the number of PV branches per section (Figure 5.12). This indicates that the PV system is expanding and adding new vessel branches, but it is doing so at a rate that is slower than the overall expansion of the liver parenchymal mass and area.

VKO mice do not exhibit a similar addition of new PV branches during this period and instead actually exhibit a loss of PV branches in section (Figure 5.12). This may indicate that the PV branches formed prior to P15 are not maintained in the VKO model. Alternatively, it may be that the decrease in isolectin^{+} ECs initially observed at E16.5 (Figure 5.11) indicates a failure to produce enough venous endothelial progenitors, limiting the elaboration of the PV system past P15. While the average number of HA branches per liver section also decreases in VKO mice over time, this decrease is not significant (Figure 5.14). Hence, the failure to maintain branches may illuminate a unique role for epithelial VEGF in the homeostasis of the PV.

We also observed a decrease in PV cast diameter in several stereotypic branch locations in the P30 VKO mice as compared to control (Figure 5.13C). Due to technical limitations, PV casts

were not generated at P15. The decrease in PV branches in P30 VKO mice may be due to a decrease in ECs that first has an effect on PV diameter and is only later manifested as a reduction in PV branches.

LSECs undergo capillarization in vivo *as a result of lost epithelial-VEGF signaling*

"Capillarization" is the loss of LSEC-specific features and involves a reduction in fenestrae, a reduction in scavenger behavior, formation of an organized basement membrane, and an upregulation of PECAM (DeLeve et al., 2004). This process is seen *in vivo* in the liver during cirrhosis and as a result of aging. *In vitro,* if LSECs are not either treated with VEGF or co-cultured with a cell type that produces VEGF, LSECs undergo capillarization, displaying reduced fenestrae and increased PECAM expression (DeLeve et al., 2004; Le Couteur et al., 2001; Yokomori et al., 2003).

In agreement with *in vitro* studies, the decrease in VEGF protein in the VKO liver results in the capillarization of LSECs. In P15 and P30 control mice, PECAM expression is restricted to the major vessels and excluded from the LSECs. However, in VKO mice, the LSECs express high levels of PECAM at P15 and P30 (Figure 5.16). Our data, along with the previous studies in culture, suggest that the LSECs in VKO mice lose their specialized LSEC identity and may have reduced function *in vivo*.

The capillarization process is believed to result in decreased function of the LSECs and can impede the transfer of both oxygen and particles between the blood stream and the hepatocytes (Le Couteur et al., 2001; Mitchell et al., 2011). This may be account, at least partially, for the observed hypoxia and the decreased liver function as seen in serum tests.

Hypoxia may occur as a result of HA paucity or LSEC capillarization.

By P15, VKO mice display a substantial increase in hypoxia in the liver as compared to controls (Figure 5.8). At this time, there are alterations observed in both the HA and the sinusoids that could contribute to the hypoxic phenotype (Figure 5.14 and 5.16).

Previous studies have indicated that capillarization and the loss of LSEC-specific characteristics, such as fenestration, correlates with changes in high energy phosphates and other metabolites in hepatocytes and a decreased ability to perform oxygen-dependent drug metabolism, consistent with a decrease in oxygen availability (Le Couteur et al., 2001). It may be that the LSECs in the VKO liver have a decreased capacity for the transfer of oxygen to hepatocytes, contributing to hypoxia in the parenchyma.

Alternately, the decrease in HA branches provides a simple explanation for the decrease of oxygen in the liver parenchyma. The blood supplied to the liver by the HA has a much higher oxygen tension than that supplied by the PV, indicating that a reduction in HA input into the liver or HA density could have a large effect on the oxygenation of the blood in the liver (Tygstrup et al., 1962). The reduction in both HAs per liver area and per liver section provides an simple explanation for the increased liver hypoxia observed in the VKO mice, especially as recent studies have been unable to find a definitive link between LSEC capillarization and hepatocyte hypoxia (Cheluvappa et al., 2007).

Hepatocyte zonation is tied to hypoxia, but hypoxia does not account for defects in VKO hepatocyte zonation.

While the regions of expanded GS expression are closely associated with hypoxia, Hypoxyprobe and GS expression do not always necessarily overlap (Figure 5.10). Instead, the two tend to frequently be juxtaposed in P30 VKO mice (Figure 5.10G-H). This indicates that hypoxia likely does not directly control GS expression in a cell-autonomous way. However, due to the close spatial association between GS and Hypoxyprobe, it remains likely that the two are connected and that hypoxia does play a role in the GS expression expansion and zonation abnormalities.

There are several potential explanations for the increased GS expression observed in P30 VKO mice, including: 1. VEGF may play a direct role on restricting GS expression in periportal hepatocytes; 2. The altered vasculature may be signaling abnormally to hepatocytes, resulting in hepatocyte zonal fate changes; 3. The hypoxia may be regulating GS expression in a non-cell-autonomous way by designating a boundary between GS^+ and GS^- hepatocytes; 4. The immature hepatocyte structure, resulting from lack of epithelial-endothelial signaling or reduced oxygen levels, may make hepatocytes less competent to signal to each other and establish a zonal boundary. There are no highly relevant published studies supporting any of these possibilities, so the explanation remains unclear. Interestingly, however, VEGF and GS expression are both frequently upregulated in cirrhosis and hepatocellular carcinoma (D'Ambrosio et al., 2012; Kwon et al., 2012; Lee et al., 2013). This provides some support against the idea that VEGF is a direct negative regulator of GS in hepatocytes.

Hnf4α and Wnt/β-catenin signaling have been found to regulate the expression of GS (CADORET et al., 2002). It is possible that these signaling pathways are affected by the hypoxia in the liver, resulting in abnormal inter-hepatocyte signaling and zonal boundaries.

One surprising finding is that hypoxia very closely overlaps with GS expression in postnatal control livers, but does not in the expanded GS^+ regions of the P30 VKO liver. This suggests that there is a different mechanism of GS regulation that emerges in the P30 VKO mice and differs from the normal mechanism of GS regulation in postnatal liver.

Influence of epithelial-VEGF provides insightful information for the use of antiangiogenic agents in the treatment of liver disease.

An upregulation of VEGF is observed in liver diseases, including hepatocellular carcinoma (Fabris et al., 2006; Marschall et al., 2001; Moon et al., 2003; Park et al., 2000). There are several VEGF inhibitor drugs approved by the FDA for the treatment of specific types of cancers; however, the use of VEGF inhibitors has been shown to have negative side effects in both pre-clinical and clinical studies (Kamba and McDonald, 2007). Global side effects include EC apoptosis and capillary regression, reduction in EC fenestrations, hypertension, hemorrhage, and thrombosis (Kamba and McDonald, 2007). The current study supports the finding that reducing hepatic VEGF levels can result in vascular regression, and specifically in the liver, we find impaired growth of the HA and PV as well as failure to maintain PV branches. We also add to this knowledge by demonstrating that reducing VEGF levels in the liver can have effects on hepatocyte zonal identity and LSEC identity. Importantly, this study does not use the complete blockage of VEGF, so we avoid disrupting the homeostasis of ECs. Use of this experimental model also allows us to distinguish that disruptions in the liver epithelial and endothelial tissues does not require a complete blockage of VEGF signaling, but can instead

occur when VEGF is simply at lower levels than normal. This suggests that dosage will be very important to minimize side effects on the liver in any VEGF inhibitor treatment.

CHAPTER 6

SUMMARY AND FUTURE DIRECTIONS

Intercellular Signaling in Development and Disease

Signals involved in BEC differentiation

Notch signaling is known to be highly important for the process of IHBD formation through ductal plate morphogenesis (Geisler et al., 2008; Hofmann et al., 2010; Jeliazkova et al., 2013; Kodama et al., 2004; Lozier et al., 2008a; Sparks et al., 2010; Tanimizu and Miyajima, 2004; Zong et al., 2009). Similarly, Notch signaling has been implicated as playing a role in hepatocyte-to-BEC conversion in the adult mouse liver (Fan et al., 2012; Jeliazkova et al., 2013; Yanger et al., 2013). However, the work demonstrated in Chapter 3 of this dissertation demonstrates that Notch is not required for the hepatocyte-to-BEC conversion. Additionally, based on the regeneration of BECs in the DKO mouse and the liver phenotypes of mice with impaired Notch signaling during ductal plate morphogenesis, it is clear that signals other than Notch are important contributors to BEC differentiation during both ductal plate morphogenesis and hepatocyte-to-BEC conversion. During ductal plate morphogenesis, disruption in Notch signaling impairs the remodeling of the ductal plate, but does not completely prevent the initial specification of ductal plate BECs. This phenotype is consistently found in a number of mouse models targeting different Notch pathway components (Hofmann et al., 2010; Kodama et al., 2004; Lozier et al., 2008b; Sparks et al., 2010). These studies suggest that Notch signaling, while necessary for the remodeling of the ductal plate into a mature IHBD, is not required for the specification of BECs and the activation of biliary genes such as Sox9 and cytokeratin19 (CK19). Thus, Notch does not act in isolation during ductal plate morphogenesis, nor is it

required for activation of BEC genes expressed in the ductal plate, such as Sox9 and cytokeratin.

The differentiation of BECs in the DKO mouse model deficient for Notch signaling confirms the idea that Notch signaling is not absolutely required for the differentiation of BECs. In the DKO mouse model, cells are able to activate Sox9 expression and, subsequently, CK19 expression while expressing no Rbpj protein (Figures 3.5, 3.7, 3.8).

The identification of signals that can induce BEC differentiation and IHBD regeneration, either independently or in collaboration with Notch signaling, could be useful for the treatment of IHBD insufficiency diseases. One pediatric IHBD insufficiency disease, Alagille syndrome, is caused by genetic disruptions in Notch signaling components; due to the genetic etiology of this disease, therapies targeting Notch signaling would not be helpful to promote BEC differentiation in Alagille syndrome patients. Notch signaling may also have limited potential as a therapeutic in other cholestatic diseases due to its demonstrated contribution to the generation of cholangiocarcinoma from hepatocytes in a mouse model (Fan et al., 2012; Sekiya and Suzuki, 2012) and the association between Notch signaling and poor prognosis observed in some studies of human hepatocellular carcinoma (Ahn S, 2013; Zhou et al., 2013).

Together, these findings indicate that there must be other pathways that are involved in normal ductal plate morphogenesis and are capable of overcoming the absence of Notch signaling during IHBD regeneration. The identity of this signal(s) is unknown. However, it is likely that Sox9 may play an important role in mediating and promoting the hepatocyte-to-BEC conversion process based on its known role controlling the timing of ductal plate morphogenesis and its expression early in the hepatocyte-to-BEC conversion process. It is likely that the proximal factors driving hepatocyte-to-BEC promote the upregulation of Sox9. Several candidate factors

are found based on molecules known to be upreguated in liver disease or with a known ability to regulate Sox9 expression.

An important future direction of this project will be to identify the signaling pathways that direct BEC differentiation and IHBD regeneration in the DKO mouse. In order to do this, molecular profiling could be done to identify pathways that are differentially activated and suppressed between cells that are at different stages along the hepatocyte-to-BEC conversion process in the P30 DKO mouse liver, including $Sox9^-$ normal hepatocytes, $Sox9^+$ hepatocytes, $CK19^+$ peripheral BECs, and $CK19^+$ mature BECs in hilar IHBDs. Targeting the P30 timepoint would provide the ability to look for gene expression differences that occur between $Sox9^+$ and $Sox9^-$ hepatocytes, at the first stage of hepatocyte-to-BEC conversion, and then in $CK19^+$ peripheral BECs at the second stage of conversion. These cells would presumably still have a gene expression profile that reflects the signals activation of the signaling pathways that drove their recent differentiation. The molecular differences between these $CK19^+$ BECs and the surrounding $Sox9^+$ hepatocytes would hopefully reveal the factor that is able to induce cells to activate CK19 and complete the process of hepatocyte-to-BEC conversion.

The role of Sox9 in hepatocyte-to-BEC conversion and liver regeneration

The expression of Sox9 seems to be an important feature of the hepatic response to cholestatic injury and the hepatocyte-to-BEC conversion process, as the expression of Sox9 in hepatocytes is observed in multiple cholestatic mouse and human liver injuries (Figures 3.5, 3.7, 3.8, 4.1, 4.3) (Yanger et al., 2013). What we cannot address at this time is what the functional significance of Sox9 expression is within the injured livers.

The function of Sox9 during hepatocyte-to-BEC conversion can, however, be hypothesized based on known interactions between Sox9 and other molecules in the liver and its demonstrated functional roles in the pancreas and intestine.

A similar role of Sox9 in cell fate conversion has been observed in the pancreas. During acinar-to-ductal metaplasia in the pancreas, pancreatic acinar cells covert to duct-like cells. These metaplastic cells can eventually lead to intraepithelial neoplasia and invasive pancreatic ductal adenocarcinoma. The role of Sox9 in this acinar-to-ductal cell conversion is illustrated by the finding that Sox9 expression is found in human metaplastic acinar cells in pancreatitis and pancreatic adenocarcinoma and that acinar-to-ductal metaplasia is severely inhibited in mouse models in the absence of Sox9 protein (Prevot et al., 2012). However, the overexpression of Sox9 in cultured cells was not sufficient to inhibit the expression of acinar genes or induce the expression of ductal genes (Prevot et al., 2012). These data suggest that Sox9 may play a central role in promoting conversion to ductal cell fates, both in the pancreas and the liver, but requires collaboration with other factors in order to induce the cell fate conversion.

At this time, we are unable to definitively state whether Sox9 is required for the hepatocyte-to-BEC conversion we see in DKO mouse livers and other liver injury models. In order to determine whether Sox9 is required of sufficient for hepatocyte-to-BEC conversion in the DKO adult mouse liver, studies inhibiting or overexpressing Sox9 would be required. To determine the requirement of Sox9 for hepatocyte-to-BEC conversion, a triple-knockout mouse model could be made where Sox9 is deleted within the hepatic epithelium in addition to Rbpj and Hnf6. Conversely, to determine whether Sox9 is sufficient to drive hepatocyte-to-BEC conversion, the overexpression of Sox9 specifically in adult mouse hepatocytes could be performed either with a genetic mouse model or by the introduction of Sox9 via an adenovirus into cultured hepatocytes. If Sox9 is sufficient to drive hepatocyte-to-BEC conversion, the transcriptional

analysis of cells undergoing that process could also provide useful information on the factors involved in the conversion process.

In the embryonic and postnatal developing liver, as well in rodent liver injuries in the DKO mouse or in BDL or DDC injury, Sox9-expressing hepatocytes and BECs are not proliferative (Figures 3.14, 4.7, 4.8) (Carpentier et al., 2011). This is consistent with known roles for Sox9 in promoting differentiation while limiting proliferation in the intestine and lung (Bastide et al., 2007; Mori-Akiyama et al., 2007)(Rockich, 2013 #340). It seems likely that Sox9 is playing the same role in the liver. However, we are not yet able to address whether the inverse correlation between Sox9 and proliferation is due to a direct influence of Sox9 in regulating the cell cycle. It may alternatively be that Sox9 plays a direct role in cell differentiation, which then in turn reduces proliferation, or that Sox9 only denotes a population of cells which are simultaneously undergoing a cell fate change and a reduction in proliferation without having a direct effect on either process. To assess the direct role of Sox9 in influencing proliferation, it would be useful to perform chromatin immunoprecipitation studies to determine if Sox9 interacts with the enhancer regions of cell cycle genes. It would also be useful to delete and overexpress Sox9 in cultured cells, specifically primary hepatocytes or BECs, to determine if the amount of Sox9, independent of any other effects on DKO hepatocytes *in vivo*, is still correlated with the proliferation status of cells.

If Sox9 is indeed playing a critical role in the hepatocyte-to-BEC conversion process, the molecules upstream and downstream of Sox9 are of interest in order to fully understand the mechanism of Notch- and Hnf6-independent BEC differentiation.

Notch and Hnf6 have both been demonstrated to regulate the expression of Sox9 in several organs (Figure 6.1) (Chen et al., 2012; Clotman et al., 2002; Haller et al., 2012; Meier-Stiegen et

al., 2010; Muto et al., 2009). However, Sox9 is still able to be upregulated and expressed in the DKO liver in the absence of both Rbpj and Hnf6, demonstrating that alternate signaling pathways or stimuli are sufficient to induce Sox9 expression. One possibility explaining the continued expression of Sox9 is the possible upregulation of redundant or compensatory molecules to Rbpj and Hnf6. Despite the loss of Hnf6, the related family member Onecut2 remains undeleted in the liver. It is possible that Onecut2 is able to compensate for the loss of Hnf6 in the DKO mouse (Figure 6.1). Furthermore, the transcription factor Hnf1β has been shown to be regulated downstream of Hnf6 and to be important for ductal plate morphogenesis (Coffinier et al., 2002). While we do not believe that Hnf1β is a crucial factor for the initiation of the hepatocyte-to-BEC conversion program, as it is not expressed in $Sox9^{+}$ hepatocytes or in any $CK19^{-}$ cells in the liver, it may be that Hnf1β is important in the later stages of the hepatocyte-to-BEC conversion process to generate mature peripheral BECs and for remodeling into peripheral IHBDs (Figure 6.1). Hnf1β may reinforce Sox9 expression or work in conjunction with Sox9 to promote the complete differentiation of peripheral BECs (Figure 6.1). Although Rbpj is required for all canonical Notch signaling, we cannot at this time rule out that noncanonical Notch signaling is able to occur and may provide some compensation for the loss of Rbpj.

There have also been findings that Sox9 can be regulated by other signaling pathways, namely Wnt (in the intestine), Fgf (in the pancreas), Shh (in the liver and esophagus) and hypoxia inducible factor (HIF) (in the bone) (Figure 6.1) (Blache et al., 2004; Mori-Akiyama et al., 2007; Seymour et al., 2012; Zhang et al., 2011). These signals are all candidates for the stimulus that is able to activate Sox9 expression in the DKO liver in the absence of Rbpj and Hnf6.

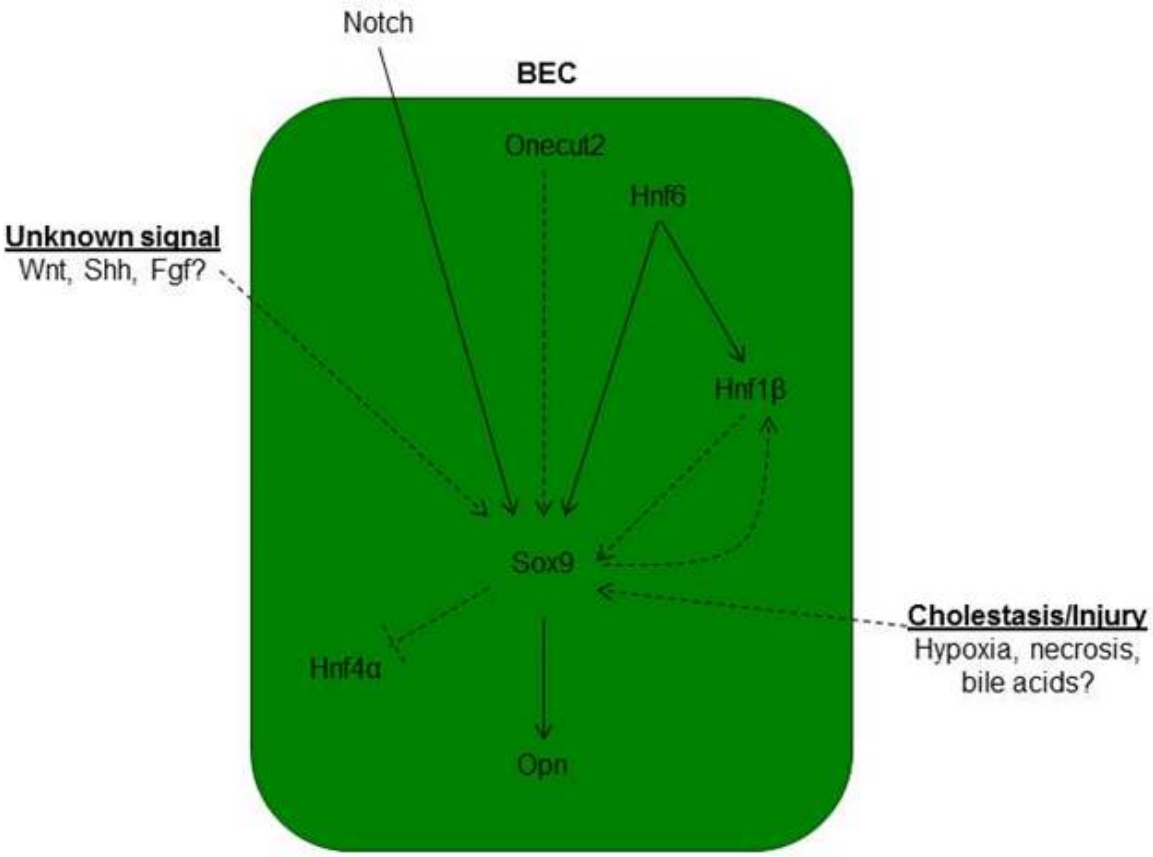

Figure 6.1. The signaling pathways promoting Sox9 expression and hepatocyte-to-BEC conversion. Both Notch signaling and Hnf6 signaling are proven mediators of Sox9 expression. However, alternate signals play a role in the upregulation of Sox9 and BEC specification in both the presence and absence of Rbpj and Hnf6. Potential intracellular signals that may function to promote Sox9 expression, and may work collaboratively with Sox9 to drive hepatocyte-to-BEC conversion, include Onecut2 and Hnf1β. Intercellular signals that may drive Sox9 expression include Wnt, Shh, and Fgf. Signals of the disease state which may function to drive the hepatocyte-to-BEC conversion process include hypoxia, necrosis, and bile acids. However, these connections to Sox9 expression are only hypothesized and have not been demonstrated. Opn has been demonstrated to be regulated downstream of Sox9, and Sox9 may also have a repressive effect on the transcription of Hnf4α. Solid lines denote relationships that have been demonstrated in BECs and dotted lines represent potential signaling relationships that may be active during hepatocyte-to-BEC conversion but have not been tested.

At this point in time, we do not believe that Wnt signaling is a promising candidate to activate Sox9 expression and drive hepatocyte-to-BEC conversion in the DKO mouse. This conclusion is based on recent findings that suggest that both canonical and non-canonical Wnt ligands (Wnt3a and Wnt5a, respectively) play an active role in suppressing biliary fates during embryonic development and liver regeneration (Boulter et al., 2012; Kiyohashi et al., 2013). Therefore, we do not hypothesize that Wnt plays a role in promoting biliary fates and activating Sox9 expression in the DKO mouse liver; however, we cannot exclude the possibility that Wnt may be involved in the hepatocyte-to-BEC process. HIF signaling has been found to regulate the expression of Sox9 in bone, providing yet another candidate factor to be involved in the expression of Sox9 in DKO mice (Zhang et al., 2011). However, this association has not been examined in the liver. Additionally, the relationship between Fgf and Sox9 has not yet been examined in the liver. Both pathways would be candidates for future testing to determine whether either pathway directly regulates the expression of Sox9.

Additionally, there is evidence that Sonic hedgehog (Shh) may regulate the expression of Sox9 in the liver and in the esophagus (Clemons et al., 2012; Pritchett et al., 2012). Interestingly, Shh expression has been found to increase after BDL, correlating with an expansion of BECs, and is believed to play a role in promoting BEC fates and ductular reactions (Omenetti et al., 2008). These data position Shh as an interesting candidate to drive hepatocyte-to-BEC morphogenesis and Sox9 expression in the DKO mice.

To test for the necessity and sufficiency of Fgf, HIF, Wnt and Shh signaling pathways in the hepatocyte-to-BEC conversion process, first the expression of pathway components and downstream targets could be assayed in $Sox9^{+}$ hepatocytes and peripheral BECs to determine if the pathway is active within the cells undergoing hepatocyte-to-BEC conversion. Additionally, a culture assay could be generated whereby isolated primary hepatocytes are treated with

agonists and antagonists of the candidate signaling pathways. The hepatocytes could be tested for expression of hepatocyte and BEC genes, such as Hnf4α, Sox9, and CK19, which has been demonstrated to change expression during the hepatocyte-to-BEC conversion process *in vivo*, to determine if the activation or repression of any signaling pathways, alone or in combination, is sufficient or necessary to promote a BEC-like gene expression profile in cultured primary hepatocytes. Pathways that demonstrate an influence over hepatocyte-to-BEC conversion *in vitro* could also be examined *in vivo* through the administration of pathway agonists or antagonists, or the genetic manipulation to delete or overexpress pathway components, in the background of the DKO mouse model. The inhibition of any pathways that are necessary for the hepatocyte-to-BEC conversion process will result in the failure to produce $Sox9^{+}$ hepatocytes and/or the failure to generate $CK19^{+}$ peripheral BECs at P30.

Specific alleles that could be crossed into the DKO mouse model to test the necessity of each of these candidate pathways for hepatocyte-to-BEC conversion *in vivo* include: floxed Patched (to eliminate Shh signaling), floxed β-catenin (to eliminate canonical Wnt signaling), floxed Fgf receptor 1, 2, or 3 (to reduce Fgf signaling), and floxed HIF1α or HIF2α (to eliminated HIF signaling).

It is possible that signaling pathways not discussed here may be involved in the hepatocyte-to-BEC conversion process. In order to test a wider variety of pathways with less biased in the pwathways analyzed, the same *in vitro* approach could be utilized to perform a screen with a small molecule library. In this experiment, small molecules would be added to isolated primary hepatocytes in culture to determine their effect on the expression of hepatocyte and BEC markers. If any molecules are determined to promote a BEC-like cell fate within primary hepatocytes, the known effects of that small molecule on signaling pathways could be used to

identify previously unexplored candidate signals involved in the hepatocyte-to-BEC conversion process *in vivo*.

In addition to what factors may be promoting Sox9 expression, it is also of interest what the role of Sox9 may be in driving hepatocyte-to-BEC conversion. Little is known about the downstream targets of Sox9 in the liver, but one molecule, osteopontin (Opn) has been shown to be directly transcriptionally regulated by Sox9 and to play a role in liver disease (Pritchett et al., 2012). Sox9 and Opn are co-localized in BECs during embryonic development and adult homeostasis in the mouse, and both genes are simultaneously increased and co-localized in rodent and human models of fibrosis (Pritchett et al., 2012). Sox9 binds a conserved enhancer region of the Opn gene, and the abrogation of Sox9 in the liver significantly decreased the production of Opn, demonstrating a direct link between the two molecules (Pritchett et al., 2012). Opn is a marker of BECs, and thus, the connection between Sox9 and Opn in the liver provides evidence that Sox9 may play an active role in upregulating BEC genes during the hepatocyte-to-BEC conversion process.

The origin of BEC-promoting signals in liver injury situations

In addition to what type of signal(s) is responsible for activating Sox9 and initiating the hepatocyte-to-BEC conversion program, it is also important to determine from whence this signal is arising, including the cell type involved and the spatial location in the tissue. If important signals are arising from a specific cell type, this would provide a potential target for pro-regenerative therapeutic interventions in cholestatic liver disease.

In the DKO mouse model, $Sox9^{+}$ intermediate cells first appear immediately surrounding necrotic lesions in the tissue (Figure 3.8). This finding presents the possibility that the

hepatocyte-to-BEC conversion in DKO mice is driven by a signal that is in some way associated with the necrosis. Previous studies have found that Wnt derived from macrophages is involved in cell fate decisions during chronic liver disease (Boulter et al., 2012); it may be that in DKO mice, immune cells that are attracted to and infiltrate focal necrotic regions release signals that drive Sox9 expression in hepatocytes and hepatocyte-to-BEC conversion.

A possible signal derived from the disease state or immune response

A remaining possibility in the question of what activates Sox9 expression is that the trigger for Sox9 expression may not be a secreted protein at all, but may be the disease state itself. The spatial expression of Sox9 around necrotic lesions may represent that an aspect of the disease state or immune response, which is associated with necrosis, could be promoting the expression of Sox9 in adjacent hepatocytes. Potential factors that could trigger the hepatocyte-to-BEC conversion include the necrosis itself, hypoxia, or cholestasis and bile acid accumulation.

While the presence of necrotic lesions clearly seems relevant to the activation of Sox9 in the DKO mouse, the presence of focal necrosis is not necessary for the expression of Sox9 in hepatocytes. Sox9 expression appears in hepatocytes in DDC and BDL liver injury models in locations where there is no focal necrosis (Figure 4.3). In these cases, it may be that the cholestatic phenotype, or necrotic signals derived from individual dying cells as opposed to large patches, is able to drive Sox9 expression. Alternatively, it may be that signals that can be associated with necrotic patches, such as secretions from immune cells, are simply deriving from other places or from a more diffuse immune infiltration in other types of liver injury.

Studies in rat have shown that VEGF expression is upregulated follow hepatic necrosis, providing another possible signal that may explain the spatial pattern of Sox9 expression (Ishikawa et al., 1999). In the injured mouse liver, VEGF receptor expression is detected in hepatocytes, but at much lower levels than it is expressed in LSECs (Yamane et al., 1994). There is no known direct connection between VEGF signaling and Sox9 expression.

Hypoxia could directly influence gene expression in hepatocytes, as hepatocytes are able to sense oxygen tension. Sox9 is regulated downstream of hypoxia in the bone. Hepatocytes have a built-in mechanism for sensing hypoxia, and it is possible that regions of hypoxia associated with focal necrotic lesions are sufficient to trigger a response in hepatocytes. To determine the direct effect of oxygen tension on the expression of Sox9 in hepatocytes, primary hepatocytes could be cultured in a variety of atmospheric oxygen pressured and assayed for differential expression of Sox9.

Another possibility is that the cholestatic disease state is responsible for driving Sox9 expression. During cholestatic injuries, such as in the DKO mouse model, the back-up of bile acids may be sensed by hepatocytes and initiate the hepatocyte-to-BEC conversion response. If the presence of a cholestatic injury is sufficient to drive Sox9 expression, this would explain the differences in Sox9 expression between cholestatic and non-cholestatic liver injury models in rodents (Figures 4.2, 4.3). Similarly, cholestasis and bile acid build-up could be a signal that more BECs are needed, explaining the response of the hepatocytes to activate Sox9 and BEC genes under cholestatic injury conditions. To test if bile acids are capable of promoting Sox9 expression in hepatocytes, a simple experiment could be performed where cultured hepatocytes are treated with exogenous bile acids to determine whether or not Sox9 becomes activated.

Comparing BEC-specification mechanisms in ductal plate morphogenesis and hepatocyte-to-BEC conversion

Ductal plate morphogenesis and hepatocyte-to-BEC conversion are similar in several ways: they both include the upregulation of Sox9 as one of the earliest steps in the BEC differentiation process, they both occur without proliferation of differentiation cells, the formation of cytokeratin-expressing BECs is spatially restricted to portal areas within zone 1 in the liver, and they both occur less efficiently without Notch signaling (Sparks et al., 2010; Yanger et al., 2013). There are also many differences between the two processes. For example, peripheral ductal plate morphogenesis cannot occur in the combined absence of Rbpj and Hnf6, but hepatocyte-to-BEC conversion can. Additionally, the BECs specified through ductal plate morphogenesis are restricted to immediately surrounding the PV, but during hepatocyte-to-BEC conversion, hepatocytes in any zone can activate Sox9, and the first Sox9 expression occurs surrounding necrotic lesions. In ductal plate morphogenesis, a mature IHBD is formed from two layers of ductal plate cells, but during hepatocyte-to-BEC morphogenesis, IHBDs are formed from remodeled ductular reactions. As the spatial location is so important for the signaling mechanism of ductal plate morphogenesis, and the spatial pattern of differentiation is different in hepatocyte-to-BEC conversion, it is likely that the differentiation mechanism is not completely conserved between the two processes.

It is likely that, despite the differences in gene requirements and spatial mechanisms, similar intracellular signaling cascades downstream of Sox9 are activated in both ductal plate morphogenesis and hepatocyte-to-BEC morphogenesis. However, the immediate upstream signal may be different between the two processes. In ductal plate morphogenesis, the first signal initiating Sox9 expression likely is derived from a periportal tissue and may be from the portal vein endothelium or the portal vein mesenchyme. In hepatocyte-to-BEC conversion,

however, and specifically in the DKO mouse model, the first signal promoting Sox9 expression is not tied to the portal area and instead appears to originate from necrotic lesions. It is possible that the same signal is involved but is derived from two different areas in embryonic and postnatal livers. Such signals might include hypoxia, immune-secreted signals, or a number of secreted signaling molecules known to be present in the liver that have already been discussed.

Regulation of Liver Zonation

The architectural zonation of liver tissues

Within the liver, zonation is found within both epithelial and endothelial tissues. With the endothelium, differences are apparent between the PV and CV as well as between the periportal and pericentral LSECs. It stands to reason that the differences between the PV and CV are important to restrict ductal plate morphogenesis. Otherwise, the origin and purpose of endothelial zonation is poorly understood. Within the epithelial tissues, there is a well-established zonal difference in gene expression across the lobule in hepatocytes. The purpose of this zonation is believed to be to segregate multiple hepatocyte functions to specific cell populations, thus generating specific groups of specialized cells. Previous work has demonstrated that Wnt/β-catenin plays a role in regulated zonal gene expression in hepatocytes (Figure 6.2A); however, the source of differential Wnt signaling between the periportal and pericentral hepatocytes is not known. Another factors hypothesized to be involved in generating and maintaining zonation in hepatocytes in oxygen tension, which varies greatly along the axis of the lobule (Figure 6.2A). In addition to hepatocytes, IHBD branches also show a zonal architecture within the liver lobule, as they appear only next to PVs.

Factors regulating IHBD zonation

The appearance of ductal plates during embryonic development is restricted to the periportal hepatocytes, indicating that either the signal inducing BEC specification is closely spatially regulated, and/or that only the periportal hepatoblasts are competent to respond to the signal that promotes BEC specification. Despite the widespread activation of Sox9 in hepatocytes throughout the parenchyma of the P30 DKO mouse (Figure 3.7), the expression of CK19 is only activated in periportal areas, and peripheral IHBDs only regenerate next to PVs. In a variety of injury models, ductular reactions are spatially restricted to the periportal areas and to the portal bridges, the areas that bridge the portal tracts along the periphery of the hepatic lobule. This spatial restriction is apparent in the location of reactive ductules in the P60 DKO mouse (Figure 3.6), and, interestingly, also in the expression of Sox9 in hepatocytes in the livers of mice subjected to BDL (Figure 4.5). Even in mouse models where activated Notch is overexpressed in all hepatoblasts or hepatocytes, conversion of hepatocytes into BEC only occurs in zone 1 and zone 2 hepatocytes; zone 3 hepatocytes did not activate a biliary program despite expressing activated Notch (Jeliazkova et al., 2013; Sparks et al., 2010; Yanger et al., 2013).

Clearly, there is some signal that limits Sox9 expression and BEC differentiation to only specific zones in the liver. However, that signal is unknown and is surprisingly not the focus of any substantial efforts of investigation (at least to the author's knowledge). The spatial restriction in BEC differentiation could reflect either a difference in competency of hepatocytes in different zones to receive and/or respond to a pro-BEC differentiation signal or the spatial restriction of a pro-BEC signal to periportal areas. The signal could be either instructive, driving the expression of Sox9 and cytokeratins, or permissive, allowing only the periportal hepatocytes to respond to pro-biliary stimuli. As the question of what signals could initial this process were contemplated previously, the remaining and related question is: from what cells is this signal derived and how

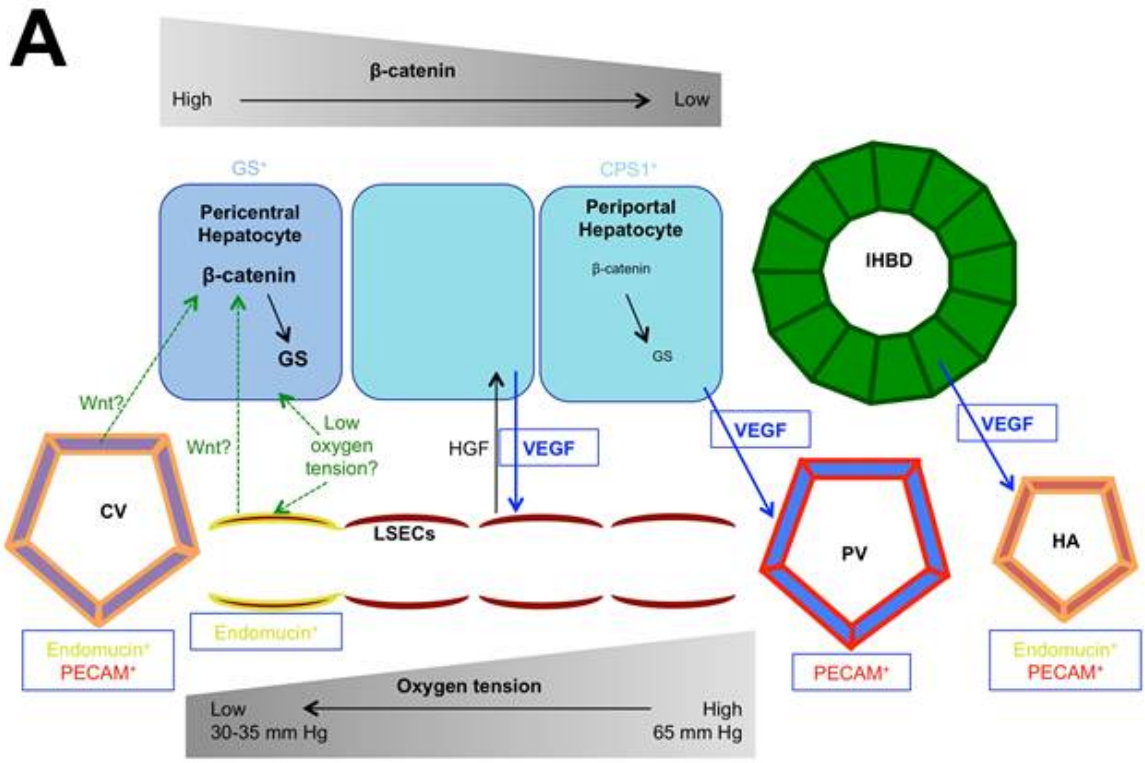
A
β-catenin
High
Low
GS+
CPS1+
Pericentral Hepatocyte
β-catenin
GS
Periportal Hepatocyte
β-catenin
GS
IHBD
Wnt?
Wnt?
Low oxygen tension?
HGF
VEGF
VEGF
VEGF
CV
LSECs
PV
HA
Endomucin+
PECAM+
Endomucin+
PECAM+
PECAM+
Endomucin+
PECAM+
Oxygen tension
Low
30-35 mm Hg
High
65 mm Hg

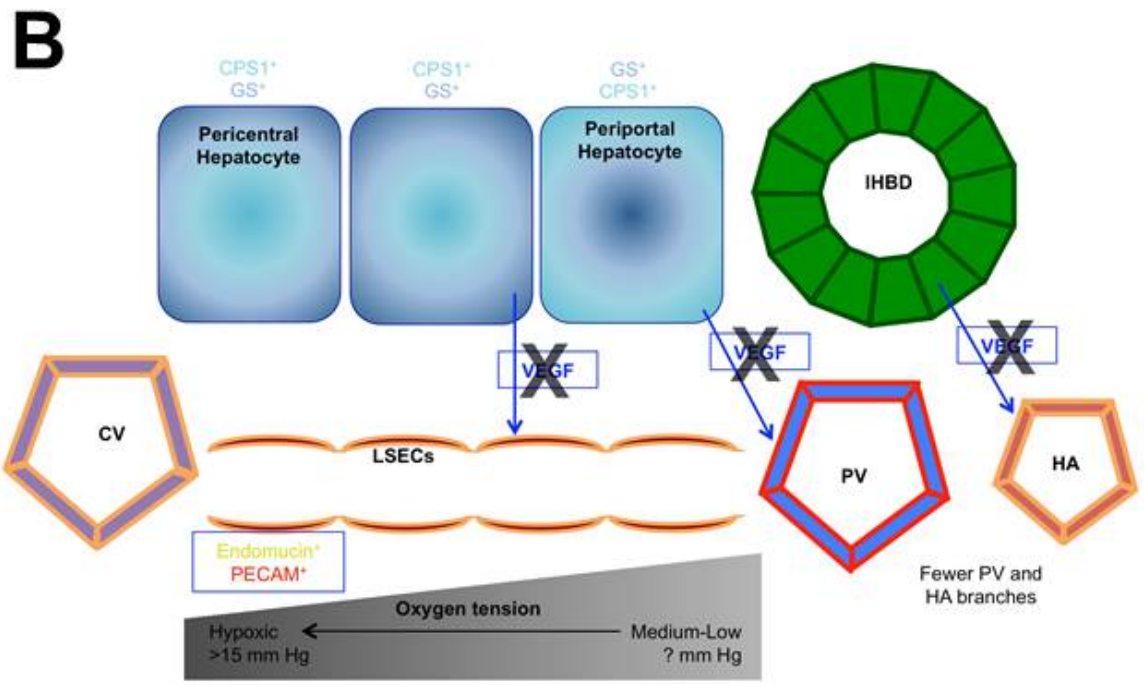
B
CPS1+
GS+
CPS1+
GS+
GS+
CPS1+
Pericentral Hepatocyte
Periportal Hepatocyte
IHBD
VEGF
VEGF
VEGF
CV
LSECs
PV
HA
Endomucin+
PECAM+
Fewer PV and HA branches
Oxygen tension
Hypoxic
>15 mm Hg
Medium-Low
? mm Hg

Figure 6.2. The regulation of zonation in control and VKO livers. Hepatocyte and endothelial cells display a high degree of zonal gene expression regulation in control mouse livers (A) which is severely disrupted in VKO mouse livers (B). In the control liver (A), there is a gradient of oxygen tension along the axis of the lobule. There is also a gradation of nuclear β-catenin in hepatocytes that is highest in the pericentral hepatocytes. The gradient of nuclear β-catenin is proposed to drive zonal hepatocyte gene expression, whereby pericentral hepatocytes express GS and periportal hepatocytes express CPS1. With in endothelial cells, there is also zonal differences in gene expression. While the CV and pericentral LSECs express endomucin, the PV and periportal LSECs do not. There is likely communication between hepatocytes and endothelial cells that define these zonal gene expression patterns. VEGF secreted from hepatocytes is known to affect LSECs, with one effect being to inhibit the expression of PECAM in LSECs. LSECs are also known to secrete HGF, which influences hepatocyte behaviors. These signals are potential candidates for mediating zonal regulation. It is also hypothesized that Wnt may be secreted from CV endothelial cells of pericentral LSECs to drive the β-catenin gradient in hepatocytes. The gradient in oxygen tension is hypothesized to play a role in zonal hepatocyte gene expression and may also play a role in zonal LSEC gene expression. The work shown in this dissertation has demonstrated that VEGF secreted from the hepatic epithelial tissues (hepatocytes and BECs) influences the gene expression and architecture in the LSECs, the PV, and the HA. Black lines denote known relationships; blue lines denote conclusions from this dissertation; green lines denote connections which have not been tested but are hypothesized. When Vegf is knocked out of the liver epithelium (B), several disruptions occur. First, there is an increase in hypoxia within the hepatocytes and thus a decrease in oxygen tension. This is likely due to a decrease in the number of PV and HA branches. There is altered gene expression in LSECs, whereby the expression of endomucin is extended into periportal LSECs and the expression of PECAM is abnormally upregulated in LSECs. Within hepatocytes, there is a loss of the zonal restrictions of GS and CPS1 expression.

is it spatially restricted?

A future direction of this work is to identify the other signal that is responsible for the spatial restriction in BEC differentiation competency. This could be performed through the molecular comparison of wsCK$^+$ ductal plate cells and surrounding wsCK$^-$ non-ductal plate hepatoblasts, especially in a Notch-impaired embryo, or of CK19$^+$ and surrounding Sox9$^+$CK19$^-$ cells in a P30 DKO mouse liver. By comparing cells in close proximity, but ultimately having a different differentiation status in terms of cytokeratin expression, the differences in intracellular signaling and/or gene expression could identify the factor(s) that is responsible for pushing cells past the signaling threshold between hepatocyte and BEC fates. These findings could then be extrapolated back to determine the extracellular cues that control the BEC differentiation competency and the cellular source of these signals.

As concurrent lobular zonation has been observed in BECs, as described above, and hepatocytes and ECs, as will be discussed following, it may be that the primary regulation of zonation occurs in only one of these tissues first and that tissue subsequently regulates the zonal patterning of the other tissues. As ductular reactions are restricted to periportal areas and portal bridges, it may be that the zonal signals spatially restricting ductular reactions are derived from either the PV, the portal mesenchyme/stroma, the periportal LSECs, or the higher oxygen tension in periportal zones. As the communication between tissues has been frequently documented, including in the case of mesenchymal-to-epithelial Notch signaling during ductal plate morphogenesis (Hofmann et al., 2010), it will be important to carefully consider the influence of certain tissues over others during the establishment and maintenance of zonation in the liver. While it may not be feasible due to challenges in the mouse model, and interesting future experiment would be to test the role of hepatocyte and endothelial zonation in regulating

ductular reaction zonation by causing a ductular reaction-inducing injury in the VKO mice who have zonation defects in hepatocytes and LSECs, as will be described below, or in another mouse model where the hepatocyte or LSEC zonation is altered.

Factors regulating endothelial zonation

There is endothelial heterogeneity between the PV and CV as well as between the periportal and perivenous LSECs (Figure 5.15, Figure 6.2A). As described in Chapter 1, the PV and CV are derived from the same fetal veins but are separated early in hepatic development. Thus far, there is no known information on how the PV and CV endothelium become distinct from each other, nor is there information known regarding the regulation of periportal and perivenous LSEC identities.

Future directions in determining the molecular factors and signals that differentiate the PV from the CV may involve transcriptional profiling of the veins early in development and in adulthood. A difference exists as early as E13.5, at the onset of ductal plate morphogenesis and just days after the two vessels become established as separate structures (Collardeau-Frachon and Scoazec, 2008; Gouysse et al., 2002). Analysis of the transcriptomes of the PV and CV endothelium early in development could identify the factor(s), if any, that is responsible for differentiating the mesenchyme around the PV and CV and/or conferring BEC specification competency in the periportal hepatoblasts only.

An interesting experiment, while technically challenging, would be to examine the role of blood flow in the divergent differentiation of the PV and CV during embryonic development. If an *ex vivo* bioreactor could be built that would support fluid flow through the embryonic liver, a reversal of fluid flow direction could be performed to determine whether fluid directionality is

sufficient to regulate the cascade of signals and events that ultimately regulates the formation of the ductal plate around only PVs and not CVs.

Novel findings on the zonal heterogeneity of LSECs are shown in Chapter 5 of this dissertation. What is found in the work discussed is that the loss of epithelial VEGF signaling results in the alteration of zonal gene expression within LSECs (Figure 6.2B). The molecule endomucin, which is normally expressed in CVs and pericentral LSECs but not in PVs or periportal LSECs, loses its spatial restrictions in the VKO mouse model and is expressed in LSECs across the lobular axis (Figure 6.2B). Without any known information on how zonal endothelial identities are regulated during normal liver development and homeostasis, it is difficult to speculate on the cause of their dysregulation in the VKO mouse model. With concurrent zonation defects in the hepatocytes and LSECs, it remains impossible at this stage to definitively determine whether the LSEC zonal defects are proximal to the hepatocyte zonal defect, or vice versa, or whether both the hepatocyte and LSEC defects are primary to the loss of epithelial VEGF and are not interdependent. Similarly, it remains unknown the reduction in VEGF protein in the liver directly or indirectly changes the zonal expression pattern of endomucin in LSECs.

There are several possibilities regarding the cause of altered LSEC zonal gene expression, including: 1. Hepatocyte-secreted VEGF gradients directly regulate expression of LSEC zonal genes; 2. Hypoxia regulates zonal identities of LSECs; 3. Altered hepatocyte fates result in altered signaling to LSECs. All of these possibilities have potential to be true, as it is known that hepatocytes can signal to LSECs through VEGF and that VEGF plays a large role in the identity of LSECs (DeLeve et al., 2004). Additionally, studies on hepatocyte-derived VEGF expression in liver injury have found that the strongest upregulation of VEGF comes from periportal hepatocytes, allowing for the possibility that a zonal VEGF gradient is generated by hepatocytes in the normal liver and is responsible for generating LSEC zonation (Taniguchi et al., 2001). It

may be that in both homeostasis and regeneration, a VEGF gradient across the liver influences endomucin expression, with high VEGF periportally inhibiting endomucin expression.

In order to test whether oxygen tension or VEGF protein levels may have a direct effect on zonal identities and gene expression in LSECs, the atmospheric oxygen pressure and the amount of exogenous VEGF could be modulated in a culture system for LSECs. The LSECs could be assayed for the expression of endomucin as a readout of zonal identity. If the culturing technique does confirm that either oxygen tension or VEGF protein levels does directly modulate the expression of endomucin, independent of indirect signals from any other cell type or source, the molecular profiling and comparison of LSECs either expressing or not expressing endomucin could be used for further identification of zonal differences within the sinusoid compartment and potentially also between PVs and CVs.

Factors regulating hepatocyte zonation

In the control liver, expression of zonal genes, such as GS and CPS1, demarcate tight boundaries in zonal hepatocyte subpopulations (Figure 6.2A). In the VKO mouse, however, there are disruptions in hepatocyte zonal gene expression, and abnormal co-expression of GS and CPS1is apparent in hepatocytes (Figure 6.2B). In P30 VKO mice, the expression of the perivenous gene GS is expanded periportally and the expression of the periportal gene CPS1 is expanded pericentrally; overlap between the two proteins is observed both in pericentral and periportal hepatocytes, indicating a breakdown in the establishment and/or maintenance of the zonal hepatocyte boundaries (Figure 5.9). In addition to zonal hepatocyte disruptions, VKO mouse livers shown alterations in LSEC zonation and in oxygen tension, the latter is believed to directly result from a decrease in PV and HA branches in the VKO mouse as compared to control (Figure 6.2B). Due to these concurrent phenotypes, a number of possibilities exist to

explain the disruption in hepatocyte zonation: 1. The hepatocyte gene expression could be directly regulated through VEGF signaling and thus altered in the loss of epithelial VEGF; 2. The hepatocyte defects could be directly caused by the change in oxygen tension across the liver lobule; or 3. The hepatocyte defects could be secondary to LSEC zonation defects, which could be caused either by hypoxia or directly by VEGF signaling reductions.

There is evidence that some hepatocyte zonal genes but not others are regulated by oxygen tension. Erythropoietin, for example, as well hepatocyte zonation genes such as PEPCK and GK, are found to be influenced by oxygen tension (Jungermann and Kietzmann, 1997; Kietzmann et al., 1992; Tam et al., 2006) while others, including GS, were not (Jungermann and Keitzmann, 1996). If GS is not sensitive to hypoxia, then the hypoxia observed in VKO livers (Figure 5.10) would not be directly responsible for the expansion in GS expression (Figure 5.8). The absence of a direct regulation of GS by hypoxia is also supported by the finding that in P30 VKO mice, regions of hypoxia and regions of expanded GS expression are not necessarily overlapping (Figure 5.10).

The finding that GS expression is changed provides evidence that the defect in the VKO livers is due to more than just a decrease in oxygen tension, and may also be caused by signaling defects within the liver. While we cannot exclude the possibility that GS expression in hepatocytes is directly regulated by oxygen tension in the VKO model, several alternative explanations could be responsible for the altered GS expression, including: 1. VEGF protein has a direct role in repressing GS expression; 2. A signal derived specifically from periportal LSECs represses GS expression in hepatocytes; 3. A signal derived specifically from perivenous LSECs promotes GS expression; 4. GS expression is inhibited by a secreted molecule from the PV, HA, or associated mesenchyme, and is decreased due to the reduction in PV and HA branches. There is currently no signal that has been identified that performs any of the roles

described above. However, one potential signaling candidate can be inferred based on the known regulation of GS signaling.

Wnt/β-catenin signaling is known to directly regulate the expression of GS in the liver. β-catenin is both necessary and sufficient to induce the expression of GS in hepatocytes (Benhamouche et al., 2006; Colletti et al., 2009; Colnot and Perret, 2011). While there has been no direct evidence that Wnt secreted from LSECs drives zonal gene expression in hepatocytes, it has been demonstrated that LSECs in the adult mouse liver express multiple Wnt ligands, whereas hepatocytes express multiple Frizzled receptors of Wnt (Zeng et al., 2007). The expression of Wnt ligands and receptors in LSECs and hepatocytes, respectively, enhances the hypothesis that signals from the endothelium could be responsible for the altered hepatocyte zonation. A future direction in this area will be to address the role of hypoxia in the altered hepatocyte zonation.

The influence of hypoxia on GS expression can be tested by separating the effects of hypoxia from the direct effects of VEGF protein reduction. This can be accomplished by inducing a hypoxic state in animals without inhibiting VEGF signaling. Additionally, the effects of VEGF inhibition could be tested without the associated hypoxia by inhibiting VEGF signaling in the liver with an inducible gene disruption of VEGF in a postnatal mouse or through the administration of VEGF inhibitors. By separating the hypoxia and the VEGF loss, it could be determined which of these factors is responsible for the alterations in hepatic zonation.

Another future direction in this project would be to determine the role of β-catenin in the VKO phenotype. It has already been shown by altering Wnt/β-catenin pathway components genetically that Wnt/β-catenin is both required and sufficient for GS expression. By combining a conditional knockout of β-catenin and Vegf within the liver epithelium, we would be able to

determine whether the VKO phenotype of expanded GS expression is mediated by β-catenin signaling.

Cellular Plasticity in Development and Disease

Differential responses in cell plasticity depending on degree and type of injury

In the various genetic, chemical, and surgical injury models examined in this dissertation, the cellular responses to injury varied widely. In the DKO model, new BECs were formed from hepatocytes, an extensive ductular reaction was formed, and functional peripheral IHBDs were generated (Figures 3.1, 3.3). In the DDC model, $Sox9^+$ hepatocytes and a $CK19^+$ ductular reaction were both induced by injury. In the BDL model, a large number of $Sox9^+$ hepatocytes were induced by injury, but no ductular reactions were observed. In the 2-AAF/PHx model, a ductular reaction was observed, but no $Sox9^+$ hepatocytes were present. Finally, in the PHx model, no $Sox9^+$ hepatocytes or ductular reactions were observed (Figures 4.2, 4.3). This variation in response indicates that the mechanisms of cellular reactions vary based on the specific injury. This variation could be caused by the degree of injury or the specific tissues affected.

$Sox9^+$ hepatocytes were observed in all the cholestatic injury models examined, including the DKO, DDC, and BDL models, but not in the non-cholestatic injuries. However, there is no simple consistency in which injuries did or did not generate reactive ductules. Interestingly, a previous study has indicated that reactive ductules can have one of two molecular profiles, either a $Notch^+$ profile or a Wnt^+ profile (Wang et al., 2009). This may indicate that there are multiple ways that the ductular reaction can be induced and that it may not be possible to identify one commonality between all ductular reaction-inducing injuries.

Future directions include determining the role of the ductual reaction in the injury, and specifically trying to determine whether the emergence of the ductular reaction serves a function in alleviating the disease state. To test the role of the ductular reaction in a cholestatic liver injury model, we could induce a ductular reaction with DDC in control mice and mice with genetical manipulations impairing the ductular reaction, such as inhibitions in Notch signaling. Between the control and mutant mice, we could perform tests on liver function and damage to determine whether, in the same liver injury model, there are differences in severity of liver damage depending on the extent of the ductular reaction.

Signals influencing liver injury and regeneration

Signaling molecules that have known importance in liver regeneration also play roles in liver regeneration and cell plasticity in the postnatal liver. The role of Sox9 has already been discussed. Of specific interest are Hnf6 and Wnt.

Hnf6 is an important mediator of IHBD morphogenesis during embryonic development and is sufficient to promote biliary cell fates in the pancreas when overexpressed in cultured cells (Clotman et al., 2002; Prevot et al., 2012). Hnf6 has been found to be downregulated in the liver after BDL and to inhibit the proliferation of BECs when overexpressed after BDL in mice (Holterman et al., 2002). Hnf6 regulates several critical liver functions, including cholesterol catabolism and bile acid synthesis, through the direct transcriptional control of cholesterol 7-alpha hydroxylase (CYP7A1) (Wang et al., 2004). Similarly to Sox9, is appears that Hnf6 promotes cellular differentiation and function while restricting proliferation, but that the repression of Hnf6 during liver injury may be an important tool for promoting cellular proliferation and regeneration. While we know that Hnf6 is not absolutely required for BEC specification and

IHBD regeneration in DKO mice, we do not at this time know the role of Hnf6 in hepatocyte-to-BEC conversion, and overall liver response to injury, in the non-genetic injury models examined. As Hnf6 promotes the expression of BEC genes, including Sox9, we may hypothesize that Hnf6 is involved in the hepatocyte-to-BEC conversion mechanism and may work coordinately with Sox9 to inhibit proliferation in the cells undergoing conversion.

Another molecule of interest for its role in liver regeneration is Wnt signaling. As previously mentioned, a recent study has demonstrated that Wnt3a, secreted from macrophages, opposes Notch signaling and promotes the hepatocyte cell fates in a liver injury model (Boulter et al., 2012). Within the adult mouse liver, β-catenin has demonstrated roles in the export of bile (Behari et al., 2010), and β-catenin-null livers demonstrated reduced regeneration after acetaminophen-induced injury (Apte et al., 2009). During liver injury in the rat, β-catenin was found to promote the differentiation of reactive BECs into hepatocytes (Williams et al., 2010). Despite the positive regulation of Sox9 by Wnt in other organs, in the liver, Wnt/β-catenin may function to promote hepatocyte, and not BEC, fates.

Significance of Sox9 expression in human liver disease and regeneration

Sox9 is not required for BEC differentiation or IHBD formation (Antoniou et al., 2009). However, it does play a role in ductal plate morphogenesis and clearly identifies, and may play a role in, cells that have progenitor characteristics or lineage conversion potential (Figures 3.7, 4.3) (Antoniou et al., 2009; Dorrell et al., 2011; Malato et al., 2011; Yanger et al., 2013). Additionally, Sox9 is expressed in hepatocytes or hepatobiliary intermediate cells in a variety of different human liver diseases (Figure 4.1) (Yanger et al., 2013). However, what these Sox9-expressing hepatobiliary intermediate cells in human liver disease actually represent is unknown.

In the pediatric liver disease Alagille syndrome, some patients recover from cholestasis seemingly spontaneously after a few years of age. Others, however, do not. The only treatment for Alagille syndrome currently is liver transplantation. Due to the stress of undergoing transplantation and the shortage of transplantable livers, there is a real need to better methods of predicting prognosis in Alagille patients, so that we can avoid transplantations in those patients who would have recovered on their own otherwise and identify the patients who will not recover earlier. As Sox9 is one of the first markers of hepatocytes undergoing a BEC conversion, the presence of $Sox9^+$ hepatocytes in Allagille syndrome patients, and potentially patients of other liver diseases, may be useful as an indicator of prognosis.

In the DKO mouse model, it appears that the expression of Sox9 denotes the first stage or regeneration, as $Sox9^+$ hepatocytes precede $CK19^+$ peripheral BECs and, subsequently, mature peripheral IHBDs. As the regeneration progresses and the injury resolves, widespread expression of Sox9 in the liver subsides. In the DDC and DKO injuries, however, where the injury persists, the expression of Sox9 persists. It is unclear if the persistent and increasing $Sox9^+$ cells are primarily indicative of either and increase in regenerative efforts or an increase in the disease state. Similarly, although we observe the expression of Sox9 in several human liver diseases, we do not know if the presence alone of $Sox9^+$ intermediate cells in human liver disease is indicative of degree of injury, ongoing regeneration, both, or neither.

A future direction for this project is to perform a thorough analysis of $Sox9^+$ intermediate cells in the liver of human liver disease patients and determine whether the presence of $Sox9^+$ intermediate cells has any correlation to disease severity and progression and/or outcome. To do this, a number of biopsy samples will be required, hopefully from patients in different stages of disease progression. By matching patients with similar disease indicators on lab tests (for

example, total bilirubin levels) to control for differences in disease severity, we can determine if there are cellular differences in the extent of Sox9 expression that correlate with outcome.

APPENDIX A

USE OF THE *ENDOTHELIAL-SCL-CRE^T* MOUSE LINE TO LINEAGE TRACE ENDOTHELIAL CELLS AND DELETE RPBJ WITHIN ENDOTHELIUM DURING HEPATIC DEVELOPMENT

Introduction

The vascular tissues of the liver, the portal vein (PV) central vein (CV), hepatic artery (HA), and liver sinusoidal endothelial cells (LSECs), have highly distinct functions and architectures. Similarly, their development is thought to be very different; while the PV and CV are proposed to arise from the remodeled vitelline and umbilical veins (Collardeau-Frachon and Scoazec, 2008), the HA is thought to arise through angiogenesis from the dorsal aorta, and the LSECs from resident endothelial cells (ECs) in the septum transversum mesenchyme (Gouysse et al., 2002). However, no studies have definitively answered the fundamental questions regarding the development of the hepatic vascular tissues, including what EC populations contribute to each structure and whether angiogenesis, vasculogenesis, or both are responsible for their formation.

Notch signaling has been implicated as being a crucial regulator of both angiogenesis and vasculogenesis and to interact cooperatively with VEGF signaling in multiple organs and species (Herbert and Stainier, 2011). Yet, it is not known whether Notch plays a role in the development of any hepatic vascular tissues. As the hepatic vasculature of the liver is highly unique in both function and development, the characterization of angiogenesis as it occurs in other organs cannot necessarily be assumed to hold true in the liver. Hence, the involvement of Notch in hepatic vascular development remains unknown.

In this study, we utilized a mouse model of tamoxifen inducible Cre-mediated recombination of a

reporter allele in ECs in an attempt to characterize their contribution to hepatic vascular development. The *endothelial-SCL-CreER^T* (Göthert et al., 2004) transgenic allele utilizes the 5' enhancer region of the *stem cell leukemia* (*SCL*) locus previously shown to be expressed specifically in ECs and a subset of hematopoietic cells (Gottgens et al., 2004). For several reasons, we have chosen to use the *Gt(ROSA)*26*Sor*$^{tm1(EYFP)Cos}$ (ROSA26R-EYFP) (Srinivas et al., 2001) reporter allele, which is silent until Cre excises a transcriptional stop cassette. First, enhanced yellow fluorescent protein (EYFP) is easily detected with antibodies and thus will allow us to immunostain for markers of cell identity and proliferation along with the EYFP lineage marker. Second, the ROSA26 promoter provides a promoter that is active in all cells, so that once Cre activates this allele, EYFP will remain expressed regardless of the cell fate. Third, activation of EYFP expression occurs via recombination of DNA and thus is a heritable event that will ensure EYFP expression even when Cre is no longer present. Thus, we will be able to perform a spatio-temporal analysis of the populations of ECs present at different developmental timepoints and identify the structure to which they and their progeny contribute.

We used the endothelial-*SCL-CreER^T* in combination with ROSA26R-EYFP reporter mouse model to lineage trace ECs over several timepoints and to delete the Notch signaling mediator *Rbpj* to assess the role of Notch signaling in hepatic vascular development. We found that the endothelial-SCL-lineage label was not able to distinguish between the populations of ECs in terms of their contribution to different vascular structures at different timepoints. We additionally found no phenotype in mice with Rbpj deleted in ECs. However, the absence of phenotype may be due to an incomplete recombination of *Rbpj*.

Results

To determine whether the expression of the endothelial-SCL-lineage label is able to differentiate subpopulations of ECs at different developmental stages, we performed a series of lineage tracing experiments in *endothelial-SCL-CreER^T; ROSA26R-EFYP* mice where recombination was either induced at different timepoints and recombination within the tissue was analyzed at a common timepoint, or where recombination was induced at one common timepoint and then recombination within the tissue assessed at a variety of later timepoints. Timepoints were targeted over a variety of different developmental stages, including prior to liver bud formation (before E9.5), during disruption and remodeling of the vitelline and umbilical veins (E10-E12.5), embryonic development after venous remodeling (E12.5-P0), and postnatal growth of the vascular tissues (P0-P30). See Figure A.1 for a graphic summary of timepoints analyzed for endothelial-SCL-lineage tracing.

We found no differences in which vascular tissues expressed the endothelial-SCL-lineage label in any experiments. For example, we found that whether we induced endothelial-SCL-lineage-labeling at E12.5 or P15, very different developmental stages, we still saw that endothelial-SCL-lineage-labeled cells contributed to the mature PV, HA, and sinusoids when the livers were analyzed at P30 (Figure A.2).

Next, we attempted to determine whether Notch signaling, and the Notch mediator Rbpj, is required for any of the crucial stages of liver vascular development. We induced recombination of the *Rbpj^{tm1Hon}* allele (*Rbpj$^{flox/flox}$*) (Han et al., 2002) at a variety of timepoints (See Figure A.3 for a graphic summary of timepoints analyzed for *endothelial-SCL-CreER^T* mediated deletion of Rbpj). In no experimental paradigm did we find a difference between the control and

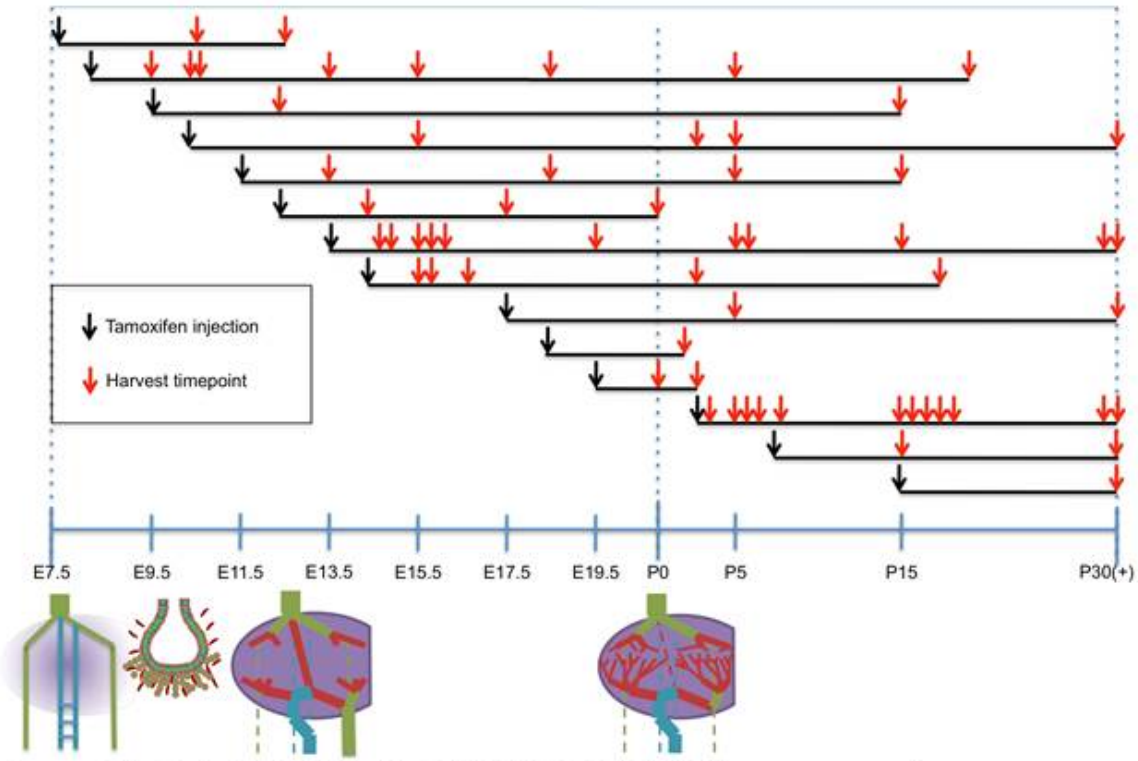

Figure A.1. *Endothelial-SCL-CreER^T; ROSA26R-EYFP* lineage trace embryos were analyzed at a variety of timepoints spanning important developmental stages. Timepoints for tamoxifen injections and harvests are shown. For each Tamoxifen timepoint, represented by a black arrow, at least one litter was harvested at each of the corresponding harvest timepoints indicated by a red arrow. Developmental events that were encompassed in these timepoints include: formation of liver bud (E9.0-E10.0), liver bud disruption of the fetal veins and fetal vein remodeling (E10-E12.5), embryonic vascular growth (E12.5-P0), collapse of the ductus venosus (P0), and postnatal growth (P0-P30+).

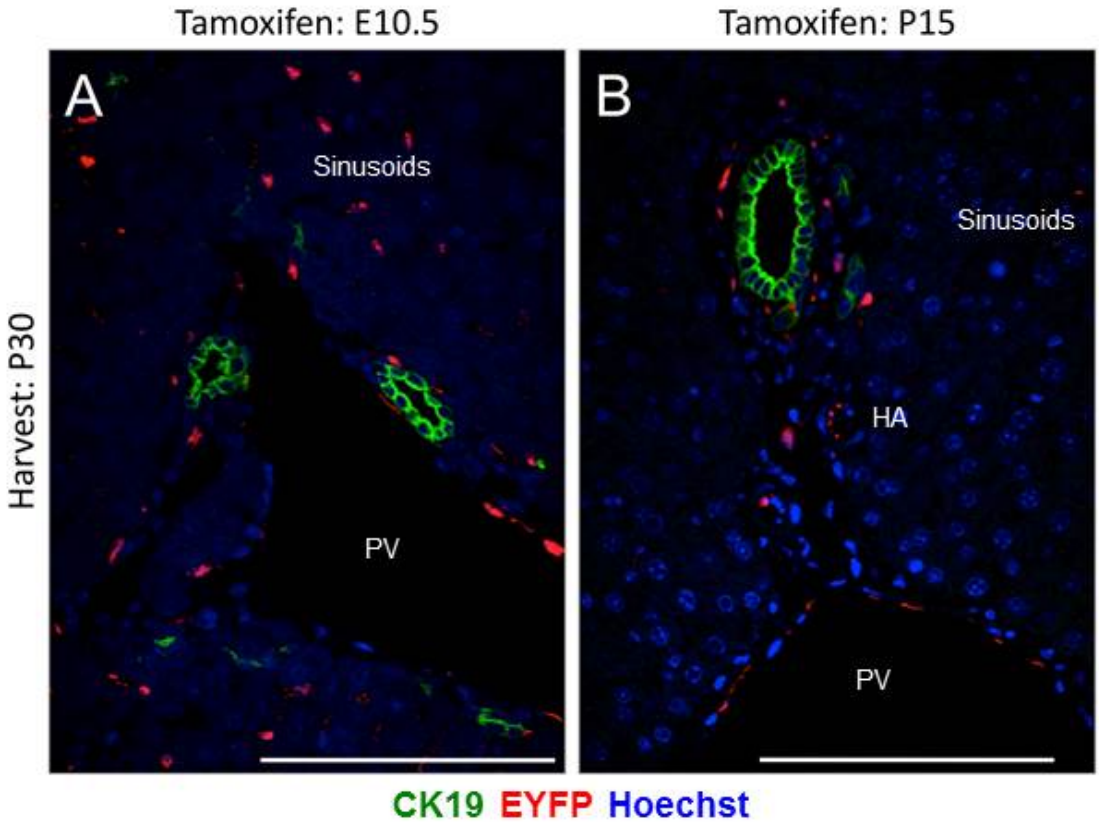

Figure A.2. Lineage labeling with *endothelial-SCL-CreER^T; ROSA26R-EYFP* at different developmental timepoints does not reveal differential contribution to mature vascular structures. Mice were injected with Tamoxifen either at E10.5, early in embryonic hepatic development (A) or at P15, during postnatal growth (B). Mice were harvested and analyzed at P30. Liver sections were stained for CK19 (green), the YFP lineage label (red), and Hoechst for nuclei (blue). With both Tamoxifen injection timepoints, lineage-labeled cells are seen in the PV, HA, and sinusoids. Scale bar is 100 μm.

endothelial-SCL-CreER^{T}; Rbpj$^{flox/flox}$; ROSA26R-EYFP (Rbpj$^{\Delta endo}$). The Rbpj$^{\Delta endo}$ mice did not display any lethality. When we analyzed the postnatal masses of control and Rbpj$^{\Delta endo}$ mice, we found no difference (Figure A.4). This was surprising, as previous studies have shown that Rbpj is required in the endothelium, and either global or endothelial-specific disruptions in Rbpj lead to severe vascular malformations (Dou et al., 2008; Gridley, 2007; Oka et al., 1995; Siekmann and Lawson, 2007).

To determine whether we were getting complete recombination and deletion of Rbpj, we performed immunohistochemistry for Rbpj protein in knockout mouse livers. When comparing Rbpj$^{\Delta endo}$ mice and controls that were injected with Tamoxifen at E12.5 and analyzed at E17, no differences were observed. In both genotypes, some cells that resemble ECs demonstrated the expression of Rbpj (Figure A.5A-B). We additionally analyzed a P30 Rbpj$^{\Delta endo}$ mouse that was injected with Tamoxifen at E11.5 (Figure A.5C). In this mouse, we were able to visualize mature veins and see morphologically-determined ECs. Several ECs retained expression of Rbpj.

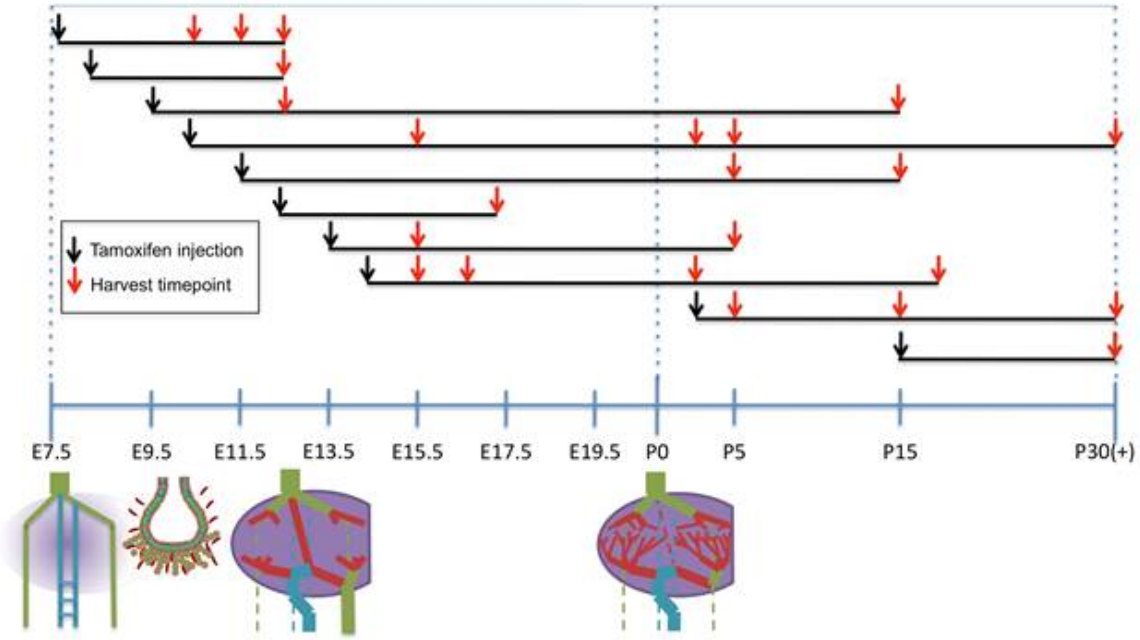

Figure A.3. ***Endothelial-SCL-CreER^{T}; Rbpj$^{flox/flox}$; ROSA26R-EYFP*** **embryos and mice were analyzed at a variety of timepoints.** Timepoints for tamoxifen injections and harvests are shown. For each Tamoxifen timepoint, represented by a black arrow, at least one litter was harvested at each of the corresponding harvest timepoints indicated by a red arrow.

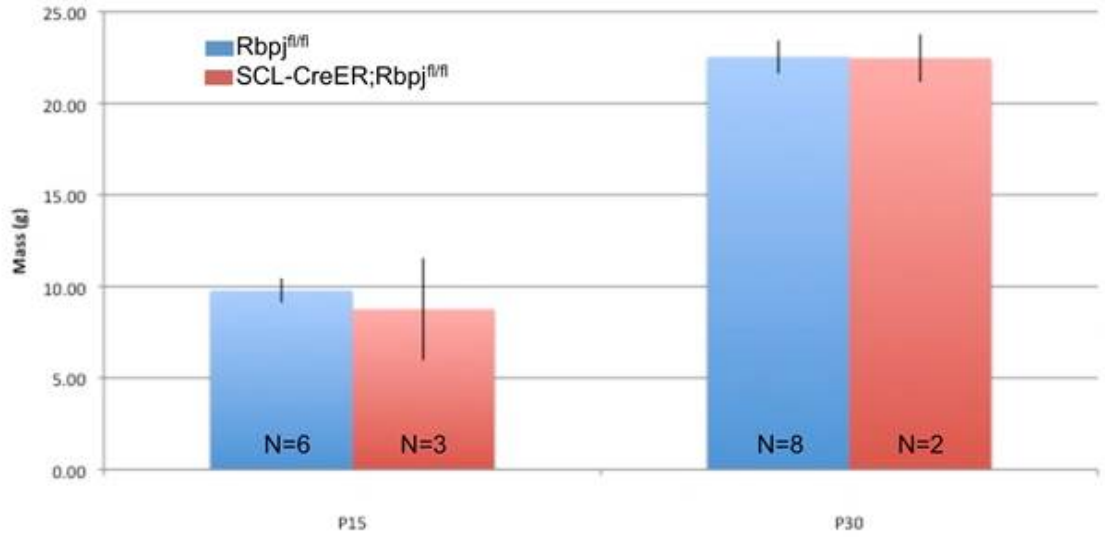

Figure A.4. ***Endothelial-SCL-CreER^{T}; Rbpj$^{flox/flox}$; ROSA26R-EYFP*** **mice had normal postnatal body mass**. Rbpj$^{\Delta endo}$ and control mice were injected with Tamoxifen at various timepoints and weighed at sacrifice at either P15 or P30. At both P15 and P30, no change in body mass was observed between Rbpj$^{\Delta endo}$ mice and controls, either within each individual litter (data not shown) or as analyzed in a group.

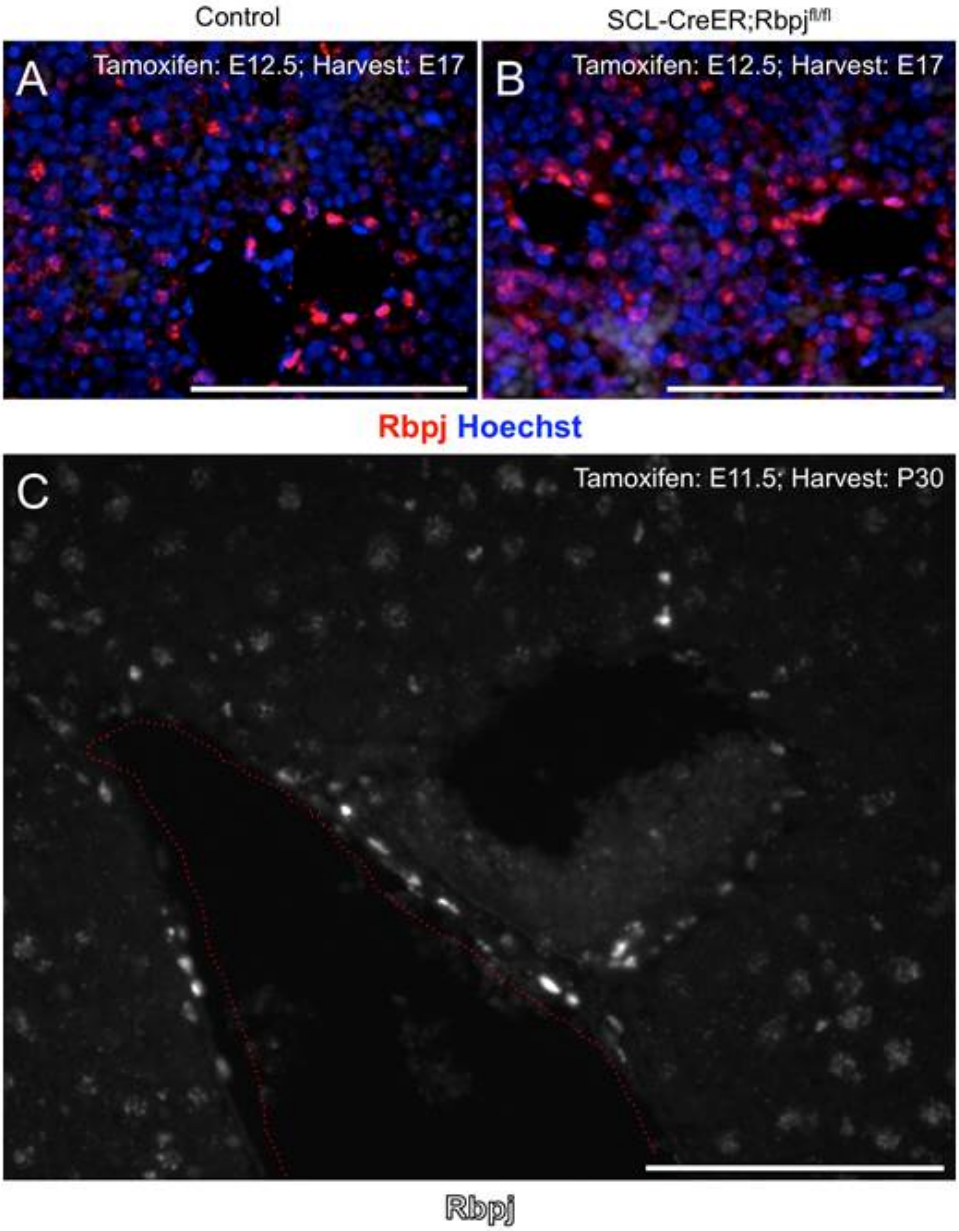

Figure A.5. ***Endothelial-SCL-CreER^{T}; Rbpj$^{flox/flox}$; ROSA26R-EYFP*** **mice display incomplete Rbpj recombination in the liver**. (A-B) Control and Rbpj$^{\Delta endo}$ mice were injected with Tamoxifen at E12.5 and harvested at E17. Immunohistochemistry was performed for Rbpj protein (red). There is no observed difference between Rbpj expression between the control and Rbpj$^{\Delta endo}$ livers. In both controls and Rbpj$^{\Delta endo}$ mice, some cells that morphologically resemble ECs retain Rbpj expression. (C) Rbpj protein (white) was visualized in the liver of a Rbpj$^{\Delta endo}$ mouse injected with Tamoxifen at E11.5 and harvested at P30. Rbpj protein is observed in cells that morphologically resemble ECs and line a vein (red dotted line). Scale bar is 100 μm.

Conclusion

The lineage tracing experiments demonstrate that the *endothelial-SCL-CreER^T* mouse line is not able to distinguish between EC subpopulations that have different contributions to the different hepatic vascular tissues. This result may be explained in several ways: 1. There are no EC subpopulations with different contributions to different hepatic vascular structures; 2. There are different EC subpopulations that have different contributions to the different hepatic vascular tissues, but the expression of *endothelial-SCL-CreER^T* is not able to distinguish between them potentially due to its expression in an early EC common progenitor or in a hematopoietic progenitor lineage (Gottgens et al., 2004); or 3. There are different EC subpopulations, but the persistence of Tamoxifen in the system (Reinert et al., 2012) makes it impossible to get precise enough temporal specificity of recombination. With the current tools, it is not possible to distinguish between these possibilities.

Methods

Lineage tracing was performed on *endothelial-SCL-CreER^{T}; ROSA26R-EYFP* mice (Göthert et al., 2004; Srinivas et al., 2001). Rpbj deletion in ECs was performed with *endothelial-SCL-CreER^{T};Rbpj$^{flox/flox}$;ROSA26R-EYFP* (Göthert et al., 2004; Han et al., 2002; Srinivas et al., 2001) mice. Tamoxifen was suspended in corm oil and given as a single dose of 2mg/mouse intraperitoneal injection to induce recombination. See Chapter 2 of this dissertation for details on immunohistochemistry.

APPENDIX B

A SYSTEM FOR CULTURING THE FETAL LIVER BUD

Introduction

The signals and intercellular interactions that direct the development of the hepatic bud after specification are of high interest to researchers. Previous studies have shown suggestive evidence that epithelial-endothelial interactions are important in hepatogenesis (Matsumoto et al., 2001); however, these findings have not been able to be confirmed in an *in vivo* model due to insufficient tools to specifically target the hepatic bud-surrounding endothelial cells (ECs) and avoid global vascular disruptions leading to embryonic lethality prior to liver bud vascularization. In order to circumvent this *in vivo* challenge and to characterize the endothelial-epithelial signaling and interactions, it is necessary to generate an *in vitro* system that is able to closely recapitulate the process of *in vivo* hepatic bud development and expansion.

Results

We have developed an *in vitro* culture system where the liver bud, as early as E9.0, can be cultured with both epithelial and endothelial tissues. In this system, the fetal liver bud explant can survive for several days in culture and the endothelial cells survive and form branching vascular networks. This method was adapted from a previously published technique (Matsumoto et al., 2001).

Live fluorescent lineage-specific labels facilitate the process of liver bud dissection and aid the ability to distinguish epithelial and endothelial cells while in culture. In the mouse model utilized, the endothelial cells are inducibly labeled with enhanced yellow fluorescent protein (EYFP) expression through *endothelial-SCL-CreER*^{T} (Göthert et al., 2004) and *Gt(ROSA)26Sor*$^{tm1(EYFP)Cos}$ (*ROSA26R-EYFP*) (Srinivas et al., 2001) alleles. In these mice, the *ROSA26R-EYFP* allele is silent until Cre-mediated excision of the transcriptional stop cassette. Induction of EYFP expression can either be done through a maternal injection of tamoxifen prior to harvest, or through the addition of 4-hydroxytamoxifen in the culture media.

The foregut endoderm and hepatic bud is labeled by a transgene, *Tg(Ttr-RFP)*^{1Hadj}*,* using transthyretin (Ttr) regulatory elements to drive expression of red fluorescent protein (RFP) (Kwon and Hadjantonakis, 2009). Ttr is known to be expressed in the embryonic endoderm, including the liver, pancreas, stomach, and intestine (Kwon and Hadjantonakis, 2009).Through crossing these transgenes and alleles together, we generated a mouse where both the hepatic bud and endothelium are fluorescently marked.

At E9.5, Ttr-RFP can be seen throughout the gut tube of the embryo and the liver bud is visible (Figure B.1A). After resecting the liver bud, the RFP fluorescence is still visible in the epithelial

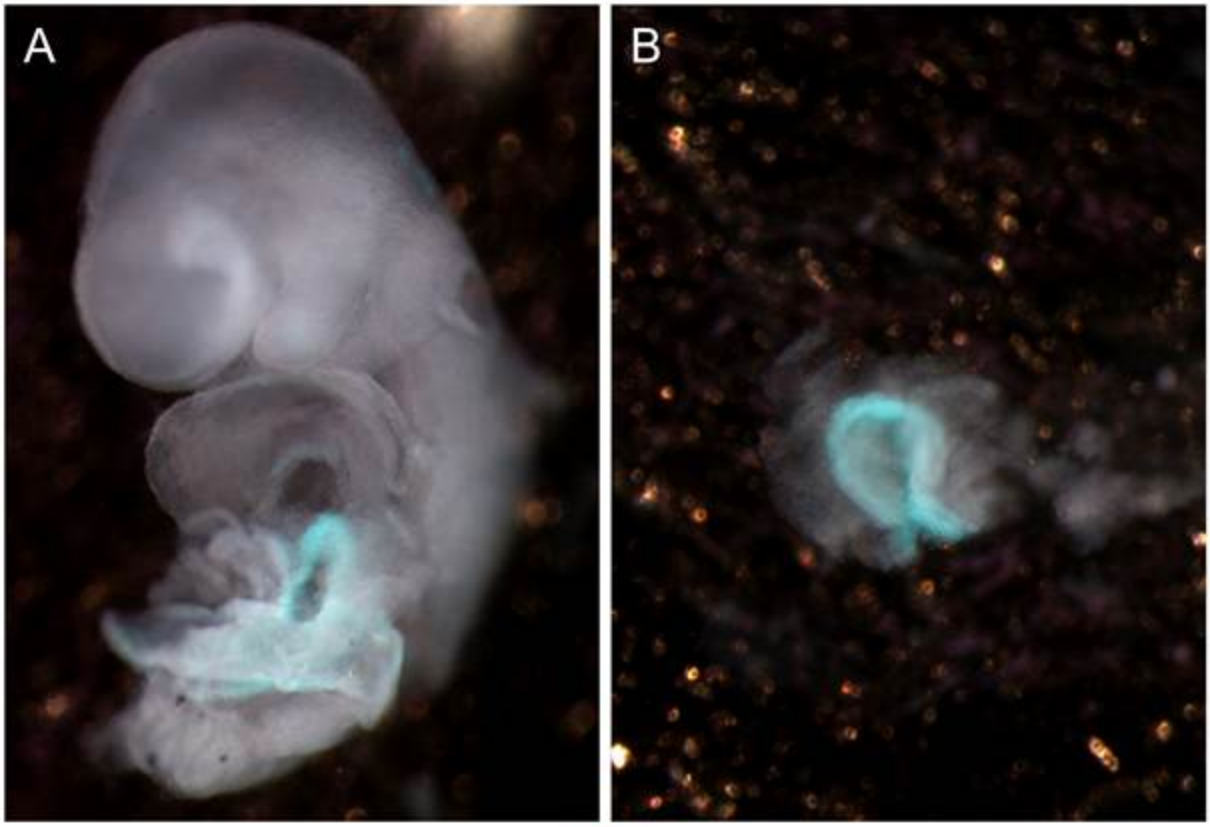

Figure B.1. Ttr-RFP expression allows for *in vivo* and *ex vivo* visualization of the hepatic endoderm. Ttr-RFP (turquoise) expression was imaged live on E9.5 embryos with the posterior of the embryo removed (A) and in the dissected liver bud (B). Fluorescent signal was overlayed on a bright field image of the embryo or tissue. The RFP expression marks the hepatic endoderm. Liver buds also included the septum transversum, which is visible via bright field but is not fluorescent.

hepatic primordium (Figure B.1B). The liver explants also contained the septum transversum mesenchyme, which does not express RFP (Figure B.1B).

The injection of tamoxifen *in vivo* results in a highly efficient recombination of the *ROSA26R-EYFP* allele and expression of EYFP in vasculature (Figure B.2). Tamoxifen injection at E7.5 into a pregnant female is sufficient to lineage label endothelium throughout the embryo at E9.5 (Figure B.2).

After several days in culture, vascular networks formed that expressed the EC marker platelet cell-derived endothelial cell adhesion molecule (PECAM) (Figure B.3).

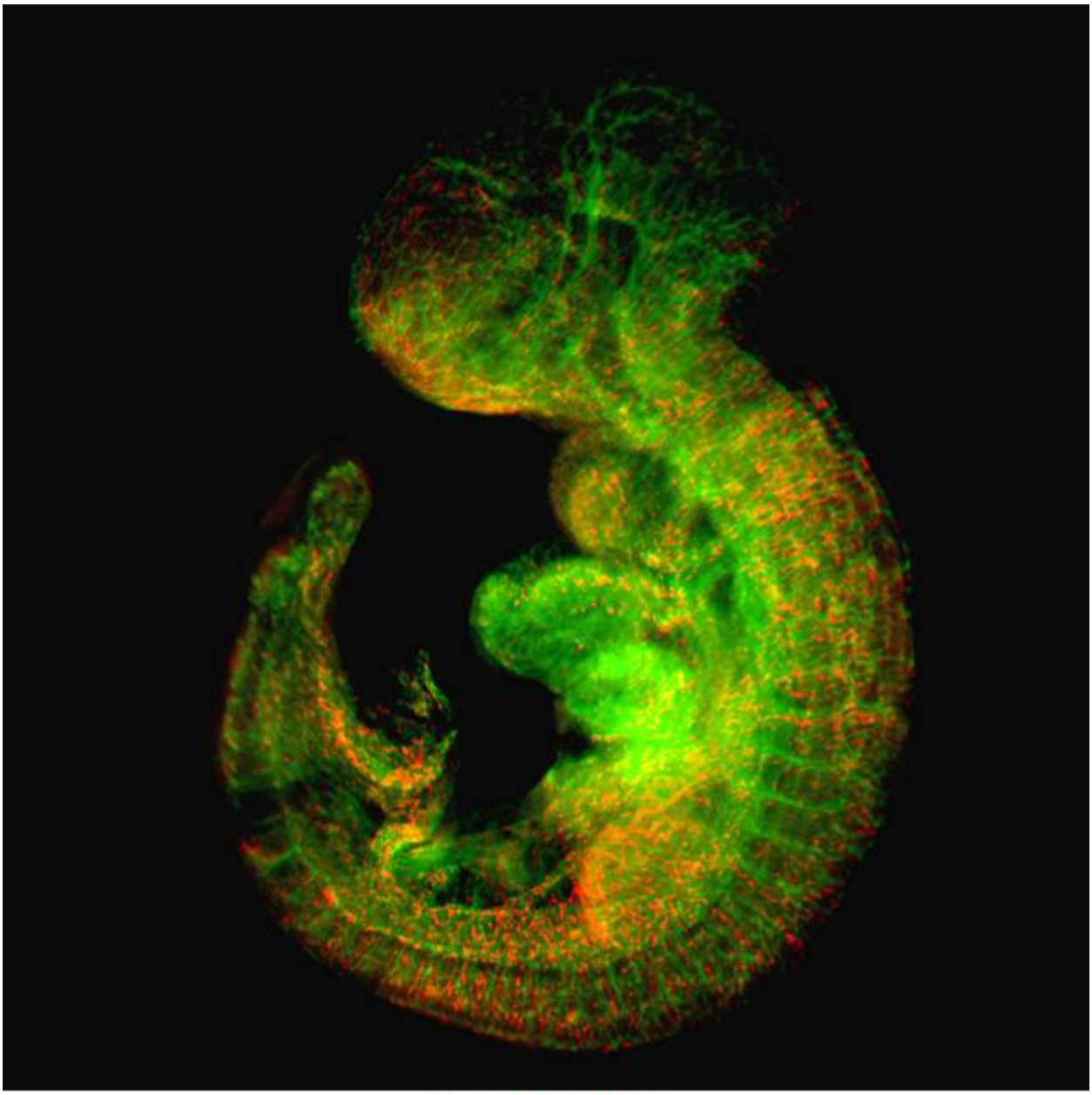

Figure B.2. *Endothelial-SCL-CreER^T; ROSA26R-EYFP* embryos express EYFP lineage label in endothelium after injection with tamoxifen. An *endothelial-SCL-CreER^T; ROSA26R-EYFP* embryo was treated with tamoxifen via maternal injection at E7.5 and analyzed at E9.5. The embryo was wholemount immunostained for PECAM (green) and EYFP (red). EFYP is expressed throughout the embryo and overlaps with PECAM expression in the vasculature.

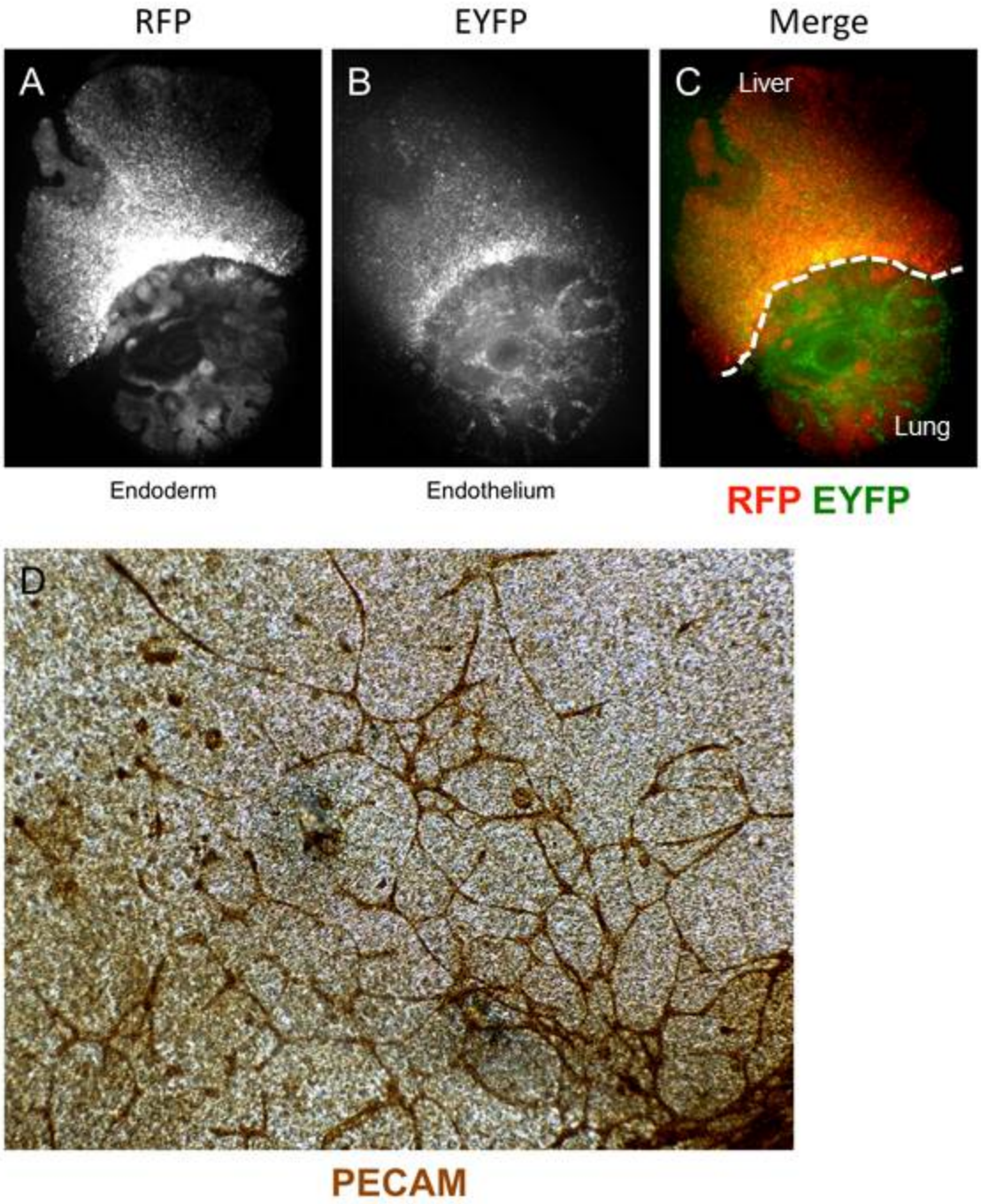

Figure B.3. Liver bud explant cultures allow for the growth of both epithelial and endothelial tissues. (A-C) A chunk of liver from an E11.5 *endothelial-SCL-CreER^T;ROSA26R-EYFP;Ttr-RFP* embryo was explanted and cultured for 4 days. The tissue survived in culture, demonstrating the presence of both endoderm (RFP-red) (A) and endothelium (EYFP-green) (B). In this explant, both liver and lung tissues grew, and the endothelium around each tissue formed a distinct pattern (liver and lung tissue separated by dotted line). This does not occur in all explants. (D). E9.5 liver bud from an *endothelial-SCL-CreER^T;ROSA26R-EYFP;Ttr-RFP* embryo was cultured for 7 days, after which it was fixed and stained for PECAM (brown) to visualize endothelium. ECs form into branched vessel-like structures.

Conclusion

The culture system allows for the concurrent growth and expansion of both the epithelial and endothelial tissues.

Methods

Mice with dual-fluorescent tissue labels were generated by combining the alleles *Ttr-RFP* (Kwon and Hadjantonakis, 2009)*; endothelial-Scl-CreER*^{T} (Göthert et al., 2004)*;* and *ROSA26R-EYFP* (Srinivas et al., 2001).

The culture protocol was done as follows:

Materials needed:

- Transwell polycarbonate filter membranes and plates: 6.5mm diameter, 0.45mm pore size (Corning, Corning, NY, product #3413)
- Dulbecco's modified Eagle medium (Gibco 11885: Low glucose, pyruvate, .37% NaHCO3)
- Fetal bovine serum
- Matrigel (Becton Dickinson, Franklin Lakes, NJ)
- Pen-Strep
- Etched tungsten micro needles, 0.5mm rod diameter, 1 um tip diameter (FST, Foster City, CA, item no. 10130-20)
- Pin holder
- No. 5 forceps

Dissection and culture protocol:

1. To make 50 mLs of dissection solution, mix 49.5 mL PBS with 0.5 mL 1% Pen-Strep. The dissection solution will stay good for 2-4 weeks at 4°C.
2. To make 50 mL of culture medium mix (without Matrigel) 44.5 mL DMEM, 5 mL 10% fetal bovine serum, and 0.5 mL Pen-Strep. Filter the mixture. The culture medium

without matrigel is good for 2-4 weeks at 4°C. At the time of use, add 10 µL Matrigel per 5 mL media. The culture medium with Matrigel will not keep.

3. Add 250 µL culture media with Matrigel to each well of the 24-well Transwell plate below the filter membranes. Put plate at 37°C.
4. Under a fluorescent stereoscope, dissect E9-E10 embryos out of the uterus in dissecting solution.
5. Use the RFP fluorescence to visualize the hepatic endoderm bud. Cut embryos transversely caudal to fetal liver bud. Carefully resect the hepatic bud, including the RFP-expressing hepatic endoderm with surrounding mesenchyme tissue.
6. In a cell culture hood, transfer hepatic buds onto Transwell filter inserts and put into 24-well plate.
7. Culture buds at 37°C in a humidified atmosphere of 5% CO_2 and 95% air.
8. Change media every 2 days. Use previously made culture medium and add Matrigel fresh each time.

To induce EYFP expression *in vivo* prior to dissection, intraperitneally inject 100 µL of 2 mg/mL tamoxifen solution. Tamoxifen is dissolved in 10% ethanol; 90% corn oil.

To induce EYFP expression in culture after resection, add 1 µM 4-hydroxytamoxifen (Sigma-Aldrich, St. Louis, MO) to culture media and incubate for 2 days before replacing with fresh media.

<u>Wholemount immunofluorescence was performed with the following protocol:</u>

Fix whole E9.5 embryo overnight at 4C. Wash embryo thoroughly with PBS. Permeabilize with 0.5% Triton X-100 in PBS (0.5% PBT) for 30 minutes at room temperature, rocking. Block overnight at 4C in blocking solution (5% normal donkey serum and 1% bovine serum albumin in

0.5% PBT. Incubate embryo with primary antibody diluted in blocking serum overnight at 4C. Dilute rat α PECAM antibody 3/500 and rabbit α GFP antibody 1/500 (see Chapter 2 for antibody information). Wash the embryo 3 x 20 minutes at room termperature in 0.1% PBT. Wash in PBS overnight at 4C. Incubate embryo with secondary antibody diluted 1:1 in blocking buffer and 0.1% PBT. Dilute α rat-Cy2 1:500 and α rabbit-Cy3 1:500. Wash embryo 2 x 1 hour in 0.1% PBT at room temperature, rocking. Incubate in a nuclear staining agent, such as DAPI or bis-benzamide, if desired, for 20 minutes at room temperature. Wash 3 times in PBS for at least 30 minutes each at room temperature, rocking, or overnight at 4C for one of the final washes.

APPENDIX C

THE RESULTS OF EPITHELIAL-OVEREXPRSSION OF VEGF IN THE FETAL LIVER

Introduction

The studies described in Chapter 5 of this dissertation illustrate the requirement of epithelial-secreted VEGF protein in liver development through the knockout of VEGF specifically in the liver epithelium. To further clarify the role of VEGF during liver development, we performed the complementary experiment and induced the overexpression of VEGF in the liver epithelium. For further information on VEGF and its role in liver development, please see Chapter 5.

Results

To determine the role of VEGF in embryonic liver development, we generated a mouse that overexpresses VEGF specifically within the liver epithelium. The VEGF-overexpression (VFOE) mouse uses an Tg(Alb-Cre)^{21Mgn}/J (*Albumin-Cre*) transgene to drive the Cre-mediated recombination of the Gt(ROSA)26Sor$^{tm1(tTA)Roos}$/J (*ROSA26-tTA*) allele to remove the stop codon and drive the expression of tetracycline. Tetracycline then binds to tetracycline-dependent promoter elements in a transgene upstream of the full-length cDNA of $VEGF_{165}$ (Ohno-Matsui et al., 2002; Sun et al., 2007). All *Albumin-Cre*-recombined lineages will overexpress $VEGF_{165}$.

Previous studies have found that *Albumin-Cre*-mediated recombination occurs in hepatoblasts during embryonic development, with recombination of the ROSA26 locus occurring in the majority of cells by E16 (Sparks et al., 2010). Immunostaining using an antibody that detects all major isoforms of VEGF, including $VEGF_{165}$, demonstrates that, the levels of VEGF protein are visually increased in the liver of VFOE mice by E15.5 (Figure C.1).

VFOE is embryonic lethal, with no surviving embryos past E16.5. The number of mice collected with control and VFOE genotypes at each age is shown in Table C.1.

To determine the effect of hepatic epithelial-overexpression of VEGF on liver histomorphology, liver tissues from E13.5, E15.5, and E16.5 VFOE and control mice were analyzed by hematoxylin and eosin stain. At E13.5, no differences are observed between control and VFOE mice (Figure C.2A-B). By E15.5, differences can be found between VFOE and control mice. At this time, VFOE mice display abnormal disruptions

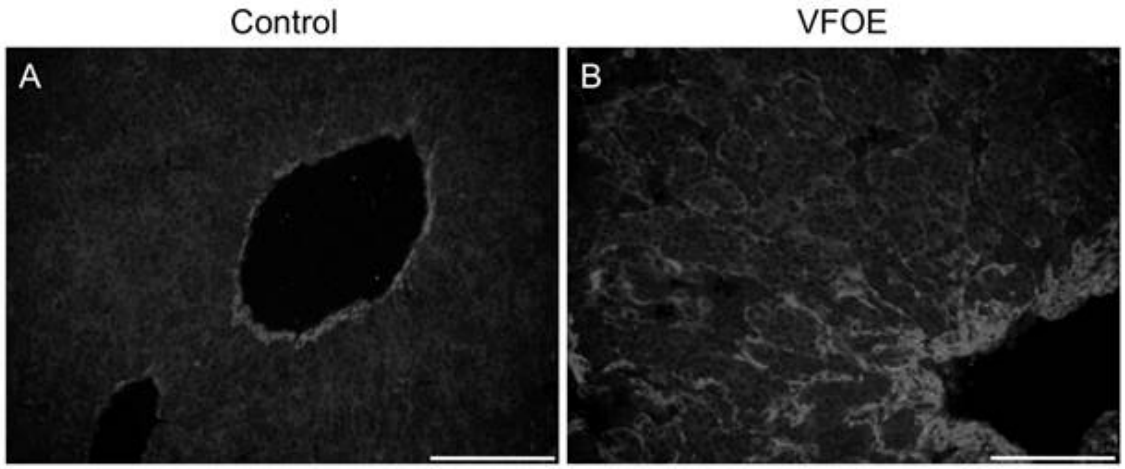

Figure C.1. VFOE embryos have increased VEGF protein in the liver by E15.5.
Immunostaining was performed for VEGF isoforms (white) in E15.5 control (A) and VFOE (B) embryo livers. In E15.5 control livers, VEGF protein is predominantly localized around veins (A). In E15.5 VFOE livers, the amount of VEGF protein around veins is increased over controls, and there is an increased amount of VEGF protein in the liver parenchyma (B). Scale bar is 100 μm.

Age	Number of litters	Number of control embryos	Number of VFOE embryos	% embryos VFOE
E13.5	2	11	2	15.4%
E15.5	2	8	3	27.3%
E16.5	1	8	1	11.1%
E17.5	2	18	1 (dead)	5.3%
P0	1	7	0	0.0%

Table C.1. Mendelian ratios of VFOE genotype. For each age at which litters were collected, the number of litters collected, number of control embryos, number of VFOE embryos, and the percentage of embryos that had the VFOE genotype are shown.

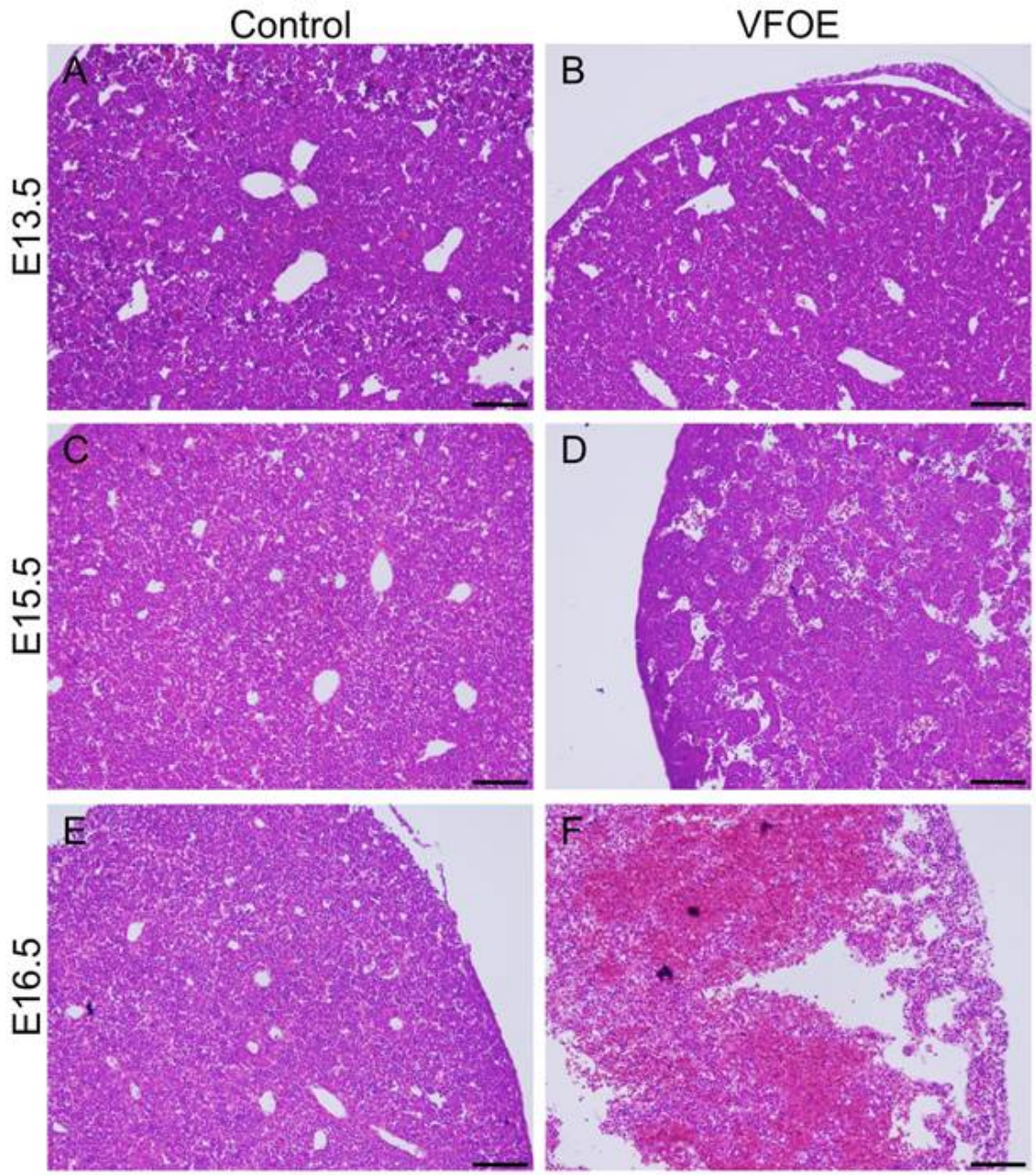

Figure C.2. VFOE embryos display histological abnormalities and architectural disruption of the liver. The livers of E13.5 (A-B), E15.5 (C-D), and E16.5 (E-F) control and VFOE mice were examined by hematoxylin and eosin staining. No obvious differences are observed between E13.5 control (A) and VFOE (B) livers. At E15.5, VFOE livers show vascular dilations (D) compared to littermate controls (C). By E16.5, VFOE livers show severe disruptions in the liver epithelial architecture and large dilations or hemorrhages in the liver (F) compared to littermate controls (E). Scale bar is 100 μm.

in the epithelial architecture, yielding large spaces filled with circulating hematopoietic lineage cells (Figure C.2C-D). By E16.5, there is a complete disruption of the epithelial architecture in VFOE mouse livers, with a further expansion of the vascular spaces and similar increase in the number of hematopoietic lineage cells observed in the liver (Figure C.2E-F). There is almost no identifiable epithelial organization in the VFOE liver at this time.

To determine the effect of the VFOE on the cellular identity of the liver epithelium, we assessed the expression of several liver cell fate markers in control and VFOE mouse livers at E15.5 and E16.5. We first examined the expression of biliary cell markers widespread cytokeratin (wsCK), a marker of several cytokeratin proteins that is expressed in the ductal plate and in mature biliary cells, and Sox9, a marker of both biliary epithelial cells (BECs) in the ductal plate and in intrahepatic bile ducts and a marker of hepatic progenitor cells (Carpentier et al., 2011). We were surprised to find a large increase in wsCK expression in VFOE mice, specifically at E16.5 (Figure C.3D) and in the areas where tissues disruptions, including large gaps in the epithelial structure that appear to be filled with hematopoietic lineage cells, were observed in the peripheral regions of the liver (Figure C.2F). However, when we examined expression of Sox9, we did not find a similar expansion of the Sox9 expressing cells as wsCK (Figure C.4D). We also examined the expression of the hepatocyte marker Hnf4α. While Hnf4α was seen throughout the parenchyma in E15.5 and E16.5 control livers, the expression was decreased in E15.5 VFOE livers and absent from E16.5 VFOE livers (Figure C.5).

With the abnormal protein expression observed in these cells, we stained the livers for Hnf1α/β, or Hnf1, which should mark all hepatic epithelial cells at these embryonic timepoints. In E13.5, E15.5, and E16.5 control mice, Hnf1 expression was seen

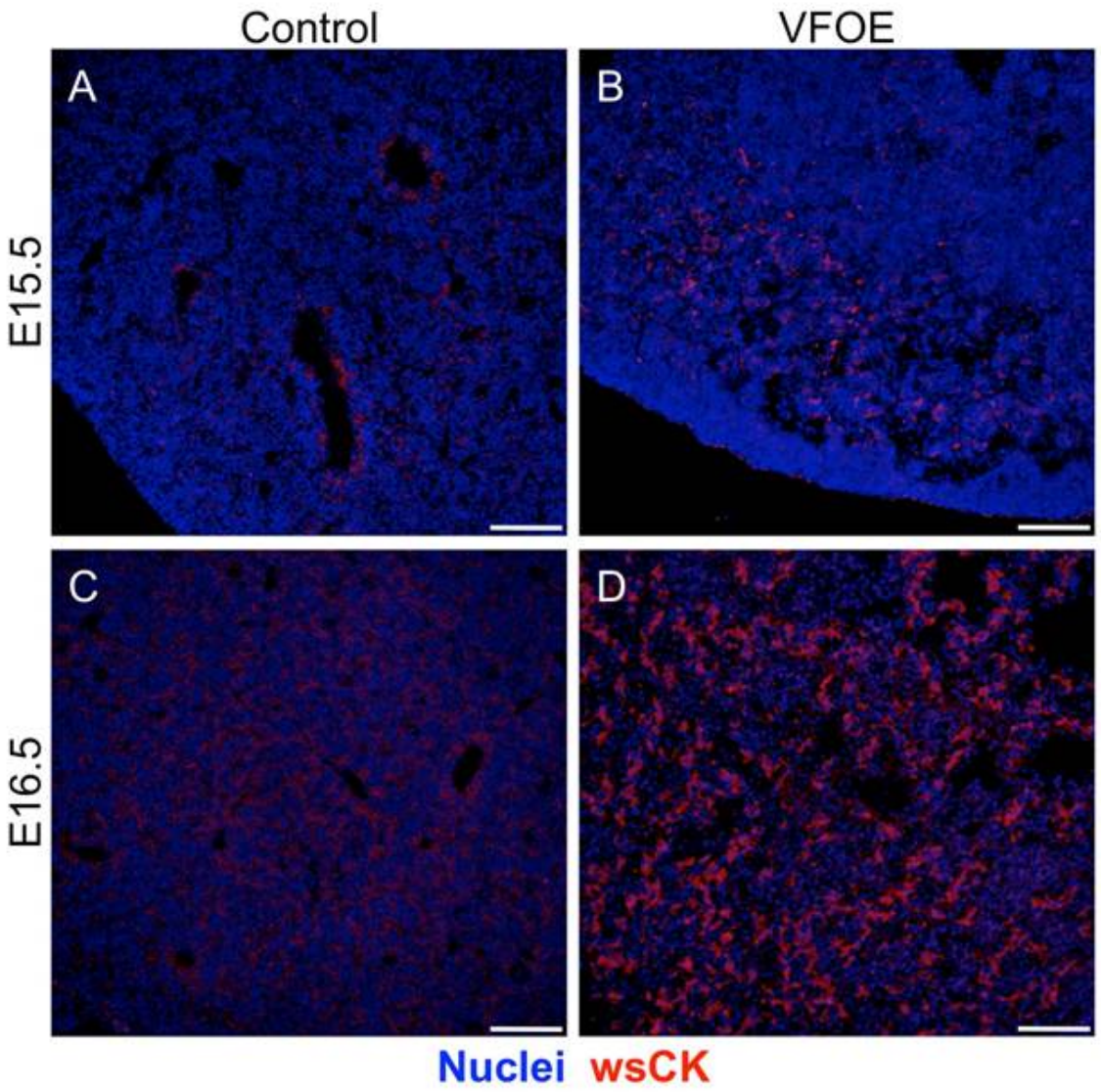

Figure C.3. VFOE embryos display abnormal expression of cytokeratin in the liver. Immunostaining was performed for wsCK (red), and nuclei (blue) in E15.5 (A-B) and E16.5 (C-D) control and VFOE embryos. In E15.5 (A) and E16.5 (C) control livers, wsCK is expressed most highly in the ductal plates surrounding portal veins. In E15.5 VFOE livers, some additional wsCK is observed in the liver periphery in the areas of vascular dilations (B). By E16.5, VFOE livers display widespread abnormal expression of wsCK (D). Scale bar is 100 μm.

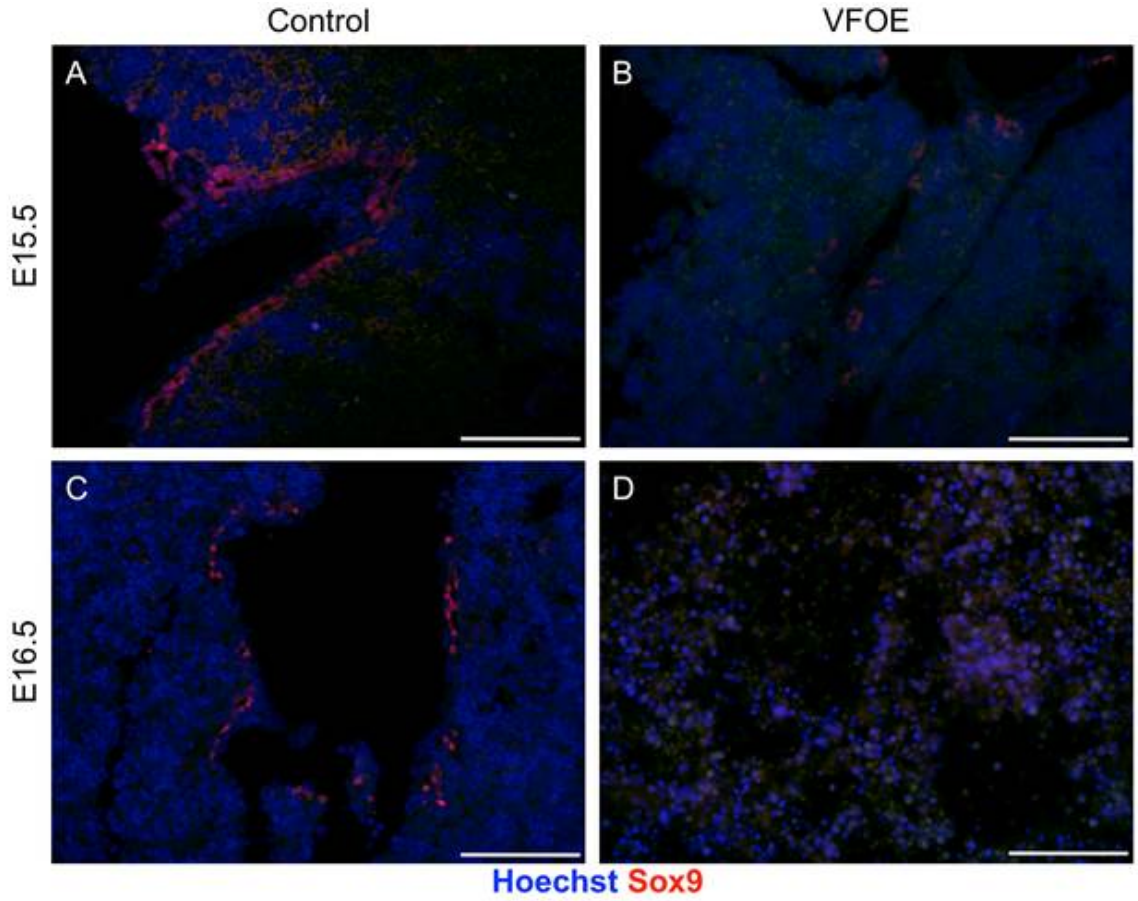

Figure C.4. Sox9 expression is not expanded coincident with cytokeratin in E16.5 VFOE livers. Immunostaining was performed for Sox9 (red) and nuclei (blue) in E15.5 (A,C) and E16.5 (B-D) control and VFOE embryos. In E15.5 controls (A), E15.5 VFOE (C), and E16.5 controls (B), Sox9 expression is observed in the ductal plate structures surrounding portal veins. In E16.5 VFOE livers, Sox9 expression is absent from the liver and is not found in corresponding regions where wsCK$^+$ cells are present. Scale bar is 100 μm.

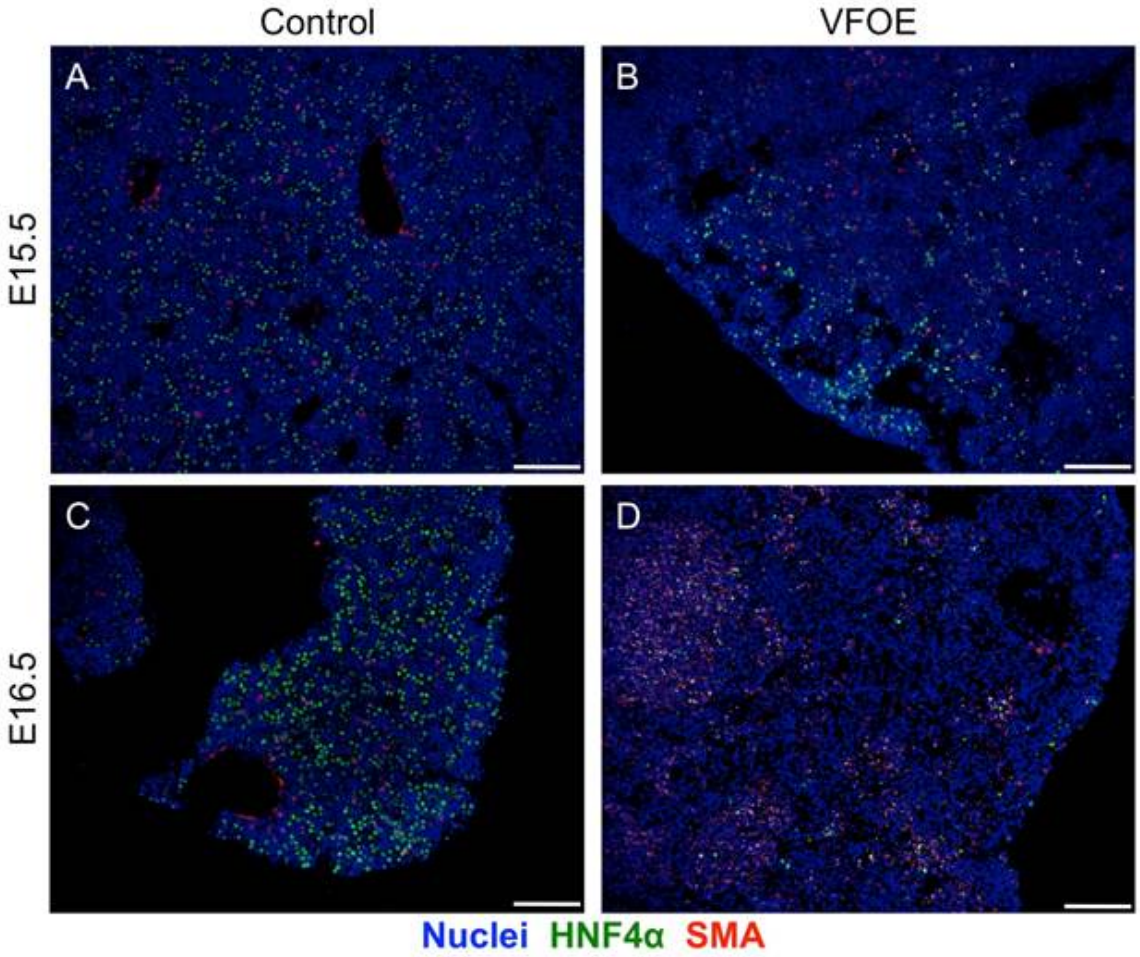

Figure C.5. VFOE embryos lose expression of Hnf4α in the liver. Immunostaining was performed for Hnf4α (green), SMA (red), and nuclei (blue) in E15.5 (A-B) and E16.5 (C-D) control and VFOE embryos. At E15.5, Hnf4α expression is seen throughout the parenchyma in control liver (A) and in several locations in VFOE liver (B). However, some regions at the periphery of E15.5 VFOE livers appear to lose Hnf4α expression in some cells. By E16.5, Hnf4α expression is lost in the VFOE (D) liver. It remains expressed in the control liver (C). There is no increase in SMA staining in the E16.5 VFOE embryo. Immune cells display autofluorescence in both green and red channels. Scale bar is 100 μm.

throughout the liver in hepatoblasts and in ductal plate structures (Figure C.6A,C,E). Hnf1 was also seen in VFOE livers at E13.5 and E15.5 (Figure C.6B,D), but was not observed in the VFOE liver at E16.5 (Figure C.6F). This confusing data suggests that the liver epithelial tissue has either disappeared from the embryonic liver and been replaced with cells that express only wsCK, or that the liver epithelium has adopted an abnormal fate by which the cells express only wsCK but no other liver lineage markers.

To determine whether changes in proliferation or apoptosis could explain the changes observed in the E16.5 VFOE livers, we assessed proliferation at E15.5 (Figure C.7) and apoptosis at E15.5 and E16.5 (Figure C.8). No changes in either proliferation or apoptosis were found between control and VFOE livers.

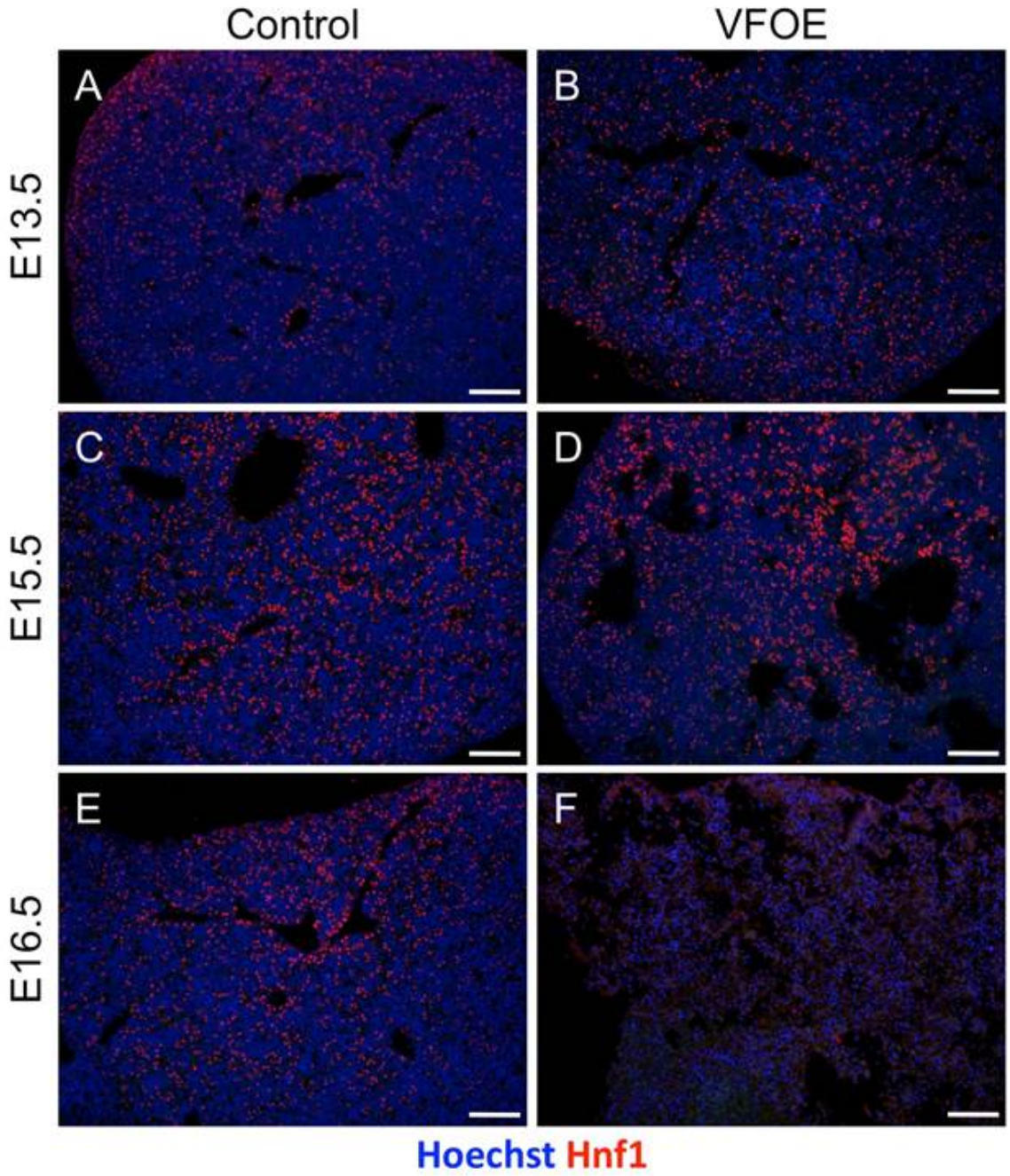

Figure C.6. VFOE embryos lose expression of Hnf1 in the liver. Immunostaining was performed for Hnf1, or Hnf1α/β (red) and nuclei (blue) in E13.5 (A-B), E15.5 (C-D) and E16.5 (E-F) control and VFOE embryos. At E13.5 and E15.5, Hnf1 expression is seen throughout the parenchyma in both control (A,C) and VFOE (B,D) livers. By E16.5, Hnf1 expression is lost in the VFOE (F) liver. It remains expressed in the control liver (E). Scale bar is 100 μm.

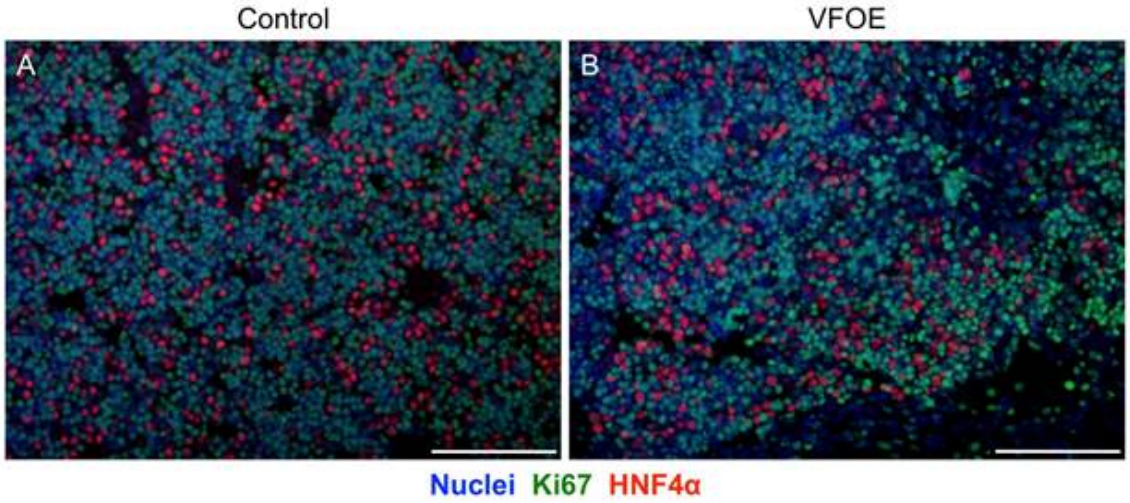

Figure C.7. VFOE embryos do not display changes in proliferation at E15.5.
Immunostaining was performed for Hnf4α (red), Ki67 (green), and nuclei (blue) in E15.5 control (A) and VFOE (B) embryos. In both control and VFOE liver, a high amount of proliferation is observed, with most proliferation occurring in Hnf4α- cells. Visually, there is no difference in proliferation observed between the control and VFOE embryos. Scale bar is 100 μm.

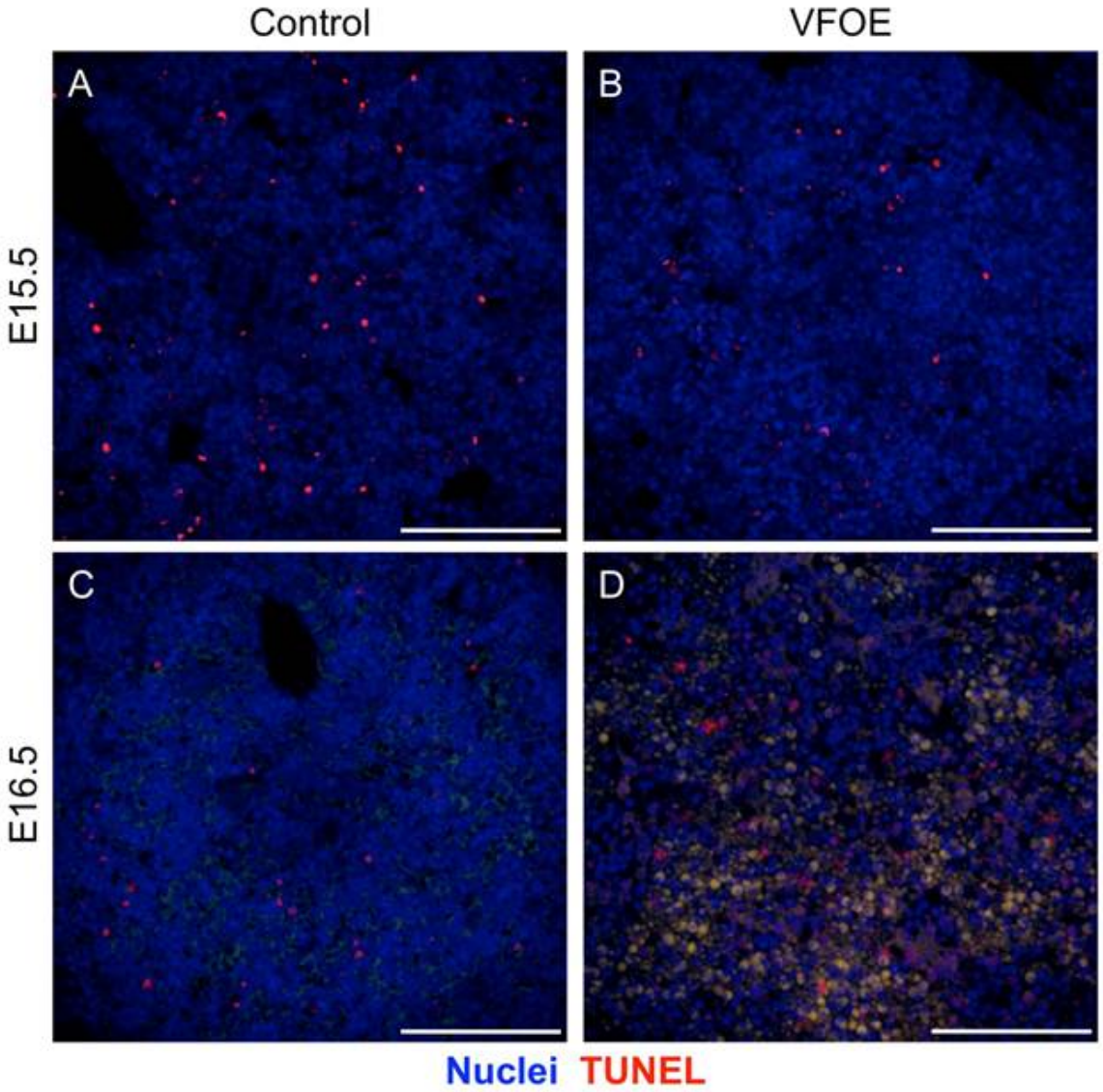

Figure C.8. No increase in apoptosis is observed in VFOE livers. TUNEL staining for apoptotic cells (red) was performed on liver tissue from E15.5 (A-B) and E16.5 (C-D) control and VFOE embryos. Nuclei are blue. A low level of apoptosis is observed in both control and VFOE livers at E15.5 and E16.5. No increase in apoptosis over controls is observed in VFOE livers at either E15.5 (B) or E16.5 (D). In E16.5 VKOE mice, blood cells exhibit autofluorescence in both green and red channels, appearing yellow. Scale bar is 100 μm.

Conclusion

VEGF overexpression causes major disruptions in the epithelial structure and identity of the liver epithelial cells. These disruptions include both physical disruptions in the liver tissue architecture and disruptions in the gene expression of liver cell type markers.

At this time, it is unclear what is causing these disruptions. It could be that the expression of VEGF has direct effects on the hepatoblasts, and VEGF overexpression promotes abnormal gene expression and cell fate. Alternatively, the direct effect could be on the hematopoietic lineages that appear to expand in the VFOE tissues. The enormous expansion of the hematopoietic population may induce secondary effects on the epithelial tissue, either through altered signaling or through physically changing the structure of the liver, through crowding out the epithelial cells or causing hemorrhages, for example.

The overexpression of VEGF in this specific mouse model will not be able to be used to study the role of VEGF in the architectural establishment and growth of the hepatic blood vessels.

Methods

VFOE mice were generated by crossing *Albumin-Cre* (Postic and Magnuson, 2000) mice, *ROSA26-tTA* (Wang et al., 2008) mice, and *TRE/VEGF* (Ohno-Matsui et al., 2002) mice.

See Chapter 2 for histology and immunostaining methods.

Acknowledgements

Tet-O-Vegfa mice were generated by Peter Campochiaro and were generously provided to us by Dr. Alvin Powers. ROSA26-tTA mice were generated by Raymond Roos.

APPENDIX D

A TECHNIQUE FOR CASTING THE HEPATIC PORTAL VEIN WITH OR WITHOUT THE SIMULTANEOUS CAST OF THE INTRAHEPATIC BILE DUCT

Introduction

The three-dimensional tissue structures in the liver pose a challenge for studying hepatic morphogenesis: how can we assess the *in vivo* architecture of one structure alone within its context in the liver, or the spatial and developmental relationship between two structures?

The question of tissue architecture interrelatedness is of special interest in the liver, as it is believed that the architectural pattern of the portal vein (PV) dictates the structure of the intrahepatic bile duct (IHBD), the hepatic artery (HA), and the hepatic nerves. The portal vein is the first of these structures to form, followed by the IHBD and then the HA. The IHBD and HA follow the pattern of the portal vein as they undergo their own morphogenesis. Indeed, there are, under normal conditions, no branches of the IHBD or HA that exist away from a PV branch.

With this intimate developmental and spatial connection between tissues, it is of interest to assess how changes in one tissue are manifested in the other. This requires a way to view both tissues in three-dimensions at the same time. Unfortunately, the liver, because of its dense nature, is not amenable to techniques such as fluorescent labeling and *in vivo* imaging of cells contributing to ductal and vascular elements.

Results

Our lab has generated a technique for the visualization of three-dimensional resin casting of the IHBD (Sparks et al., 2010). This technique has subsequently been adapted to use in the portal vein (Walter et al., 2012) and for double-casts of the PV and IHBD simultaneously (Figure D.1).

In the double resin cast of the IHBD and the PV, we can see that one PV is followed by several IHBD branches, and that the IHBD will occasionally wrap around the PV. The IHBD branches are various sizes, even when they are following the same PV branch (Figure D.1).

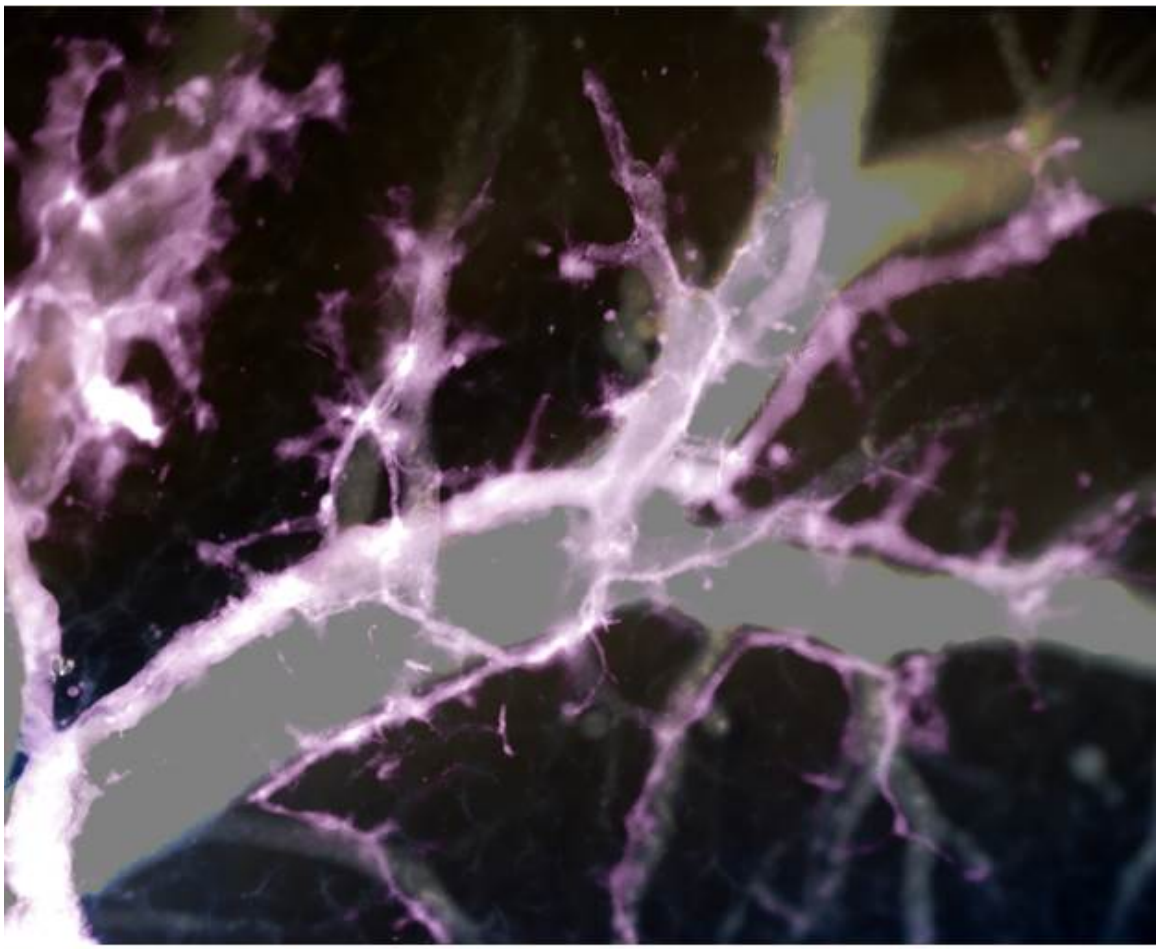

Figure D.1. A double resin cast shows the architectural relationship between the PV and the IHBD. The PV (white) was cast with non-fluorescent resin and the IHBD (pink) was cast with the fluorescent Nile red dye added to the resin. The fluorescent image of the IHBD cast was overlayed onto the bright field image of both casts. The IHBD is seen to follow the PV, with several branches wrapping around the PV.

Conclusion

The double resin cast provides a novel way to visualize the architecture of two 3-dimensional tissues at the same time and to analyze their relationship to each other. In this case, we were able to visualize both the IHBD and the PV. In 2-dimensions, we can see the IHBD branches next to the PV and we can see that there can be a variety of IHBD sizes next to the same PV branch. These findings are confirmed in the 3-dimensional double resin casts of the IHBD and PV. Additionally, the double casts allow us to see the way that the two structures relate to each other along their lengths; we see that large IHBD branches tend to follow the PV in a fairly parallel manner, while small IHBD branches can either run parallel to the PV or can wrap around the PV (Figure D.1.)

This technique could be adapted to any other two luminal structures that can be cast.

Methods

Resin casts were performed as previously described (Walter et al., 2012). Please see Walter et al. (2012) for a detailed protocol and videos.

To generate a cast of the portal vein, first sacrifice a mouse, expose the abdominal cavity, and flush the PV by cutting a nick in the cardinal vein and injecting PBS into the extrahepatic PV. Then, tie a tight ligature around the cardinal vein, anterior to the nick, and a loose ligature around the portal vein near the base of the liver. Attach a cannula made of stretched PE10 tubing to a 32 gauge, ½ inch needle and insert the cannula into the portal vein. Tighten the ligature to hold the cannula in place. Mix 0.1 grams of catalyst with 1 mL of resin and pull into a syringe. Attach the syringe to the cannula-needle and push resin into the portal vein. Allow the resin to harden at room temperature, then remove the liver from the mouse and fix in 4% paraformaldehyde. Wash in PBS, then dehydrate to methanol. Wash the liver in a 1:2 solution of benzyl alcohol and benzyl benzoate to clear the liver tissue and visualize the resin cast.

Double resin casts were performed using the previously described method with some modifications to accommodate casts in both the IHBD and the PV. After the mouse was sacrificed, the PV was immediately flushed with PBS. Afterward, ligatures were tied around the cardinal vein above the site of the nick, the extrahepatic PV and the extrahepatic IHBD. The ligature around the cardinal vein is tightened, but the others remain loose. The portal vein is cast first and is done as described above (Walter et al., 2012). Next, the IHBD is cast as described but with fluorescent resin. To generate fluorescent resin, add 0.05 mg/mL Nile Red (Sigma Aldrich, St. Louis, MO) to resin. The fluorescence is able to withstand the clearing process with BABB. To image the double resin cast, first take a bright field image of both casts. Then, take an image of the fluorescence in the IHBD casts at 543λ. Apply a false color to the

fluorescent image and overlay it on the bright field image using Photoshop or a comparable photo editing program. The image resulting from this process will show the PV in the white color of the resin and the IHBD in the false color assigned to the fluorescent image.

APPENDIX E

CYTOKERATIN19-EXPRESSING CELLS DO NOT FUNCTION AS BIPOTENTIAL LIVER PROGENITORS DURING DDC-INDUCED LIVER INJURY OR REGENERATION

Introduction

The origin and identity of the adult liver stem cell has been a focus of investigation due to the therapeutic potential of this cell for chronic liver disease. A definitive liver stem cell has not been identified. This is partly due to disparate findings between different liver injury models that vary both in liver phenotype and severity of injury, suggesting that potential hepatic progenitor cell (HPC) populations are heterogeneous morphologically and molecularly as wells as in their response to injury (Dorrell et al., 2011; Español-Suñer et al., 2012; Glaser et al., 2009; Shin et al., 2011; Strazzabosco and Fabris, 2008; Tietz and LaRusso, 2006).

A common feature of chronic liver disease in human and mouse models is the emergence of a ductular reaction. Cytokeratin19 (CK19)-expressing reactive ductular cells are thought to arise from previously differentiated biliary epithelial cells (BECs) or HPCs lining bile ducts and ductules, and to contain bipotential progenitors called “oval cells.” While these reactive BEC populations have demonstrated capacity to differentiate into both hepatocytes and BECs (Dorrell et al., 2011; Shin et al., 2011; Wang et al., 2003), the *in vivo* regenerative contribution of these cells to hepatic physiology and architecture remain debated.

Results

To examine the origin and contribution potential of reactive BECs, we performed lineage tracing using different mouse lines designed to express the Cre recombinase protein in specific cell lineages in a chemical liver injury mouse model. 3,5-diethoxycarbonyl-1,4-dihydrocollidine (DDC), a derivative of the anti-fungal compound griseofulvin, feeding induces the emergence of a ductular reaction and a chronic cholestatic liver injury model in mice.

We performed hepatoblast lineage tracing using a mouse containing *Tg(Alb-cre)*^{21Mgn} *(Albumin-Cre)* (Postic and Magnuson, 2000) and *Gt(ROSA)*26*Sor*$^{tm1(EYFP)Cos}$ (*ROSA26R-EYFP)* (Srinivas et al., 2001). The ROSA26R-EYFP allele is a Cre-activated reporter, which upon recombination results in EYFP expression that is stably inherited by all descendants regardless of their differentiated fate. We found that all BECs and hepatocytes express the EYFP lineage label in an uninjured adult mouse liver (Figure E.1A). After three weeks of DDC treatment, all reactive BECs similarly possessed the EYFP lineage label, indicating an *Albumin-Cre*-expressing hepatoblast origin (Figure E.1B).

To determine the contribution potential of reactive BECs, we performed temporal-specific lineage labeling of BECs with *Krt19*$^{tm1(cre/ERT)Ggu}$ (*Cytokeratin19-CreER*^{T}*)* (Means et al., 2008) in combination with the Cre-mediated reporter *ROSA26R-EYFP* (Srinivas et al., 2001). To indelibly label BECs of quiescent IHBDs and reactive ductules, we injected tamoxifen at different times to induce reporter allele recombination and expression of EYFP. To ensure that the lineage label is specific, we analyzed the expression of EYFP after tamoxifen injection with no DDC injury (Figure E.2A). To assess any interlineage

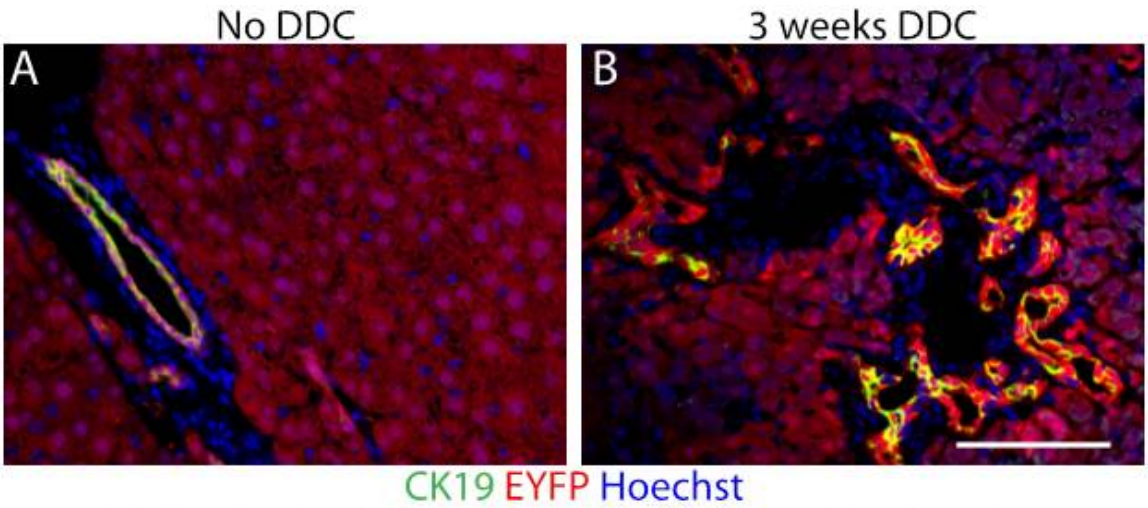

Figure E.1. Reactive ductules in DDC liver injury arise from an *Albumin-Cre* lineage. *Albumin-Cre;ROSA26R-EYFP* mice were analyzed without DDC feeding (A) or after being fed a DDC-supplemented diet for 3 weeks (B). Liver sections were stained for CK19 (green), EYFP (red), and Hoechst (blue). *Albumin-Cre* is expressed in embryonic bipotential hepatic progenitors and lineage labels both hepatocytes and BECs. All hepatocytes and BECs express the EYFP lineage label at P60 (A). After DDC-induced liver injury, reactive ductules appear that express the EYFP lineage label, indicating that they arise from a hepatic origin (B). Scale bar is 100 um.

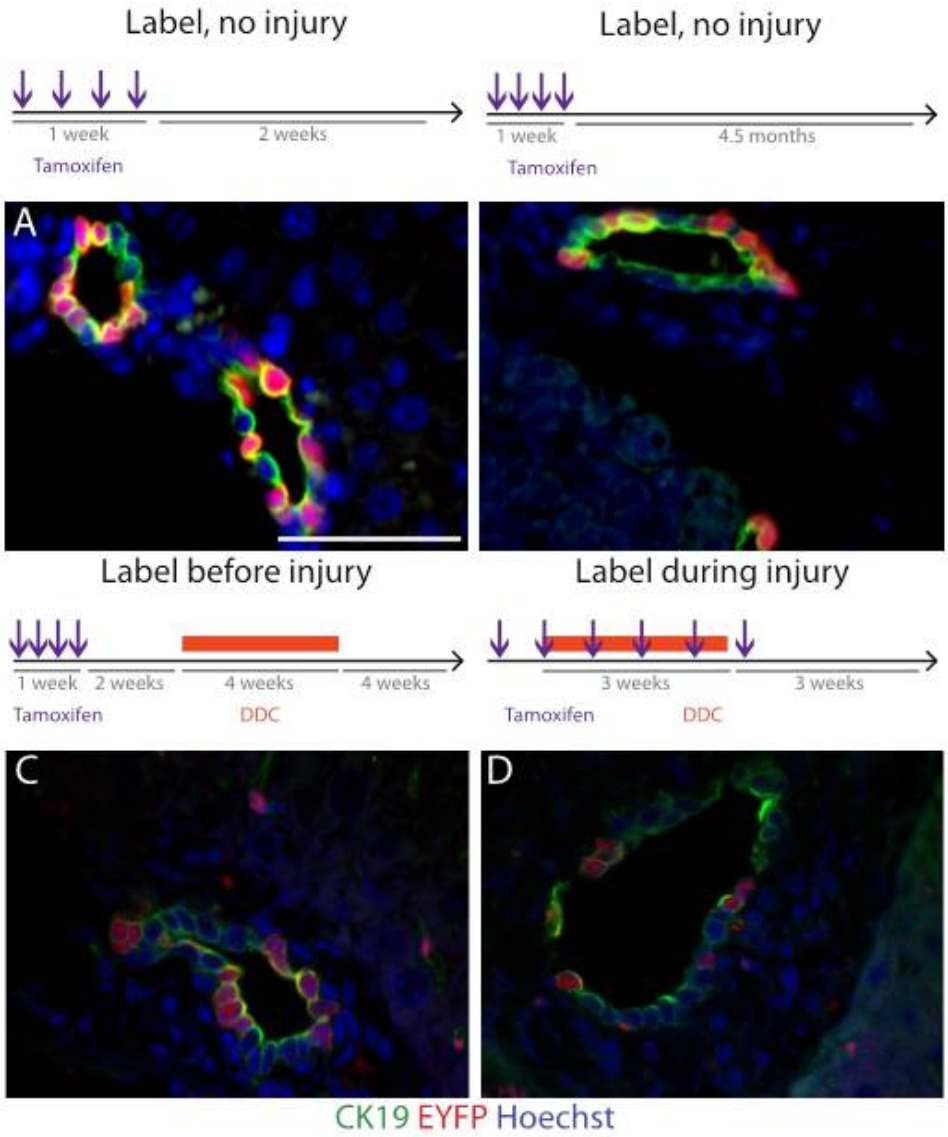

Figure E.2. *Cytokeratin19-CreER^T*-lineage labeled IHBDs and reactive ductules do not contribute to hepatocytes in a DDC liver injury model. *Cytokeratin19-CreER^T;ROSA26R-EYFP* mice were subjected to three different lineage label regimens, including: lineage labeling BECs with no DDC injury (A,B), lineage labeling BECs prior to 4 weeks of DDC feeding (C), and lineage labeling BECs over the course of a three week DDC feeding (D). Mice were analyzed after a period of recovery and regeneration, either 4 (C) or 3 (D) weeks after DDC feeding was stopped. Liver sections were stained for CK19 (green), EYFP (red), and Hoechst (blue). *Cytokeratin19-CreER^T* labels only BECs and not hepatocytes in an uninjured liver (A,B). After DDC injury, the lineage label is retained in BECs and not found in any hepatocytes (C). Additionally, when lineage labeling occurs throughout the period of injury, targeting both mature IHBDs and reactive ductules resulting from injury, BECs retain the lineage label but no hepatocytes express the lineage label (D). Scale bar is 50 um.

conversion of BECs to hepatocytes during normal homeostatic maintenance, we injected tamoxifen and waited for 4.5 months before analyzing the mice (Figure E.2B). We found that after 4.5 months of homeostatic maintenance, the lineage label was still not observed in any hepatocytes.

To assess the bipotentiality of CK19-expressing cells in response to an injury, we injected tamoxifen either before or throughout the DDC treatment. We found that whether we labeled BECs prior to the injury, targeting quiescent BECs (Figure E.2C), or during the injury, targeting reactive BECs (Figure E.2D), we found no hepatocytes expressing the lineage label after a period of recovery. This indicates that CK19-expressing cells that are present in an uninjured liver and that are present under a DDC injury condition do not provide any substantial contribution to hepatocytes during or after DDC injury.

To further test if a quiescent progenitor exists that expresses CK19 under injury but has a slow rate of expansion, we induced lineage labeling after 1 week of DDC treatment. We then allowed the mice to recover for 1 week. At this point, no hepatocytes expressed the EYFP lineage label (Figure E.3A). We then re-subjected the mice to another week of DDC feeding to re-activate any labeled quiescent stem cell that may exist. After one week of re-injury, we still did not see any hepatocytes that expressed the EFYP lineage label (Figure E.3B).

Finally, we assessed whether CK19-expressing cells during embryonic hepatogenesis may give rise to adult bipotential progenitor cells. Previous studies have suggested that ductal plate cells that regress into hepatocytes may serve as a bipotential progenitor compartment in adult mice (Carpentier et al., 2011). We induced lineage labeling

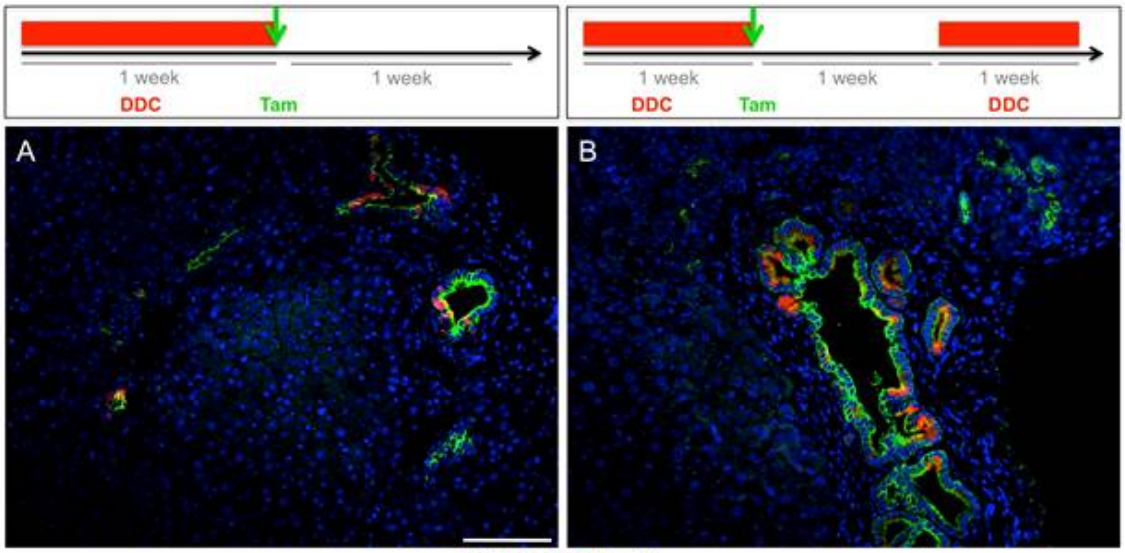

Figure E.3. *Cytokeratin19-CreER^T*-lineage labeled cells that are present during DDC injury do not constitute bipotential stem cells that are activated upon re-injury. Mice were fed DDC for 1 week, at the end of which, a single dose of 4mg Tamoxifen was injected intraperitoneally. Mice were allowed to recover for 1 week, after which they were either analyzed (A) or re-injured with DDC feeding for 1 additional week (B). Liver sections were stained for CK19 (green), EYFP (red), and Hoechst for nuclei (blue). When performing lineage-labeling at the end of one week of DDC treatment, no hepatocytes are present that express the EYFP lineage marker after either 1 week of recovery (A) or 1 week of recovery and 1 week of re-injury (B). Scale bar is 100 μm.

embryonically by injecting pregnant females with tamoxifen between embryonic day (E)17.5-19.5. We allowed the mice to age for 8 weeks, at which time the lineage label was observed only in CK19-expressing BECs (Figure E.4A). We subjected the mice to 3 weeks of DDC treatment. After DDC treatment, no hepatocytes were observed that possessed the EYFP lineage label (Figure E.4B). We also assessed mice after 3 weeks of DDC treatment and a recovery period of 3 weeks; again, no hepatocytes were found that expressed the lineage label (Figure E.4C).

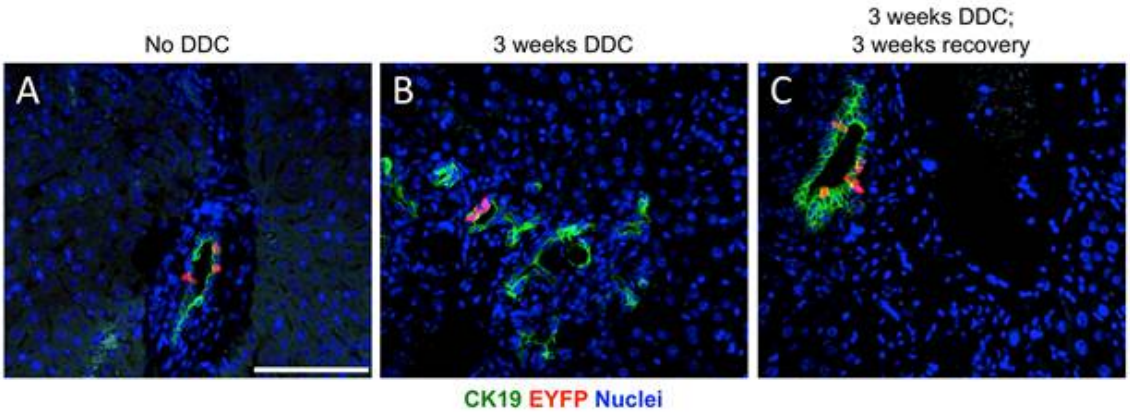

Figure E.4. *Cytokeratin19-CreER^T*-lineage labeled cells in embryonic liver do not give rise to a bipotential adult liver stem cell. Tamoxifen was injected into a pregnant female at E17.5-E19.5. Progeny mice were born and allowed to age to adulthood, at which time they received no DDC treatment (A), DDC diet for 3 weeks (B), or DDC diet for 3 weeks with 3 weeks of recovery (C). Liver sections were stained for the EYFP lineage label (red), CK19 (green), and Hoechst (blue). With all treatments, EYFP lineage-labeling was observed in a small percentage of BECs but in no hepatocytes or CK19$^-$ cells types. Scale bar is 100 μm.

Conclusion

The lineage-tracing data indicate that DDC injury does not stimulate an abundant bipotential progenitor that expresses CK19 and provides a substantial contribution to the hepatocyte lineage. We assessed several CK19-expressing populations, including quiescent and activated BECs along with CK19-expressing cells in the embryonic ductal plate. None of these populations contained a bipotential progenitor cell that gave rise to hepatocytes under DDC injury conditions.

Due to the incomplete recombination observed with the *Cytokeratin19-CreER^T* mouse, we are not able to conclude that no *Cytokeratin19-CreER^T*–lineage cells have the potential to give rise to hepatocytes; we only state that it is unlikely that CK19-expressing populations contribute significantly to hepatocytes in a DDC-induced injury model.

It may also be that the *Cytokeratin19-CreER^T* recombination occurs most frequently in the cells that express the highest amount of CK19 and may also be the most differentiated BECs. Hence, we may be missing a population of weakly-expressing CK19$^+$ cells that do have bipotentiality. This idea is somewhat supported by the finding that no cells lineage-traced embryonically gave rise to hepatocytes. Previous data utilizing another BEC marker, Sox9, has been able to lineage-trace ductal plate cells and find that some of them regress into periportal hepatocytes (Carpentier et al., 2011). The lack of lineage-traced hepatocytes in our *Cytokeratin19-CreER^T* mouse line may indicate that the cells that express CK19, and *Cytokeratin19-CreER^T*, may represent a more highly-differentiated subset of ductal plate cells that are already committed to the BEC lineage and do no regress into hepatocytes.

It may also be that the DDC feeding injury model is not the correct model to activate a CK19-expressing bipotential progenitor. Please see Chapter 4 of this dissertation for a comparison of different rodent liver injury models.

Methods

Hepatoblast-specific lineage-tracing mice were generated by crossing the *Albumin-Cre* allele (Postic and Magnuson, 2000) with the *ROSA26R-EYFP* allele (Srinivas et al., 2001). BEC lineage tracing mice were generated by crossing the *Cytokeratin19-CreER^T* allele (Means et al., 2008) with the *ROSA26R-EYFP* allele (Srinivas et al., 2001).

Tamoxifen was prepared at 40 mg/mL in a solution of 90% corn oil; 10% ethanol.

Embryonic lineage tracing was performed by injecting 2mg of tamoxifen into a pregnant female at 17.5-19.5 days of gestation.

Lineage tracing before injury was done by injecting a series of 4 tamoxifen injections, 4 mg each, ever other day over the course of 7 days.

Lineage tracing over the course of injury was done by injecting a series of tamoxifen injections into mice, starting before DDC feeding and ending after DDC food was removed. For the first injection, 4 mg tamoxifen was administered 5 days before starting DDC feeding. For the second injection, 4 mg of tamoxifen was administered on the first day of DDC feeding. The third, fourth, and fifth injections were each 2 mg of tamoxifen and were administered after 7, 14, and 21 days of DDC feeding, respectively. The final dose of tamoxifen was 4 mg and was administered 4 days after the removal of DDC food.

Lineage tracing after 1 week of DDC and prior to re-injury was done by injecting a single dose of 4mg tamoxifen on the 7th day of DDC feeding, at which time the DDC food was removed from the mice.

See Chapter 2 of this dissertation for immunohistochemistry methods.

REFERENCES

Abdel-Samad, R., Zalzali, H., Rammah, C., Giraud, J., Naudin, C., Dupasquier, S., Poulat, F., Boizet-Bonhoure, B., Lumbroso, S., Mouzat, K., Bonnans, C., Pignodel, C., Raynaud, P., Fort, P., Quittau-Prevostel, C., Blache, P., 2011. MiniSOX9, a dominant-negative variant in colon cancer cells. Oncogene 30, 2493-2503.

Ahn S, H.J., Park CK, 2013. Notch1 and Notch4 are markers for poor prognosis of hepatocellular carcinoma. Hepatobiliary Pancreat Dis Int 12, 286-294.

Aird, W.C., 2007. Phenotypic heterogeneity of the endothelium II. Representative vascular beds. Circulation research 100, 174-190.

Allen, J.W., Bhatia, S.N., 2003. Formation of steady-state oxygen gradients in vitro: Application to liver zonation. Biotechnology and Bioengineering 82, 253-262.

Andersson, E.R., Sandberg, R., Lendahl, U., 2011. Notch signaling: simplicity in design, versatility in function. Development 138, 3593-3612.

Antoniou, A., Raynaud, P., Cordi, S., Zong, Y., Tronche, F.ß., Stanger, B.Z., Jacquemin, P., Pierreux, C.E., Clotman, F., Lemaigre, F.P., 2009. Intrahepatic Bile Ducts Develop According to a New Mode of Tubulogenesis Regulated by the Transcription Factor SOX9. Gastroenterology 136, 2325-2333.

Apte, U., Singh, S., Zeng, G., Cieply, B., Virji, M.A., Wu, T., Monga, S.P.S., 2009. Beta-Catenin Activation Promotes Liver Regeneration after Acetaminophen-Induced Injury. The American journal of pathology 175, 1056-1065.

Apte, U., Thompson, M.D., Cui, S., Liu, B., Cieply, B., Monga, S.P.S., 2008. Wnt/β-catenin signaling mediates oval cell response in rodents. Hepatology 47, 288-295.

Bai, H., Zhang, N., Xu, Y., Chen, Q., Khan, M., Potter, J.J., Nayar, S.K., Cornish, T., Alpini, G., Bronk, S., Pan, D., Anders, R.A., 2012. Yes-associated protein regulates the hepatic response after bile duct ligation. Hepatology 56, 1097-1107.

Bastide, P., Darido, C., Pannequin, J., Kist, R., Robine, S., Marty-Double, C., Bibeau, F.d.r., Scherer, G., Joubert, D., Hollande, F.d.r., Blache, P., Jay, P., 2007. Sox9 regulates cell proliferation and is required for Paneth cell differentiation in the intestinal epithelium. The Journal of Cell Biology 178, 635-648.

Behari, J., Yeh, T.-H., Krauland, L., Otruba, W., Cieply, B., Hauth, B., Apte, U., Wu, T., Evans, R., Monga, S.P.S., 2010. Liver-Specific β-Catenin Knockout Mice Exhibit Defective Bile Acid and Cholesterol Homeostasis and Increased Susceptibility to Diet-Induced Steatohepatitis. The American journal of pathology 176, 744-753.

Benedito, R., Roca, C., Sörensen, I., Adams, S., Gossler, A., Fruttiger, M., Adams, R.H., 2009. The Notch Ligands Dll4 and Jagged1 Have Opposing Effects on Angiogenesis. Cell 137, 1124-1135.

Benhamouche, S., Decaens, T., Godard, C., Chambrey, R., Rickman, D.S., Moinard, C., Vasseur-Cognet, M., Kuo, C.J., Kahn, A., Perret, C., Colnot, S., 2006. Apc Tumor Suppressor Gene Is the Zonation-Keeper of Mouse Liver. Developmental cell 10, 759-770.

Bhatia, S.N., Toner, M., Foy, B.D., Rotem, A., O'Neil, K.M., Tompkins, R.G., Yarmush, M.L., 1996. Zonal liver cell heterogeneity: effects of oxygen on metabolic functions of hepatocytes. Cellular Engineering.

Blache, P., van de Wetering, M., Duluc, I., Domon, C., Berta, P., Freund, J.-N.I., Clevers, H., Jay, P., 2004. SOX9 is an intestine crypt transcription factor, is regulated by the Wnt pathway, and represses the CDX2 and MUC2 genes. The Journal of Cell Biology 166, 37-47.

Bockhorn, M., Goralski, M., Prokofiev, D., Dammann, P., Grünewald, P., Trippler, M., Biglarnia, A., Kamler, M., Niehues, E.M., Frilling, A., Broelsch, C.E., Schlaak, J.F., 2007. VEGF is Important for Early Liver Regeneration After Partial Hepatectomy. The Journal of surgical research 138, 291-299.

Bolós, V., Grego-Bessa, J., de la Pompa, J.L., 2007. Notch Signaling in Development and Cancer. Endocrine Reviews 28, 339-363.

Bort, R., Signore, M., Tremblay, K., Barbera, J.P.M., Zaret, K.S., 2006. Hex homeobox gene controls the transition of the endoderm to a pseudostratified, cell emergent epithelium for liver bud development. Developmental Biology 290, 44-56.

Boulter, L., Govaere, O., Bird, T.G., Radulescu, S., Ramachandran, P., Pellicoro, A., Ridgway, R.A., Seo, S.S., Spee, B., Van Rooijen, N., Sansom, O.J., Iredale, J.P., Lowell, S., Roskams, R., Forbes, S.J., 2012. Macrophage-derived Wnt opposes Notch signaling to specify hepatic progenitor cell fate in chronic liver disease. Nat Med 18, 572-579.

CADORET, #160, Axelle, OVEJERO, #160, Christine, TERRIS, #160, Benoit, SOUIL, #160, Evelyne, LEVY, #160, Laurence, LAMERS, #160, H., W., KITAJEWSKI, #160, Jan, KAHN, #160, Axel, PERRET, #160, Christine, 2002. New targets of β-catenin signaling in the liver are involved in the glutamine metabolism. Nature Publishing Group, Basingstoke, ROYAUME-UNI.

Campbell, K.M., Sabla, G.E., Bezerra, J.A., 2004. Transcriptional reprogramming in murine liver defines the physiologic consequences of biliary obstruction. Journal of Hepatology 40, 14-23.

Carlson, T.R., Yan, Y., Wu, X., Lam, M.T., Tang, G.L., Beverly, L.J., Messina, L.M., Capobianco, A.J., Werb, Z., Wang, R., 2005. Endothelial expression of constitutively active Notch4 elicits reversible arteriovenous malformations in adult mice. Proceedings of the National Academy of Sciences of the United States of America 102, 9884-9889.

Carmeliet, P., Ferreira, V., Breier, G., Pollefeyt, S., Kieckens, L., Gertsenstein, M., Fahrig, M., Vandenhoeck, A., Harpal, K., Eberhardt, C., Declercq, C., Pawling, J., Moons, L., Collen, D., Risau, W., Nagy, A., 1996. Abnormal blood vessel development and lethality in embryos lacking a single VEGF allele. Nature 380, 435-439.

Carpenter, B., Lin, Y., Stoll, S., Raffai, R.L., McCuskey, R., Wang, R., 2005. VEGF is crucial for the hepatic vascular development required for lipoprotein uptake. Development 132, 3293-3303.

Carpentier, R., Español-Suñer, R., van Hul, N., Kopp, J.L., Beaudry, J.Ä., Cordi, S., Antoniou, A., Raynaud, P., Lepreux, S., Jacquemin, P., Leclercq, I.A., Sander, M., Lemaigre, F.P., 2011. Embryonic Ductal Plate Cells Give Rise to Cholangiocytes, Periportal Hepatocytes, and Adult Liver Progenitor Cells. Gastroenterology 141, 1432-1438.e1434.

Carpino, G., Cardinale, V., Onori, P., Franchitto, A., Berloco, P.B., Rossi, M., Wang, Y., Semeraro, R., Anceschi, M., Brunelli, R., Alvaro, D., Reid, L.M., Gaudio, E., 2012. Biliary tree stem/progenitor cells in glands of extrahepatic and intraheptic bile ducts: an anatomical in situ study yielding evidence of maturational lineages. Journal of Anatomy 220, 186-199.

Cheluvappa, R., Hilmer, S.N., Kwun, S.Y., Jamieson, H.A., O'Reilly, J.N., Muller, M., Cogger, V.C., Le Couteur, D.G., 2007. The effect of old age on liver oxygenation and the hepatic expression of VEGF and VEGFR2. Experimental Gerontology 42, 1012-1019.

Chen, S., Tao, J., Bae, Y., Jiang, M.-M., Bertin, T., Chen, Y., Yang, T., Lee, B., 2012. Notch gain of function inhibits chondrocyte differentiation via Rbpj-dependent suppression of Sox9. Journal of Bone and Mineral Research, n/a-n/a.

Clemons, N.J., Wang, D.H., Croagh, D., Tikoo, A., Fennell, C.M., Murone, C., Scott, A.M., Watkins, D.N., Phillips, W.A., 2012. Sox9 drives columnar differentiation of esophageal squamous epithelium: a possible role in the pathogenesis of Barrett's esophagus. American Journal of Physiology - Gastrointestinal and Liver Physiology 303, G1335-G1346.

Clotman, F., Lannoy, V., Reber, M., Cereghini, S., Cassiman, D., Jacquemin, P., Roskams, T., Rousseau, G., Lemaigre, F., 2002. The onecut transcription factor HNF6 is required for normal development of the biliary tract. Development 129, 1819 - 1828.

Coffinier, C., Gresh, L., Fiette, L., Tronche, F., Schutz, G., Babinet, C., Pontoglio, M., Yaniv, M., Barra, J., 2002. Bile system morphogenesis defects and liver dysfunction upon targeted deletion of HNF1beta. Development 129, 1829 - 1838.

Collardeau-Frachon, S., Scoazec, J.-Y., 2008. Vascular Development and Differentiation During Human Liver Organogenesis. The Anatomical Record: Advances in Integrative Anatomy and Evolutionary Biology 291, 614-627.

Colletti, M., Cicchini, C., Conigliaro, A., Santangelo, L., Alonzi, T., Pasquini, E., Tripodi, M., Amicone, L., 2009. Convergence of Wnt Signaling on the HNF4α-Driven Transcription in Controlling Liver Zonation. Gastroenterology 137, 660-672.

Colnot, S., Perret, C., 2011. Liver Zonation, in: Monga, S.P.S. (Ed.), Molecular Pathology of Liver Diseases. Springer, pp. 7-15.

Connolly, D.T., Heuvelman, D.M., Nelson, R., Olander, J.V., Eppley, B.L., Delfino, J.J., Siegel, N.R., Leimgruber, R.M., Feder, J., 1989. Tumor vascular permeability factor stimulates endothelial cell growth and angiogenesis. The Journal of Clinical Investigation 84, 1470-1478.

Crawford, L.W., Foley, J.F., Elmore, S.A., 2010. Histology atlas of the developing mouse hepatobiliary system with emphasis on embryonic days 9.5-18.5. Toxicologic pathology 38, 872-906.

D'Ambrosio, R., Aghemo, A., Rumi, M.G., Ronchi, G., Donato, M.F., Paradis, V., Colombo, M., Bedossa, P., 2012. A morphometric and immunohistochemical study to assess the benefit of a sustained virological response in hepatitis C virus patients with cirrhosis. Hepatology 56, 532-543.

Darwiche, H., Oh, S.-H., Steiger-Luther, N.C., Williams, J.M., Pintilie, D.G., Shupe, T.D., Petersen, B.E., 2011. Inhibition of Notch signaling affects hepatic oval cell response in rat model of 2AAF-PH. Hepatic medicine: evidence and research 3, 89.

DeLeve, L.D., Wang, X., Hu, L., McCuskey, M.K., McCuskey, R.S., 2004. Rat liver sinusoidal endothelial cell phenotype is maintained by paracrine and autocrine regulation. American Journal of Physiology - Gastrointestinal and Liver Physiology 287, G757-G763.

Delous, M., Yin, C., Shin, D., Ninov, N., Debrito Carten, J., Pan, L., Ma, T.P., Farber, S.A., Moens, C.B., Stainier, D.Y.R., 2012. *sox9b* Is a Key Regulator of Pancreaticobiliary Ductal System Development. PLoS Genet 8, e1002754.

Desmet, V., 2011. Ductal plates in hepatic ductular reactions. Hypothesis and implications. I. Types of ductular reaction reconsidered. Virchows Archiv 458, 251-259.

Desmet, V., Roskams, T., Van Eyken, P., 1995. Ductular reaction in the liver. Pathol Res Pract 191, 513 - 524.

Desmet, V.J., 1992. Congenital diseases of intrahepatic bile ducts: Variations on the theme “ductal plate malformation”. Hepatology 16, 1069-1083.

Dessaud, E., McMahon, A.P., Briscoe, J., 2008. Pattern formation in the vertebrate neural tube: a sonic hedgehog morphogen-regulated transcriptional network. Development 135, 2489-2503.

Dill, M.T., Tornillo, L., Fritzius, T., Terracciano, L., Semela, D., Bettler, B., Heim, M.H., Tchorz, J.S., 2013. Constitutive Notch2 signaling induces hepatic tumors in mice. Hepatology 57, 1607-1619.

Ding, B.-S., Nolan, D.J., Butler, J.M., James, D., Babazadeh, A.O., Rosenwaks, Z., Mittal, V., Kobayashi, H., Shido, K., Lyden, D., 2010. Inductive angiocrine signals from sinusoidal endothelium are required for liver regeneration. Nature 468, 310-315.

Discher, D.E., Mooney, D.J., Zandstra, P.W., 2009. Growth Factors, Matrices, and Forces Combine and Control Stem Cells. Science 324, 1673-1677.

Dorrell, C., Erker, L., Schug, J., Kopp, J.L., Canaday, P.S., Fox, A.J., Smirnova, O., Duncan, A.W., Finegold, M.J., Sander, M., Kaestner, K.H., Grompe, M., 2011. Prospective isolation of a bipotential clonogenic liver progenitor cell in adult mice. Genes & Development 25, 1193-1203.

Dou, G.-R., Wang, Y.-C., Hu, X.-B., Hou, L.-H., Wang, C.-M., Xu, J.-F., Wang, Y.-S., Liang, Y.-M., Yao, L.-B., Yang, A.-G., Han, H., 2008. RBP-J, the transcription factor downstream of Notch receptors, is essential for the maintenance of vascular homeostasis in adult mice. The FASEB Journal 22, 1606-1617.

Eichmann, A., Makinen, T., Alitalo, K., 2005. Neural guidance molecules regulate vascular remodeling and vessel navigation. Genes & development 19, 1013-1021.

Español-Suñer, R., Carpentier, R., Van Hul, N., Legry, V., Achouri, Y., Cordi, S., Jacquemin, P., Lemaigre, F., Leclercq, I.A., 2012. Liver Progenitor Cells Yield Functional Hepatocytes in Response to Chronic Liver Injury in Mice. Gastroenterology 143, 1564-1575.e1567.

Fabris, L., Cadamuro, M., Fiorotto, R., Roskams, T., Spirlì, C., Melero, S., Sonzogni, A., Joplin, R.E., Okolicsanyi, L., Strazzabosco, M., 2006. Effects of angiogenic factor overexpression by human and rodent cholangiocytes in polycystic liver diseases. Hepatology 43, 1001-1012.

Fabris, L., Cadamuro, M., Guido, M., Spirli, C., Fiorotto, R., Colledan, M., Torre, G., Alberti, D., Sonzogni, A., Okolicsanyi, L., Strazzabosco, M., 2007. Analysis of Liver Repair Mechanisms in Alagille Syndrome and Biliary Atresia Reveals a Role for Notch Signaling. The American Journal of Pathology 171, 641-653.

Fabris, L., Cadamuro, M., Libbrecht, L., Raynaud, P., Spirlì, C., Fiorotto, R., Okolicsanyi, L., Lemaigre, F., Strazzabosco, M., Roskams, T., 2008. Epithelial expression of angiogenic growth factors modulate arterial vasculogenesis in human liver development. Hepatology 47, 719-728.

Factor, V.M., Jensen, M.R., Thorgeirsson, S.S., 1997. Coexpression of C-myc and transforming growth factor alfa in the liver promotes early replicative senescence and diminishes regenerative capacity after partial hepatectomy in transgenic mice. Hepatology 26, 1434-1443.

Falkowski, O., An, H.J., Ianus, I.A., Chiriboga, L., Yee, H., West, A.B., Theise, N.D., 2003. Regeneration of hepatocyte ‚Äòbuds‚Äô in cirrhosis from intrabiliary stem cells. Journal of Hepatology 39, 357-364.

Fan, B., Malato, Y., Calvisi, D.F., Naqvi, S., Razumilava, N., Ribback, S., Gores, G.J., Dombrowski, F., Evert, M., Chen, X., Willenbring, H., 2012. Cholangiocarcinomas can originate from hepatocytes in mice. The Journal of Clinical Investigation 122, 2911-2915.

Ferrara, N., Carver-Moore, K., Chen, H., Dowd, M., Lu, L., O'Shea, K.S., Powell-Braxton, L., Hillan, K.J., Moore, M.W., 1996. Heterozygous embryonic lethality induced by targeted inactivation of the VEGF gene. Nature 380, 439-442.

Ferrara, N., Davis-Smyth, T., 1997. The Biology of Vascular Endothelial Growth Factor. Endocrine Reviews 18, 4-25.

Fiorotto, R., Raizner, A., Morell, C.M., Torsello, B., Scirpo, R., Fabris, L., Spirli, C., Strazzabosco, M., 2013. Notch signaling regulates tubular morphogenesis during repair from biliary damage in mice. Journal of hepatology 59, 124-130.

Fong, G.-H., Rossant, J., Gertsenstein, M., Breitman, M.L., 1995. Role of the Flt-1 receptor tyrosine kinase in regulating the assembly of vascular endothelium. Nature 376, 66-70.

Franco, M., Roswall, P., Cortez, E., Hanahan, D., Pietras, K., 2011. Pericytes promote endothelial cell survival through induction of autocrine VEGF-A signaling and Bcl-w expression. Blood 118, 2906-2917.

Furuyama, K., Kawaguchi, Y., Akiyama, H., Horiguchi, M., Kodama, S., Kuhara, T., Hosokawa, S., Elbahrawy, A., Soeda, T., Koizumi, M., 2010. Continuous cell supply from a Sox9-expressing progenitor zone in adult liver, exocrine pancreas and intestine. Nature genetics 43, 34-41.

Furuyama, K., Kawaguchi, Y., Akiyama, H., Horiguchi, M., Kodama, S., Kuhara, T., Hosokawa, S., Elbahrawy, A., Soeda, T., Koizumi, M., Masui, T., Kawaguchi, M., Takaori, K., Doi, R., Nishi, E., Kakinoki, R., Deng, J.M., Behringer, R.R., Nakamura, T., Uemoto, S., 2011. Continuous cell supply from a Sox9-expressing progenitor zone in adult liver, exocrine pancreas and intestine. Nature genetics 43, 34-41.

Gaudio, E., Barbaro, B., Alvaro, D., Glaser, S., Francis, H., Franchitto, A., Onori, P., Ueno, Y., Marzioni, M., Fava, G., 2006. Administration of r-VEGF-A prevents hepatic artery ligation-induced bile duct damage in bile duct ligated rats. American Journal of Physiology-Gastrointestinal and Liver Physiology 291, G307-G317.

Geisler, F., Nagl, F., Mazur, P.K., Lee, M., Zimber-Strobl, U., Strobl, L.J., Radtke, F., Schmid, R.M., Siveke, J.T., 2008. Liver-specific inactivation of Notch2, but not Notch1, compromises intrahepatic bile duct development in mice. Hepatology (Baltimore, Md.) 48, 607-616.

Gerber, H.-P., Malik, A.K., Solar, G.P., Sherman, D., Liang, X.H., Meng, G., Hong, K., Marsters, J.C., Ferrara, N., 2002. VEGF regulates haematopoietic stem cell survival by an internal autocrine loop mechanism. Nature 417, 954-958.

Gerber, H.P., Hillan, K.J., Ryan, A.M., Kowalski, J., Keller, G.A., Rangell, L., Wright, B.D., Radtke, F., Aguet, M., Ferrara, N., 1999. VEGF is required for growth and survival in neonatal mice. Development 126, 1149-1159.

Gerhardt, H., Golding, M., Fruttiger, M., Ruhrberg, C., Lundkvist, A., Abramsson, A., Jeltsch, M., Mitchell, C., Alitalo, K., Shima, D., Betsholtz, C., 2003. VEGF guides angiogenic sprouting utilizing endothelial tip cell filopodia. The Journal of Cell Biology 161, 1163-1177.

Glaser, S.S., Gaudio, E., Rao, A., Pierce, L.M., Onori, P., Franchitto, A., Francis, H.L., Dostal, D.E., Venter, J.K., DeMorrow, S., Mancinelli, R., Carpino, G., Alvaro, D., Kopriva, S.E., Savage, J.M., Alpini, G.D., 2009. Morphological and functional heterogeneity of the mouse intrahepatic biliary epithelium. Lab Invest 89, 456-469.

Goldman, O., Han, S., Sourrisseau, M., Dziedzic, N., Hamou, W., Corneo, B., D,ÄôSouza, S., Sato, T., Kotton, D.N., Bissig, K.-D., Kalir, T., Jacobs, A., Evans, T., Evans, M.J., Gouon-Evans, V., 2013. KDR Identifies a Conserved Human and Murine Hepatic Progenitor and Instructs Early Liver Development. Cell Stem Cell 12, 748-760.

Göthert, J.R., Gustin, S.E., van Eekelen, J.A.M., Schmidt, U., Hall, M.A., Jane, S.M., Green, A.R., Göttgens, B., Izon, D.J., Begley, C.G., 2004. Genetically tagging endothelial cells in vivo: bone marrow-derived cells do not contribute to tumor endothelium. Blood 104, 1769-1777.

Gottgens, B., Broccardo, C., Sanchez, M.-J., Deveaux, S., Murphy, G., G√∂thert, J.R., Kotsopoulou, E., Kinston, S., Delaney, L., Piltz, S., Barton, L.M., Knezevic, K., Erber, W.N., Begley, C.G., Frampton, J., Green, A.R., 2004. The scl +18/19 Stem Cell Enhancer Is Not Required for Hematopoiesis: Identification of a 5‚Ä≤ Bifunctional Hematopoietic-Endothelial Enhancer Bound by Fli-1 and Elf-1. Molecular and Cellular Biology 24, 1870-1883.

Gouw, A.S.H., Clouston, A.D., Theise, N.D., 2011. Ductular reactions in human liver: Diversity at the interface. Hepatology 54, 1853-1863.

Gouysse, G., Couvelard, A., Frachon, S., Bouvier, R., Nejjari, M., Dauge, M.-C., Feldmann, G., Hénin, D., Scoazec, J.-Y., 2002. Relationship between vascular development and vascular differentiation during liver organogenesis in humans. Journal of hepatology 37, 730-740.

Gridley, T., 2007. Notch signaling in vascular development and physiology. Development 134, 2709-2718.

Gualdi, R., Bossard, P., Zheng, M., Hamada, Y., Coleman, J.R., Zaret, K.S., 1996. Hepatic specification of the gut endoderm in vitro: cell signaling and transcriptional control. Genes & Development 10, 1670-1682.

Guilak, F., Cohen, D.M., Estes, B.T., Gimble, J.M., Liedtke, W., Chen, C.S., 2009. Control of Stem Cell Fate by Physical Interactions with the Extracellular Matrix. Cell Stem Cell 5, 17-26.

Guo, X., Xiong, L., Sun, T., Peng, R., Zou, L., Zhu, H., Zhang, J., Li, H., Zhao, J., 2012. Expression features of SOX9 associate with tumor progression and poor prognosis of hepatocellular carcinoma. Diagnostic Pathology 7, 44.

Haller, R., Schwanbeck, R., Martini, S., Bernoth, K., Kramer, J., Just, U., Rohwedel, J., 2012. Notch1 signaling regulates chondrogenic lineage determination through Sox9 activation. Cell Death Differ 19, 461-469.

Hamaguchi, Y., Yamamoto, Y., Iwanari, H., Maruyama, S., Furukawa, T., Matsunami, N., Honjo, T., 1992. Biochemical and Immunological Characterization of the DNA Binding Protein (RBP-Jx) to Mouse Jx Recombination Signal Sequence. Journal of Biochemistry 112, 314-320.

Han, H., Tanigaki, K., Yamamoto, N., Kuroda, K., Yoshimoto, M., Nakahata, T., Ikuta, K., Honjo, T., 2002. Inducible gene knockout of transcription factor recombination signal binding protein,RBPJ reveals its essential role in T versus B lineage decision. International Immunology 14, 637-645.

Hardingham, T.E., Oldershaw, R.A., Tew, S.R., 2006. Cartilage, SOX9 and Notch signals in chondrogenesis. Journal of Anatomy 209, 469-480.

Hellström, M., Phng, L.-K., Hofmann, J.J., Wallgard, E., Coultas, L., Lindblom, P., Alva, J., Nilsson, A.-K., Karlsson, L., Gaiano, N., 2007. Dll4 signalling through Notch1 regulates formation of tip cells during angiogenesis. Nature 445, 776-780.

Herbert, S.P., Stainier, D.Y.R., 2011. Molecular control of endothelial cell behavior during blood vessel morphogenesis. Nature Reviews Molecular Cellular Biology 12, 551-564.

Hoeben, A., Landuyt, B., Highley, M.S., Wildiers, H., Van Oosterom, A.T., De Bruijn, E.A., 2004. Vascular Endothelial Growth Factor and Angiogenesis. Pharmacological Reviews 56, 549-580.

Hofmann, J.J., Zovein, A.C., Koh, H., Radtke, F., Weinmaster, G., Iruela-Arispe, M.L., 2010. Jagged1 in the portal vein mesenchyme regulates intrahepatic bile duct development: insights into Alagille syndrome. Development 137, 4061-4072.

Holterman, A.-X.L., Tan, Y., Kim, W., Yoo, K.W., Costa, R.H., 2002. Diminished hepatic expression of the HNF-6 transcription factor during bile duct obstruction. Hepatology 35, 1392-1399.

Ishikawa, K., Mochida, S., Mashiba, S., Inao, M., Matsui, A., Ikeda, H., Ohno, A., Shibuya, M., Fujiwara, K., 1999. Expressions of Vascular Endothelial Growth Factor in Nonparenchymal as Well as Parenchymal Cells in Rat Liver after Necrosis. Biochemical and Biophysical Research Communications 254, 587-593.

Jeliazkova, P., Jörs, S., Lee, M., Zimber-Strobl, U., Ferrer, J., Schmid, R.M., Siveke, J.T., Geisler, F., 2013. Canonical Notch2 signaling determines biliary cell fates of embryonic hepatoblasts and adult hepatocytes independent of Hes1. Hepatology, n/a-n/a.

Jung, J., Zheng, M., Goldfarb, M., Zaret, K.S., 1999. Initiation of Mammalian Liver Development from Endoderm by Fibroblast Growth Factors. Science 284, 1998-2003.

Jungermann, K., Keitzmann, T., 1996. Zonation of Parenchymal and Nonparenchymal Metabolism in Liver. Annual Review of Nutrition 16, 179-203.

Jungermann, K., Kietzmann, T., 1997. Role of oxygen in the zonation of carbohydrate metabolism and gene expression in liver : Oxygen sensing on the cellular and molecular level. Nature Publishing Group, Basingstoke, ROYAUME-UNI.

Jungermann, K., Kietzmann, T., 2000. Oxygen: Modulator of metabolic zonation and disease of the liver. Hepatology 31, 255-260.

Kaestner, K.H., 2005. The Making of the Liver: Competence in the Foregut Endoderm and Induction of Liver-Specific Genes. Cell Cycle 4, 1146-1148.

Kamba, T., McDonald, D.M., 2007. Mechanisms of adverse effects of anti-VEGF therapy for cancer. British Journal of Cancer 96, 1788-1795.

Kato, T., Ito, Y., Hosono, K., Suzuki, T., Tamaki, H., Minamino, T., Kato, S., Sakagami, H., Shibuya, M., Majima, M., 2011. Vascular endothelial growth factor receptor-1 signaling promotes liver repair through restoration of liver microvasculature after acetaminophen hepatotoxicity. Toxicological Sciences 120, 218-229.

Kietzmann, T., Schmidt, H., Probst, I., Jungermann, K., 1992. Modulation of the glucagon-dependent activation of the phosphoenolpyruvate carboxykinase gene by oxygen in rat hepatocyte cultures Evidence for a heme protein as oxygen sensor. FEBS Letters 311, 251-255.

Kietzmann, T., Schmidt, H., Unthanfechner, K., Probst, I., Jungermann, K., 1993. A Ferro-Heme Protein Senses Oxygen Levels, Which Modulate the Glucagon-Dependent Activation of the Phosphoenolpyruvate Carboxykinase Gene in Rat Hepatocyte Cultures. Biochemical and Biophysical Research Communications 195, 792-798.

Kiyohashi, K., Kakinuma, S., Kamiya, A., Sakamoto, N., Nitta, S., Yamanaka, H., Yoshino, K., Fujiki, J., Murakawa, M., Kusano-Kitazume, A., Shimizu, H., Okamoto, R., Azuma, S., Nakagawa, M., Asahina, Y., Tanimizu, N., Kikuchi, A., Nakauchi, H., Watanabe, M., 2013. Wnt5a signaling mediates biliary differentiation of fetal hepatic stem/progenitor cells in mice. Hepatology 57, 2502-2513.

Kodama, Y., Hijikata, M., Kageyama, R., Shimotohno, K., Chiba, T., 2004. The role of notch signaling in the development of intrahepatic bile ducts. Gastroenterology 127, 1775-1786.

Krueger, J., Liu, D., Scholz, K., Zimmer, A., Shi, Y., Klein, C., Siekmann, A., Schulte-Merker, S., Cudmore, M., Ahmed, A., le Noble, F., 2011. Flt1 acts as a negative regulator of tip cell formation and branching morphogenesis in the zebrafish embryo. Development 138, 2111-2120.

Kwon, G.S., Hadjantonakis, A.-K., 2009. Transthyretin mouse transgenes direct RFP expression or Cre-mediated recombination throughout the visceral endoderm. genesis 47, 447-455.

Kwon, S., Jeong, S., Jang, J., Lee, J., Lee, S., Kim, S., Kim, Y.Y., Kim, H., Kim, B., Jin, S.-Y., 2012. Cyclooxygenase-2 and vascular endothelial growth factor in chronic hepatitis, cirrhosis and hepatocellular carcinoma. Clinical and Molecular Hepatology 18, 287-294.

Lassau, J., Bastian, D., 1983. Organogenesis of the venous structures of the human liver: a hemodynamic theory. Anatomia Clinica 5, 97-102.

Lautt, W.W., 2009. Hepatic Circulation: Physiology and Pathopysiology. Morgan & Claypool Life Sciences, San Rafael, CA.

Le Couteur, D.G., Cogger, V.C., Markus, A.M.A., Harvey, P.J., Yin, Z.-L., Ansselin, A.D., McLean, A.J., 2001. Pseudocapillarization and associated energy limitation in the aged rat liver. Hepatology 33, 537-543.

Lee, C.S., Friedman, J.R., Fulmer, J.T., Kaestner, K.H., 2005. The initiation of liver development is dependent on Foxa transcription factors. Nature 435, 944-947.

Lee, J.M., Yang, J., Newell, P., Singh, S., Parwani, A., Friedman, S.L., Nejak-Bowen, K.N., Monga, S.P., 2013. Beta-Catenin signaling in hepatocellular cancer: Implications in inflammation, fibrosis, and proliferation. Cancer Letters.

Lee, S., Chen, T.T., Barber, C.L., Jordan, M.C., Murdock, J., Desai, S., Ferrara, N., Nagy, A., Roos, K.P., Iruela-Arispe, M.L., 2007. Autocrine VEGF Signaling Is Required for Vascular Homeostasis. Cell 130, 691-703.

Leung, A., Ciau-Uitz, A., Pinheiro, P., Monteiro, R., Zuo, J., Vyas, P., Patient, R., Porcher, C., 2013. Uncoupling VEGFA Functions in Arteriogenesis and Hematopoietic Stem Cell Specification. Developmental Cell 24, 144-158.

Limaye, P., Alarcon, G., Walls, A., Nalesnik, M., Michalopoulos, G., Demetris, A., Ochoa, E., 2008a. Expression of specific hepatocyte and cholangiocyte transcription factors in human liver disease and embryonic development. Lab Invest 88, 865 - 872.

Limaye, P., Bowen, W., Orr, A., Apte, U., Michalopoulos, G., 2010. Expression of hepatocytic- and biliary-specific transcription factors in regenerating bile ducts during hepatocyte-to-biliary epithelial cell transdifferentiation. Comparative Hepatology 9, 9.

Limaye, P.B., Bowen, W.C., Orr, A.V., Luo, J., Tseng, G.C., Michalopoulos, G.K., 2008b. Mechanisms of hepatocyte growth factor–mediated and epidermal growth factor–mediated signaling in transdifferentiation of rat hepatocytes to biliary epithelium. Hepatology 47, 1702-1713.

Lobov, I.B., Renard, R.A., Papadopoulos, N., Gale, N.W., Thurston, G., Yancopoulos, G.D., Wiegand, S.J., 2007. Delta-like ligand 4 (Dll4) is induced by VEGF as a negative regulator of angiogenic sprouting. Proceedings of the National Academy of Sciences 104, 3219-3224.

Loebel, D.A.F., Watson, C.M., De Young, R.A., Tam, P.P.L., 2003. Lineage choice and differentiation in mouse embryos and embryonic stem cells. Developmental Biology 264, 1-14.

Lozier, J., McCright, B., Gridley, T., 2008a. Notch signaling regulates bile duct morphogenesis in mice. PLoS ONE 3, e1851-e1851.

Lozier, J., McCright, B., Gridley, T., 2008b. Notch Signaling Regulates Bile Duct Morphogenesis in Mice. PLoS ONE 3, e1851.

Malato, Y., Naqvi, S., Sch√ºrmann, N., Ng, R., Wang, B., Zape, J., Kay, M.A., Grimm, D., Willenbring, H., 2011. Fate tracing of mature hepatocytes in mouse liver homeostasis and regeneration. The Journal of Clinical Investigation 121, 4850-4860.

Mancinelli, R., Onori, P., Gaudio, E., Franchitto, A., Carpino, G., Ueno, Y., Alvaro, D., Annarale, L.P., DeMorrow, S., Francis, H., 2009. Taurocholate Feeding to Bile Duct Ligated Rats Prevents Caffeic Acid-Induced Bile Duct Damage by Changes in Cholangiocyte VEGF Expression. Experimental Biology and Medicine 234, 462-474.

Marschall, Z.v., Cramer, T., Höcker, M., Finkenzeller, G., Wiedenmann, B., Rosewicz, S., 2001. Dual mechanism of vascular endothelial growth factor upregulation by hypoxia in human hepatocellular carcinoma. Gut 48, 87-96.

Matsumoto, K., Yoshitomi, H., Rossant, J., Zaret, K.S., 2001. Liver Organogenesis Promoted by Endothelial Cells Prior to Vascular Function. Science 294, 559-563.

Mazur, P.K., Riener, M.-O., Jochum, W., Kristiansen, G., Weber, A., Schmid, R.M., Siveke, J.T., 2012. Expression and Clinicopathological Significance of Notch Signaling and Cell-Fate Genes in Biliary Tract Cancer. Am J Gastroenterol 107, 126-135.

McCright, B., Lozier, J., Gridley, T., 2002. A mouse model of Alagille syndrome: Notch2 as a genetic modifier of Jag1 haploinsufficiency. Development 129, 1075-1082.

Means, A.L., Xu, Y., Zhao, A., Ray, K.C., Gu, G., 2008. A CK19CreERT knockin mouse line allows for conditional DNA recombination in epithelial cells in multiple endodermal organs. genesis 46, 318-323.

Meier-Stiegen, F., Schwanbeck, R., Bernoth, K., Martini, S., Hieronymus, T., Ruau, D., Zenke, M., Just, U., 2010. Activated Notch1 Target Genes during Embryonic Cell Differentiation Depend on the Cellular Context and Include Lineage Determinants and Inhibitors. PLoS ONE 5, e11481.

Michalopoulos, G., Barua, L., Bowen, W., 2005. Transdifferentiation of rat hepatocytes into biliary cells after bile duct ligation and toxic biliary injury. Hepatology 41, 535 - 544.

Michalopoulos, G., Bowen, W., Mule, K., Lopez-Talavera, J., Mars, W., 2002. Hepatocytes undergo phenotypic transformation to biliary epithelium in organoid cultures. Hepatology 36, 278 - 283.

Michalopoulos, G.K., DeFrances, M.C., 1997. Liver Regeneration. Science 276, 60-66.

Mitchell, S.J., Huizer-Pajkos, A., Cogger, V.C., McLachlan, A.J., Le Couteur, D.G., Jones, B., de Cabo, R., Hilmer, S.N., 2011. Age-Related Pseudocapillarization of the Liver Sinusoidal Endothelium Impairs the Hepatic Clearance of Acetaminophen in Rats. The Journals of Gerontology Series A: Biological Sciences and Medical Sciences 66A, 400-408.

Miyoshi, H., Rust, C., Roberts, P.J., Burgart, L.J., Gores, G.J., 1999. Hepatocyte apoptosis after bile duct ligation in the mouse involves Fas. Gastroenterology 117, 669-677.

Moeini, A., Cornellà, H., Villanueva, A., 2012. Emerging signaling pathways in hepatocellular carcinoma. Liver Cancer 1, 83-93.

Mohanty, S., Shivakumar, P., Sabla, G., Bezerra, J., 2006. Loss of interleukin-12 modifies the pro-inflammatory response but does not prevent duct obstruction in experimental biliary atresia. BMC Gastroenterol 6, 1-10.

Moon, W.S., Rhyu, K.H., Kang, M.J., Lee, D.G., Yu, H.C., Yeum, J.H., Koh, G.Y., Tarnawski, A.S., 2003. Overexpression of VEGF and ANgiopoietin 2: A Key to High Vascularity of Hepatocellular Carcinoma? Modern Pathology 16, 552.

Morell, C.M., Fabris, L., Strazzabosco, M., 2013. Vascular biology of the biliary epithelium. Journal of Gastroenterology and Hepatology 28, 26-32.

Mori-Akiyama, Y., van den Born, M., van Es, J.H., Hamilton, S.R., Adams, H.P., Zhang, J., Clevers, H., de Crombrugghe, B., 2007. SOX9 Is Required for the Differentiation of Paneth Cells in the Intestinal Epithelium. Gastroenterology 133, 539-546.

Muto, A., Iida, A., Satoh, S., Watanabe, S., 2009. The group E Sox genes Sox8 and Sox9 are regulated by Notch signaling and are required for Muller glial cell development in mouse retina. Experimental Eye Research 89, 549-558.

Oda, T., Elkahloun, A.G., Pike, B.L., Okajima, K., Krantz, I.D., Genin, A., Piccoli, D.A., Meltzer, P.S., Spinner, N.B., Collins, F.S., Chandrasekharappa, S.C., 1997. Mutations in the human Jagged1 gene are responsible for Alagille syndrome. Nat Genet 16, 235-242.

Oe, H., Kaido, T., Mori, A., Onodera, H., Imamura, M., 2004. Hepatocyte growth factor as well as vascular endothelial growth factor gene induction effectively promotes liver regeneration after hepatectomy in Solt-Farber rats. Hepato-gastroenterology 52, 1393-1397.

Ohno-Matsui, K., Hirose, A., Yamamoto, S., Saikia, J., Okamoto, N., Gehlbach, P., Duh, E.J., Hackett, S., Chang, M., Bok, D., Zack, D.J., Campochiaro, P.A., 2002. Inducible Expression of Vascular Endothelial Growth Factor in Adult Mice Causes Severe Proliferative Retinopathy and Retinal Detachment. The American Journal of Pathology 160, 711-719.

Oka, C., Nakano, T., Wakeham, A., de la Pompa, J.L., Mori, C., Sakai, T., Okazaki, S., Kawaichi, M., Shiota, K., Mak, T.W., 1995. Disruption of the mouse RBP-J kappa gene results in early embryonic death. Development 121, 3291-3301.

Omenetti, A., Popov, Y., Jung, Y., Choi, S.S., Witek, R.P., Yang, L., Brown, K.D., Schuppan, D., Diehl, A.M., 2008. The hedgehog pathway regulates remodelling responses to biliary obstruction in rats. Gut 57, 1275-1282.

Owen, M.R., Sherratt, J.A., Wearing, H.J., 2000. Lateral Induction by Juxtacrine Signaling Is a New Mechanism for Pattern Formation. Developmental Biology 217, 54-61.

Park, Y.N., Kim, Y.-B., Yang, K.M., Park, C., 2000. Increased Expression of Vascular Endothelial Growth Factor and Angiogenesis in the Early Stage of Multistep Hepatocarcinogenesis. Archives of Pathology & Laboratory Medicine 124, 1061-1065.

Parviz, F., Matullo, C., Garrison, W.D., Savatski, L., Adamson, J.W., Ning, G., Kaestner, K.H., Rossi, J.M., Zaret, K.S., Duncan, S.A., 2003. Hepatocyte nuclear factor 4alpha controls the development of a hepatic epithelium and liver morphogenesis. Nature Genetics 34, 292-296.

Petersen, B.E., Bowen, W.C., Patrene, K.D., Mars, W.M., Sullivan, A.K., Murase, N., Boggs, S.S., Greenberger, J.S., Goff, J.P., 1999. Bone Marrow as a Potential Source of Hepatic Oval Cells. Science 284, 1168-1170.

Petersen, B.E., Goff, J.P., Greenberger, J.S., Michalopoulos, G.K., 1998. Hepatic oval cells express the hematopoietic stem cell marker thy-1 in the rat. Hepatology 27, 433-445.

Phng, L.K., Gerhardt, H., 2009. Angiogenesis: A Team Effort Coordinated by Notch. Developmental Cell 16, 196-208.

Postic, C., Magnuson, M.A., 2000. DNA excision in liver by an albumin-Cre transgene occurs progressively with age. genesis 26, 149-150.

Prado, I.B., Santos, M.H.H.d., Lopasso, F.P., Iriya, K., Laudanna, A.A., 2003. Cholestasis in a murine experimental model: lesions include hepatocyte ischemic necrosis. Revista do Hospital das Clínicas 58, 27-32.

Preisegger, K.H., Factor, V.M., Fuchsbichler, A., et al., 1999. Atypical ductular proliferation its inhibition by transforming growth factor beta1 in the 3,5-diethoxycarbonyl-1,4-dihydrocollidine mouse model for chronic alcoholic liver disease. Lab Invest 79, 103-109.

Preissegger, K.H., Factor, V.M., Fuchsbichler, A., Stumptner, C., Denk, H., Thorgeirsson, S.S., 1999. Atypical ductular proliferation and its inhibition by transforming growth factor beta1 in the 3,5-diethoxycarbonyl-1,4-dihydrocollidine mouse model for chronic alcoholic liver disease. Laboratory Investigation 79, 103-109.

Prevot, P.-P., Simion, A., Grimont, A., Colletti, M., Khalaileh, A., Van den Steen, G., Sempoux, C., Xu, X., Roelants, V., Hald, J., Bertrand, L., Heimberg, H., Konieczny, S.F., Dor, Y., Lemaigre, F.P., Jacquemin, P., 2012. Role of the ductal transcription factors HNF6 and Sox9 in pancreatic acinar-to-ductal metaplasia. Gut.

Pritchett, J., Harvey, E., Athwal, V., Berry, A., Rowe, C., Oakley, F., Moles, A., Mann, D.A., Bobola, N., Sharrocks, A.D., Thomson, B.J., Zaitoun, A.M., Irving, W.L., Guha, I.N., Hanley, N.A., Hanley, K.P., 2012. Osteopontin is a novel downstream target of SOX9 with diagnostic implications for progression of liver fibrosis in humans. Hepatology 56, 1108-1116.

Ramalingam, S., Daughtridge, G.W., Johnston, M.J., Gracz, A.D., Magness, S.T., 2012. Distinct levels of Sox9 expression mark colon epithelial stem cells that form colonoids in culture. American Journal of Physiology - Gastrointestinal and Liver Physiology 302, G10-G20.

Reinert, R.B., Kantz, J., Misfeldt, A.A., Poffenberger, G., Gannon, M., Brissova, M., Powers, A.C., 2012. Tamoxifen-Induced Cre-loxP Recombination Is Prolonged in Pancreatic Islets of Adult Mice. PLoS ONE 7, e33529.

Ren, X.S., Sato, Y., Harada, K., Sasaki, M., Yoneda, N., Lin, Z.H., Nakanuma, Y., 2011. Biliary infection may exacerbate biliary cystogenesis through the induction of VEGF in cholangiocytes of the polycystic kidney (PCK) rat. The American journal of pathology 179, 2845-2854.

Roskams, T.A., Libbrecht, L., Desmet, V.J., 2003. Progenitor Cells in Diseased Human Liver. Semin Liver Dis 23, 385-396.

Rosmorduc, O., Wendum, D., Corpechot, C., Galy, B., Sebbagh, N., Raleigh, J., Housset, C., Poupon, R., 1999. Hepatocellular hypoxia-induced vascular endothelial growth factor expression and angiogenesis in experimental biliary cirrhosis. The American journal of pathology 155, 1065-1073.

Rossi, J.M., Dunn, N.R., Hogan, B.L.M., Zaret, K.S., 2001. Distinct mesodermal signals, including BMPs from the septum transversum mesenchyme, are required in combination for hepatogenesis from the endoderm. Genes & Development 15, 1998-2009.

Sackett, S.D., Li, Z., Hurtt, R., Gao, Y., Wells, R.G., Brondell, K., Kaestner, K.H., Greenbaum, L.E., 2009. Foxl1 is a marker of bipotential hepatic progenitor cells in mice. Hepatology 49, 920-929.

Sekiya, S., Suzuki, A., 2012. Intrahepatic cholangiocarcinoma can arise from Notch-mediated conversion of hepatocytes. The Journal of Clinical Investigation 0.

Seymour, P.A., Freude, K.K., Tran, M.N., Mayes, E.E., Jensen, J., Kist, R., Scherer, G., Sander, M., 2007. SOX9 is required for maintenance of the pancreatic progenitor cell pool. Proceedings of the National Academy of Sciences 104, 1865-1870.

Seymour, P.A., Shih, H.P., Patel, N.A., Freude, K.K., Xie, R., Lim, C.J., Sander, M., 2012. A Sox9/Fgf feed-forward loop maintains pancreatic organ identity. Development 139, 3363-3372.

Shalaby, F., Rossant, J., Yamaguchi, T.P., Gertsenstein, M., Wu, X.-F., Breitman, M.L., Schuh, A.C., 1995. Failure of blood-island formation and vasculogenesis in Flk-1-deficient mice. Nature 376, 62-66.

Shimizu, H., Mitsuhashi, N., Ohtsuka, M., Ito, H., Kimura, F., Ambiru, S., Togawa, A., Yoshidome, H., Kato, A., Miyazaki, M., 2005. Vascular endothelial growth factor and angiopoietins regulate sinusoidal regeneration and remodeling after partial hepatectomy in rats. World Journal of Gastroenterology 11, 7254.

Shimizu, H., Miyazaki, M., Wakabayashi, Y., Mitsuhashi, N., Kato, A., Ito, H., Nakagawa, K., Yoshidome, H., Kataoka, M., Nakajima, N., 2001. Vascular endothelial growth factor secreted by replicating hepatocytes induces sinusoidal endothelial cell proliferation during regeneration after partial hepatectomy in rats. Journal of Hepatology 34, 683-689.

Shin, S., Walton, G., Aoki, R., Brondell, K., Schug, J., Fox, A., Smirnova, O., Dorrell, C., Erker, L., Chu, A.S., Wells, R.G., Grompe, M., Greenbaum, L.E., Kaestner, K.H., 2011. Foxl1-Cre-marked adult hepatic progenitors have clonogenic and bilineage differentiation potential. Genes & Development 25, 1185-1192.

Shteyer, E., Liao, Y., Muglia, L.J., Hruz, P.W., Rudnick, D.A., 2004. Disruption of hepatic adipogenesis is associated with impaired liver regeneration in mice. Hepatology 40, 1322-1332.

Si-Tayeb, K., Lemaigre, F.P., Duncan, S.A., 2010. Organogenesis and Development of the Liver. Developmental Cell 18, 175-189.

Siekmann, A.F., Lawson, N.D., 2007. Notch signalling limits angiogenic cell behaviour in developing zebrafish arteries. Nature 445, 781-784.

Sosa-Pineda, B., Wigle, J.T., Oliver, G., 2000. Hepatocyte migration during liver development requires Prox1. Nature Genetics 25, 254-255.

Sparks, E.E., Huppert, K.A., Brown, M.A., Washington, M.K., Huppert, S.S., 2010. Notch signaling regulates formation of the three-dimensional architecture of intrahepatic bile ducts in mice. Hepatology 51, 1391-1400.

Sparks, E.E., Perrien, D.S., Huppert, K.A., Peterson, T.E., Huppert, S.S., 2011. Defects in hepatic Notch signaling result in disruption of the communicating intrahepatic bile duct network in mice. Disease Models & Mechanisms 4, 359-367.

Spee, B., Carpino, G., Schotanus, B.A., Katoonizadeh, A., Borght, S.V., Gaudio, E., Roskams, T., 2010. Characterisation of the liver progenitor cell niche in liver diseases: potential involvement of Wnt and Notch signalling. Gut 59, 247-257.

Srinivas, S., Watanabe, T., Lin, C.-S., William, C., Tanabe, Y., Jessell, T., Costantini, F., 2001. Cre reporter strains produced by targeted insertion of EYFP and ECFP into the ROSA26 locus. BMC Developmental Biology 1, 4.

Stanulović, V.S., Kyrmizi, I., Kruithof-de Julio, M., Hoogenkamp, M., Vermeulen, J.L.M., Ruijter, J.M., Talianidis, I., Hakvoort, T.B.M., Lamers, W.H., 2007. Hepatic HNF4α deficiency induces periportal expression of glutamine synthetase and other pericentral enzymes. Hepatology 45, 433-444.

Strazzabosco, M., Fabris, L., 2008. Functional Anatomy of Normal Bile Ducts. The Anatomical Record: Advances in Integrative Anatomy and Evolutionary Biology 291, 653-660.

Strazzabosco, M., Fabris, L., 2013. The balance between Notch/Wnt signaling regulates progenitor cells' commitment during liver repair: Mystery solved? Journal of hepatology 58, 181-183.

Streuli, C.H., 2009. Integrins and cell-fate determination. Journal of Cell Science 122, 171-177.

Suchting, S., Freitas, C., le Noble, F., Benedito, R., Bréant, C., Duarte, A., Eichmann, A., 2007. The Notch ligand Delta-like 4 negatively regulates endothelial tip cell formation and vessel branching. Proceedings of the National Academy of Sciences 104, 3225-3230.

Sun, Y., Chen, X., Xiao, D., 2007. Tetracycline-inducible Expression Systems: New Strategies and Practices in the Transgenic Mouse Modeling. Acta Biochimica et Biophysica Sinica 39, 235-246.

Swift, M.R., Weinstein, B.M., 2009. Arterial–Venous Specification During Development. Circulation Research 104, 576-588.

Tam, B.Y.Y., Wei, K., Rudge, J.S., Hoffman, J., Holash, J., Park, S.-k., Yuan, J., Hefner, C., Chartier, C., Lee, J.-S., Jiang, S., Nayak, N.R., Kuypers, F.A., Ma, L., Sundram, U., Wu, G., Garcia, J.A., Schrier, S.L., Maher, J.J., Johnson, R.S., Yancopoulos, G.D., Mulligan, R.C., Kuo, C.J., 2006. VEGF modulates erythropoiesis through regulation of adult hepatic erythropoietin synthesis. Nature Medicine 12, 793-800.

Tanaka, A., Tsuneyama, K., Mikami, M., Uegaki, S., Aiso, M., Takikawa, H., 2007. Gene expression profiling in whole liver of bile duct ligated rats: VEGF-A expression is up-regulated in hepatocytes adjacent to the portal tracts. Journal of gastroenterology and hepatology 22, 1993-2000.

Taniguchi, E., Sakisaka, S., Matsuo, K., Tanikawa, K., Sata, M., 2001. Expression and Role of Vascular Endothelial Growth Factor in Liver Regeneration After Partial Hepatectomy in Rats. Journal of Histochemistry & Cytochemistry 49, 121-129.

Tanimizu, N., Miyajima, A., 2004. Notch signaling controls hepatoblast differentiation by altering the expression of liver-enriched transcription factors. Journal of Cell Science 117, 3165-3174.

Tao, X.-R., Li, W.-L., Su, J., Jin, C.-X., Wang, X.-M., Li, J.-X., Hu, J.-K., Xiang, Z.-H., Lau, J.T.Y., Hu, Y.-P., 2009. Clonal mesenchymal stem cells derived from human bone marrow can differentiate into hepatocyte-like cells in injured livers of SCID mice. Journal of Cellular Biochemistry 108, 693-704.

Tietz, P.S., LaRusso, N.F., 2006. Cholangiocyte Biology. Current Opinion in Gastroenterology 22, 279-287.

Tremblay, K.D., Zaret, K.S., 2005. Distinct populations of endoderm cells converge to generate the embryonic liver bud and ventral foregut tissues. Developmental Biology 280, 87-99.

Trindade, A., Ram Kumar, S., Scehnet, J.S., Lopes-da-Costa, L., Becker, J., Jiang, W., Liu, R., Gill, P.S., Duarte, A., 2008. Overexpression of delta-like 4 induces arterialization and attenuates vessel formation in developing mouse embryos. Blood 112, 1720-1729.

Tygstrup, N., Winkler, K., Mellemgaard, K., Andreassen, M., 1962. DETERMINATION OF THE HEPATIC ARTERIAL BLOOD FLOW AND OXYGEN SUPPLY IN MAN BY CLAMPING THE HEPATIC ARTERY DURING SURGERY. The Journal of Clinical Investigation 41, 447-454.

Vanderpool, C., Sparks, E.E., Huppert, K.A., Gannon, M., Means, A.L., Huppert, S.S., 2012. Genetic interactions between hepatocyte nuclear factor-6 and notch signaling regulate mouse intrahepatic bile duct development in vivo. Hepatology 55, 233-243.

Wagenaar, G.T.M., Chamuleau, R.A.F.M., de Haan, J.G., Maas, M.A.W., de Boer, P.A.J., Marx, F., Moorman, A.F.M., Frederiks, W.M., Lamers, W.H., 1993. Experimental evidence that the physiological position of the liver within the circulation is not a major determinant of zonation of gene expression. Hepatology 18, 1144-1153.

Wagenaar, G.T.M., Chamuleau, R.A.F.M., Maas, M.A.W., De Bruin, K., Korfage, H.A.M., Lamers, W.H., 1994. The physiological position of the liver in the circulation is not a major determinant of its functional capacity. Hepatology 20, 1532-1540.

Walter, T.J., Sparks, E.E., Huppert, S.S., 2012. 3-Dimensional Resin Casting and Imaging of Mouse Portal Vein or Intrahepatic Bile Duct System. J Vis Exp, e4272.

Wang, L., Sharma, K., Deng, H.-X., Siddique, T., Grisotti, G., Liu, E., Roos, R.P., 2008. Restricted expression of mutant SOD1 in spinal motor neurons and interneurons induces motor neuron pathology. Neurobiology of Disease 29, 400-408.

Wang, L., Wang, X., Xie, G., Wang, L., Hill, C.K., DeLeve, L.D., 2012. Liver sinusoidal endothelial cell progenitor cells promote liver regeneration in rats. The Journal of Clinical Investigation 122, 1567-1573.

Wang, M., Tan, Y., Costa, R.H., Holterman, A.-X.L., 2004. In vivo regulation of murine CYP7A1 by HNF-6: A novel mechanism for diminished CYP7A1 expression in biliary obstruction. Hepatology 40, 600-608.

Wang, M., Xue, L., Cao, Q., Lin, Y., Ding, Y., Yang, P., Che, L., 2009. Expression of Notch1, Jagged1 and β-catenin and their clinicopathological significance in hepatocellular carcinoma. Neoplasma 56, 533-541.

Wang, X., Foster, M., Al-Dhalimy, M., Lagasse, E., Finegold, M., Grompe, M., 2003. The origin and liver repopulating capacity of murine oval cells. Proceedings of the National Academy of Sciences of the United States of America 100, 11881-11888.

Watt, A.J., Zhao, R., Li, J., Duncan, S.A., 2007. Development of the mammalian liver and ventral pancreas is dependent on GATA4. BMC Developmental Biology 7.

Williams, J.M., Oh, S.-H., Jorgensen, M., Steiger, N., Darwiche, H., Shupe, T., Petersen, B.E., 2010. The Role of the Wnt Family of Secreted Proteins in Rat Oval “Stem” Cell-Based Liver Regeneration: Wnt1 Drives Differentiation. The American journal of pathology 176, 2732-2742.

Wisse, E., De Zanger, R., Charels, K., Van Der Smissen, P., McCuskey, R., 1985. The liver sieve: considerations concerning the structure and function of endothelial fenestrae, the sinusoidal wall and the space of Disse. Hepatology 5, 683-692.

WÖLfle, D., Jungermann, K., 1985. Long-term effects of physiological oxygen concentrations on glycolysis and gluconeogenesis in hepatocyte cultures. European Journal of Biochemistry 151, 299-303.

Yamamoto, C., Yagi, S., Hori, T., Iida, T., Taniguchi, K., Isaji, S., Uemoto, S., 2010. Significance of Portal Venous VEGF During Liver Regeneration After Hepatectomy. The Journal of surgical research 159, e37-e43.

Yamane, A., Seetharam, L., Yamaguchi, S., Gotoh, N., Takahashi, T., Neufeld, G., Shibuya, M., 1994. A new communication system between hepatocytes and sinusoidal endothelial cells in liver through vascular endothelial growth factor and Flt tyrosine kinase receptor family (Flt-1 and KDR/Flk-1). Oncogene 9, 2683.

Yang, L., Jung, Y., Omenetti, A., Witek, R.P., Choi, S., Vandongen, H.M., Huang, J., Alpini, G.D., Diehl, A.M., 2008. Fate-Mapping Evidence That Hepatic Stellate Cells Are Epithelial Progenitors in Adult Mouse Livers. STEM CELLS 26, 2104-2113.

Yanger, K., Zong, Y., Maggs, L.R., Shapira, S.N., Maddipati, R., Aiello, N.M., Thung, S.N., Wells, R.G., Greenbaum, L.E., Stanger, B.Z., 2013. Robust cellular reprogramming occurs spontaneously during liver regeneration. Genes & Development.

Yao, Z., Mishra, L., 2009. Cancer stem cells and hepatocellular carcinoma. Cancer Biology & Therapy 8, 1691-1698.

Yokomori, H., Oda, M., Yoshimura, K., Nagai, T., Ogi, M., Nomura, M., Ishii, H., 2003. Vascular endothelial growth factor increases fenestral permeability in hepatic sinusoidal endothelial cells. Liver International 23, 467-475.

Zeng, G., Awan, F., Otruba, W., Muller, P., Apte, U., Tan, X., Gandhi, C., Demetris, A.J., Monga, S.P.S., 2007. Wnt'er in liver: Expression of Wnt and frizzled genes in mouse. Hepatology 45, 195-204.

Zhang, C., Yang, F., Cornelia, R., Tang, W., Swisher, S., Kim, H., 2011. Hypoxia-inducible factor-1 is a positive regulator of Sox9 activity in femoral head osteonecrosis. Bone 48, 507-513.

Zhang, H., Ables, E.T., Pope, C.F., Washington, M.K., Hipkens, S., Means, A.L., Path, G., Seufert, J., Costa, R.H., Leiter, A.B., Magnuson, M.A., Gannon, M., 2009. Multiple, temporal-specific roles for HNF6 in pancreatic endocrine and ductal differentiation. Mechanisms of Development 126, 958-973.

Zhao, R., Watt, A.J., Li, J., Luebke-Wheeler, J., Morrisey, E.E., Duncan, S.A., 2005. GATA6 Is Essential for Embryonic Development of the Liver but Dispensable for Early Heart Formation. Molecular and Cellular Biology 25, 2622-2631.

Zhou, L., Zhang, N., Song, W., You, N., Li, Q., Sun, W., Zhang, Y., Wang, D., Dou, K., 2013. The Significance of Notch1 Compared with Notch3 in High Metastasis and Poor Overall Survival in Hepatocellular Carcinoma. PLoS ONE 8, e57382.

Zong, Y., Panikkar, A., Xu, J., Antoniou, A., Raynaud, P., Lemaigre, F., Stanger, B.Z., 2009. Notch signaling controls liver development by regulating biliary differentiation. Development 136, 1727-1739.